OPTICAL COHERENCE TOMOGRAPHY APPLIED TO INVESTIGATIONS OF OPTICAL PROPERTIES OF PAINTINGS

BORISLAVA PERIC

A thesis submitted in partial fulfilment of the
requirements of Nottingham Trent University
for the degree of Master of Philosophy

December 2008

Acknowledgements

I would here like to express my thanks to the people who have been very supportive to me during this project.

I would like to express my gratitude to my supervisor, Dr. Haida Liang, for her great support from the start of the project until the long way to writing up the thesis. I am particularly grateful for her and my second supervisor, Dr. Mike Newton, for help, suggestions and encouragement through the rough times of the project.

I would like to thank Marika Spring for introducing me to the field of art conservation and her explanations of the investigated paintings regarding their conservational history. I am also grateful for the opportunity to investigate paintings at the National Galllery London.

Most of the paint samples used for the investigations have been prepared by Sophie Martin-Simpson and still a lot have been painted out by Rachel Morrison, Marika Spring and myself at the National Gallery London. I am very grateful to them for their effort and their patience as they have taught me to mix paint in a traditional way.

I also would like to thank the lecturers, post-docs and research students from the Physics Department at the Nottingham Trent University for their support. The financial support offered by The Leverhulme Trust is greatly appreciated.

Finally I must thank Chris, my family and my friends, who encouraged me to start the project and also for being very supportive during that time.

Abstract

Optical Coherence Tomography (OCT), a fast 3D scanning Michelson interferometer normally applied to biomedical applications has recently been applied to art related subjects. In this thesis, the various applications of OCT to the non invasive imaging of paintings are explored in detail. The spectral reflectance and transparency of a variety of historic artists' pigments in linseed oil or egg tempera medium are investigated and the best spectral window is found for OCT imaging of paintings. Different methods of OCT measurements of refractive indices of paint layers are presented. The first attempt of monitoring the cleaning treatment of a painting was presented in order to detect whether there was a change in the original paint surface after solvent cleaning of old varnish layers above the paint surface. Methods of revealing underdrawings (preparatory sketches) below the paint layers using OCT are explored to obtain the highest contrast images of underdrawings. One of the largest OCT underdrawing images is presented for the first time.

Contents

1. Introduction 1

1.1 Time domain OCT (TD-OCT) 4

1.2 Fourier Domain OCT (FD-OCT) 6

1.3 OCT Resolution 8

1.3.1 Source and Axial Resolution 8

1.3.2 Transversal Resolution 8

1.4 OCT Applications 9

1.4.1 Applications in Material Science 9

1.4.2 Art Related Applications 9

1.5 OCT Systems In This Project 12

2. Spectral Properties of Paint 16

2.1 Introduction 16

2.2 Theory 18

2.3 Sample Preparation 21

2.4 Experimental Method 23

2.5 Results 28

2.5.1 Effect of Binding Media 29

2.5.2 Effect of Concentration 31

2.5.3 Effect of Particle Size 34

2.5.4 Effect of Paint Mixtures 37

2.5.5 Spectral Transparency 38

3. OCT Application to Art Conservation 44

3.1 OCT Measurements of Refractive Indices 44

3.1.1 Refractive Indices 45

3.1.2 Overview of Methods of Refractive Index Measurements 48

3.1.2.1 Conventional Methods 48

3.1.2.2 OCT Methods 50

3.1.3 Refractive Index Measurements of Paint Samples 53

3.2 Monitoring of Cleaning Treatment 62

3.2.1 Monitoring of Cleaning 65

4. OCT Application to Art History 69
4.1 Introduction 69
4.2 Visibility of Underdrawing Materials 72
4.3 Method for the Best Underdrawing Images 74
4.4 Underdrawings of Paintings 83

5. Conclusion 87

References 90

Appendix 94
A Reflectance Graphs 94
a. Blue Pigments in Egg Tempera and Linseed Oil 94
b. Green Pigments in Egg Tempera and Linseed Oil 98
c. Red Pigments in Egg Tempera and Linseed Oil 101
d. Yellow Pigments in Egg Tempera and Linseed Oil 106
e. Purple Pigments in Egg Tempera and Linseed Oil 110
f. White and Black Pigments in Egg Tempera and Linseed Oil 111
B List of Publications 113

1. Introduction

This thesis is devoted to Optical Coherence Tomography (OCT) applied to paintings or paint samples. When Optical Coherence Tomography (OCT) was first introduced by Huang et al. in 1991, it was for biomedical applications. OCT is an imaging technique that is capable of scanning a 3D subsurface image. The system is basically a fast high-resolution 3D scanning Michelson interferometer. The basic OCT set-up consists of a fibre optic Michelson interferometer, a superluminescent light source, a reference and sample arm and a detector system. The light beam passes through the beam splitter and half of the light travels towards the reference mirror in the reference arm and the other half towards the sample in the sample arm. The reflected light from the sample and the reference mirror is combined and the interference signal is measured. An interference signal is only detected when the sample path length matches the reference path length within the coherence length. The physics of OCT will be explained in this chapter.

In Chapter 2, the optical properties of historic artist pigments in linseed oil and egg tempera are investigated. The spectral reflectance was measured over the visible and near infrared range (400 - 2400 nm). As the reflectance of the paint-outs was measured over a highly scattering and a highly absorbing target the spectral transparency of each paint-out is calculated. The set of reflectance spectra will provide the basis for information to further understand the optical properties of pigments as well as a reference library for spectral pigment identification. In this study, the differences in particle size, pigment concentration in the binding medium, pigment mixtures with lead white and the effect of two binding media were presented in terms of how these parameters affect the reflectance. Through the reflectance and transparency information of each paint-out a prediction of the OCT image can be made.

In Chapter 3, the potential of refractive index measurements of paint and varnish using OCT is shown. As the most important attribute of a painting is its visual appearance and it is defined partly by the refractive index, it is important to monitor refractive index for conservation as the refractive index of paint or varnish may change over time.
As OCT registers only optical thickness, the measurements of refractive index could also be used for the thickness correction of individual layers in order to obtain the physical thickness. This could reduce the necessity of taking samples from a painting in order to get the layer structure information. The potential of monitoring cleaning treatments using OCT is also shown. Through the correction of the thickness of the varnish layer, the paint surface under varnish can be compared to the cleaned paint surface. This can be done in order to detect if there is a loss of the original paint through the cleaning process.

In Chapter 4, revealing drawings beneath the paint surface is the main focus. A common technique of revealing these so called underdrawings is the application of infrared reflectography. The approach in this thesis is to use OCT to obtain depth selected images for the best image of underdrawings. The method of getting the best underdrawing image will be described. The advantage of OCT underdrawing images compared to infrared reflectography images will be demonstrated.
Finally, Chapter 5 gives the overall conclusions of the thesis.

Before we introduce OCT, we should introduce some terms which will be used throughout the thesis. Most OCT images are collected in cross-sections. Let us consider a cross-section image in a Cartesian coordinate system, where the y-axis is into the depth and the x-axis is parallel to the surface. A cross-sectional image consists of a certain number of 'A-scans' which is a depth scan along the y axis at one position of the

x-axis. A piezo electrically driven mirror within the probe head scans through the x-axis and produces a 'B-scan' which is the cross-sectional image. The y-axis gives us the depth information. The resolution of the y-axis is the axial resolution, which depends on the light source. In OCT there are two resolutions. These are independent from each other. The second resolution is in the transversal plane that is parallel to the x-axis and is defined through the objective lens. A second piezo electrically driven mirror can scan in the third direction. This scan collects a range of B-scans in order to create a 3D image. Alternatively, another means of scanning is the actual movement of the probe head through a motorised stage. This has the potential of scanning a much larger area than the earlier method.

There are two kinds of OCTs. One is the time-domain OCT (TD-OCT) that generates the depth profile through moving the reference arm. The other one is the Fourier-domain OCT (FD-OCT) that has a fixed reference arm and the signal is detected through a spectrometer and then Fourier transformed into the image domain in order to get the depth profile. FD-OCT operates much faster as there is no mechanical scanning involved in the depth ranging.

1.1. Time domain OCT (TD-OCT)

The OCT technique introduced by Huang et al. in 1991 is the TD-OCT. A schematic diagram is shown in Fig. 1.1. The system consists of a fibre optic Michelson interferometer, superluminescent light source and a detector system.

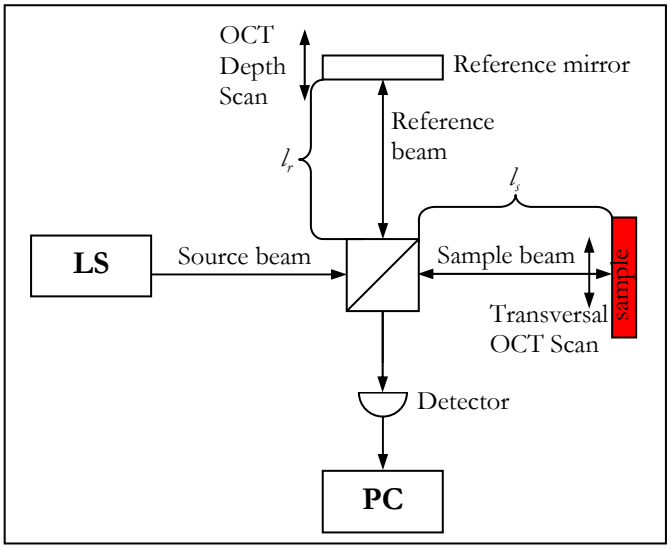

Figure 1.1. Schematic Time-domain OCT. LS: low coherence light source.

The source beam can be expressed as monochromatic complex plane wave

$$E_{SB} = E_0 e^{-ik(\omega)z} \qquad k = 2\pi/\lambda \qquad (1.1)$$

where ω is the angular frequency of the light wave. When the light travels through the 50/50 beam splitter the beam in the reference arm can be described as

$$E_r = -1/\sqrt{2}\, E_{SB} \qquad (1.2)$$

and in the sample arm respectively as

$$E_s = i/\sqrt{2}\, E_{SB} \qquad (1.3)$$

where the 90 degree phase shift at the beam splitter is taken into account. The reflected beam from the reference mirror and the sample can be expressed as

$$E_{r2} = r_r (1/\sqrt{2}) E_{SB} e^{-i2kl_r} \qquad (1.4)$$

$$E_{s2} = -r_s (i/\sqrt{2}) E_{SB} e^{-i2kl_s} \qquad (1.5)$$

where l_r is the distance between the beam splitter and the reference mirror and l_s is the distance between the sample and the beam splitter. r_r and r_s are the reflectivity from the reference mirror and the sample. The sum of E_{r2} and E_{s2} after they pass the beam splitter can be described as the signal at the detector.

$$E_D = E_R e^{-i2kl_r} + E_S e^{-i2kl_s} \qquad (1.6)$$

where $E_R = (1/2) r_r E_{SB}$ and $E_S = -(i/2) r_s E_{SB}$. The irradiance is measured at the detector rather than the electric field. The irradiance is proportional to the electric field multiplied by its complex conjugate (the angled brackets represent time-averages):

$$I_D = \left\langle E_D E_D^* \right\rangle = \left\langle E_R E_R^* \right\rangle + \left\langle E_S E_S^* \right\rangle + 2\Re\left\{ \left\langle E_S E_R^* \right\rangle \right\} \qquad (1.7)$$

The first two terms of the Eq. (1.7) are due to self-interference or autocorrelation. The signal of the interference between the sample and reference arm is the last term. The following formula is given by substitution of Eq. (1.6) into (1.7)

$$I_D = I_R + I_S + 2\left|\gamma(\Delta l)\right| \sqrt{I_r I_s} \cos(2k\Delta l) \qquad (1.8)$$

where I_R is the irradiance from the reference arm which is proportional to the autocorrelation of the source electric fields, I_S is the irradiance from the sample arm which is proportional to the autocorrelation of the sample fields and $\gamma(\Delta l)$ is the complex degree of coherence. Coherence can be described as how well the correlation is between two interfering light waves. When the degree of coherence is 1, we have total coherence and 0 when there is no coherence. When the degree of coherence is between 0 and 1, we have partial coherence. The coherence time is defined as time interval where the phase of the light beams is constant. The coherence length is the product of the coherence time and the speed of light. When the difference of the path length between the reference arm mirror and the sample arm mirror is much greater than the coherence length the signal at the detector is only the sum of the intensities of the sample and reference arm. There will be no interference fringes. The interference is detected when

the path length difference is within the coherence length (Brezinski 2006, Fercher et al. 2003, Tomlins et al. 2005).

In the case of OCT, the source is broadband rather than monochromatic. The third term in Eq. 1.8 is the cross-correlation between the reference and sample fields which gives the depth information of the sample. The cross-correlation term gives fringes as the mirror position varies in the case of time domain OCT. The envelope of the fringes corresponds to the autocorrelation of the source field and the FWHM of the envelope gives the depth resolution.

1.2. Fourier Domain OCT (FD-OCT)

FD-OCT has nearly the same set up as TD-OCT, only that the reference mirror is fixed and the detection system differs. The depth information using FD-OCT is acquired through the spectrum of the light obtained using a spectrometer. This signal is then Fourier transformed that gives the depth profile of the sample. A schematic set-up of a FD-OCT is shown in Fig. 1.2.

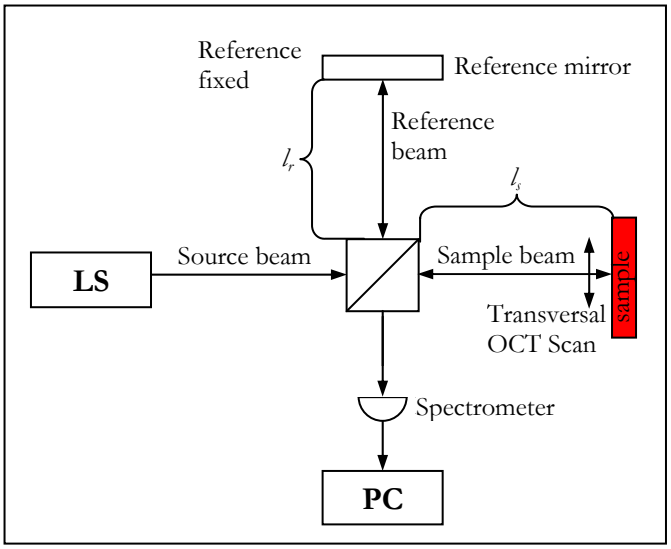

Figure 1.2. Schematic Fourier-domain OCT. LS: low coherence light source.

When light is back reflected from the sample, the light carries information of different depths within the sample. An interference signal is given through the combination of

the reference arm intensity and the sample arm intensity. The intensity can be described as in Eq. 1.8. The raw data of an A-scan is seen in Fig. 1.3. The data was obtained with a Thorlabs OCT at 930 nm.

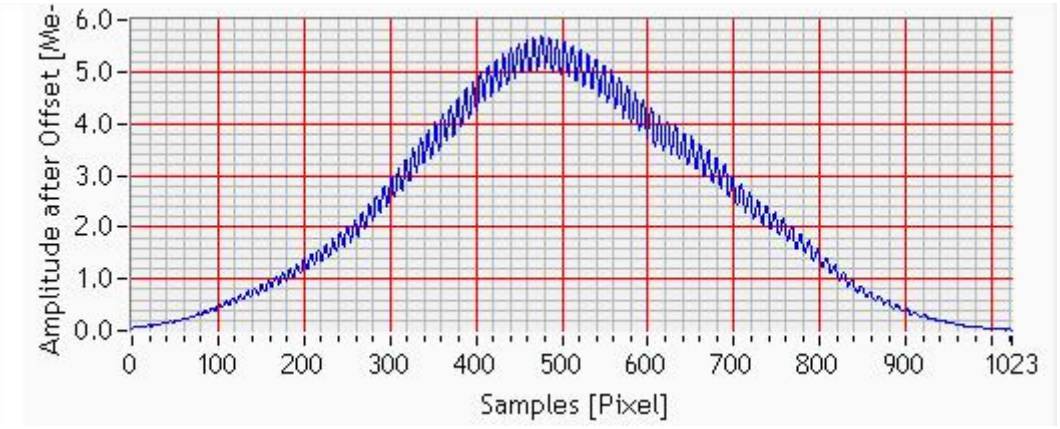

Figure 1.3. Raw data of an A-Scan obtained with Thorlabs OCT at 930nm.

The cross-correlation term (Eq. 1.8) varies as the wavelength changes in the case of FD-OCT. The intensity as a function of the depth is obtained through a Fourier transform of the intensity in frequency domain (Brezinski 2006, Fercher et al. 2003, Tomlins et al. 2005).

$$I(t) = FT\{I(k)\} \qquad (1.9)$$

An A-scan of a microscope slide is presented in Fig. 1.4 as the function of the depth.

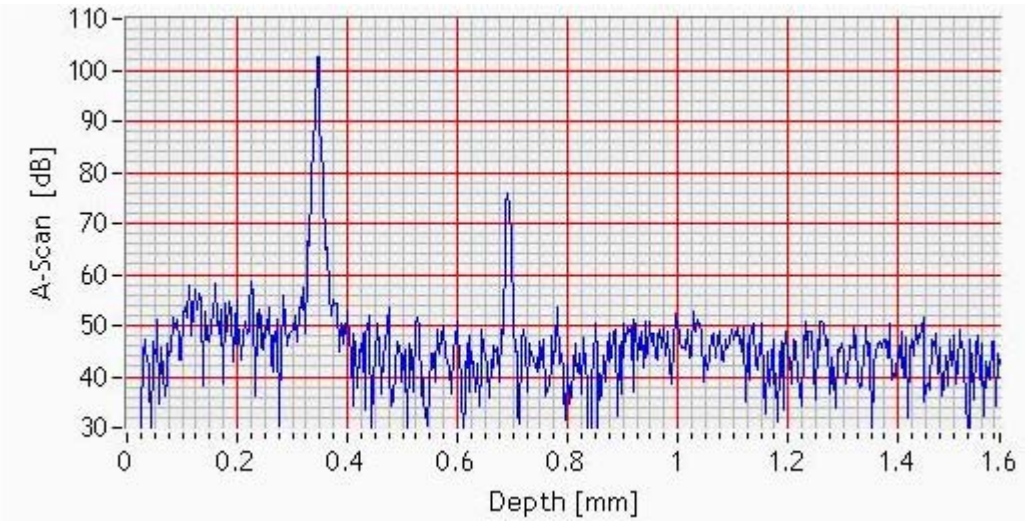

Figure 1.4. An A-Scan after Fourier transformation of the raw data.

1.3. OCT Resolution

1.3.1. Source and Axial Resolution

The light source is a very important part of an OCT. As the temporal coherence of the source determines the axial resolution and the wavelength of the source affects the depth penetration. A high axial resolution is important in order to distinguish between paint layers or even to separate the varnish layer from the paint layer. Varnish layers can have a thickness of about 10 μm. The axial resolution of an OCT is given by

$$\Delta z = \frac{2\ln(2)}{\pi}\frac{\lambda_0^2}{\Delta\lambda} = 0.44\frac{\lambda_0^2}{\Delta\lambda} \qquad (1.10)$$

where λ_0 is the wavelength and $\Delta\lambda$ is the spectral band width of the light source. Axial resolution depends on the square of the wavelength and the bandwidth of the source. Due to the round-trip path length of the light the axial resolution is half the coherence length.

1.3.2. Transversal Resolution

The transversal resolution is separated from the axial resolution in OCT. The axial resolution is determined through the light source and their coherence length. On the other hand the transversal resolution is given by the numerical aperture of the objective lens. Therefore the transversal resolution can be varied without a resolution change in the axial direction. However there is an interdependence between axial resolution and the depth of focus. The transversal resolution Δx is given by Abbe's equation (Wang et al. 2002).

$$\Delta x = 1.22\frac{\lambda}{2N.A._{obj}} \qquad (1.11)$$

The depth of focus of the objective lens is expressed by (Born and Wolf 1999):

$$d = 2\frac{\lambda n}{N.A._{obj}^2} \qquad (1.12)$$

Therefore for a high transversal resolution, the depth of focus is reduced which means the depth range is reduced.

1.4. OCT Applications

1.4.1. Applications in Material Science

Over the last seventeen years OCT was applied to a variety of different areas, such as botany, micro fluidics, art diagnostics, material science and medical applications. The main application is in the medical.

In material science there are a variety of different materials OCT is applied to in order to characterise the material. The materials are: ceramics, glass, optical components, polymers, fibre composites and paper. OCT scans of ceramics can show micro damages in the surface and sub-surface. These damages would decrease the strength of ceramics and therefore their performance. Another application to material science is the investigation of laser damages to optical parts. The results can help to prevent further growth of the damage. That is more interesting for larger and more expensive optical components. OCT can also measure the outer diameter and the thickness of the fibre coating simultaneously. A different area for the application of OCT is botany. A study was dedicated to the measurement of the hull thickness of lupin seeds as the thickness is a quality factor for the plant. A comprehensive review of OCT applications in material science is given by Stifter (2007).

1.4.2. Art Related Applications

The application of OCT to art related objects is mostly towards paintings. The main areas are the study of varnish which is the top layer of an oil painting and the

investigation of drawings below the paint surface. In this section, OCT applications to art objects are reviewed.

In 2004, three papers on the application of OCT to heritage science were published for the first time. Yang et al. (2004) used two time-domain OCTs to examine ancient jade objects. First an OCT at a central wavelength of 800 nm and an axial resolution of 3.5 μm in the jade object and the second with a central wavelength of 1240 nm and an axial resolution of 7.5 μm in the jade object. They investigated the subsurface of jades and also compared the jade without whitening (caused by weathering) to natural and artificial whitening. The results were that there is a difference in scattering behaviour between these areas, however, the conclusions were not definitive. Targowski et al. (2004) investigated porcelain, ceramics and paintings using a FD-OCT demonstrating the potential of OCT applied to a variety of art objects. Liang et al. (2004) used TD-OCTs at 800nm and 1300nm to demonstrate the capabilities of OCT at resolving paint and varnish layers and giving thickness information of varnish and paint layers for paintings.

Subsequently, Liang et al. showed in several publications the potential of OCT applied to art works including the differentiation between old and new varnish and between paint layers, the imaging of underdrawing using OCT which gave superior underdrawing images than any other imaging methods and the measurement of the refractive indices of varnish layers with OCT (Liang et al. 2005a, Liang et al. 2005b).

Arecchi et al. compared an OCT cross-section of a conventional cross-section that is acquired with a microscope in 2005. The two cross-sections were then super-imposed and presented that the two cross-sections taken with two different methods match (Arecchi et al. 2005). There is no mention about a thickness correction of the OCT

image. As the thickness of the layers in the OCT images is the optical thickness and the thickness of the conventional method is the physical thickness.

Gorczynska et al. 2006 showed the thickness measurement of varnish, but also the correction of the varnish layer thickness into physical thickness. The changes of the paint surface and canvas due to humidity were investigated by Targowski et al (2006a) and Bajraszewski et al. (2006). A sample was exposed to 100% relative humidity and the movement of the canvas was monitored. After 60 minutes, the paint surface moved by about 170 μm (Bajraszewski et al. 2006). Another area of interest is the applicability of OCT to paint samples, that is how many types of paint can OCT penetrate. The applicability of OCT for imaging paint layers was investigated by examining 47 commercial oil paint samples at 823 and 1550 nm which showed that more paints are transparent to OCT at 1550nm than 823nm (Szkulmowska et al. 2006).

The latest publications by Liang et al. were devoted to OCT applications to paintings at The National Gallery and to objects at The British Museum, and further investigations of how to extract the optical properties of paint samples using OCT (Liang et al. 2007a, Liang et al. 2007b). The applications to paintings aspects of these publications are mostly based on work in this thesis which will be described in detail in the following chapters.

Adler et al. (2007) presented the 3D characterisation of gold punch marks on wood panels using an OCT. Through these marks the paintings can be characterised to a specific workshop and also mocks of paintings can be revealed. It is feasible to measure punch marks with OCT quantitatively and also it was shown that OCT is capable of illustrating small feature which cannot be seen in high resolution photography. Also the

revealing of underdrawings was investigated and compared to high resolution IR photography. The authors concluded in the case of paintings with highly transparent layers, IR photography images are comparable to OCT images and since the imaging and processing time is much lower for OCTs, IR photography has the advantage. However, for more opaque paint layers, OCT has the advantage.

In this project we have applied OCT to art conservation and art history. The application to art history is mainly focussed on the study of underdrawings. The application to art conservation is focussed on the measurement of refractive indices of paint samples, the comparison of spectral reflectance data to OCT images and the monitoring of the removal of a varnish layer.

1.5. OCT Systems In This Project

There were two OCT systems applied to art related objects in this thesis. A time-domain OCT (TD-OCT) from Carl Zeiss Meditec and a Fourier-domain OCT (FD-OCT) from Thorlabs. The Carl Zeiss Meditec Visante™ OCT has a central wavelength of 1310 nm (Fig. 1.5). The system is designed for medical use (ophthalmology). It is a bench-top instrument with everything included in one box, except the keyboard and the mouse. As the system is for examination of the eye it has a chin rest. The latter was modified with a self-made microscope slide holder in order to be able to measure the variety of paint-outs on the microscope slides. The axial resolution is 18 μm. It is possible to choose between three transversal resolutions that are 78, 63 and 20 μm. The acquisition time of one B-scan depends on the chosen transversal resolution, but is in all cases less than a second.

Figure 1.5. Carl Zeiss Meditec Visante™ OCT with a central wavelength of 1310 nm (Carl Zeiss Meditec AG 2006, p. 1).

The second OCT system is a Thorlabs Spectral Radar OCT [Fourier-domain OCT (FD-OCT)] with a central wavelength of 930 nm. The system is portable and therefore it can be applied to samples and to paintings. The OCT is adapted to scan a reasonably large area by attaching the probe to a XYZ stage. In Figure 1.6 the main parts of the system are shown: the spectral OCT engine, handheld scanning probe, motorised XYZ translation stage, computer and motor controller.

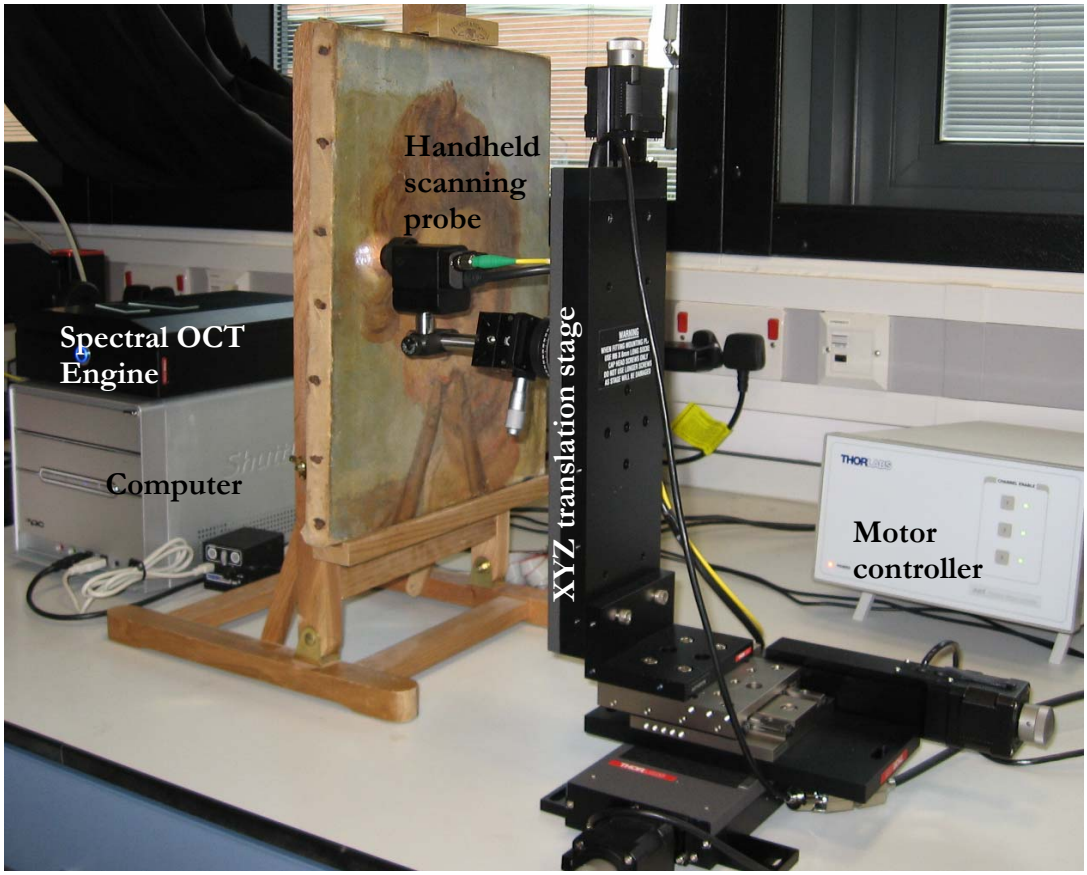

Figure 1.6. Thorlabs Spectral Radar Optical Coherence Tomography. Handheld scanning probe is mounted onto a motorised XYZ translation stage.

The handheld probe is mounted to a motorised three axes stage (Fig. 1.6). The latter gives a range of 15 cm by 15 cm scan area. Cross-sectional images can be adjusted to a maximum size of 10 mm in width by 1.6 mm in depth. The axial resolution of 6.2 μm is limited by the spectral bandwidth (100 nm) of the light source and the depth range is inversely proportional to the spectral wavelength resolution. However, the limitation of the transverse resolution of 9.2 μm is dependent on the objective lens. The signal degradation as a function of depth is measured by placing a glass microscope slide at different distances to the probe head. The results are shown in Fig. 1.7. The OCT reference mirror position and the objective lens focus can both be adjusted at the initial calibration stage. In Fig. 1.7, the setup corresponds to an optimum signal strength at pixel 44. The signal degradation increases as both the distance away from the zero path

length difference increases and as the distance from best focus increases. The working distance, which is the distance between the sample and the probe, is about 1 cm.

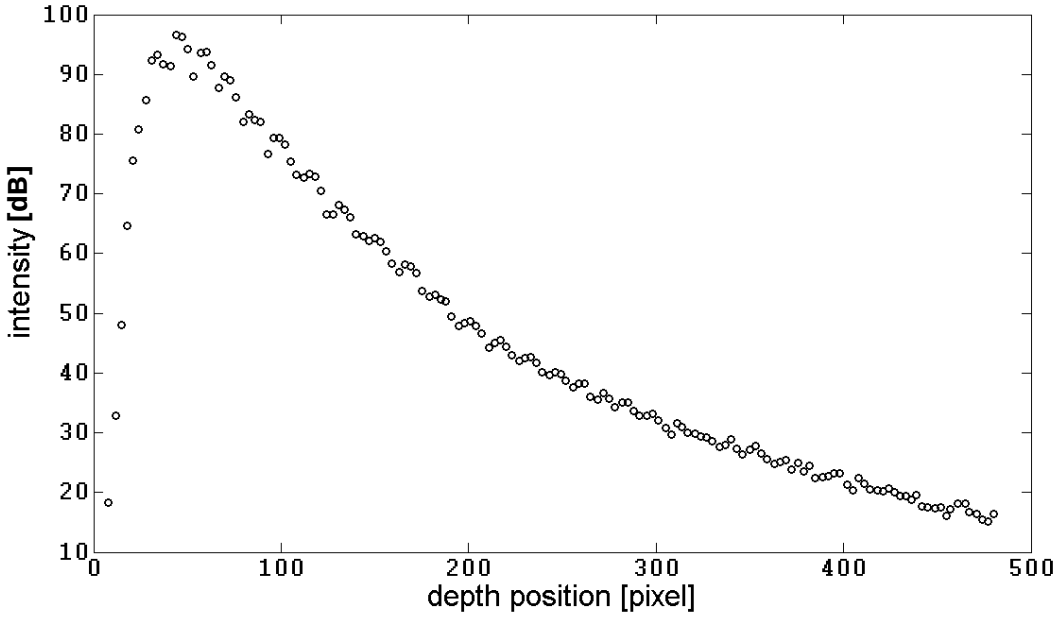

Figure 1.7. Intensity versus depth position of Thorlabs Spectral Radar Optical Coherence Tomography.

A 3D image can be captured by collecting a number of B-scans through scanning in one direction by moving the motorised stage. The sampling resolution in the scanning direction is adjustable through the speed of the scan. All 3D images in this thesis have a resolution of about 20 μm in scanning direction. 3D scans have a maximum width of 1 cm determined by the optics of the probe and a maximum length of 15 cm defined by the maximum travel of the translation stage. Larger areas of interest can be scanned in separate parts and joined together afterwards with an image processing program.

2. Spectral Properties of Paint

2.1. Introduction

As it was discovered that paint is more transparent in the infrared region then in the visible, the focus of the investigation of the underdrawings (preparatory sketches) of paintings was placed in the infrared region. Infrared photography had been used since the 1930s. The infrared-sensitive film has a limited wavelength range from 750 nm up to 900 nm which leads to the poor penetration through for example copper-containing paint layers (van Asperen de Boer 1966). Another imaging technique is infrared reflectography that uses longer wavelengths up to 2μm, so that the penetration through copper containing paint layers is achievable. This technique was developed in the 1960s and is the fundamental application for revealing underdrawings (van Asperen de Boer 1969).

Since the application of infrared reflectography (IRR) to paintings, it is an important aim to study the optical properties of historic artists' pigments. This was done directly and indirectly in order to determine the best spectral window for IRR (van Asperen de Boer 1969, Delaney et al. 1993, Gargano et al. 2006, Walmsley et al 1993). Van Asperen de Boer has developed the infrared reflectography for revealing non-destructively underdrawings of paintings in 1969. In the publication the hiding thickness was used as a parameter for transparency. The optimum wavelength range was obtained around 2.0 μm for revealing underdrawings, but there were only eight paint-outs in linseed oil investigated. The pigments were vermilion, malachite, azurite, ochre, lead white, verdigris, iron oxide and raw sienna. In 1993 Delaney et al. investigated the spectral reflectance of six blue pigments (azurite, lapis lazuli, indigo, Prussian blue, cobalt and thalo blue) in linseed oil for pigment identification. The transparency was determined using multispectral images of test panels with drawings below the paint. Another study

of the best spectral bandwidth was published by Walmsley et al. in 1993. Reflectography of eight underdrawing test panels were investigated in four different spectral bands. Each test panel had paint with one single pigment painted over eight different drawings. The background of the test panel was a microscope slide. Lapis lazuli, malachite, azurite, chrome oxide green, indigo, Mars yellow, raw sienna and lead-tin yellow were the pigments mixed with oil that were applied on the test panels. The bands were in the visible and near infrared range (0.4 - 0.8, 0.9 - 1.5, 1.5 - 1.8, 2.0 - 2.5 μm). The reflectography was collected with a silicon CCD camera, a vidicon camera, a germanium detector and a PtSi camera. The best visibility was achieved from 1.0 up to 2.5 μm depended on the paint and the underdrawing material. Gargano et al. (2006) compared five multispectral cameras in the wavelength range of 800 to 5000 nm for investigating underdrawings of paintings. The transparency was measured with a contrast value which was defined as ratio of the difference between the black areas (e.g. underdrawings) and white areas (e.g. background) below the paint layer and of the difference between the black areas and white areas without a paint layer. In this study only some selected results were shown and the full range of investigated paint samples was not presented. Only the results of 17 paint-outs, three in egg tempera (indigo, natural ultramarine and light natural sienna) and the rest in oil as binding medium (azurite, smalt blue, green earth, malachite, verdigris, veronese green, lead yellow, lead yellow red, yellow ochre, red lake, vermilion, haematite, red ochre and red earth) were published. Their results showed that the majority of pigments they investigated are more transparent in the 1330 to 2200 nm range.

In 1958 a study of reflectance of pigments in the *photographic* near infrared (700 nm – 900 nm) was published by Taylor. Here the reflectance of a variety of paint films (56 samples) was measured over a white, which is highly reflecting, and over a black, which is highly absorbing, surface. The combination of the scattering and absorbing property

of the paint describes the hiding power of a paint film. The results of the reflectance over white (RW) and over black (RB) were calculated as contrast ratio of these two values (100 RB/RW), which was used to describe the hiding power of the paint film.

The current study is a comprehensive survey of the transparency of historic artist pigments over the visible and near infrared (NIR) range (400 nm - 2400 nm). The spectral reflectance of 50 pigments in egg tempera and linseed oil were measured from the visible to the near infrared. The transparency of paint layers determines the effective depth range that the non-contact cross-sectional imaging technique OCT can probe into the painting. OCT has recently been applied to paintings (e.g. Liang et al. 2004, 2005, Targowski et al. 2004, 2006b, Szkulmowska et al. 2006).

In this study different aspects were taken into account to investigate the changes in spectral reflectance due to the differences in particle size, binding medium, pigment concentration and pigment mixtures with lead white. The set of reflectance spectra will provide the basis for information to further understand the optical properties of pigments as well as a reference library for spectral pigment identification. Another application for the reflectance measurements is to determine the best spectral window for NIR imaging for revealing underdrawings with IRR and OCT imaging or to determine the best spectral band for OCT imaging of paintings so that the deepest penetration into the paint is achieved. In order to achieve that it is necessary to convert the reflectance into a relative transparency of the paint samples.

2.2. Theory

When incident light hits the boundary of air and the paint layer, the light is divided into a reflected and refracted part, if the condition for total reflection is not fulfilled. The

refracted part can either be absorbed or scattered in the media or transmitted through the paint layer. The reflection and transmission can by described by Fresnel as:

$$R_{\perp}{}^{2} = \left(-\frac{\sin(\Theta_i - \Theta_t)}{\sin(\Theta_i + \Theta_t)} \right)^2 = \left(\frac{n_i \cos\Theta_i - n_t \cos\Theta_t}{n_i \cos\Theta_i + n_t \cos\Theta_t} \right)^2 \qquad T_{\perp} = 1 - R_{\perp} \qquad (2.1)$$

$$R_{||}{}^{2} = \left(\frac{\tan(\Theta_t - \Theta_i)}{\tan(\Theta_t + \Theta_i)} \right)^2 = \left(\frac{n_i \cos\Theta_t - n_t \cos\Theta_i}{n_i \cos\Theta_t + n_t \cos\Theta_i} \right)^2 \qquad T_{||} = 1 - R_{||} \qquad (2.2)$$

$R_{\perp}$ is the reflection coefficient when the electric field is perpendicular to the plane of incident and $R_{||}$ is when the electric field is parallel to the plane of incident. These equations are for the case that the reflection is specular, i.e. mirror-like. In the case of the diffuse reflection the light is reflected into different directions due to the surface roughness of the object. The reflections within a volume can be described as diffuse scattering. For example light that is transmitted into a paint layer is scattered diffuse by the particles.

When an object is illuminated there are several actions which might occur. The light could be absorbed, transmitted or scattered by the object or a combination of these actions could happen. The colour of an object is defined by the absorption and scattering of the light. Absorption of light in matter results in either the excitation of the matter to a higher energy state or the conversion of the energy of the incident light into other forms of energy such as thermal energy. Scattering is the change of the original light propagation direction through the interactions of light with particles in the matter.
The colour of the sample is due to the backscattered part of the white light, so that when light at certain wavelengths is absorbed or/and transmitted, the remaining light is scattered and some of which backscattered. The spectrum of the backscattered light is then different from the incident white light. This gives rise to colour of the sample. The transmittance of an object at a specific wavelength can be described as the ratio between

light that passed through the object and the incident light. Extinction is used to describe the absorption and scattering of light by matter. The higher the extinction is, the stronger the absorption and/or scattering and lower the transparency. Extinction depends on the wavelength, the chemical composition of the particle, size, shape, concentration and the medium it is in.

Mie theory describes the scattering of an electromagnetic wave from a single spherical particle of arbitrary size but of the order comparable to the wavelength of light. The theory was first published by Gustav Mie in 1908. Rayleigh scattering is a limiting case of the Mie theory, where the particle size is smaller than the wavelength of light. Through the Mie theory the absorption and scattering coefficient can be obtained and also the intensity of the scattered light. The latter can be calculated so that the scattering behaviour around the particle is described. These calculations demand that the medium surrounding the particle is not absorbing the light, the refractive index is known and only single scattering occurs (McNeil et al. 2001, Phillips-Invernizzi et al. 2001, Bohren et al. 2004). As pigment particles are not perfectly spherical nor of the same regular shape and more often than not in the multiple scattering regime, the theory cannot be easily applied to paint films.

In 1931 a theory for relating reflectance measurements to scattering and absorption properties was published by Kubelka and Munk (Kubelka and Munk 1931). Instead of considering the interaction of single particle with the incident light, the average interaction was considered to describe the scattering and absorption properties. An infinitely thick layer is illuminated by a diffuse light, which is assumed to propagate diffusely in the entire sample. The theory considers a thin layer *dx* in the infinitely thick sample which is hit by the incident light *i* from the top surface and the back reflected

light *j* from the bottom of the sample. Therefore the total change *di* of the incident light beam *i* is weakened by scattering *S* and absorption *K* in the forward direction, but strengthened by the scattering *S* in the media in the backward direction. Thus the total change *dj* of the reflected light can be similarly described by these differential equations:

$$-di = -(K+S)i\,dx + S\,j\,dx \qquad (2.3)$$

$$dj = -(K+S)\,j\,dx + S\,i\,dx \qquad (2.4)$$

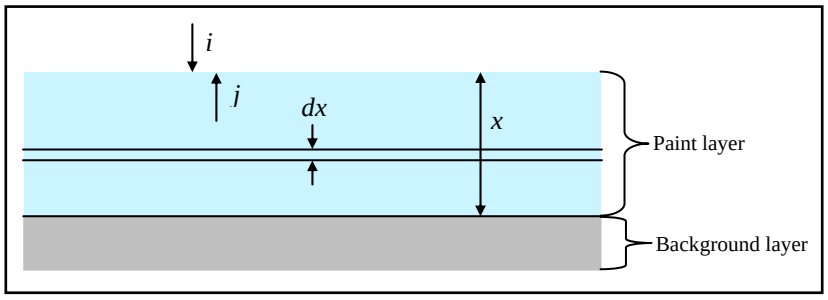

Figure 2.1. Schematic diagram for the Kulbelka-Munk model.

The negative signs in the equations are due to the opposite direction of the flux, as can be seen in Fig. 2.1.

Equation 2.5 can be derived from the equations 2.3, 2.4 and R(λ)=j/i. In this formula the reflectance is only dependant on the scattering and absorbing constants.

$$\frac{K(\lambda)}{S(\lambda)} = \frac{(1-R(\lambda))^2}{2R(\lambda)} \qquad (2.5)$$

This very simple version of the Kubelka-Munk theory assumes complete hiding of the paint layer. The reflectance of the paint can also be described such that the thickness *x*, reflectance of the background R_o, the effective scattering constant *S* and the effective absorption constant *K* are taken into account in the equation.

2.3. Sample preparation

A set of paint-outs consisting of a wide variety of historic artist's pigments in both egg tempera and linseed oil has been prepared. A total of 50 pigments were included. Some

pigments such as azurite, malachite and smalt blue were painted out in different particle sizes, as this has an effect on the colour and spectral reflectance of the resulting paint. The pigments were chosen to be representative of what is found on paintings.

Mixing paints requires experience in order to recognize a good paint mixture and therefore it is qualitative. Here the procedure of mixing paint is described. As the amount of oil necessary to make a paint varies significantly from pigment to pigment, it is recommended to start with a couple of drops of oil and continue adding more until the paint mixture reaches a consistency suitable for traditional oil paintings. The pigment powder was weighed and then placed onto a glass plate. A small amount of oil, which was also weighed, was added to the pigment and mixed well together with a spatula. At this stage the mixture should not be too stiff or runny, but still shinny. The next step was to grind the paint up to 15 minutes. Sometimes it was necessary to add a bit more oil or even pigment powder after the grinding procedure and to grind it again in order to get the optimum consistency. This was achieved when the paint was glossy and smooth, but not too runny. As the oil and the pigment powder were weighed, these samples have a known pigment volume concentration. The same procedure can be applied to pigments mixed with egg tempera. These paint samples were prepared at the Scientific Department of the National Gallery.

In order to measure the transparency of the paint layers, the set of paint-outs was prepared over thin glass microscope slides. A template of a known thickness (50 μm, 100 μm or 200 μm) was placed onto the microscope slide and the paint was then applied by hand, so that the wet thickness of the paint is known. A list of the pigments is shown in Table 2.1 and few samples are shown in Figure 2.2.

Figure 2.2. Paint samples on glass microscope slides.

BLUE		GREEN	
Azurite	The Pigment Factory Bejing	Artificial malachite	Kremer Pigmente
Azurite MP	L. Cornelissen and Son	Bavarian green earth	Kremer Pigmente
Artificial Ultramarine dark	Kremer Pigmente	Cobalt bottle green	Kremer Pigmente
Artificial Ultramarine light	Kremer Pigmente	Cobalt turquoise	L. Cornelissen and Son
Cerulean blue	Kremer Pigmente	Natural malachite	The Pigment Factory Bejing
Cobalt blue	Kremer Pigmente	Natural malachite*	Kremer Pigmente
Indigo	Kremer Pigmente	Phthalo (Mona) green	L. Cornelissen and Son
Lapis Lazuli deep°	L. Cornelissen and Son	Verdigris synthetic	Kremer Pigmente
Manganese blue	Kremer Pigmente	Viridian green	L. Cornelissen and Son
Prussian blue (milori)	Kremer Pigmente		
Smalt	L. Cornelissen and Son		
RED		**YELLOW**	
Cadmium red	L. Cornelissen and Son	Cadmium yellow deep	L. Cornelissen and Son
Chrome red	Kremer Pigmente	Cadmium yellow light	L. Cornelissen and Son
Cochineal lake	G8/EU-Artech	Chrome yellow medium	Kremer Pigmente
Lac lake	NG Jan 2003	Cobalt yellow (Aureolin)	L. Cornelissen and Son
Madder lake (2005, from dyed wool)	COST-G8 from 2ii residue	Dyer's broom lake 1 (buckthorn lake)	G8/EU-Artech
Madder lake 1 (MODHT)	COST G8/EU-ARTECH	Italian golden ochre	Kremer Pigmente
Natural red earth	Kremer Pigmente	Lead tin yellow (type 1)	Kremer Pigmente
Red lead	Kremer Pigmente	Lemon yellow (Barium Chr.)	L. Cornelissen and Son
Red ochre (RTFLES)	Kremer Pigmente	Naples yellow light	Kremer Pigmente
Rose madder	L. Cornelissen and Son	Nat. Italian tierra di Sienna	Kremer Pigmente
Sappanwood lake (Brazilwood lake)	G8/EU-ARTECH 18/10/2005	Orpiment (grade 3)	The Pigment Factory Bejing
Vermillion Chinese grade 3	The Pigment Factory Bejing	Weld lake	EU-Artech
Vermillion light	Kremer Pigmente		
WHITE		**PURPLE**	
Lead white	Kremer Pigmente	Cobalt violet dark	Kremer Pigmente
Titanium white	L. Cornelissen and Son	Cobalt violet light	Kremer Pigmente
Zinc white*	L. Cornelissen and Son	Manganese violet	Kremer Pigmente
BLACK			
Bone black	Kremer Pigmente	Charcoal (made from beech)	Kremer Pigmente
* only with linseed oil; ° only in egg tempera			

Table 2.1. Pigment list including the supplier information.

2.4. Experimental Method

The reference set of spectral reflectance of paint in both egg tempera and linseed oil was measured between 400 nm and 2400 nm. An Ocean Optics HR2000 fibre optic spectrometer (200 - 1100 nm), a Polychromix DTS 1700 (900 - 1700 nm) and DTS 2500 (1700 - 2500 nm) fibre optic spectrometer were used to cover the measurement range. The spectral resolutions of the three spectrometers are 0.9 nm, 12 nm and 22 nm.

There is a difference of the method of operation between the spectrometer for the visible and infrared range. The main parts of a spectrometer are the grating and the detector. When light hits the sample, specific frequencies are absorbed. Absorption in the near infrared corresponds to the transition between various vibrational modes of molecular bonds (Bacci 2000). In the case of the visible range the absorption results in electronic transitions. The light which enters the visible spectrometer is collimated onto

the grating mirror, which separates the light into the different wavelengths. The dispersed light is then focussed onto the Charge-coupled device (CCD) detector. The latter detects light with different wavelengths on different pixels. The CCD detector has an array of light sensitive pixels.

The Ocean Optics spectrometer (HR2000) for the visible range works with a silicon-based detector (CCD) and the Polychromix spectrometers (DTS1700 and DTS2500) for the near infrared range use InGaAs detector.

The signal of the CCD detector is influenced by readout and dark noise. The dark signal, which is when there is no light at the detector, should be zero, but due to thermal excitation of electrons into the conduction band and the CCD potential, the dark signal is never zero. The dark signal can be subtracted out, but the noise associated with the dark signal remains (Birney et al. 2006). The infrared spectrometers subtract automatically the dark signal from the sample signal and therefore the dark correction is only necessary for the visible spectrometer. The latter has a special feature (electric dark correction) in the software implemented so that the thermal drift between measurements is compensated. This is possible as a part of the CCD detector in the spectrometer is covered and no light can reach this part of the sensor. The signal of each pixel in the covered part is averaged and then subtracted from the signal of the rest of the CCD sensor. The subtraction influences only the thermal drift and not the pixel dependent dark signal. Therefore the pixel dependent dark signal needs to be subtracted after the full data set is taken. By investigating the electric dark correction, it showed that the dark signal measured with the software implemented tool was more stable than the dark signal measured without the automated correction. This is due to the fact that the electric dark correction is done with every measurement and therefore it is adjusted

to the changed thermal conditions. This setting was applied to all measurements.

As the collected signals are given in counts at the each wavelength, the reflectance over white (R_W) and over black (R_B) can be calculated. In the case of the Ocean Optics spectrometer (200 - 1100 nm) the dark signal D had to be taken into account. The dark signal was subtracted from the reference signal R_R and the paint signal measured when the sample is placed over white R_{SW} and black R_{SB}. The reference signal is the spectrum of the light reflected from a white standard (~100% reflectance) target placed at the same relative position to the spectrometer probe as the sample. The following formulas give the reflectance respectively over a white and black target.

$$R_W(\lambda) = \frac{(R_{SW}(\lambda) - D(\lambda))}{(R_R(\lambda) - D(\lambda))} \qquad (2.6)$$

$$R_B(\lambda) = \frac{(R_{SB}(\lambda) - D(\lambda))}{(R_R(\lambda) - D(\lambda))} \qquad (2.7)$$

The reflectance calculations for the wavelength range from 900 to 2500 nm were done without the dark subtraction, as the dark signal has already been subtracted from the output data. Therefore the formulas are as follows:

$$R_W(\lambda) = \frac{R_{SW}(\lambda)}{R_R(\lambda)} \qquad (2.8)$$

$$R_B(\lambda) = \frac{R_{SB}(\lambda)}{R_R(\lambda)} \qquad (2.9)$$

As transparency depends on both the scattering and absorption properties, the measurement method was chosen to differentiate between scattering and absorption. This was done by measuring the reflectance of the sample placed over a highly reflecting (white) and a highly 'absorbing' (black) reference. Out of these results it is possible to derive that a sample is highly transparent, when the reflectance of the sample placed over white is high and the reflectance of the sample placed over black is low. In other

words, such a sample would have a poor hiding power. The Kubelka-Munk theory presented in subsection 2.2 assumes complete hiding of the paint. A correction for that formulation is given with the following equation for incomplete hiding (Kubelka 1948).

$$R_{KM} = \frac{1 - R_g\left[a - b\coth(bSh)\right]}{a + b\coth(bSh) - R_g} \qquad (2.10)$$

where S is the scattering coefficient, h the thickness of the paint layer and R_g is the diffuse reflectance of the substrate.

The variables a and b are defined as:

$$a = \frac{(S + K)}{S} \qquad (2.11)$$

$$b = \left(a^2 - 1\right)^{1/2} \qquad (2.12)$$

As we can obtain the information about the layer thickness through the OCT images, the scattering and absorption coefficient could be calculated.

Another case would be when both reflectances (over white and black) are high, the sample is expected to be highly scattering. The setup was constructed in a way that a white target could be placed under the sample without changing the position of the measuring spot on the sample. A highly absorbing paint layer would have low reflectance over a white or black background.

In Figure 2.3 the setup for the reflectance measurements is displayed. The probe head was adjusted to 45 degrees to the normal above the sample holder. A Tungsten light source was connected with the spectrometers through a reflectance probe fibre. The highly reflecting reference was a Labsphere Spectralon 99% reflective target. A large distance, ~45 cm, between the sample and the next possible reflecting surface (reflecting in black paper) was used as an alternative for a highly absorbing reference, as can be

seen in Fig. 2.3. There was a difference of 0.1% between the results of using a 2% reflecting black target and our alternative 'black' reference. This is insignificant for the results as the spectrometer specifications state that error due to the stray light effects is 0.1%.

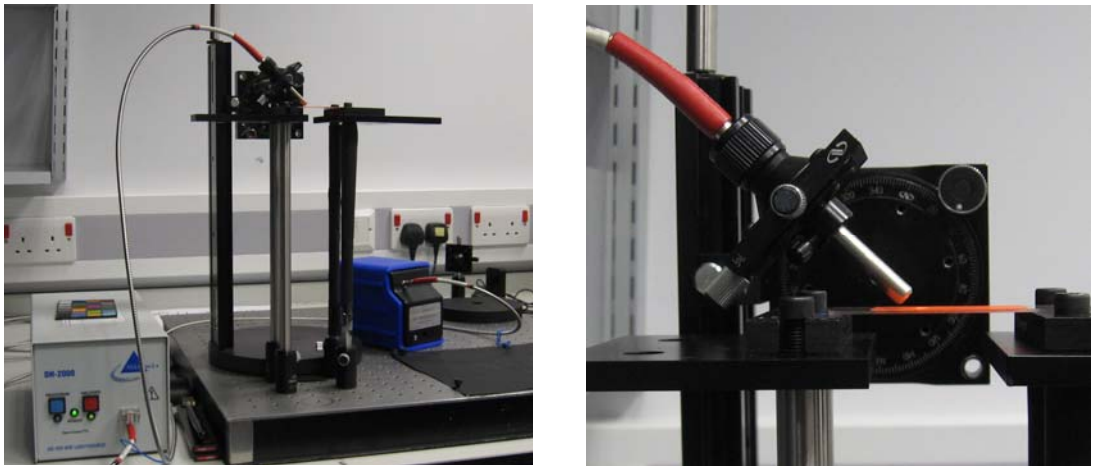

Figure 2.3. Experimental setup for reflectance measurements: the sample is placed on a stage ~30cm from the optical table (covered in black) such that no light will be reflected back from the background into the fibre.

A dark signal measurement was collected with the cap on the input of the Ocean Optics HR2000 spectrometer. After the warming up of the Tungsten light source (~30 minutes) a reference measurement was taken of the highly reflecting reference standard (white) with the first spectrometer to cover the visible range and part of the near infrared. The next step was to place the sample onto the sample holder with the reference target below it and to take a picture of the light spot in order to record the exact measurement position. Then the signal was captured and the highly reflecting white target was removed without moving the sample. The position of the target in the sample holder is constructed in such a way that the white reference target can be removed without changing the position of the measuring spot onto the paint sample. A signal of the sample over the 'black' reference was then taken and the optical fibre was connected to the next spectrometer (Polychromix DTS2500) with the range of 1700 to 2500 nm. The paint signals over the white and black reference was captured and then

the same measurements were done with the last spectrometer (Polychromix DTS1700) with the range of 900 to 1700 nm. After the whole paint data was collected the white reference signal for the last spectrometer was measured. Following that the white reference data was also taken for the spectrometer DTS 2500. These measurement steps were repeated for all paint samples. The reflectance of each paint sample can be separately selected with the wavelength range, the data over white and black. As we have measured the reflectance over white and black of the paint-outs, a transparency factor needs to be introduced in order to find the best wavelength window for OCT applied to paintings. The transparency η is defined as:

$$\eta(\lambda) = S_W(\lambda) - S_B(\lambda) \qquad (2.13)$$

where S_W is the spectral reflectance of a paint sample over a white target and S_B is the spectral reflectance of a paint sample over a black target.

Additional paint samples of five mixtures of different proportions of lead white with another pigment, different concentrations of the binding medium and different particle sizes for a couple of pigments were also prepared and measured. The data was analysed with Matlab®.

2.5. Results

The main objective of the spectral reflectance measurements was to determine the best wavelength for OCT to penetrate deeper into the sample. As the measurements were done over white and 'black' reflecting references it was possible to determine the optimum wavelength band for transparency for all paint samples. The changes in the spectral reflectance of the paint samples were also investigated in terms of different particle sizes, concentrations and binding media. This information is relevant for pigment identification.

2.5.1. Effect of Binding Media

In Fig. 2.4 the difference between the two binding media, egg tempera and linseed oil, on two pigments are demonstrated in terms of their reflectance. The transparency of the paint samples can be determined through the difference of the reflectance over a white and black target. Therefore a large difference means a high transparency of the paint. Paints in egg tempera are significantly less transparent compared to oil paints. This is partly due to the difference in refractive indices of egg tempera (n=1.346) and linseed oil (n=1.478) (Brill 1980). The refractive index of linseed oil is measured in wet condition and tends to increase during the drying process (de la Rie 1987). Pigments tend to have larger refractive indices than either medium. High scattering properties of paint are due to a high difference between the refractive index of the pigment and the binding medium. In addition, egg tempera is less homogeneous compared with linseed oil and hence more scattering.

The higher reflectance over white of the oil paints in Fig. 2.4 is due to the fact that these paint samples are more transparent than the egg tempera paints. Therefore the light is transmitted through the paint layer and back reflected from the white target through the paint layer to the detector.

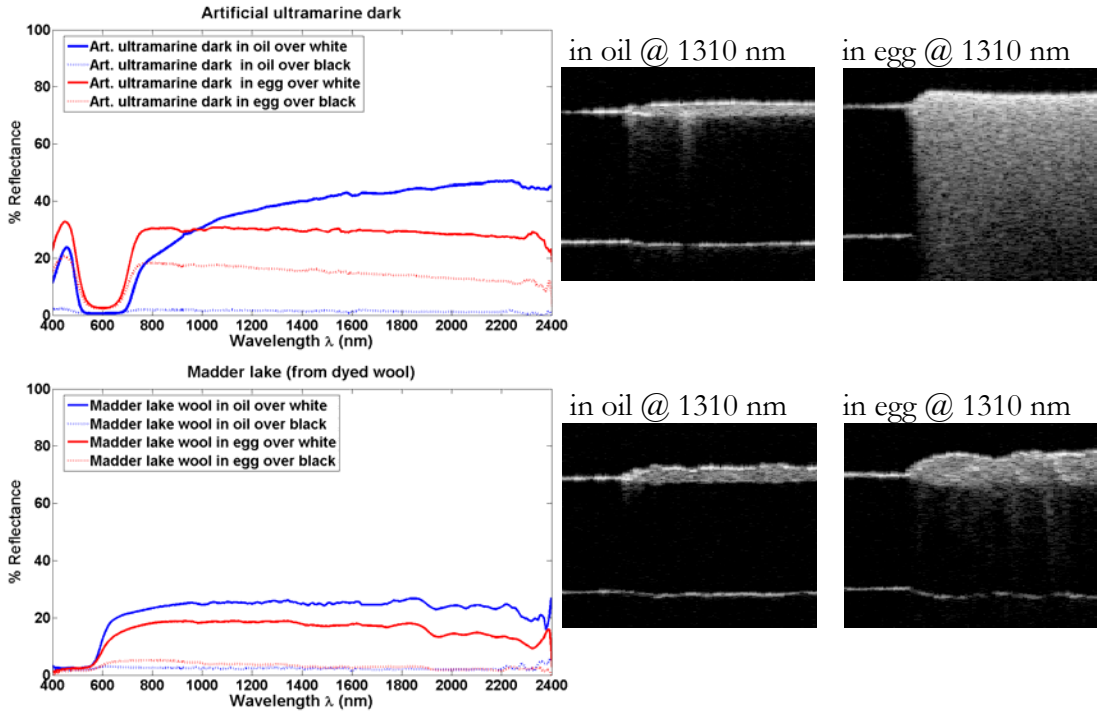

Figure 2.4. Spectral reflectance and OCT images (about 2mm x 2 mm) at 1310 nm of the same pigments with egg tempera and linseed oil as binding medium. a) Artificial ultramarine dark. b) Madder lake (from dyed wool).

In Fig. 2.5 the difference between the binding media, linseed oil and egg tempera, is shown. The reflectance of linseed oil is higher over the whole range and also more transparent. The cross-sectional OCT images at 1310 nm show the layer of the binding media and due to the high transparency the bottom of the microscope slide can be seen.

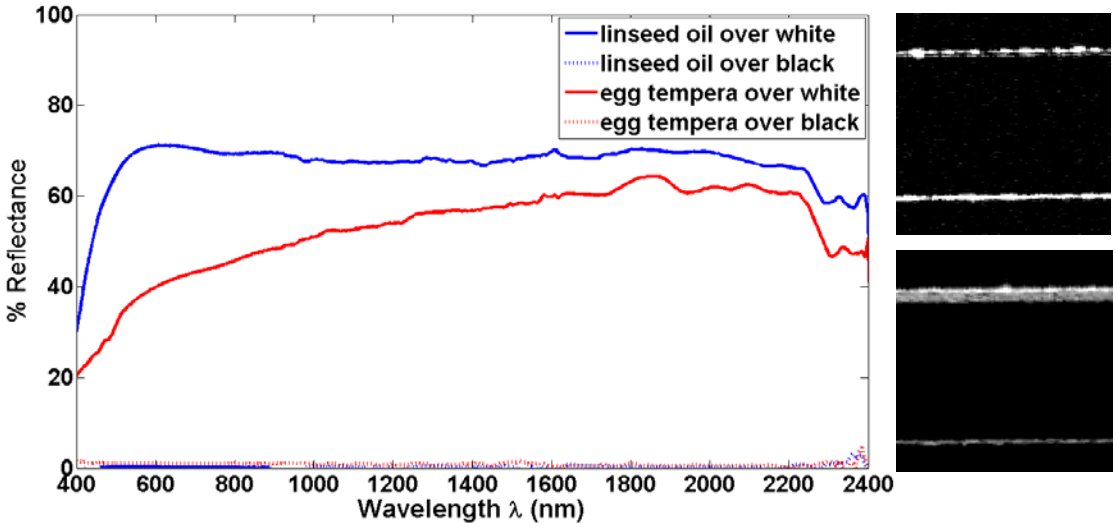

Figure 2.5. Left: Spectral reflectance of egg tempera and linseed oil and their transparency. Right top: 1310 nm OCT images of linseed oil (about 2mm x 2 mm). Right bottom: 1310 nm OCT images of egg tempera (about 2mm x 2 mm).

2.5.2. Effect of Concentration

The effect of different pigment to binding medium concentrations on reflectance was investigated. Two sets of paint-outs with four different concentrations have been prepared. Chinese azurite and malachite had been used with the binding medium egg tempera. The concentrations were described as mass concentration and were as follows 89%, 78%, 67% and 56%. As expected for both examples in Fig. 2.6, the paint with lower pigment to medium concentration is more transparent in the infrared region and lower in reflectance over black (i.e. less backscattering).

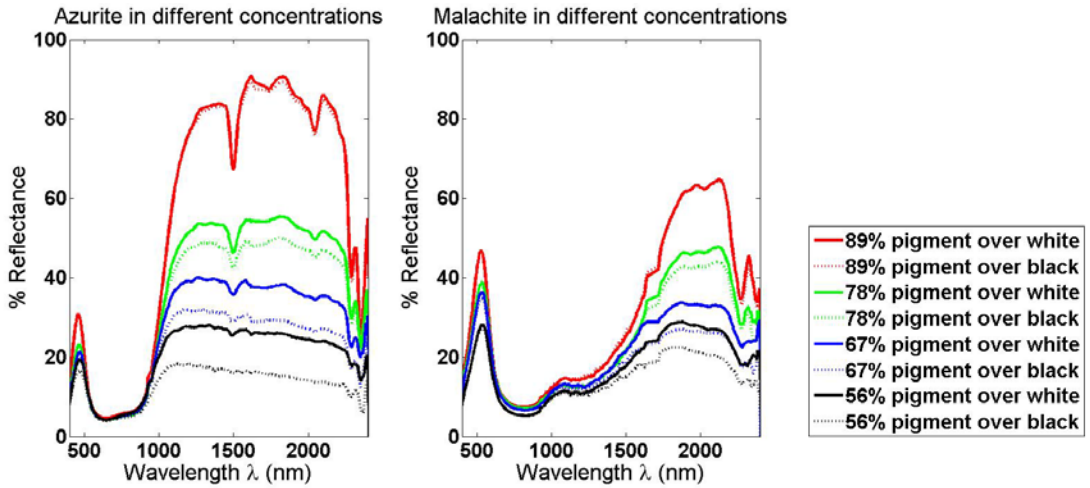

Figure 2.6. Spectral reflectance of azurite and malachite in different mass concentrations.

The paint with higher pigment to medium concentration has stronger spectral features, especially in the example of azurite indicating that most of the absorption features are due to the pigments rather than the medium. The prominent features in the reflectance spectrum of azurite are the peak at ~460nm corresponding to a *d-d* electronic transition (Bacci et al. 2000), the broad absorption band in the red and very near infrared (~600 to 900nm) corresponding to a broad *d-d* absorption band, a strong absorption feature at 1.5 μm corresponds to the asymmetric C-O bond stretching mode (Bacci. et al. 2000), and other absorption lines at ~2.1, 2.3 and 2.4 μm similar to those tabulated in Bacci et al. (2000) for pure azurite pigments. There is no shift in the absorption feature in the

reflectance spectra of azurite at ~1.5 μm, but in the visible range there is a peak shift of azurite at ~460 nm and malachite at ~530 nm (Fig.2.7). The maximum peak shift in the case of azurite is 12.0 nm and for malachite the maximum peak shift is 6.4 nm (Table 2.2). Azurite's peak shift is towards the longer wavelengths with decreasing pigment concentration. There is no peak shift for malachite in pigment concentrations of 56% up to 78%. The peak shift of malachite in pigment concentration of 89% is towards the longer wavelengths with decreasing pigment concentration. As the concentration changes, the balance between absorption and scattering may change which results in a peak shift in the reflectance spectrum. At these very high pigment concentrations, the inter-particle distance becomes comparable to or smaller than the wavelength of light and correlation effects can become important. In addition the spectral features are less prominent as the pigment concentration decreases. In terms of pigment identification, these shifts in spectral features have to be taken into account.

Pigment in egg tempera	Reflectance measurement	Peak position [nm]
Malachite 89%	over white	527.3
	over black	529.6
Malachite 78%	over white	533.2
	over black	533.7
Malachite 67%	over white	532.3
	over black	532.8
Malachite 56%	over white	532.3
	over black	532.8
Azurite 89%	over white	461.8
	over black	459.5
Azurite 78%	over white	462.7
	over black	464.1
Azurite 67%	over white	471.5
	over black	463.7
Azurite 56%	over white	470.6
	over black	463.7

Table 2.2. Peak position for azurite (in egg tempera) and malachite (in egg tempera) in different concentrations.

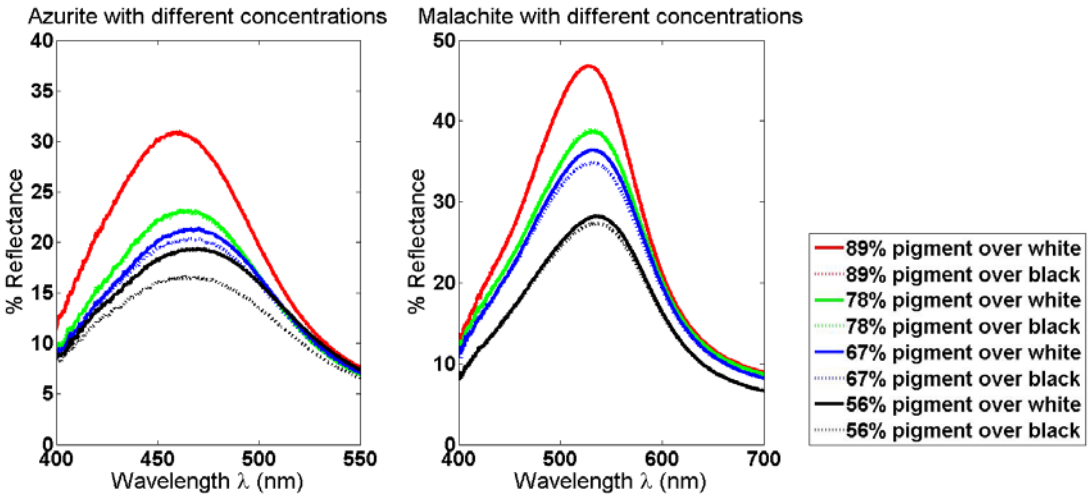

Figure 2.7. Peak shift of azurite and malachite in different mass concentrations.

In Fig.2.8 the transparency of azurite and malachite with different mass concentrations is demonstrated. In the case of azurite the less pigment the paint contains the more transparent the paint gets. The paint-outs of malachite with 67% and 58% have a similar transparency. This might be due to the fact that the paint-outs are not directly comparable in term of dry thickness even though all attempts had been made to ensure the same wet thickness.

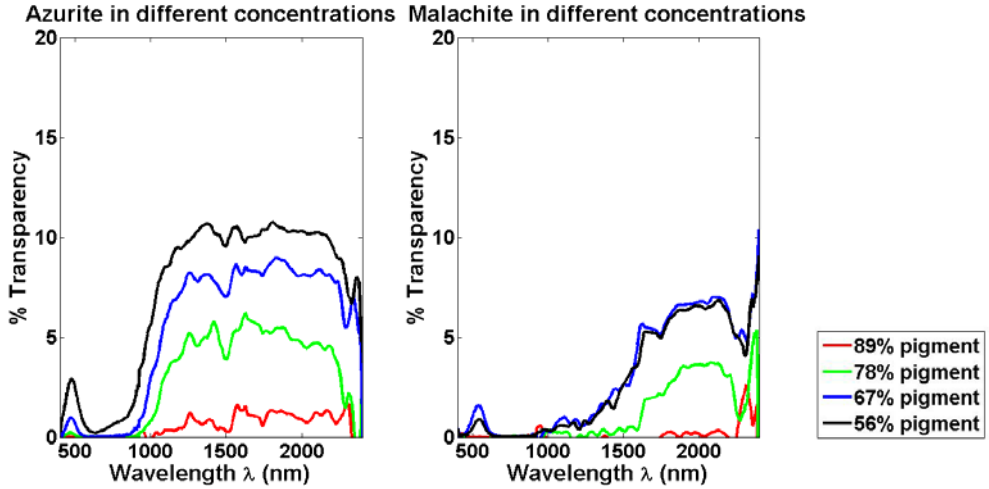

Figure 2.8. Spectral transparency of azurite and malachite in different pigment mass concentrations.

From Fig. 2.8 the OCT images can be predicted. As all of the paint outs show a strong absorption resulting in ~0% transparency at 930 nm, we concentrate on the 1310 nm OCT images where there is a range of transparency. Azurite shows a higher

transparency with the lower pigment concentrations as can be seen in the OCT images (Fig. 2.9). The bottom side of the microscope glass slides can be detected in Fig. 2.9 c) and d) as a faint line.

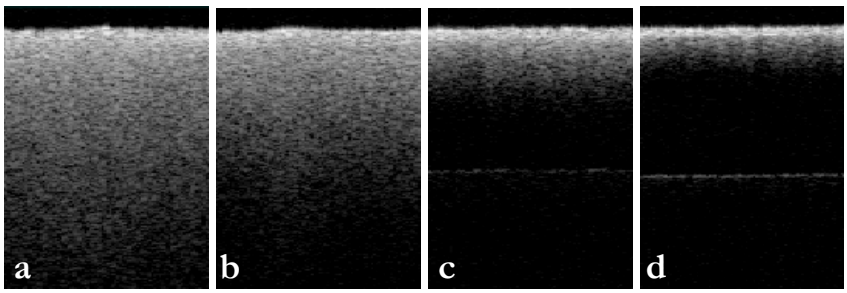

Figure 2.9. 1310 nm OCT images (about 2mm × 2.5 mm) of azurite in different mass concentrations: a) 89% pigment. b) 78% pigment. c) 67% pigment. d) 56% pigment.

2.5.3. Effect of Particle Size

The effect of different particle sizes of a pigment showed that the reflectance is higher with smaller particle size as can be seen in Fig. 2.10. It was observed that in both examples, azurite and malachite, in the infrared, the larger the particle size, the lower the reflectance and the higher the transparency. Both samples are opaque in the visible spectra. Smaller particle sizes have increased scattering properties. The two examples were prepared in three different particle sizes, which are described as grade 1, 3 and 5 (~30 μm, ~10 μm and ~3 μm in diameter).. Hence we are in the Mie scattering regime where the particles are larger than the wavelength. For those particles with size comparable to the wavelength, Mie scattering efficiency decreases linearly with wavelength. However, for particle with size much larger than the wavelength, the scattering efficiency does not depend significantly on the wavelength. In Mie scattering, the scattering efficiency for a single particle depends on the ratio of the particle size and wavelength, hence the scattering efficiency for a small particle at a short wavelength is the same as a large particle at a longer wavelength for the same particle size/wavelength ratio.

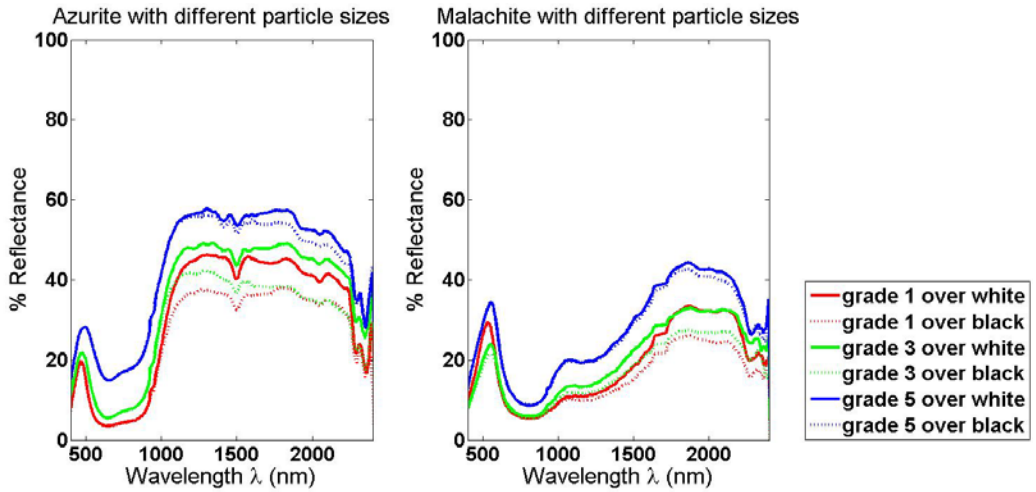

Figure 2.10. Effect of particle size for Azurite (in egg tempera) and Malachite (in egg tempera). The particle size is described as grade 1, 3 and 5. Grade 1 is the largest particle size and grade 5 the smallest.

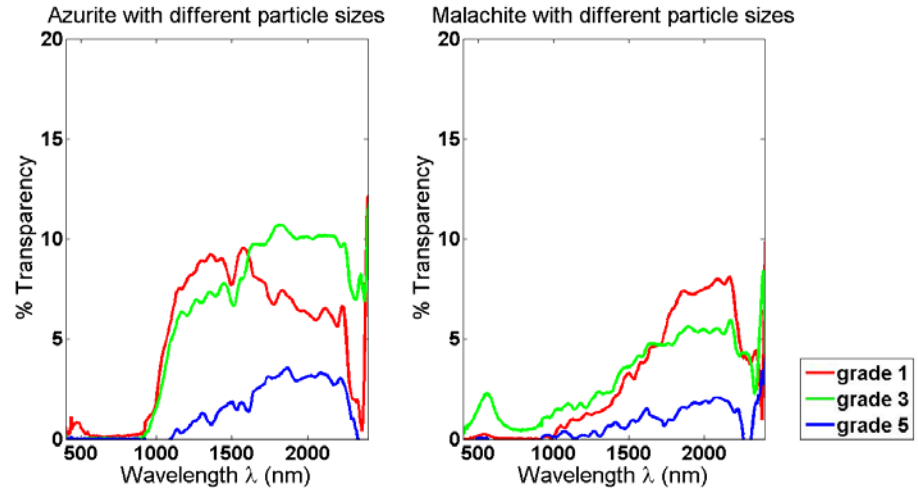

Figure 2.11. Transparency of Azurite (in egg tempera) and Malachite (in egg tempera) in different particle sizes. The particle size is described as grade 1, 3 and 5. Grade 1 is the largest particle size and grade 5 the smallest.

Malachite shows a deviation from the above general trend in the visible spectra, as the middle particle size (grade 3) paint was found to have the highest transparency as can be seen in Fig. 2.11. If the grade 3 paint mixture has a lower concentration than the other paint mixtures, then it is possible to explain the anomaly in both Fig. 2.10 and 2.11. The absorption features are stronger for the larger particle size. The effect of increasing the particle size should result into a peak shift towards longer wavelengths (McNeil et al. 2001). The opposite is observed in Fig. 2.12. Both scattering and absorption increases as the particle size decreases. As the reflectance depends on a mixture of absorption and

scattering it is rather difficult to predict the exact behaviour of the reflectance spectra. Significant multiple scattering occurs in these paint mixtures which also complicates the interpretation. A number of other factors could affect the reflectance spectra: presence of absorption edges, impurities in the pigment powder, the differences in pigment volume concentrations (PVC) between the samples or final dry thickness of the paint. Using the procedure of mixing paint described in section 2.3 (Sample preparation), it is not possible to mix the exact PVC for each paint sample. The maximum peak shift is 20.9 nm for malachite and 26.7 nm for azurite which are greater than the shift due to change in concentration. The maximum difference is between the largest and smallest particle size for both examples as can be seen in Fig. 2.12.

Pigment in egg tempera	Reflectance measurement	Peak position [nm]
Malachite grade 1	over white	534.2
	over black	534.2
Malachite grade 3	over white	552.8
	over black	551.9
Malachite grade 5	over white	555.1
	over black	555.1
Azurite grade 1	over white	470.6
	over black	470.0
Azurite grade 3	over white	478.4
	over black	475.1
Azurite grade 5	over white	496.7
	over black	495.3

Table 2.3. Peak position for azurite (in egg tempera) and malachite (in egg tempera) in different particle sizes.

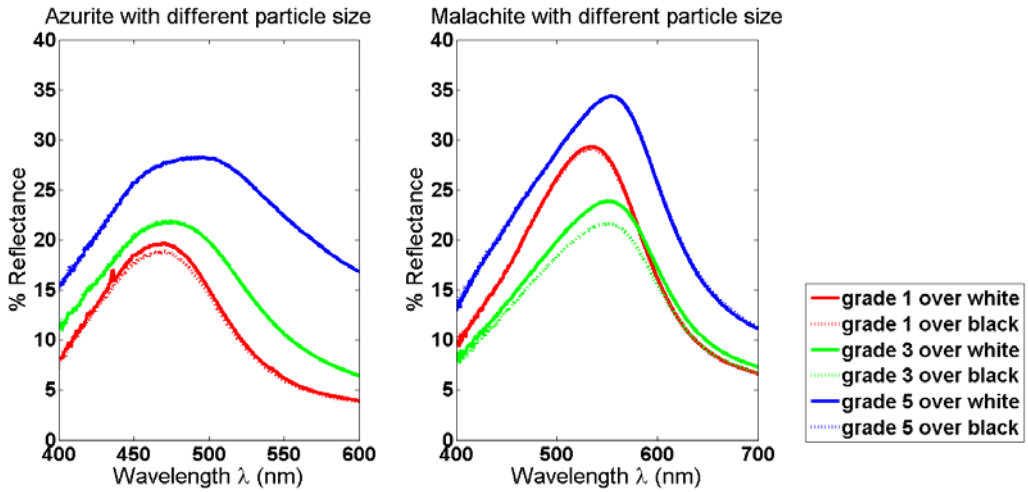

Figure 2.12. Peak shift of azurite (in egg tempera) and malachite (in egg tempera) with different particle size in the visible spectra. Grade 1 is the largest particle size and grade 5 the smallest.

2.5.4. Effect of Paint Mixtures

Another effect in the reflectance spectra which was monitored was the mixture of lead white with another pigment. Artists used to mix lead white with another pigment in order to achieve a different lightness. This was done for example for the sky of a painting with azurite and lead white. In Fig. 2.13 the effect of lead white on indigo can be seen. As expected the reflectance increases with an increased lead white concentration. The samples were prepared in three different concentrations of lead white and indigo. The amount of indigo was kept constant and lead white was changed so that the following concentrations were achieved: 1:1, 1:10 and 1:50. The measurement of lead white corresponds to an unusually thin area of the paint sample. This was deliberate as lead white is highly scattering, it is necessary to select a very thin layer in order to study the change in transparency as a function of wavelength. In Fig.2.14 the corresponding OCT images are shown. It is possible to see the bottom of glass for the egg tempera OCT image (Fig. 2.14a) due to its high transparency and also for the indigo in egg tempera sample (Fig. 2.14b). In the case of the mixtures the bottom of the glass cannot be seen (Fig. 2.14c and Fig. 2.14d) and with higher amount

of lead white, the sample is more scattering as expected. In Fig. 2.14e lead white in egg tempera is shown.

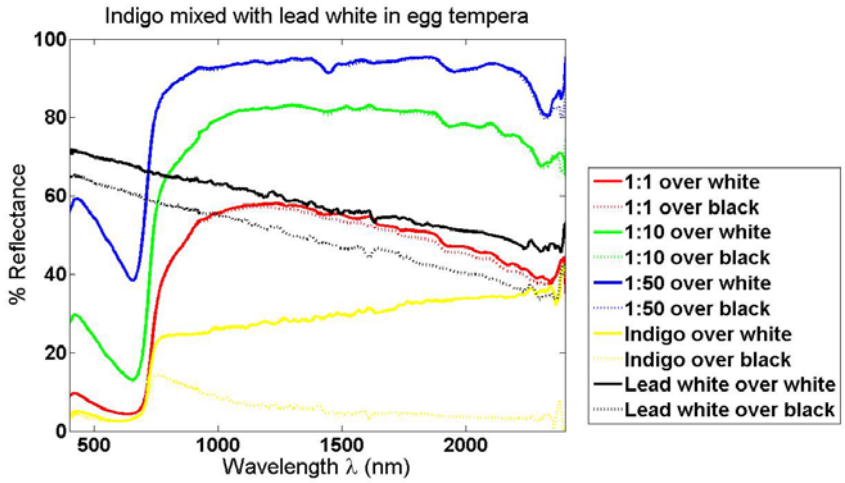

Figure 2.13. Indigo mixed with lead white in egg tempera in three different concentrations and just indigo and lead white in egg tempera.

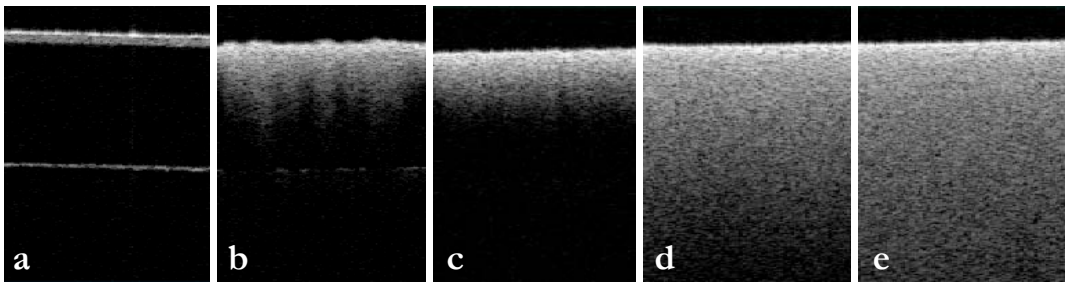

Figure 2.14. 1310 nm OCT images (about 2mm x 2.5 mm) of: a) egg tempera. b) indigo in egg tempera. c) indigo mixed with lead white (1:1) in egg tempera. d) indigo mixed with lead white (1:50) in egg tempera. e) lead white in egg tempera.

2.5.5. Spectral Transparency

In Fig. 2.15 the spectral reflectance of two pigments (verdigris and cobalt blue, both in oil) are compared to the cross-sectional OCT images at 1310 nm and 930 nm. This shows that a prediction of the OCT images can be made with the use of the spectral reflectance over a white and a black target. Verdigris in linseed oil is demonstrated first in Fig. 2.15. The cross-sectional OCT images at 1310 nm and 930 nm are consistent with the reflectance measurements. This can be explained with the reflectance graph, as the reflectances over a white and black target at 930 nm are both ~0%; the transparency is also zero and the paint sample is highly absorbent at this wavelength. On the other

hand the paint sample is highly transparent at 1310 nm as the reflectance over white is high and there is no reflectance over black. Therefore it is transparent and this is confirmed with the OCT images: it is possible to see the bottom glass/air interface of the microscope glass slide in the image at 1310 nm, but not at 930 nm. The second reflectance graph in Fig. 2.15 is cobalt blue in linseed oil and it is absorbent at 1310 nm and scattering at 930 nm. High scattering is the cause of opacity when the reflectance over white is high and the difference of the reflectance over white and black is low, as it is the case for cobalt blue at 930 nm. Paint that is absorbent has a low reflectance and for transparent paint layers the reflectance over white is high and the difference of the reflectance over white and black is also high. This knowledge can be helpful in order to predict how OCT image will look like and to know which wavelength is the optimum for OCT applied to paintings.

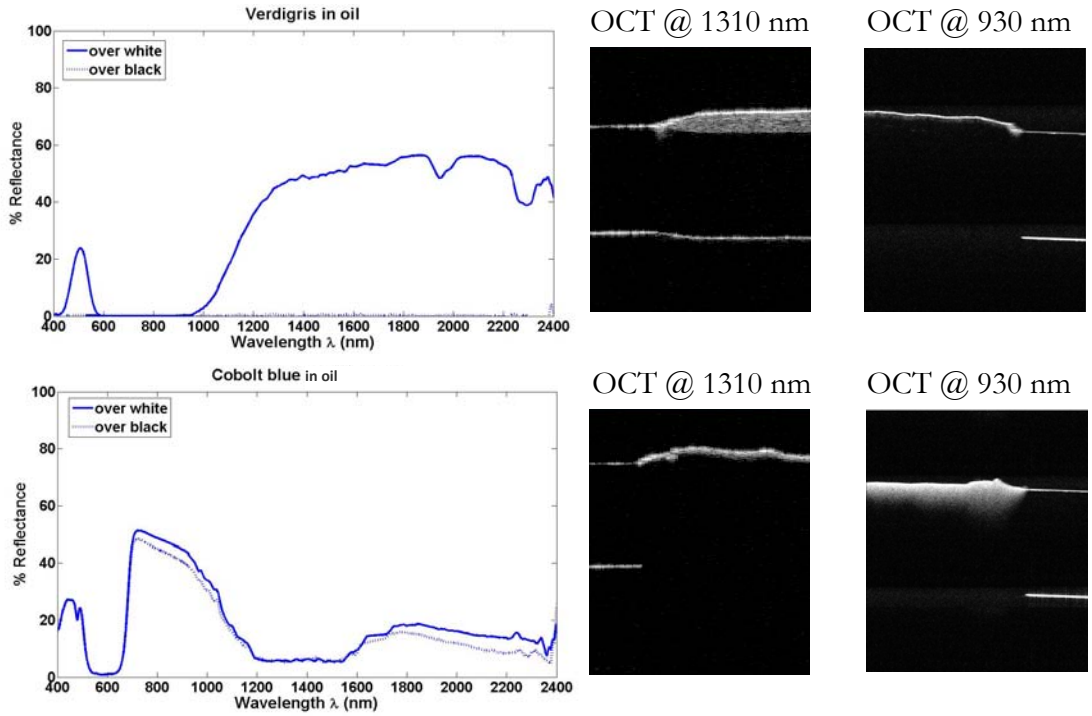

Figure 2.15. Spectral reflectance and OCT images (about 2 mm x 3 mm) at 930 nm and 1310nm of verdigris and cobalt blue in linseed oil.

In Fig. 2.16 to 2.21 the transparency is split into six groups: blue (shown in two graphs), green, red lake, red (excluding red lake), yellow (shown in two graphs) and purple paint.

In Table 2.1 the pigments that are used for each group are shown. The transparency of one paint sample cannot be directly compared to the other paints as the thickness differs. However, the transparency over the wavelength range from 400 nm up to 2400 nm for each individual paint can be deduced.

In general it can be said that the higher the wavelength the more transparent the paint is. In Fig. 2.16 there are a few exceptions, e.g. smalt in linseed oil and egg tempera. In this case the paint is more transparent between 750 nm and 1000 nm than at longer wavelength.

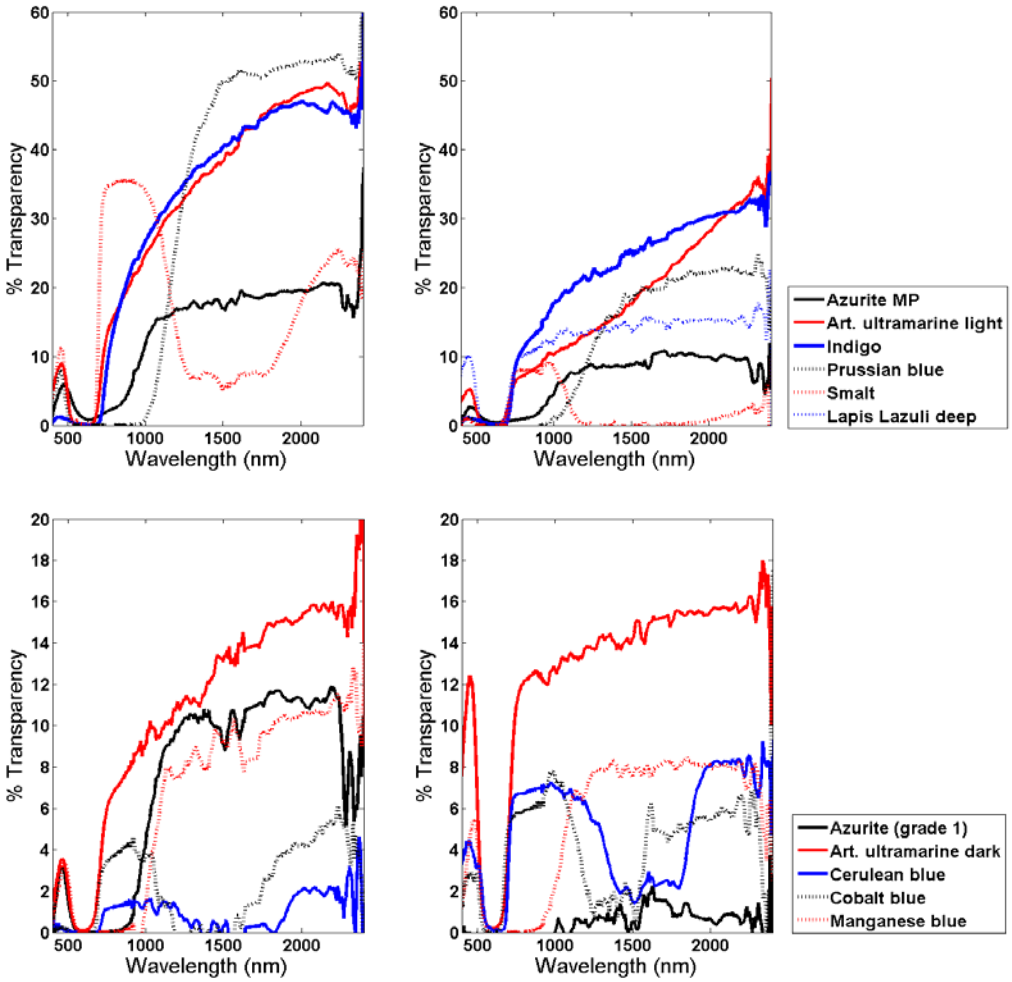

Figure 2.16. Transparency of the samples of blue pigments in oil (left) and egg tempera (right) as defined in Eq. (2.13) is plotted as a function of the wavelength.

In the case of the green pigments (Fig. 2.17) the best transparency is at higher wavelengths except for a few exceptions such as cobalt turquoise where the

transparency has a minimum around 1500 nm. The red paint (red lake paints excluded, Fig. 2.20), yellow paint (Fig. 2.20) and the purple paints (Fig. 2.21) all have transparency increasing as the wavelength increases.

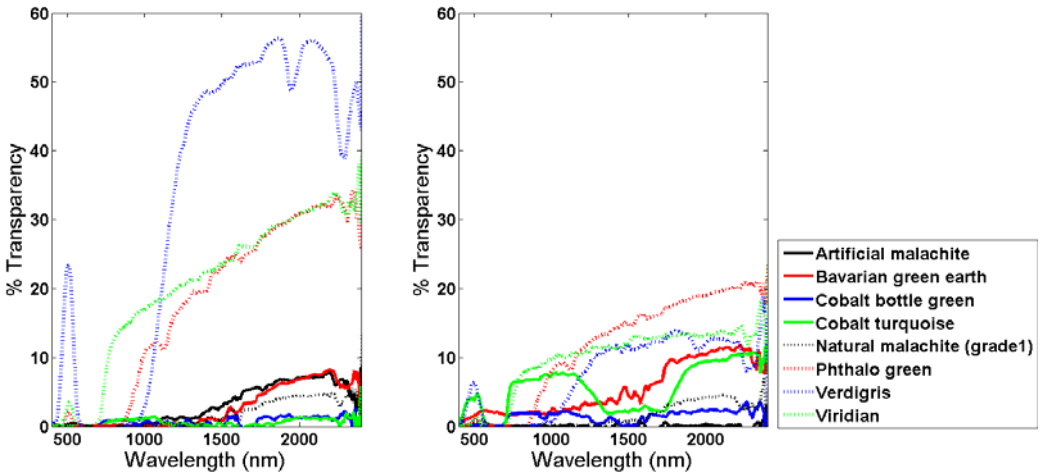

Figure 2.17. Transparency of the samples of green pigments in oil (left) and egg tempera (right) as defined in Eq. (2.13) is plotted as a function of the wavelength.

The red lake paints (Fig. 2.18) show a relative constant transparency over the wavelength range from 600 nm up to 2300 nm.

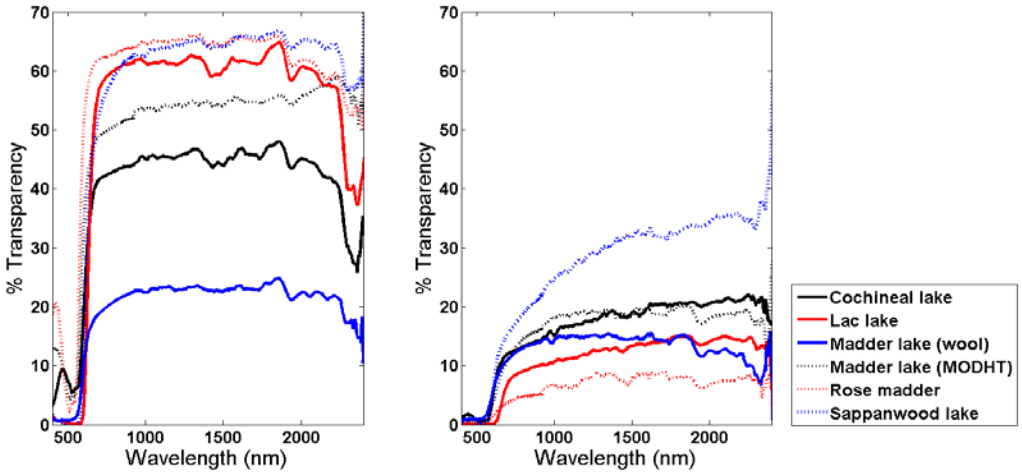

Figure 2.18. Transparency of the samples of red lake pigments in oil (left) and egg tempera (right) as defined in Eq. (2.13) is plotted as a function of the wavelength.

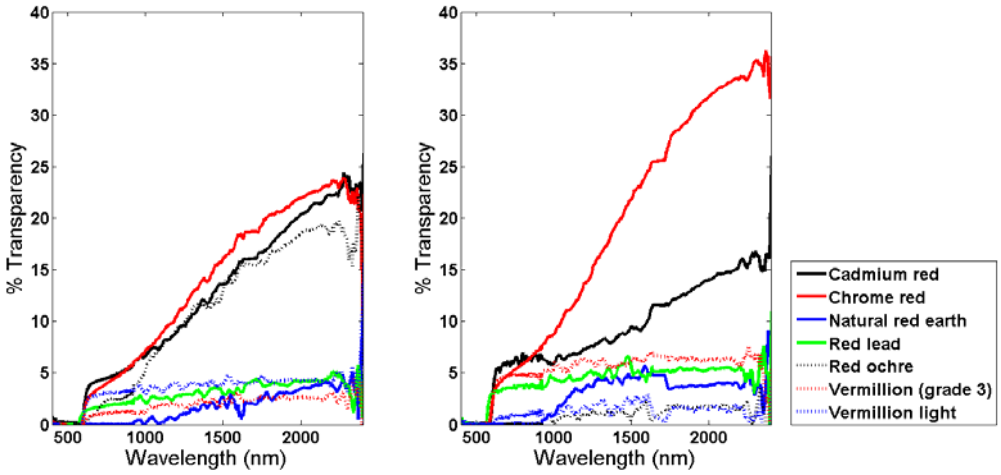

Figure 2.19. Transparency of the samples of red pigments (red lakes excluded) in oil (left) and egg tempera (right) as defined in Eq. (2.13) is plotted as a function of the wavelength.

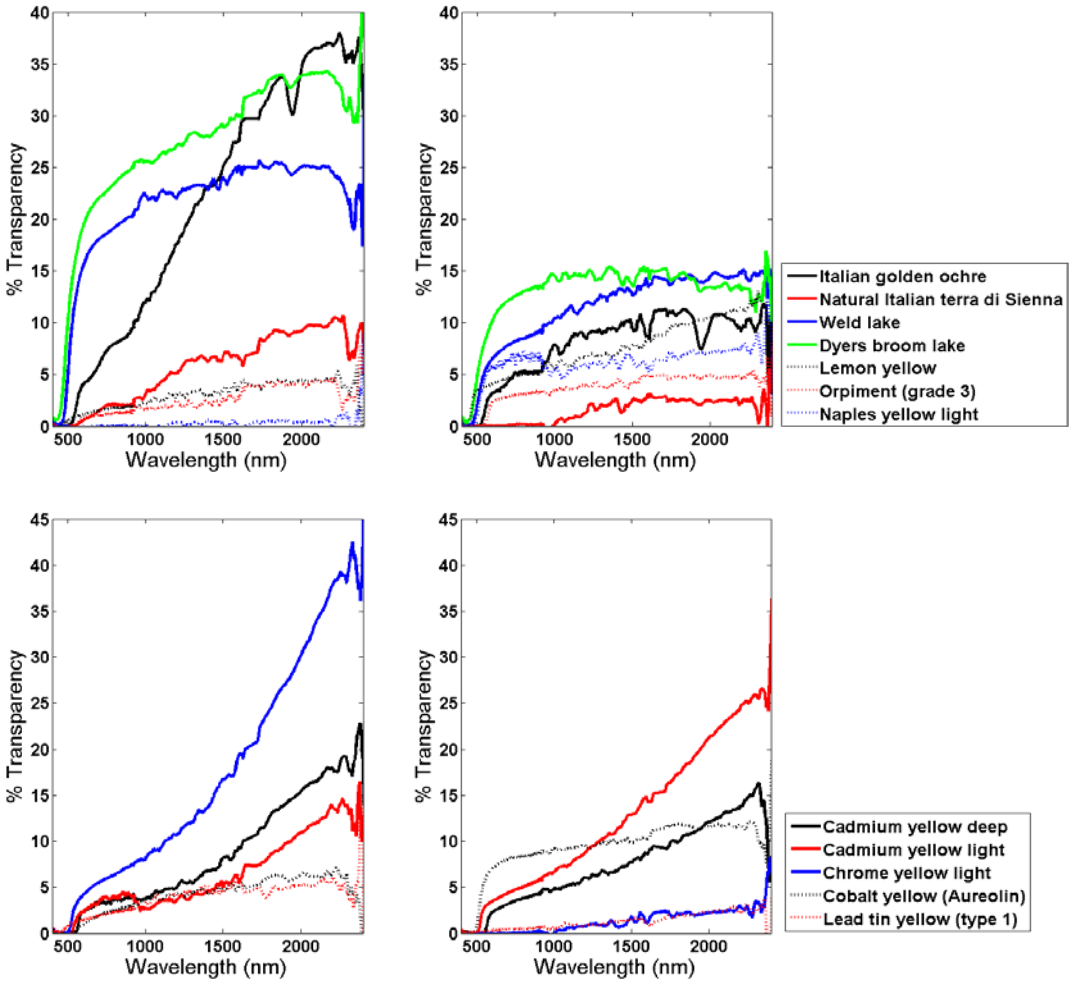

Figure 2.20. Transparency of the samples of yellow pigments in oil (left) and egg tempera (right) as defined in Eq. (2.13) is plotted as a function of the wavelength.

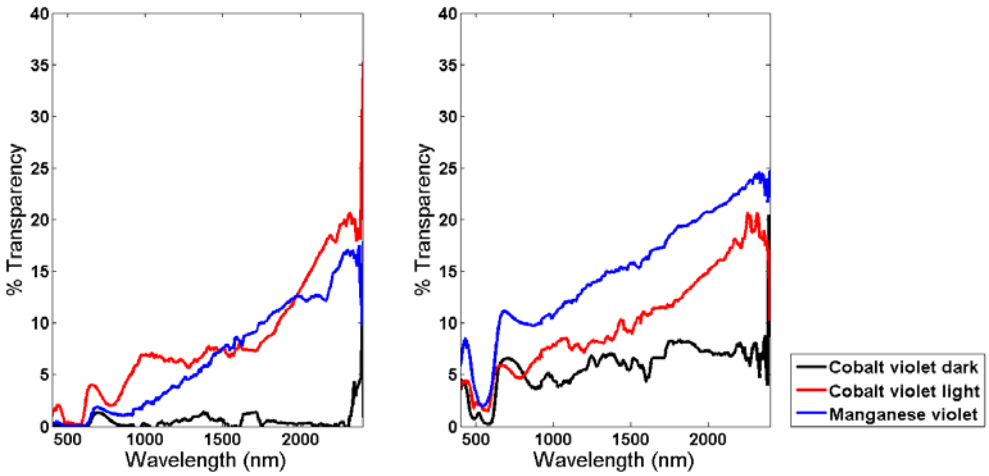

Figure 2.21. Transparency of the samples of purple pigments in oil (left) and egg tempera (right) as defined in Eq. (2.13) is plotted as a function of the wavelength.

In general it can be said that the best transparency is at higher wavelength with a few exceptions.

3. OCT Application to Art Conservation

3.1. OCT Measurements of Refractive Indices

The most important attribute of a painting is its visual appearance. Conservator's aim is to preserve the original aspect of a painting. Visual appearance is defined by optical parameters such as the refractive index, absorption and scattering coefficient, thickness of the layers and the surface roughness of the varnish and the paint layers. Therefore it is important to monitor these parameters for conservation records. The refractive index (RI) of paint or varnish may change over time. An increased RI of varnish would affect the appearance of a painting in such a way that more light would be reflected (Berns et al. 2002). This chapter is devoted to the measurement of the RI of paint and varnish.

OCT could reduce the need of taking samples from a painting in order to get the layer structure information. As OCT images measure the optical path difference between sample and reference arm, the directly measured thickness of a layer is the optical thickness. The physical thickness can be calculated by dividing the optical thickness by the RI of the layer of interest. Therefore cross-sectional OCT images, which are images into the depth of the sample, are distorted. The problem of distorted cross-sectional images could be solved through image post processing by correcting the thickness of the individual layers of paint and varnish. This correction needs RI information. While OCT can give thickness, refractive index, scattering and absorption information, it could not replace the need for sampling of paintings to deduce chemical composition.

3.1.1. Refractive Indices

The RI of a material is primarily described by the reduction of the velocity of light in the material compared to the one in vacuum (c=299,792.458 km/s). Here we need to differentiate between group and phase velocity of a wave. The rate at which planes of monochromatic waves of constant phase propagates in space can be described by the phase velocity,

$$v_{phase} = \frac{\omega}{k} = \lambda \cdot f \qquad (3.1)$$

where ω is the angular frequency, k the wave number, λ the wavelength and f the frequency. The group velocity is the rate the envelope of a superposition of different monochromatic waves (wave packet) propagates in space.

$$v_{group} = \frac{d\omega}{dk} \qquad (3.2)$$

It can also be expressed in terms of the phase velocity.

$$v_{group} = v_{phase} + k\frac{dv_{phase}}{dk} = v_{phase} - \lambda\frac{dv_{phase}}{d\lambda} \qquad (3.3)$$

When in a medium where no dispersion effect is taking place, the group velocity v_{group} is equal to the phase velocity v_{phase}, as $dv_{phase}/dk=0$. In dispersive media, the group velocity v_{group} differs from the phase velocity v_{phase}. The phase refractive index is the ratio of the phase velocity v_{phase} of the light in the medium and the speed of light in vacuum c.

$$n = \frac{c}{v_{phase}} \qquad (3.4)$$

In analogy to the phase refractive index, the group refractive index is the ratio of the group velocity v_{group} of the light in the medium and the speed of light in vacuum c.

$$n_{group} = \frac{c}{v_{group}} \qquad (3.5)$$

Equation 3.5 can be expressed in terms of the phase refractive index dependence on the wavelength (Hecht 2003)

$$n_{group} = n(\lambda) - \lambda \frac{dn(\lambda)}{d\lambda} \qquad (3.6)$$

When an incident monochromatic plane wave hits the boundary of two homogenous media with different optical properties, the wave is divided into a reflected and refracted part, if the condition for total reflection is not fulfilled. The refracted wave has a different phase which leads to a change of velocity of the light in the medium which is due to the RI. In order to describe the RI it is necessary to derive the dispersion relation as a function of the frequency.

To understand dispersion, where the refractive index changes as a function of wavelength, we consider a simple model by Lorentz where an atom or molecule has positively charged nuclei and negatively charged electrons. Equation 3.7 describes the effect of the incident light onto the matter. The force F_E which is applied through the electric field $E(t)$ of the incident electromagnetic wave to an electron with the charge q_e is:

$$F_E = q_e E(t) = q_e E_0 \cos(\omega t) \qquad (3.7)$$

The next step is to get the relative displacement of the electrons. Therefore the sum of all forces, the driving force F_E and restoring force, is equal to the mass m_e multiplied by the acceleration:

$$q_e E_0 \cos(\omega t) - m_e \omega_0^2 x = m_e \frac{d^2 x}{dt^2} \qquad (3.8)$$

where E_0 is the amplitude of the electric field, ω_0 is the angular resonance frequency. It can be assumed that the electron oscillates at the same frequency as the electric field F_E and therefore:

$$x(t) = x_0 \cos(\omega t) \qquad (3.9)$$

Through substitution we get the relative displacement:

$$x(t) = \frac{q_e / m_e}{(\omega_0^{\,2} - \omega^2)} E_0 \cos(\omega t) = \frac{q_e / m_e}{(\omega_0^{\,2} - \omega^2)} E(t) \qquad (3.10)$$

The electric field induces a dipole which oscillates at a frequency dependent on its natural frequency and the driving frequency. We define the electric polarisation *P* as the dipole moment per unit volume:

$$P = (\varepsilon - \varepsilon_0)E \qquad (3.11) \qquad P = q_e x N \qquad (3.12)$$

where ε is the permittivity of the medium, ε_0 is the vacuum permittivity and N is the number of the electrons per unit volume.

Substitution of Eq. 3.10 into Eq. 3.12 yields to:

$$P = \frac{q_e^{\,2} N E / m_e}{(\omega_0^{\,2} - \omega^2)} \qquad (3.13)$$

Substitution of Eq. 3.13 into Eq. 3.11 leads to:

$$\varepsilon = \varepsilon_0 + \frac{P(t)}{E(t)} = \varepsilon_0 + \frac{q_e^{\,2} N / m_e}{(\omega_0^{\,2} - \omega^2)} \qquad (3.14)$$

Through the fact that $n^2 = \varepsilon / \varepsilon_0$ the refractive index can be described as a function of frequency, which is also the dispersion relation:

$$n^2(\omega) = 1 + \frac{N q_e^{\,2}}{\varepsilon_0 m_e}\left(\frac{1}{\omega_0^{\,2} - \omega^2}\right) \qquad (3.15)$$

Therefore if $(\omega_0^{\,2} - \omega^2) < 0$ the refractive index is smaller than 1 and if $(\omega_0^{\,2} - \omega^2) > 0$ the refractive index is greater than 1 (Hecht 2003). When the frequency range of the waves is small, group velocity is also the velocity at which energy or signal propagates. However, group velocity is not always the same as the velocity at which energy is propagated and it can be greater than the speed of light. Equation 3.15 is a simple

classical calculation that does not include effects of damping. In reality, refractive index is not infinite at the resonance frequency or absorption peaks.

3.1.2. Overview of Methods of Refractive Index Measurements

3.1.2.1. Conventional Methods

The two main conventional methods of measuring the RI are the immersion method and the use of a refractometer. The first method for RI measurements that is described here is the immersion method. In 1993 a work by Townsend was published on RI measurements of paint media. The method demands a sub-milligram sample of the paint, glaze or varnish layer. This sample is then placed under a microscope and immersed in liquids of different known RI. When the RI of the sample matches the RI of the liquid, the edge of the samples becomes invisible, so that it looks like that the sample had disappeared. Only RI of glasses and pigments are measured with this method, but it can also be applied to any transparent material which is not too heavily pigmented and does not dissolve in the calibration liquids (Townsend 1993). This method is limited as opaque paint samples cannot be measured. Nevertheless the method is capable of measuring RI samples of test paint-outs and historical painting as long as the sample is transparent enough. The disadvantage of the method is that it is destructive and therefore the paintings would be harmed.

Another method of measuring the RI is the use of a refractometer which makes use of the Snell's law that is:

$$n_1 \sin\theta_1 = n_2 \sin\theta_2 \qquad (3.16)$$

A refractometer consists basically of four parts: light source, illuminating prism, sample holder and a scale to read out the critical angle. The propagation of light from one medium n_1 to another medium n_2 leads to a change of the incident (critical) angle α_c to the refractive angle β in the second medium (Fig. 3.1). The medium of RI n_1 is known,

the medium of n_2 is the sample where the RI should be measured. The critical angle is the angle of incidence for which the refractive angle is 90°. This is done by changing the angle of the ocular of the instrument. The critical angle can be read out on the scale. Equation (3.17) gives the RI of the sample.

$$n_2 = n_1 \sin \alpha_c \qquad (3.17)$$

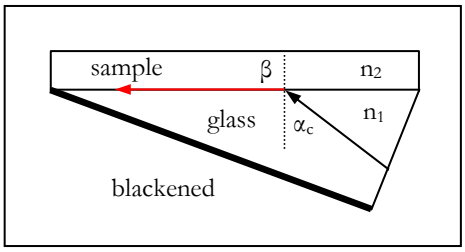

Figure 3.1. Schematic diagram of a refractometer. The arrows indicate the path of light.

Liquids and glasses are common samples for refractometers. The results of the RI for paint or varnish samples are less precise as the contact to the prism is not perfect. This is due to the fact that the paint samples have a rough surface and therefore there is a prism-air and air-sample interface. However this method can be used for new (liquid) paint which can be applied onto the prism. But a study of historical paint samples cannot be done. Another drawback is that samples for refractometers need to be larger than just a sub-milligram as needed for the immersion method. The samples for glass and liquids used in the publication of Townsend in 1993 were 5 x 8 mm and they had a comparable accuracy as the results of the immersion method. The error was from ±0.005 to ±0.007.

Both conventional methods cannot be applied to opaque paint samples. The refractometer method cannot measure the RI of paint-outs or samples of paintings. Both are suitable for transparent samples, such as glazes, varnish and some paint. These measurements cannot be done non-destructively. Methods of measuring the RI non-destructively using OCT will be introduced in the next section. The measurement of RI

using OCT can be applied to transparent samples only. But as OCT operates in the near infrared, samples are more transparent than in the visible.

3.1.2.2. OCT Methods

The capability of non-invasively measuring the RI of varnish using OCT was first shown by Liang et al. (2005b). OCT uses infrared light and as paint is more transparent in the infrared region of the spectrum than in the visible, a wider collection of different paints can be studied. There are two main methods of determining the RI using OCT. The basic principle of one method is to measure the physical (t_p) and optical (t_o) thickness of the paint or varnish. RI is given by the ratio $n=t_o/t_p$. In 1995 Tearney et al. demonstrated this method for human tissue and glass. The approximately 500 μm samples were placed onto a metal surface and imaged with a 1300 nm TD-OCT with an axial resolution of 20 μm. Optical and physical thickness were measured from the OCT images. As the samples were approximately 500 μm, the error of the group index was only from ±0.007 up to ±0.012. In OCT images the optical thickness of layers can easily be measured, but to measure the real thickness in air directly from the OCT images it is necessary to have a clear edge or a crack in the top layer. While this limitation of requiring the presence of a clear edge or a crack in the top layer means that it is only suitable for paintings with cracks, the study of RI of a range of different paint and varnish samples is, however, feasible.

Another method for the measurement of RI is the focus tracking method using TD-OCT (Tearney et al. 1995, Wang X. et al. 2002, Maruyama et al. 2002). Basically the difference of the stage position where the focus is set onto the top and the bottom layer and the difference of the optical path difference are taken into account for this method.

RI can be measured in situ and non-invasively with this method anywhere on a painting or sample.

After the sample with the thickness d_s and the refractive index n_s is placed under the instrument such that the top of the sample is in focus and the reference arm position is adjusted so that it matches the sample arm. This means that the signal is maximum at this position. Then the sample was moved so that the focus position is at the bottom of the sample. After that the reference arm was adjusted so that the signal reaches the maximum. If this adjustment is given by z_r and the distance the focus lens is moved by z_f then the refractive index using focus tracking method can be derived with the followings steps:

$$n_0(z_r + z_f) = n_s d_s \qquad (3.18)$$

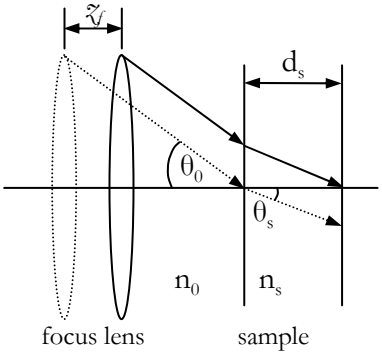

Figure 3.2: Schematic OCT focus tracking method.

The relationship between the incident angle θ_0 and the angle of refraction θ_s with respect to the thickness of the sample d_s and the movement of the focus lens z_f can be described as:

$$d_s \tan\theta_s = z_f \tan\theta_0 \qquad (3.19)$$

From Eqs. (3.18) and (3.19)

$$\tan\theta_s = \frac{z_f n_s}{n_0(z_r + z_f)} \tan\theta_0 \qquad (3.20)$$

Equation 3.20 can be substituted into the equation $n_s \sin\theta_s = n_o \sin\theta_0 = N.A.$

$$n_s \cdot \sin\left[\tan^{-1}\left(\frac{z_f n_s}{n_0(z_r + z_f)}\tan\theta_0\right)\right] = N.A. \qquad (3.21)$$

where N.A. is the numerical aperture, n_0 the refractive index of air (Tearney et al. 1995). Eq. 3.21 can alternatively be expressed as

$$n_s^2 = \frac{1}{2}\left[N.A.^2 + \sqrt{N.A.^4 + 4(n_0^2 - N.A.^2)\left(\frac{z_r + z_f}{z_f}\right)^2}\right] \qquad (3.22)$$

The thickness of the sample is:

$$d_s = n_0(z_r + z_f)/n_s \qquad (3.23)$$

For small N.A., the refractive index n_s can be approximated by:

$$n_s = \sqrt{1 + \frac{z_r}{z_f}} \qquad (3.24)$$

The approximation in Eq. 3.24 will give a higher RI value than that derived by Eq. 3.22. Figure 3.3 shows the difference between the full calculation of RI in Eq. 3.22 and the approximation given by Eq. 3.24 as a function of N.A.. The term *(zr+zf)/zf* was set in such a way that the RI calculated with the Eq. 3.24 is 1.5, 1.58, 1.66 and 1.72. For N.A. less than 0.1, the approximation overestimates the RI by less than 0.002 for a refractive index of 1.5. For the same N.A., the higher the RI, the less accurate the approximation becomes.

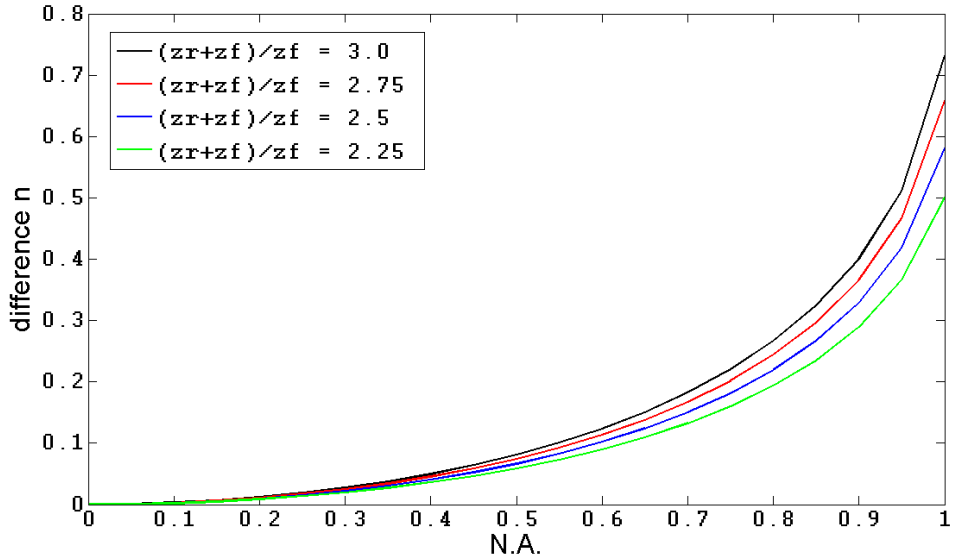

Fig. 3.3. Validity of the small N.A. approximation for RI estimates using the focus tracking method. Difference between RI calculated from the approximation in Eq. 3.24 and the full equation in Eq. 3.22 for different N.A..

In the publication of Tearney et al. the RI of human tissue were measured with the focus tracking method. The group showed the results of three RI, one measured *in vitro* and two *in vivo*. The maximum error for the RI was ±0.03 and the minimal was ±0.01. Wang et al. in 2002 presented two results for the focus tracking method. One achieved with a 1300 nm OCT and the other with 850 nm OCT. The sample used was a fused silica with a thickness of about 1000 μm. The error for both measurements was ±0.01. This method would also be suitable for the in situ and non-invasive measurement of RI of paint and varnish of paintings. The advantage is that the layer thickness and the RI could be monitored simultaneously.

3.1.3. Refractive Index Measurements of Paint Samples

The simplest approach to measure the RI of paint and varnish using OCT is to take the ratio of the optical and physical thickness. A couple of paint-outs were chosen from the wide variety of ~50 historic artist's pigments, which have been prepared in both egg tempera and linseed oil. The reason for only selecting certain types of paint was that the

method is limited in terms of the transparency of the paint. In order to measure the transparency in chapter 2 and to measure the RI of the paint layers, the set of paint-outs was prepared over thin glass microscope slides.

The method which was applied to determine the RI of paint using OCT measures the optical path length in air and in the samples. The ratio of these two parameters is the RI. In Figure 3.4 the first method is shown to measure the RI using OCT. A cross-sectional image of the sample was taken such that the air-paint interface and the air-glass interface were captured. The extrapolated surface of the air-microscope slide interface was used to measure the actual thickness of the paint layer, i.e. the path length t_r of the paint in air. On the other hand the optical path length t_o was obtained by measuring the thickness of the apparent paint layer. Therefore the ratio of these two values is the RI.

$$n_1 = \frac{t_o}{t_r} \qquad (3.25)$$

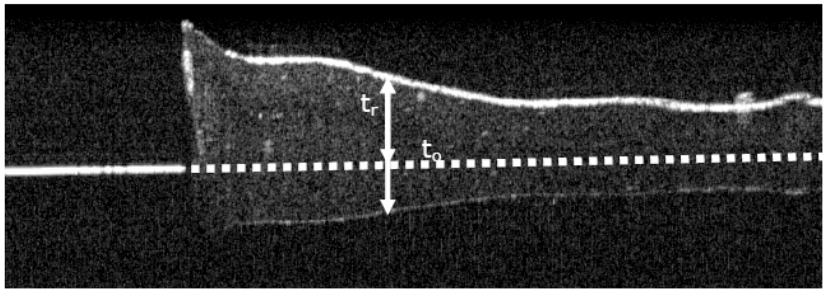

Figure 3.4. Refractive index measurement of rose madder in linseed oil using a 930 nm FD-OCT (method 1).

The second method shown in Figure 3.5, includes the thickness of the microscope slide into the measurement. This serves to check the result of the first method and is potentially more accurate as the glass/air interface of the bottom side of the microscope glass is more prominent than the paint/glass interface. The RI was calculated by the following equation:

$$n_2 = \frac{(t_w - t_g)}{t_r} \qquad (3.26)$$

where t_w is the optical thickness of the paint and the microscope slide, t_g the optical thickness of the microscope slide and t_r the physical thickness of the paint.

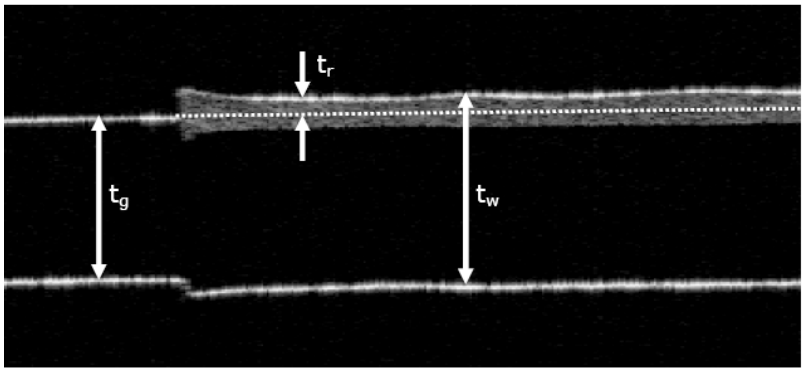

Figure 3.5. Refractive index measurements of rose madder in linseed oil using a 1310 nm TD-OCT (method 2).

The importance of measuring the RI in the case of OCT images is to determine the real thickness of the paint or varnish layer. In order to convert the optical thickness t_o into the physical thickness t_r the following equation must be applied:

$$t_r = \frac{t_o}{n_1} \qquad (3.27)$$

where n_1 is the refractive index of paint sample. The thickness of the samples was measured with the collected OCT images. Therefore a Matlab® program was used to detect the air-paint, paint-glass and air-glass interface.

The two methods, method 1 and method 2, were applied to several paint-outs. Two OCT systems were used for these measurements. Unfortunately, the second method could only be done with the 1310 nm TD-OCT (depth resolution 18 μm) as the 930 nm FD-OCT (depth resolution 6 μm) has a limited depth range. Eleven paint-outs were chosen to measure the RI with method 1 and 2. The criterion was that the samples were

transparent enough in order to detect the bottom of the microscope glass slide or in the case of the 930 nm OCT that the paint-glass interface had a clear edge.

It has to be taken in account that the two OCT systems have different pixel sizes. The axial pixel sizes are 12.9 μm and 3.125 μm for the 1300 nm and 930 nm OCTs respectively. In order to consider the pixel size for the error calculation in Fig. 3.6 and Fig. 3.7 the theoretical error for both OCT systems and two sample thicknesses are shown. The error calculation was applied to both methods. As in method 2 the clearer bottom glass/air interface was used instead of the paint/glass interface, the error is smaller than for method 1.

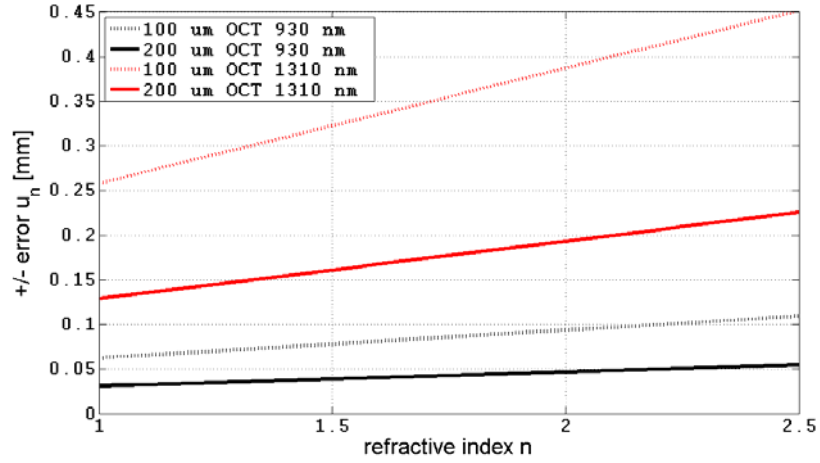

Figure 3.6. Pixel size error in the case of OCT at 930 nm and 1310 nm for RI calculations for samples with 100 μm and 200 μm wet thickness using method 1.

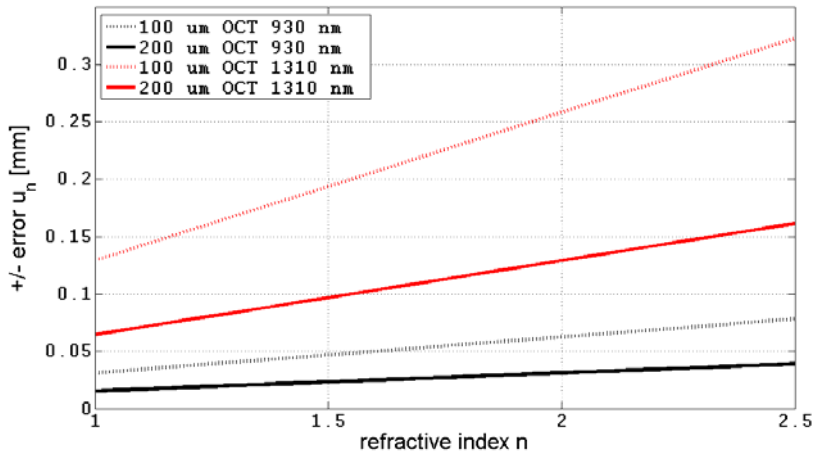

Figure 3.7. Pixel size error in the case of OCT at 930 nm and 1310 nm for RI calculations for samples with 100 μm and 200 μm wet thickness using method 2.

In Table 3.1 the RI of the selected paint-outs of either 100 or 200 μm wet thickness are shown. The reason that verdigris in linseed oil is only measured with one of the two OCT systems is due to the different transparency of the samples at different wavelengths. Verdigris in oil is highly absorbent at 930 nm, but transparent at 1310 nm as can be seen in Figure 2.15 in section 2.5.5. Bavarian green earth in linseed oil on the other hand shows a low reflectance and no transmission at 930 nm. Therefore the absorption is very high. There is an absorption trough, which means that the dispersion is anomalous and in this region there is a steep increase of the refractive index with wavelength. Therefore the RI of Bavarian green earth could not be measured using the 930 nm OCT.

Pigment	Binding medium	OCT @ 930 nm			OCT @ 1310 nm					Literature n of the pigments only	
		Method 1			Method 1		Method 2				
		n_1	STD	dp[7]	n_1	STD	n_2	STD	dp[7]		
Madder lake[1,6]	linseed oil	1.53	0.06	10	1.75	0.09	1.66	0.08	13	< 1.66[3]	
Madder lake[2,5]	linseed oil	1.51	0.02	20	1.31	0.08	1.35	0.04	7	< 1.66[3]	
Rose madder[6]	linseed oil	1.59	0.09	20	1.59	0.08	1.61	0.07	13	< 1.66[3]	
Sappanwood lake[6]	linseed oil	1.61	0.09	25	1.34	0.20	1.34	0.12	9		
Weld lake[5]	linseed oil	1.62	0.04	18							
Bavarian green earth[5]	linseed oil				1.67	0.10	1.59	0.03	9	1.62[3]	2.5 - 2.7[4]
Cochineal lake[6]	linseed oil	1.55	0.02	25	1.45	0.12	1.53	0.07	10		
Dyers broom lake[5]	linseed oil	1.82	0.21	17	1.76	0.22	1.06	0.20	8		
Verdigris[6]	linseed oil				1.45	0.09	1.51	0.06	10	α = 1.53[3]	γ = 1.56[3]
Madder lake[1,6]	egg tempera	1.55	0.03	5						< 1.66[3]	
Madder lake[2,6]	egg tempera	1.47	0.21	10						< 1.66[3]	

[1] from dyed wool; [2] from ground madder root; [3] The Pigment Compedium; [4] Brill, [5] 100 μm wet thickness; [6] 200 μm wet thickness, [7] number of data points

Table 3.1. Refractive indices of different paint-outs measured with method 1 and 2.

The RI was measured several times (Table 3.1) at different positions of the OCT image with both methods and the uncertainties are quoted with one standard deviation. The samples with higher standard deviations did not have a completely clear paint-glass interface. Dyer's broom lake in linseed oil has the highest deviation. This can be explained by investigating the OCT images. In Figure 3.8a it can be seen that the paint-

glass interface does not have a clear edge as in Figure 3.8b for sappanwood lake. The first peak in the profile graph is the air-paint interface and the second peak for the case of sappanwood lake is the paint-glass interface. The profile of Dyer's broom lake shows a decreasing signal where the paint-glass interface is. Through the blurred edge the variance of the RI results is higher compared to the samples with a clear interface.

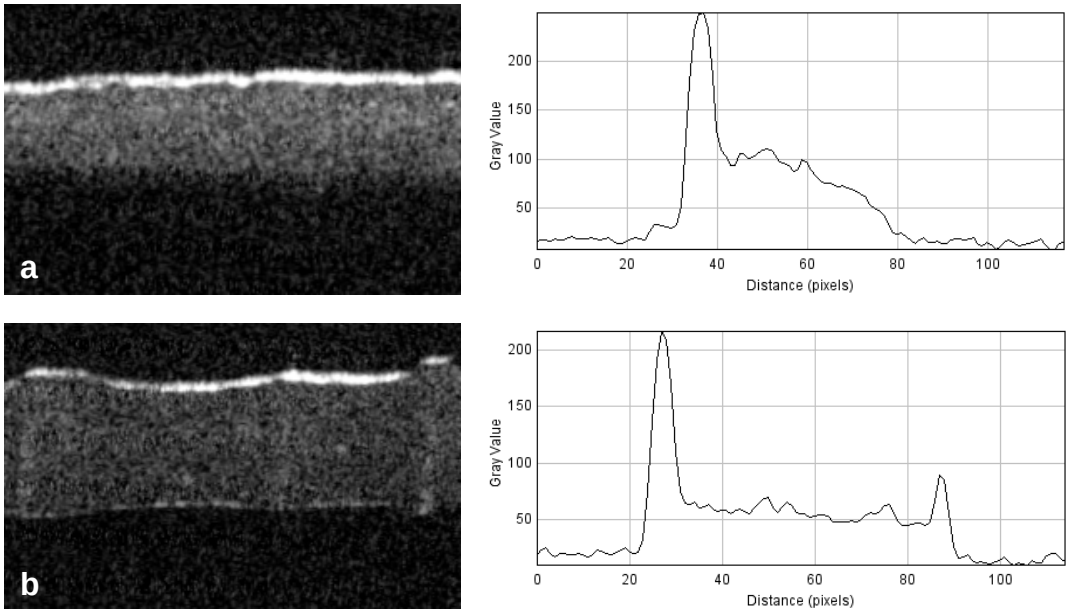

Figure 3.8. a) 930 nm OCT image (2.75 mm x 0.5 mm) of Dyer's broom lake in linseed oil and a profile through the paint layer. b) 930 nm OCT image (2.75 mm x 0.5 mm) of sappanwood lake in linseed oil and a profile through the paint layer.

A 930 nm OCT image of rose madder in linseed oil was corrected so that the paint thickness represents the physical thickness (Fig. 3.9b) rather than the optical thickness as in Fig. 3.9a. The RI for the correction was from the measured value of rose madder in Table 3.1. The RI of 1.6 was applied to the paint in the OCT image. A Matlab® program was written to correct this. Through the correction of the OCT images, a truer representation of the paint layer structure is obtained.

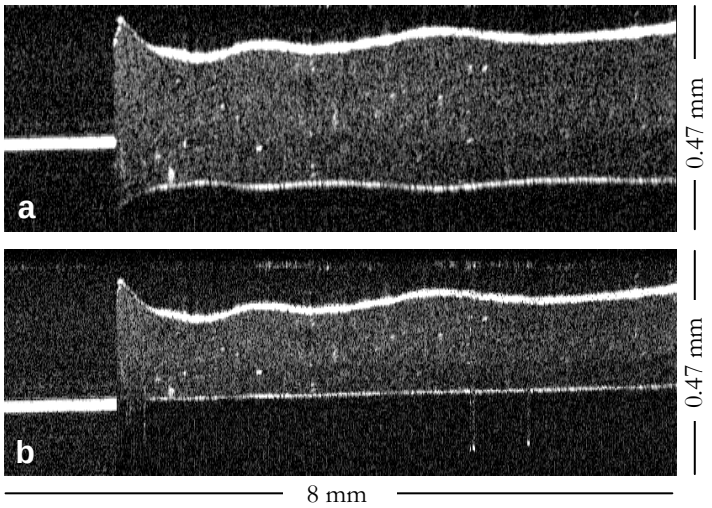

Figure 3.9. Cross-sectional 930 nm OCT images of rose madder in linseed oil on glass microscope slide. a) original images. b) optical thickness of the paint is corrected into physical thickness.

A further check on the RI determination for the sample in Fig. 3.9 can be conducted using the a priori knowledge that the microscope slide is flat. The air-glass interface in the OCT image can be extrapolated and this extrapolated glass surface should coincide with the corrected paint-glass interface. The original paint-glass interface was detected and then corrected with different RI using Eq. 3.25. The difference of the extrapolated air-glass interface and the RI corrected paint-glass interface is plotted as a function of RI in Fig. 3.10. This was done by subtracting the extrapolated air-glass interface by the RI corrected paint-glass over the whole sample. About 650 measurements were taken for each RI. The median difference for each RI is presented as the y axis in Fig. 3.10. The RI at zero difference between the extrapolated air-glass interface and the RI corrected paint-glass interface is 1.60± 0.03. Compared to the measurement with method 1, the error is nearly half the error for rose madder measured with the 930 nm OCT in Table 3.1.

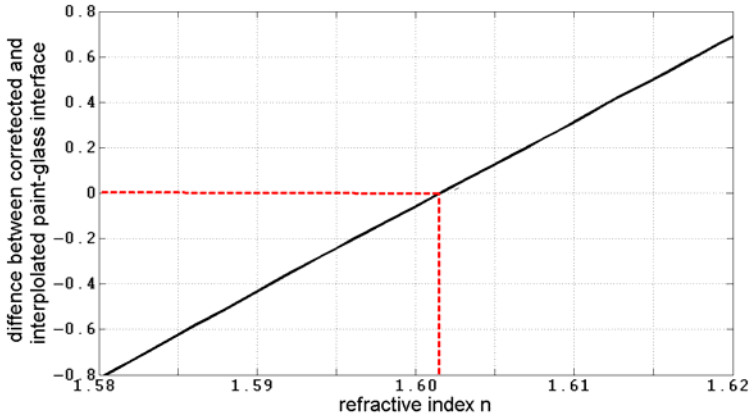

Figure 3.10. Difference between the RI corrected paint-glass interface and the extrapolated air-glass interface in the case of rose madder in linseed oil on glass microscope slide.

The correction of the thickness in OCT images can also be applied to cleaning treatments of paintings, which will be discussed in more detail in section 3.2. In Figure 3.11 we show an example of correcting the varnish layer of a painting by assuming a RI of 1.5. The aim is to change the optical thickness of the varnish into the real thickness in order to show the estimated real paint surface profile. This is done by calculating the physical thickness with a variety of refractive indices using Eq. 3.25. The corrected paint profile is the result of these calculations. By comparing the estimated paint profiles with the paint profile of the cleaned painting the information about paint loss through cleaning treatments can be gained. In addition, the RI of the varnish can be measured simultaneously.

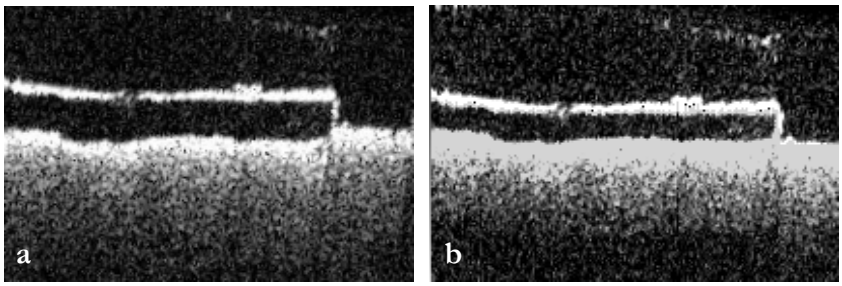

Figure 3.11. Cross-sectional OCT images (2.1mm × 0.46 mm) of a 16th painting. a) varnish on top of a paint layer. b) same as a) but the optical thickness of the varnish layer is corrected into physical thickness with a RI of 1.5.

Finally, the theoretical error of the focus tracking method is estimated for the Thorlabs 930nm OCT in order to know how accurate this in situ non-invasive measuring method can be. The error propagation is calculated for Eq. 3.24 where the accuracy of the translation stage and different RI are considered. The error σ_n of the RI is shown in Eq. 3.29.

$$\sigma_n^2 = \left(\frac{\partial n_s}{z_r}\right)^2 \sigma_r^2 + \left(\frac{\partial n_s}{\partial z_f}\right)^2 \sigma_f^2 \tag{3.28}$$

$$\sigma_n = \sqrt{\frac{1}{4z_f^2\sqrt{1+z_r/z_f}}\left(\sigma_r^2 + \frac{z_r^2}{z_f^2}\sigma_f^2\right)} \tag{3.29}$$

where the σ_r is the resolution of z_r, σ_f is the resolution of z_f and σ_n the error of n_s. The accuracy of z_r is the one that we intend to get. Solving the equation we get:

$$\sigma_r = \sqrt{4z_f^2 n_s \sigma_n^2 - (n_s^2 - 1)^2 \sigma_z^2} \tag{3.30}$$

The ratio of the calculated error σ_r of the reference arm and the adjustment to the focus is shown in Fig. 3.12. The accuracy σ_n of RI is set to 0.005, 0.01, 0.05 and 0.1 and the accuracy of the stage for the focus adjustment is 3 μm.

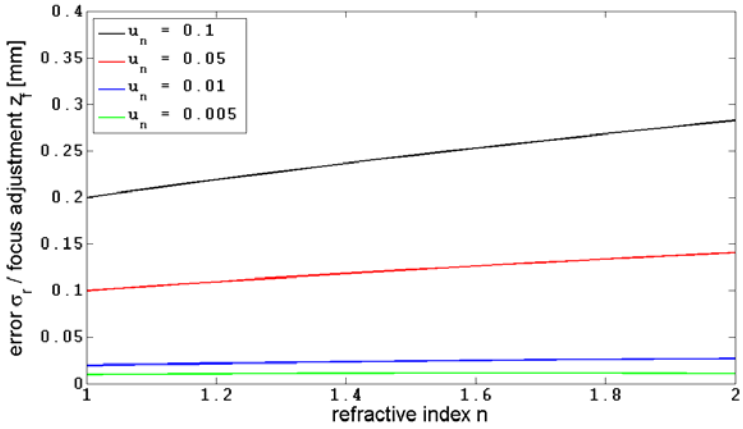

Figure 3.12. Ratio of the error for the reference mirror stage and the adjustment to the focus with four different errors for the refractive index.

A ±0.005 error for the refractive index could be achieved with an accuracy of 12 μm in the reference mirror tube movement for sample thickness of 1 mm. An RI

measurement accuracy of 0.02 can be obtained with an accuracy of 1 µm for the position of the reference arm and samples with a thickness of 100 µm (Fig. 3.13). Only a very coarse manual adjustment is possible with the current Thorlabs OCT probe head. It is necessary to fit an electronically controlled micrometer to the adjustment of the reference mirror.

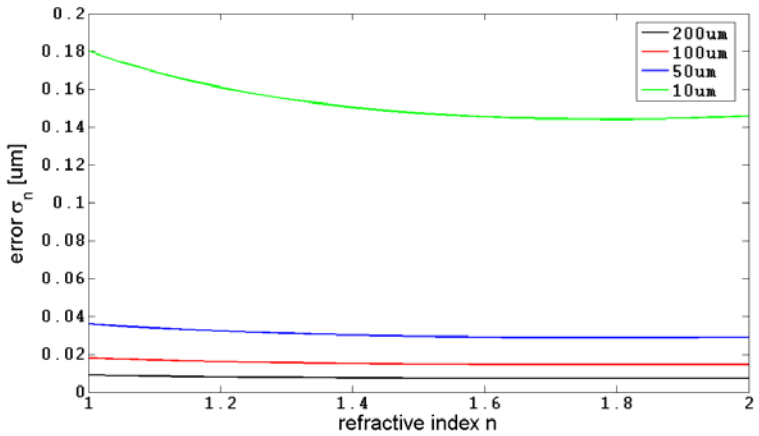

Figure 3.13. Error in the RI measurement using the focus tracking method with a reference arm translation stage of 1 µm accuracy for different thicknesses. A 3 µm accuracy is assumed for the translation stage attached to the probe.

3.2. Monitoring of Cleaning Treatment

Varnishes are applied to paintings for its visual and protective effects. So the paint layers are protected from mechanical damage and dust deposition. The more important effect is the appearance of a painting. The painting gains more saturated colour and a glossy look with a varnish layer on top of the paint surface. Glossiness is due to the surface roughness. Light that is reflected from a smooth surface is mainly specular reflection and therefore the painting has a glossy appearance. On the other hand, a rougher surface has a larger surface area and reflects diffusely which results in a reduction of the glossiness. A rougher surface also causes a less saturated colour. This is due to the combination of the scattered white light of the varnish and the reflected light at the interface of the paint and varnish layer (de la Rie 1987, Berns & de la Rie 2002). Varnish changes its optical properties with age, which results in a change of the visual qualities.

The original appearance of the painting should be preserved. Aged varnish turns yellowish or hazy which needs to be removed and a new varnish layer has to be applied. The aim is to restore the painting to its original appearance, after the conservation procedure. The cleaning process requires high precision in order to clean away the old varnish while not damaging the original paint. Conservators remove the varnish with solvents which are aggressive to the varnish and the paint. This is a standard method for the cleaning of old master paintings. It is difficult to control the cleaning of the varnish and to make sure that the original paint remains. Current method of detecting whether the old varnish has been cleaned off is by shining a UV light on the cleaned area to detect the florescence of old varnish. The cleaning controversy is about whether or how much of the old varnish needs to be removed in order to re-establish the original appearance of the painting (The Burlington Magazine 1962). Conservators at National Gallery were criticized for the cleaning treatment of historical paintings as Rubens' *Peace and War* in 1846. The critic Morris Moore saw a decrease of the richness of the colours because of the cleaning process. Another criticism was that the original glaze of some paintings, as the Titans' *Bacchus and Ariadne*, was removed and therefore the original appearance was lost (Sutherland 2001). Another important controversy is whether cleaning solvents affect the paint layer or not. The main investigations are the leaching of paint compounds and the swelling of oil paints. The latter was investigated by Stolow in the 1950s to the 1970s. It would simplify the removal of not only the varnish but also the paint film as the paint softens through the swelling with solvents. Cleaning tests with different solvents are done by conservators in order to choose the cleaning solvent which has the least effect on the paint. The decision for the right solvent depends on the swelling degree of the paint when the solvent is applied. Stolow's experiments showed that the swelling degree of solvents on reference paint films reached a maximum within a few minutes. The leaching effect occurred in Stolow's experiments

after the maximum of the swelling degree was reached. Swelling was measured as the change in the thickness of the reference paint film in microns. The decrease of the thickness was due to the leaching of compounds in the paint. This can cause a change of the physical properties as the brittleness and the optical properties of the paint. Conservators cannot control this effect on a painting (Phenix and Sutherland 2001). The publication of White & Roy in 1998 on whether the paint surface was affected or not by the cleaning process was shown on a variety of significant paintings. The study was conducted on twelve National Gallery paintings which vary in date, support and binding medium. Areas of these paintings were monitored before and after the cleaning procedure. Solvent and mechanical cleaning of the varnish was compared in chemical composition and whether the solvent penetrated through the paint was shown through a microscopic investigation with a scanning electron microscope. One microsample of paint was taken from an area of the mechanical and solvent removed varnish in order to get the chemical composition with a gas chromatography mass spectrometer. Leaching of the paint could not be demonstrated. The microscopic investigation was carried out with samples of an uncleaned and solvent cleaned area. The main conclusion was that there was no evidence that the original paint was harmed by the cleaning process (White & Roy 1998).

There were no direct ways of checking if the original paint surface had been affected by the solvent. As sampling changes the surface and the results of the investigated sample cannot be provided immediately. It is necessary to investigate other methods. Therefore the application of OCT for monitoring the cleaning process gives a convenient, in situ and direct method of ascertaining whether or not the cleaning is complete and whether the paint surface had been affected. OCT as a monitoring equipment for laser ablation of varnish layers has been shown in 2006 by Gora et al. Here we demonstrate how OCT

can be used to monitor traditional solvent cleaning of varnish which is the most common method for the cleaning of paintings.

3.2.1. Monitoring of Cleaning

The cleaning test was done on a ~50-year-old test painting (Fig. 3.14), which is partly covered by a 50 year old yellowed mastic varnish. Aged varnish of a small area, roughly 1 cm by 1.5 cm, was removed from the bottom left hand corner of the painting. OCT monitored the area of interest before the cleaning procedure and in several stages during the removal of the varnish. The OCT system used for the cleaning scan was a Fourier domain OCT with a central wavelength of 930 nm. The size of the cross-sectional images was adjusted to 10 mm width by 1.6 mm depth. The axial resolution is 6.2 μm in air and the transverse resolution is 9.2 μm.

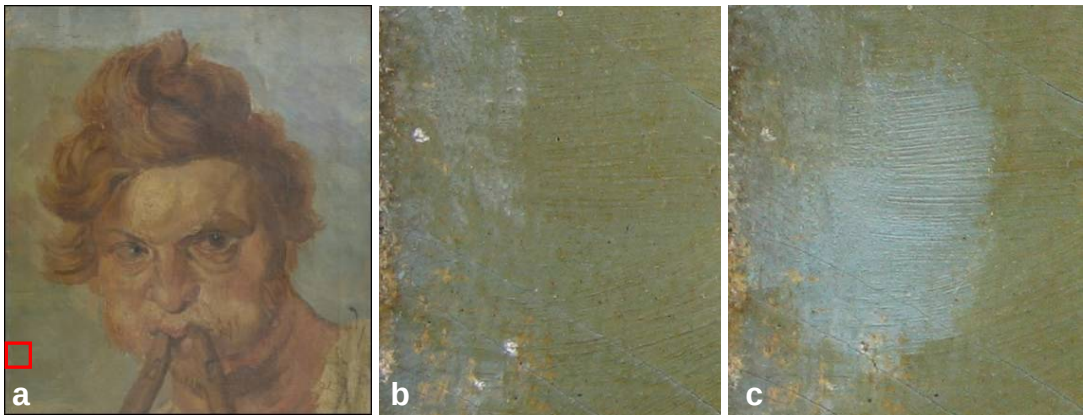

Figure 3.14. ~50-year-old test painting. a) uncleaned painting with marked cleaning area. b) detail of uncleaned area. c) detail of cleaned area.

The area of interest on the painting was first scanned with the OCT before the removal of the varnish (Fig. 3.14b). Afterwards the area was partly cleaned and scanned again to capture the cleaning procedure. The latter was done in three steps until the varnish was completely removed (Fig. 3.14c). As the cross-sectional OCT images were taken from successive scans of uncleaned, partly cleaned and cleaned areas, the alignment of them is necessary. The enface images of each scan were used for the alignment, as there are

some distinctive marks in the structure of the area of interest. For the alignment the images were cross-correlated.

The cross-correlation of two images gives the position of the best alignment of the two images. An area with some distinctive marks of the enface image before the cleaning treatment were chosen and cross-correlated with the enface images during and after the cleaning. The displacement to the enface image before the cleaning treatment can be seen in Table 3.2.

Before cleaning treatment image cross-correlated to:	Δy [pixel]	Δx [pixel]
After the first cleaning step	-4	-1
After the second cleaning step	-5	-1
After the third cleaning step	-3	-1

Table 3.2. Displacement in axial (Δy) and transversal (Δx) direction between the scans.

In Fig. 3.15a the rough paint structure and two layers of varnish are visible in the cross-section image. These two layers of varnish are easy distinguishable because of their different scattering properties. The top layer is more transparent and therefore a newer varnish. Aged varnish tends to turn yellow and becomes hazy, which increases scattering in the second varnish layer compared to the newer varnish. After the first cleaning step some areas where the newer varnish was thinner, less than 31 μm, were removed (Fig. 3.15b). In Fig. 3.15c only varnish in larger hollows still remained. Most of the varnish is removed after the last cleaning step (Fig. 3.15d).

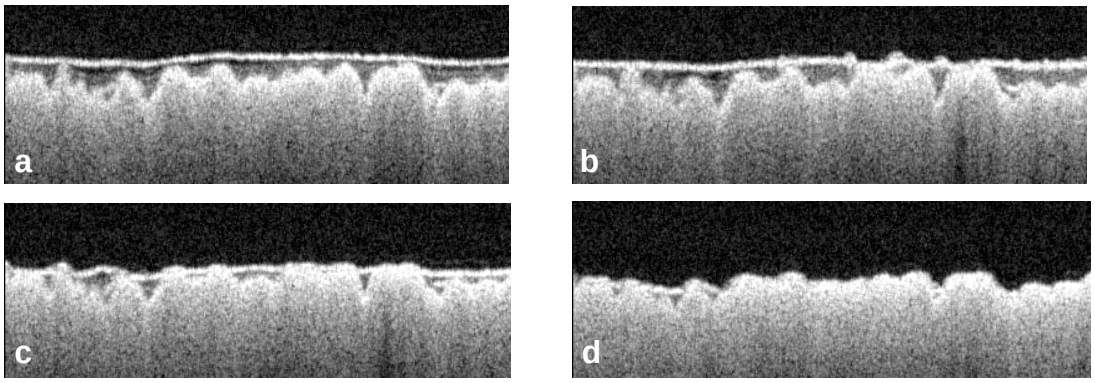

Figure 3.15. cross-sectional OCT images (4.1 mm × 0.44 mm) of an ~50-year-old test painting in the cleaning process. a) before the cleaning. b-c) during the cleaning procedure. d) after the cleaning

The cleaned paint surface (Fig. 3.15d) has a slightly different profile compared to the uncleaned paint surface in Fig. 3.15a. This is due to the RI difference between air in the cleaned image and the varnish layer in the uncleaned image. As transmitted light is slowed down in the varnish layer, which means that the optical thickness is larger than physical thickness in these images, and the different thicknesses of the varnish over the paint change the profile of the surface. It is necessary to correct the profile of the paint surface under the varnish in order to compare with the 'bare' paint surface after cleaning to detect if there is a loss of the original paint through the cleaning process. This was done with an algorithm written in Matlab®. The fundamental principle for the algorithm was to change the optical thickness of the varnish layer into the physical thickness so that it would match a sampled cross-section. In order to achieve this, the surfaces of the varnish layer and of the paint surface in the OCT image were detected automatically. The difference of these two positions is the optical thickness of the varnish layer. The physical thickness of the varnish layer can be calculated by dividing the optical thickness of the varnish by its refractive index which in turn gives the real paint surface profile. The corrected paint surface is laid over the OCT images of the cleaned painting in order to determine whether there is a change in the paint surface (see Fig.3.16).

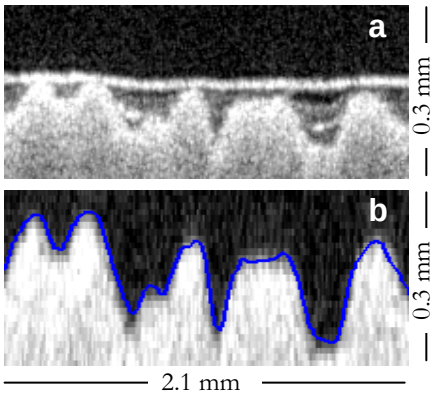

Figure 3.16. a) cross-sectional OCT image before cleaning. b) cross-sectional OCT image after cleaning with calculated paint surface (blue graph).

The maximum difference is 5 pixels, but these large deviations correspond to the larger troughs with two layers of old varnish and one layer of relatively newer varnish on top of the paint. Only one RI and one uniform layer of varnish was assumed in the calculation. Apart from these large deviations, the maximum difference was 2 pixels, i.e. 6 microns. This result shows the potential of OCT for monitoring the cleaning of paintings.

4. OCT Application to Art History

4.1. Introduction

Ever since the application of infrared imaging on paintings, the study of underdrawings has become an important part of art historical analysis. These drawings are preparatory sketches of the painter on a canvas or wood panel. Underdrawings are covered with paint layers, so they are not usually visible to the naked eye. But some paint layers reveal the underdrawing with age as the paint becomes more transparent. Art historians and scientists at galleries can gain extra information of the painting by visualising the underdrawings. The painting itself can differ from the underdrawings. The underdrawings can reveal the artist's initial composition. In the process of finishing the painting the artist may have painted objects differently or even included other objects which were not planned (Bomford 2002).

Generally speaking an underdrawing is drawn or transferred onto the canvas or the wood panel by the painter. This drawing guides the painter during the process of finishing the painting. The lines or the hatchings may have been drawn with different materials which are either dry or fluid. Through analysing the underdrawings, it may be possible to determine if a painter used a pen or a brush as drawing tool. The study of underdrawings can provide a basic understanding of the drawings themselves in terms of the type of material and method of application.

Broadly speaking there were two types of underdrawings: the ones that were drawn free hand or the ones that were traced. The latter can be done with transfer techniques which were *pouncing*, *tracing* or *squaring*. For two of these methods, *pouncing* and *tracing*, a pattern mask was applied to copy the drawing onto the panel. *Pouncing* made use of a

cartoon, which is a paper with a punctured outline of the drawing. This mask was put onto the panel or canvas and then a dark pigment or charcoal was transferred through the holes onto the surface of the canvas. Usually a fabric bag filled with loose dark charcoal or pigment was used to apply the pigment to the canvas. The remaining dots at the canvas were connected, but later on they might also have been brushed away in the process of painting. Some of the dots remained below the paint layers and can be visualized by infrared reflectography or OCT scans. *Tracing* is the other technique of transferring the drawing which made use of a mask. This is not as obvious in identifying the method of transfer as the first one. A paper with the final drawing was blackened on the back or a blackened paper was placed between the cartoon and the canvas or wood panel. The lines of the drawing were traced so that the drawing was copied on to the panel. The third method was *squaring*. A grid on the paper with the initial drawing was used to transfer the drawing free hand onto the canvas. So the painter copied the drawing of one box of the grid on to the canvas into the corresponding grid. The drawing of any size can be transferred onto the canvas as the grid gives the relative proportions. Paintings where the drawing was transferred in such a way can be easily identified as the lines of the grid are visible in the underdrawing images (Bomford 2002).

Underdrawings can be revealed by different non-invasive examination techniques such as infrared photography, infrared reflectography or OCT. Near infrared imaging is preferred as the paint layers become more transparent at longer wavelength. Infrared photography had been used since the 1930s. An infrared-sensitive film that is placed in a conventional camera and it needs to be developed in a similar fashion as a traditional photographic film. Most carbon based underdrawings absorb in the near infrared which stand out over a light-coloured highly reflective background. Nevertheless this method has some limitations. One of them is the relatively short wavelength of the sensitive

range (750 nm to 900 nm) of the film (van Asperen de Boer 1966) which leads to the poor penetration through for example copper-containing paint layers (van Asperen de Boer 1968). On the other hand, infrared reflectography uses longer wavelengths up to 2μm, so that the penetration through copper containing paint layers (e.g. azurite and malachite) is achievable. Infrared reflectography, first developed in the 1960s, uses a vidicon tube or a solid-state detector that are sensitive to the infrared in the region from 900nm up to 2200nm. Visible light, on the other hand, is filtered out so that just infrared information is obtained. Due to the low resolution of the camera, a mosaic of many images of the size of a couple of centimetres is necessary to capture a whole painting. These images are joined together with a computer program to one image (Bomford 2002).

Saunders et al. (2006) introduced a new large format infrared camera (SIRIS). An indium gallium arsenide (InGaAs) sensor was used for imaging underdrawings providing nearly an order of magnitude better sensitivity than the vidicon systems. These digital devices have better linearity compared with the analogue vidicon systems. In general the resolution of infrared sensors is low compared to CCD cameras operating in the visible range. A common size for the array of an InGaAs detector is 640 x 480 pixels. In order to reveal brushstrokes, a resolution of 10 pixels per millimetre is needed. Therefore the InGaAs sensor can only cover an area of 60 x 50 mm of the painting at such a high resolution. As paintings can be larger, it is necessary to collect a series of images to cover the whole painting. This camera is designed such that the sensor moves in the focal plane and the individual images are mosaiced together on the fly in order to get one underdrawing image of the whole painting or of an area of interest (Saunders et al. 2006).

OCT was first used for the study of underdrawings in 2005 (Liang et al. 2005). This relatively new optical technique had shown a better visibility of the underdrawings in comparison to any of the infrared imaging techniques described above. A set of OCT cross-sections images scanned over a certain transverse range, can be formed into a 3D image. The main advantage is that OCT gives depth resolved 3D images, so that it is possible to select only the *en face* images of the 3D image with underdrawing information. Infrared reflectography, however, displays the sum of the information of all layers in the image. OCT images could also show the position of the underdrawing in order to detect if it was drawn above or underneath the priming layer (*imprimatura*).

4.2. Visibility of Underdrawing Materials

For this study a set of underdrawing samples had been prepared. The background area of the underdrawings is essential for the visibility of underdrawings. The underdrawing material was drawn onto white veneered wood as most ground layers for paintings are white. The samples contained dry and fluid drawing materials. Lead-tin, silver, red conté chalk pastel, charcoal, red and black chalk are dry drawing materials. This group of material can be divided into four groups: metal-point, pastel, charcoal and chalk. The first group of the dry materials is the metal-point, which is a sharpened metal stylus. When metal-point is applied onto a canvas it leaves a greyish-silver drawing. Through oxidation of the silver and lead-tin, the drawings become darker with time, even below the protective paint layers. Metal-point drawings can be seen in infrared and OCT images. The pastel underdrawing material red conté chalk pastel could not be seen in an OCT image due to its high transparency at 930 nm. Charcoal as underdrawing material on the other hand is easily visible with IRR or OCT imaging. It could also have been used for the transfer process (as *pouncing* or *tracing*) of the underdrawing. Red chalk can't be detected with the OCT system at 930 nm, but black chalk can be detected. In this

study the fluid materials for underdrawings were lamp black water colour and iron gall ink. Fluid material can be distinguished from dry underdrawing material from the variation in width and density of the lines on the infrared or OCT image. The end of a drawn fluid line has typically a droplet and the edges of a line have a higher density when the underdrawing is applied with a brush. The background area of the underdrawings is essential for the visibility of underdrawings. In Fig. 4.2 the contrast value of the different underdrawings applied onto white veneered wood can be seen. The contrast value between the underdrawing and the background (here the white veneered wood) is defined as following equation:

$$contrast\ value = \frac{I_{\max} - I_{\min}}{I_{\max} + I_{\min}} \qquad (4.1)$$

where I_{max} is the peak position in the histogram of the background and I_{min} is the peak position in the histogram of the underdrawing area. Best visibility is achieved with a contrast value of 1.

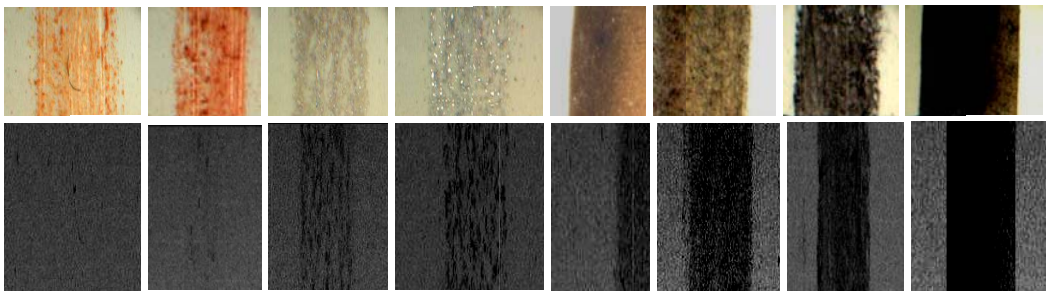

Figure 4.1.Pictures and OCT images (930 nm) of underdrawing material on white veneered wood: red chalk, red conté chalk pastel, silver, lead-tin, iron gall ink, charcoal, black chalk, lamp black water colour. These pictures and OCT images are not at the same position.

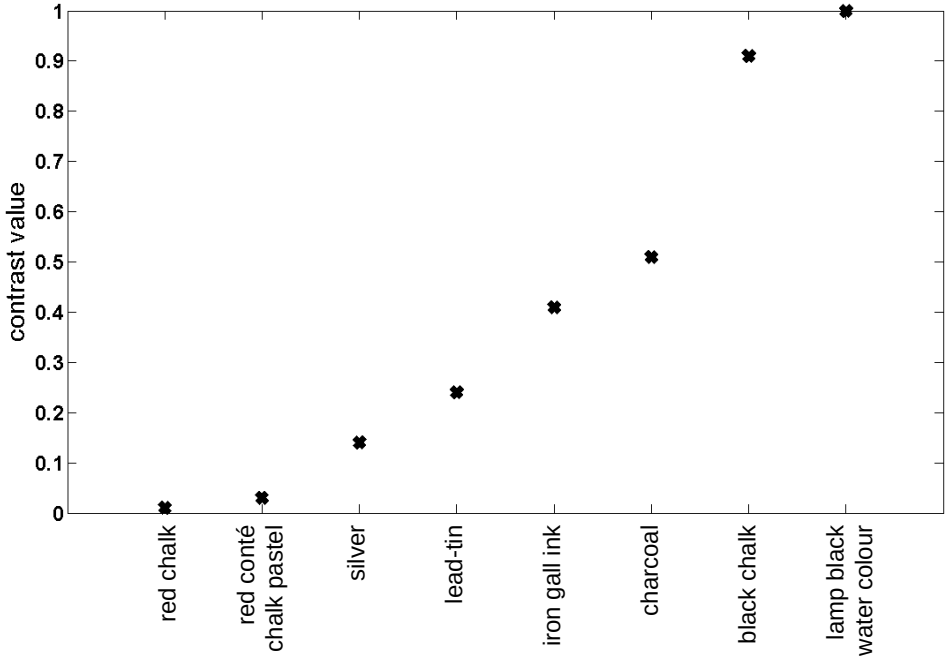

Figure 4.2.Contrast value at 930 nm of the different underdrawing materials applied onto white veneered wood.

Lamp black water colour and black chalk have the best contrast value onto white veneer wood. On the other hand red chalk and red conté chalk pastel have a poor visibility. Therefore the red underdrawing materials are not visible at 930 nm OCT images with this background, as expected.

4.3. Method for the Best Underdrawing Images

The OCT system used for all the underdrawing measurements was a Fourier domain OCT. A handheld probe is mounted to a motorised three axes stage. The latter gives a range of 15 cm by 15 cm scan area. The central wavelength is 930 nm. Cross-sectional images can be adjusted to a maximum size of 10 mm width by 1.6 mm depth.

Paintings in galleries or objects in museums are valuable. In most cases it is not possible to bring these objects or paintings to the instrument. Therefore a portable instrument, such as the Thorlabs spectral radar OCT, is needed for such an application. The OCT system has been adapted by mounting the small probe head onto translation stages in order to scan an area of interest. From assembling the system to starting the first

measurement takes about 30 minutes. The handheld probe is then aligned to the work of art in such a way that the area of interest is in focus. There is no danger for the painting as the stages are set up such that they are at maximum travel when closest to the painting. The distance between the painting and the probe is around 1 cm. The individual cross-section images are collected by the probe which has an internal piezo scanning mirror. A 3D image can be captured by scanning with the translation stage in a direction perpendicular to the cross-section images. The sampling resolution in the scanning direction is adjustable through the speed of the scan. All 3D images in this thesis have a sampling resolution of about 20 μm in scanning direction controlled by the translation stage.

In order to obtain underdrawing images it is necessary to reslice the 3D image. Through this we get enface images which are images parallel to the plane of the painting at given depths. The basic principle of obtaining a high contrast underdrawing image is to select images with underdrawing information in a range of depth positions. Either the average or the median of these selected enface images are taken to form the final underdrawing image. The visibility of the underdrawings depends on the underdrawing material itself, the background of the underdrawing and the paint layer on top of it. Through the spectral investigation of historic artists' paints in chapter 2 an optimum wavelength for the best visibility of underdrawings is given at 2.2-2.3 μm.

In Fig. 4.3 a cross-sectional images is shown. Underdrawings are the dark bands over the whole width of the image. In order to get underdrawing images a 3D image needs to be made out of the cross-sections. The 3D image is then resliced to show the underdrawing. Some depth positions are marked with a position number. Position 95 is just below the surface of the paint sample and 320 is further down in the paint layer.

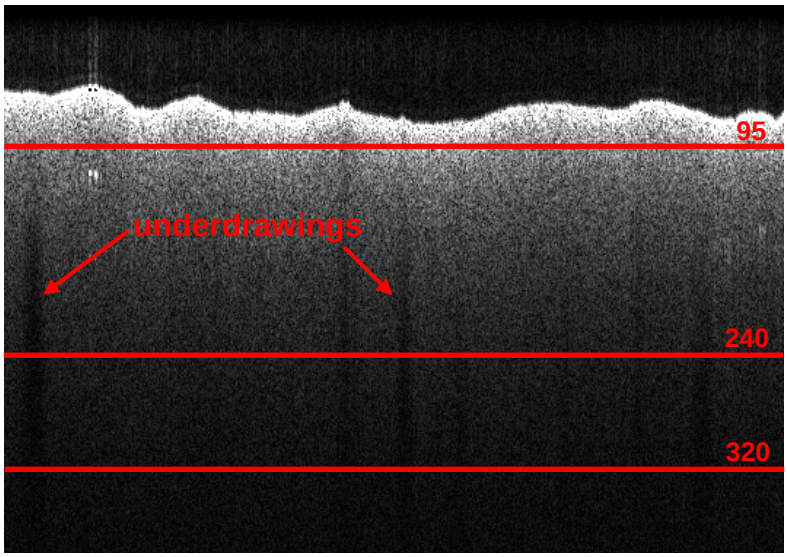

Figure 4.3.One cross-section image of the underdrawing sample with marked positions at 95, 240 and 320 (image: width 5.3 mm, height 1.2 mm).

To estimate visibility of each *en face* underdrawing image, the contrast between the pure background area and pure underdrawing area are calculated according to Equation 4.1. First of all we need to decide whether it is better to take the mean or the median of the range of underdrawing images in depth. A painted patch of two layers of lead-tin yellow over underdrawings of bone black in gum drawn with a quill pen was used as a test sample. The contrast value is calculated from the median and mean of ten up to 100 images. In Fig. 4.4 the contrast value versus the number of images used for either a mean or a median image is shown. When 30 images or more adjacent images are used to calculate the median image, the contrast value is slightly higher than for the mean image. Another advantage of median images is that it is unaffected by ghost images or artefacts in the image. Therefore we decide to use only the median for the underdrawing images.

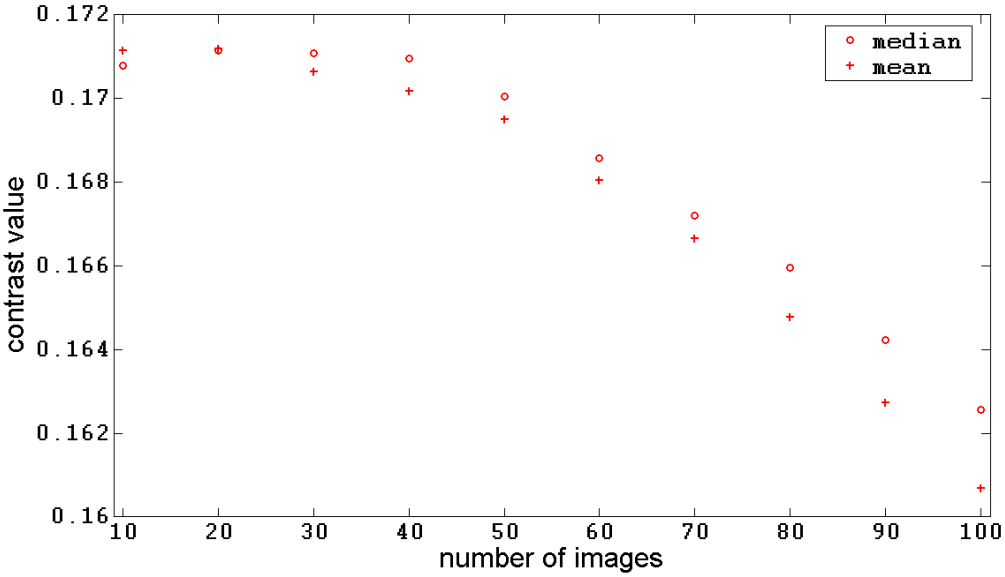

Figure 4.4.Contrast value versus the number of images used for either a mean or a median image.

In Fig. 4.5 enface images are shown at different depth positions. When we start at the top of a set of enface images we see black images which are images of noise taken just above the object surface (see Fig. 4.3). The next is the interface between air and the paint surface. This includes specular reflection which gives high signal values. In Fig. 4.5a an enface image just below the surface is shown and in Fig. 4.5b is the image slightly deeper into the paint layer. At some point we reach the level where the underdrawing has the best visibility (Fig. 4.5c) and when we penetrate deeper the visibility is decreasing (Fig. 4.5d).

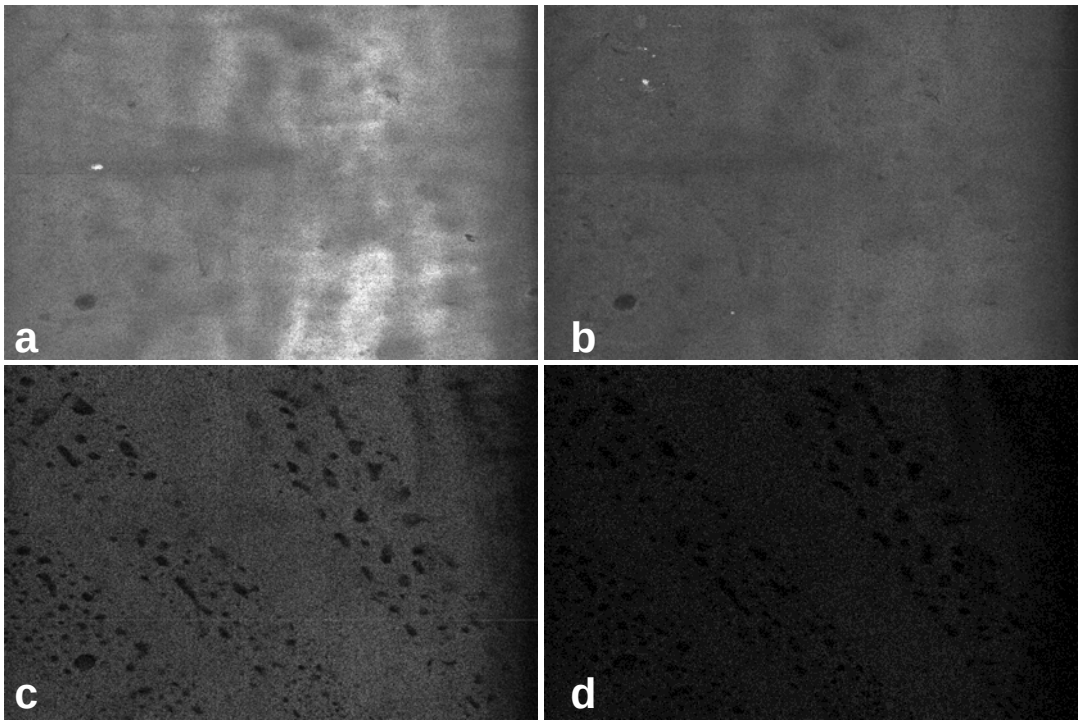

Figure 4.5. Enface images at different depths (starting at from top to bottom). a) paint layer just below the surface (position 95). b) paint layer further down (position 125). c) depth of the underdrawing (position 240). d) visibility of the underdrawing is decreasing (position 320). Image size: 10 mm × 10 mm.

This can be shown quantitatively by looking at the contrast value of individually enface images. We start at the enface image where it is possible to differentiate between underdrawing and background area. In Fig. 4.6 a graph is plotted of the contrast value versus the position of the enface image. The red circles show the results over eight underdrawing areas. As the underdrawings are relative small marks, we selected a number of them over the whole enface image. The black, green and blue circles represent the different areas. It can be seen that the contrast variation as a function of depth are similar for the different areas. Therefore the best contrast for the enface images is given from depth position 220 up to 260.

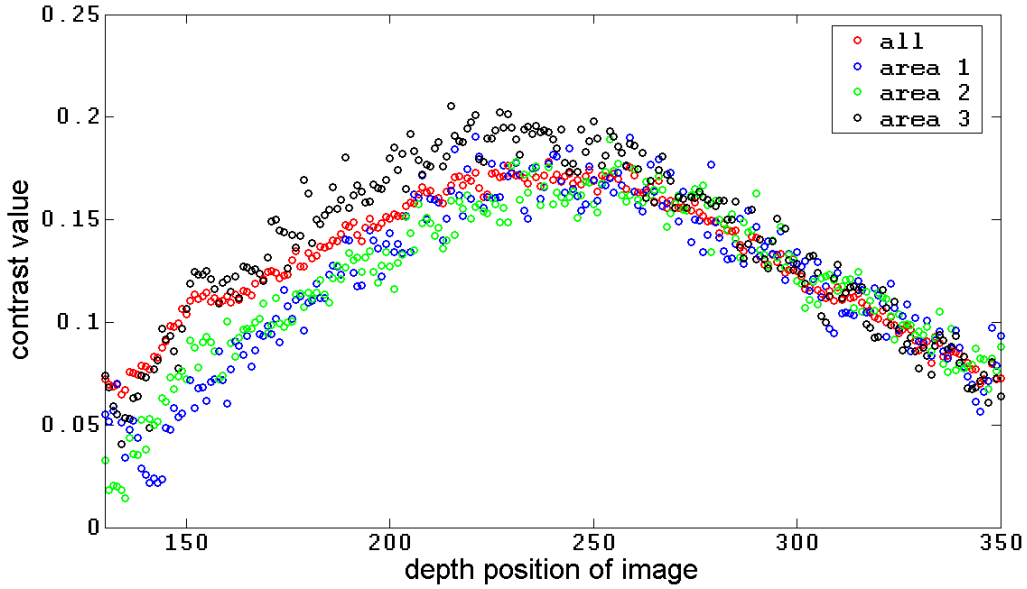

Figure 4.6. Contrast values of the individual enface images versus the depth position ('all' indicates all eight underdrawing areas, 'area1', 'area2' and 'area3' are shown to demonstrate the similar behaviour).

First we investigate the difference between taking the median of enface images at the same depth position (position 240, 10 repeated scans) and at a range of 10 different depth positions (235-244). The contrast value of the median images at different depths is higher than the one at the same depth (Fig. 4.7).

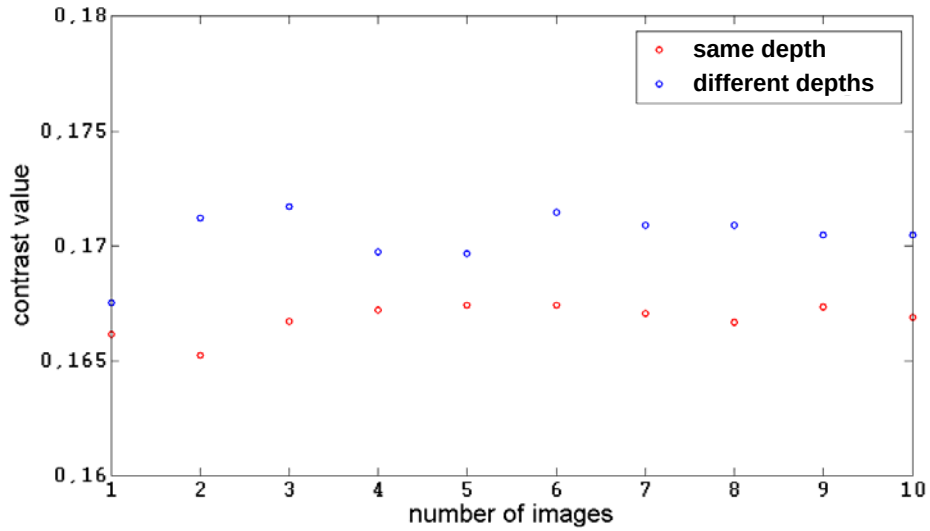

Figure 4.7. Contrast values versus the number of enface images at the same depth and different depths.

The main advantage of average at different depths is that speckle is reduced. Speckle is the unwanted signal that arises through interference between back-scattered light from

different positions in the sample volume that reach the detector. The reduction of speckle can be illustrated by the reduction of speckle contrast:

$$speckle \quad contrast = \frac{Sigma}{Peak \ \ position} \qquad (4.2)$$

In Fig.4.8 it can be seen that the speckle contrast of the background area is decreasing with number of images used for the median for the case of the different depths. Therefore the use of different depth is recommended. In Fig. 4.9 a median enface image of the same depth position and at ten different depth positions is shown.

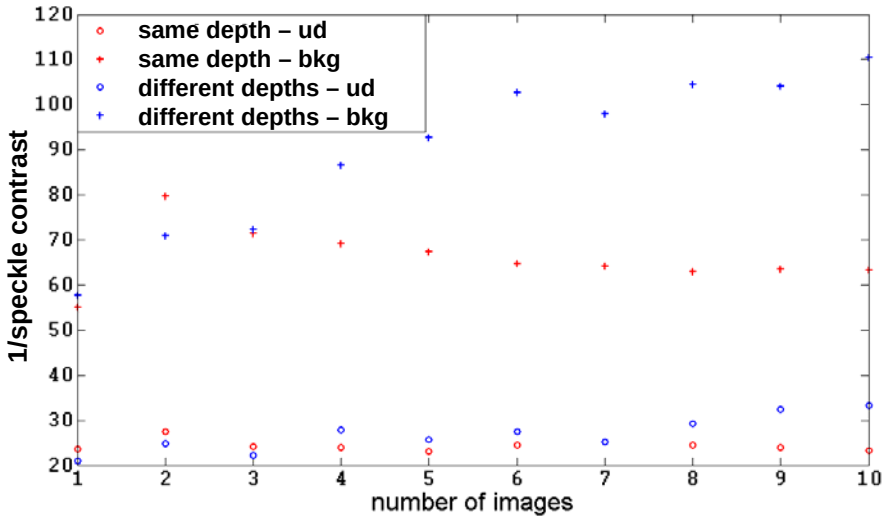

Figure 4.8. Comparison of the median image of the same depth position and a range of depth positions.

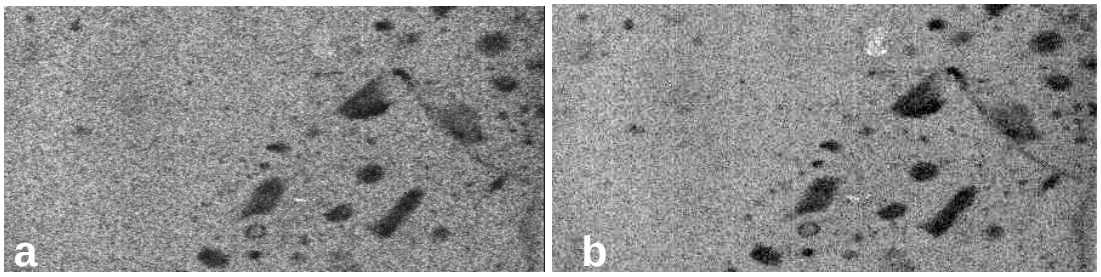

Figure 4.9. a) median image of ten enface images of the same depth position. b) median image of ten enface images at ten different depth positions. Image size: 4.5 mm × 3 mm.

The median of a range of images at different depth positions gives the best underdrawing image. As the best contrast of the individual enface images is between 220 and 260, we average a range of images above and below position 240 in order to determine the optimum number of images to use. In Fig. 4.10 the number of images

used for a median image versus the contrast value is presented. The contrast value is constant between 20 and 40 images used for the median. From Fig. 4.6 we could have expected such a result as the contrast values of the individual enface images are constant over a range of 40 images (from 221 up to 260). To include any more images at lower contrast values would only result in a degradation of the final image quality. It is possible to obtain an improved final image by including all images that contain underdrawing information but with each image weighted by it contrast value.

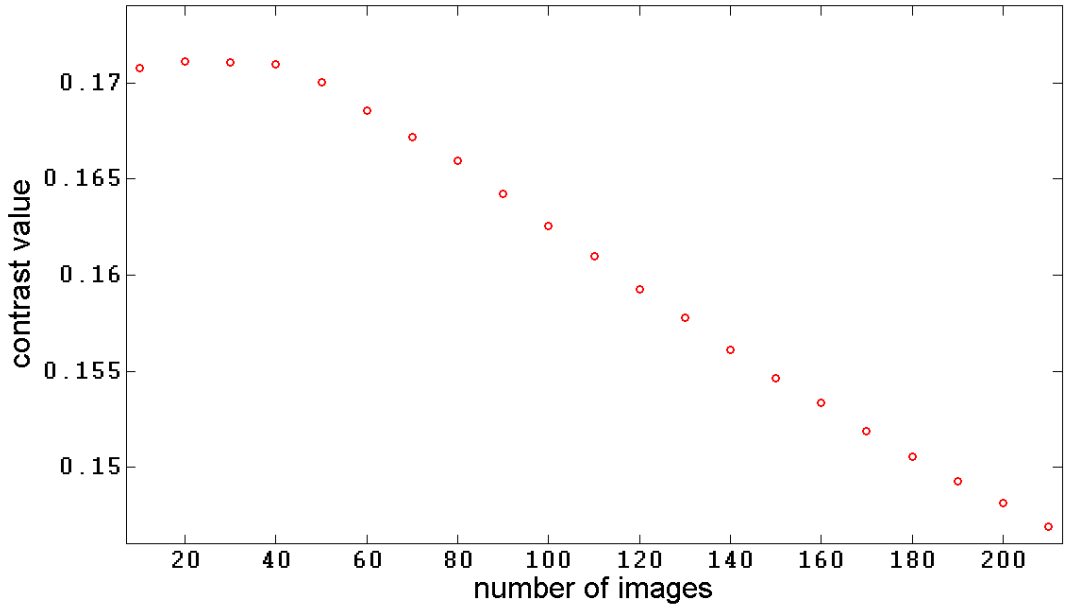

Figure 4.10. Contrast value versus the number of images used for one median image.

Fig. 4.11. shows 20 and 40 images used for a median image. The contrast value is higher and also some feature are more dominant in Fig. 4.11b compared to Fig. 4.11a. Therefore it is recommended to take the median of as many images as in the first analysis results (Fig. 4.6). In this example it means to take the median of 40 images form position 221 up to 260.

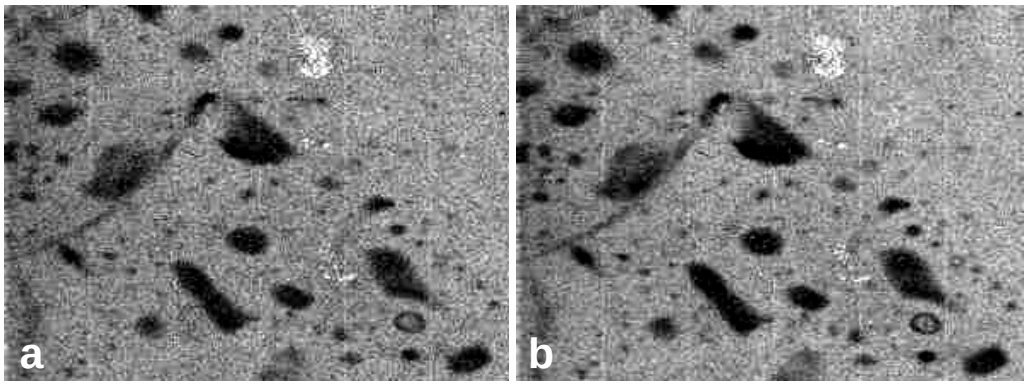

Figure 4.11. Underdrawing images. a) 20 images (position 231-250). b) 40 images used for the median (position 221-260). Image size: 3 mm x 3 mm.

In Fig. 4.12 shows the differences between the median of 40 images at the depth where the contrast value reaches a peak and at a position above (closer to the top of the underdrawing) where the contrast value is lower. The visibility is increased in Fig. 4.12a. This is partly because of the effect of multiple scattering where it is stronger at the top of the underdrawing than further down in the shadows of the underdrawing.

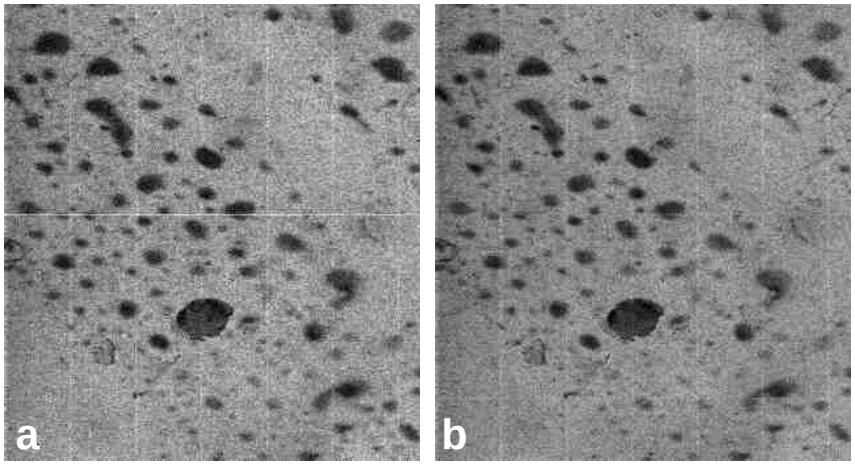

Figure 4.12. Underdrawing images. a) 40 images used for the median (position 221-260). b) 40 images used for the median (position 190-230). Image size: 3.2 mm x 5 mm.

In Fig. 4.13 the best underdrawing image is presented. This image was obtained by taking the median of 40 images at the depth positions from 221 up to 260.

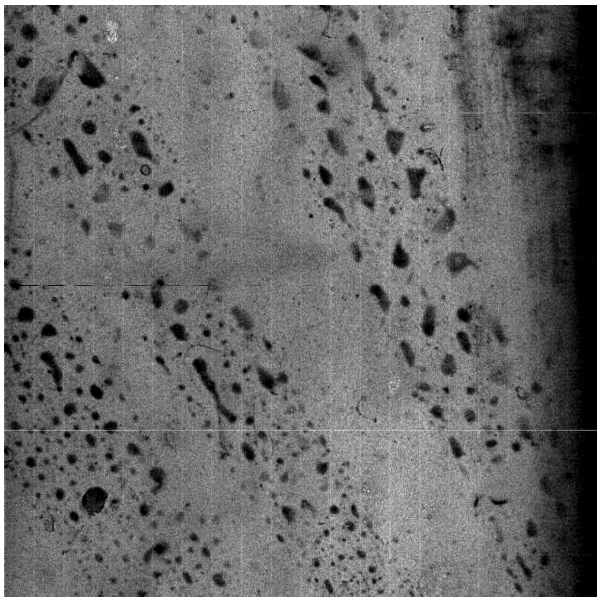

Figure 4.13. Best underdrawing image for the painted patch of two layers of lead-tin yellow over underdrawing of bone black in gum executed with a quill pen (image: width 10 mm, height 10 mm).

4.4. Underdrawings of Paintings

An example of imaging underdrawings in a 16th C painting *The Magdalen* is shown in Fig. 4.14. In this painting the underdrawing was easily visible to the naked eye (Fig. 4.14b). The area was scanned in order to determine whether the underdrawing is visible in the OCT images at 930 nm. In Fig.4.14d the different paint layers and underdrawings of the painting are shown in a cross-sectional image. It can be clearly differentiated between the top layer of varnish and the second layer of red lake. Below the red lake layer there is another layer visible, which could be either chalk ground or a priming layer. The dark bands in the cross-sectional images correspond to the underdrawing lines. The underdrawing image of the red drapery is shown in Fig. 4.14c.

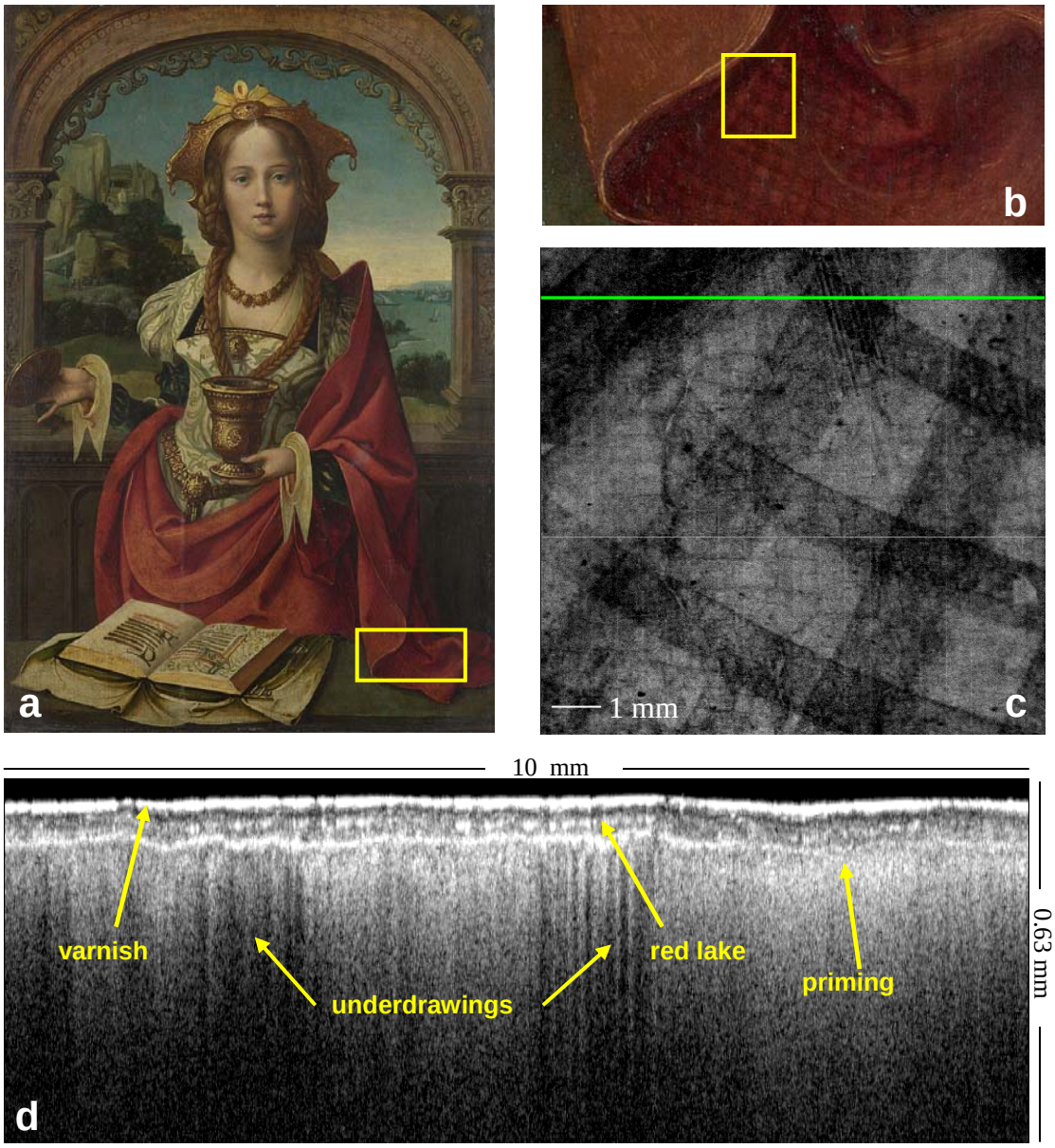

Figure 4.14. a) A region on the red drapery in the painting The Magdalen by an anonymous Netherlandish artist (National Gallery No. 719). b) detail of a). c) OCT en-face image (930 nm) at the depth of the underdrawing corresponding to the region marked by a yellow box in c). d) OCT cross-section image (930 nm) of the region marked by a green line segment in c).

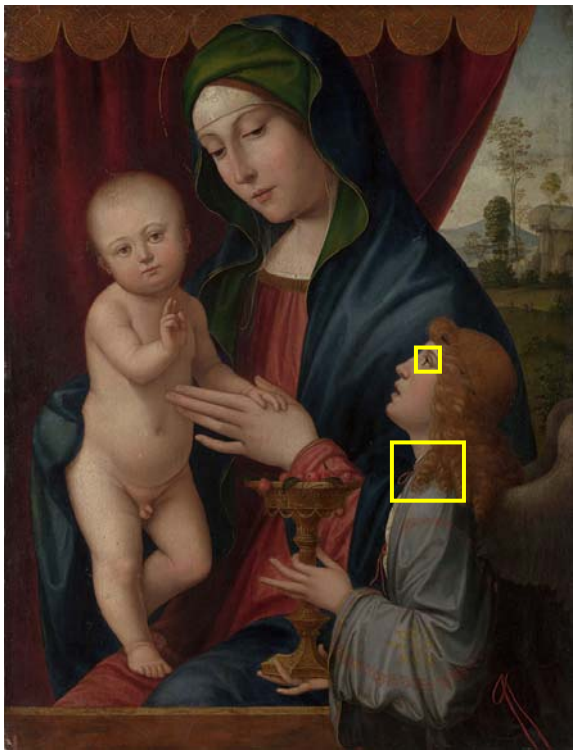

Figure 4.15. Francesco Francia, The Virgin and Child with an Angel (NG 3927). The yellow boxes indicate the position of the Fig. 4.16a and Fig. 4.17. Photo © The National Gallery, London.

Another example of imaging underdrawing of paintings is shown in Fig. 4.16. The painting *The Virgin and Child with an Angel* (Fig. 4.15) has already been imaged with a SIRIS digital infrared camera. From this image (Fig.4.16b) it can be seen that *pouncing* was used to transfer the motif onto the canvas and the underdrawing lines appear to have been drawn with a dry medium. The better resolution and contrast of the OCT image shows with greater certainty that a dry medium was used (Fig. 4.16c).

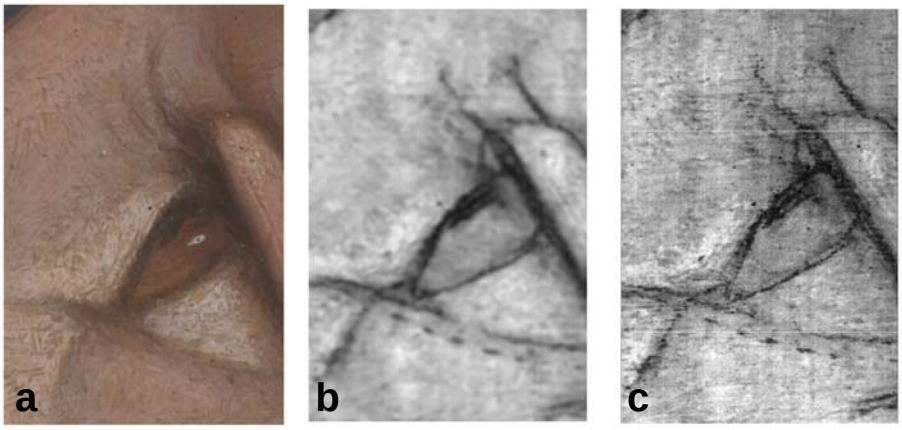

Figure 4.16. a) Francesco Francia, The Virgin and Child with an Angel (NG 3927), detail of the angel's eye. Photo © The National Gallery, London. b) near infrared image from SIRIS of the same area c) 930 nm en-face OCT image. Image size: 10 mm x 15 mm.

One of the largest OCT scans is shown in Fig. 4.17. The scan has a maximum width of 3.2 cm and a maximum length of 3.1 cm. It shows that OCT is capable of scanning larger areas than traditional thought possible. In the past OCT images have been around a maximum of 1cm x 1cm. The OCT system is able to scan areas with the maximum size of 15 cm x 15 cm with the present set-up. Through a change of the translation stages the system would be capable of much larger scans.

Figure 4.17. Francesco Francia, The Virgin and Child with an Angel (NG 3927), detail of the virgins's curls. Photo © The National Gallery, London. The 930 nm OCT images are laid over the photo of the painting.

5. Conclusion

In this thesis, applications of OCT to conservation and studies of art history have been presented. A comprehensive survey of VIS-NIR reflectance spectra provided not only the determination of the best spectral window for OCT images of paint layers, but also a reference library for the identification of historic artists' pigments. By extending the wavelength range into the NIR, additional spectral features that are unique to each pigment are revealed, allowing more conclusive identification. The positions of the peaks in the spectra are found to shift as the particle size changes, which needs to be considered when identifying pigments based on their spectra. The successes and limitations of non-invasive identification of pigments on actual paintings using this VIS-NIR reference spectral library along with newly developed algorithms for spectral identification will be based on this work.

In this project the spectral reflectance of 50 different pigments in linseed oil or egg tempera have been measured over the visible and near infrared spectral range. The effects of different concentration, particle size, binding medium and the addition of various amounts of lead white have been investigated. These effects need to be considered for pigment identification.

The optimum wavelength for revealing underdrawings (i.e. for maximum penetration into a painting) has been identified for OCT and near Infrared imaging to be ~2.2-2.3 μm over the range from 400 to 2400 nm. The general trend is that the pigments in linseed oil or egg tempera are more transparent with increasing wavelength over the VIS-NIR spectral range. By separating the paints into colour groups it had been shown that the general trend is not dependent on the colour group. There are few exceptions to the rule. For example the blue paint smalt in linseed oil and egg tempera tend to be more transparent from 750 nm up to 1100 nm, but still it is comparably transparent at 2.2-2.3 μm.

Different methods of measuring the refractive index of paint and varnish samples have been discussed. Direct methods of measuring the refractive index of samples painted on microscope glass slides using the ratio between optical and physical thickness were shown to be able to achieve accuracies of 0.03 in RI for samples of ~200 μm thickness. The focus tracking method could not be performed with the Thorlabs OCT system used in this work. An electronically controlled micrometer screw attached to the reference mirror with an accuracy of 1 micron is needed in order to achieve a 0.02 accuracy in refractive index for samples of 100 μm. Further improvements in refractive index measurement can be achieved by fitting the sample interfaces with Gaussians to obtain higher position accuracy.

The results of monitoring cleaning treatments demonstrate the potential of OCT for this new application. Preliminary results showed a difference less than 6 microns (2 pixels) between the calculated paint surface and the cleaned paint surface. This method will need further improvements, i.e. the correction of optical effects due to image distortion at large angles of incidence.

OCT applied to the study of underdrawings is a novel technique which provides better contrast and higher resolution images than conventional direct imaging techniques. In this work we have shown a method to obtain the best quality underdrawing image using an OCT. Median averaging of *enface* images in the depth range with the best contrast values gives the optimum underdrawing image. *Enface* images further below the paint/underdrawing interface or sometime below the underdrawing layer (i.e. in the shadows of the underdrawing) give better contrast because of the reduced effect from multiple scattering. One of the largest OCT scans given in Fig. 4.17 shows that OCT is

capable of scanning areas as large as 3.2 cm x 3.1 cm. In the past, the largest OCT images have been around 1cm x 1cm.

References

Adler, D. C., Stenger, J., Gorczynska, I., Lie, H., Hensick, T., Spronk, R., Wolohojian, S., Khandekar, N., Jiang, J. Y.,Barry, S., Cable, A.. E., Huber, R.., and Fujimoto, J. G., 'Comparision of three-dimensional optical coherence tomography and high resolution photography for art conservation studies' , *Opt. Express* 15, 15972-15986 (2007).

Arecchi, T., Bellini, M., Corsi, C., Fontana, R., Materazzi, M., Pezzati, L., Tortora, A., 'Optical coherence tomography for painting diagnostics', Vol. 5857 of *Proceedings of SPIE*, pp. 278–282, Munich, Germany, June 2005.

Bacci, M., 2000, 'UV-VIS-NIR, FT-IR, and FORS spectroscopies'. In *Modern Analytical Methods in Art and Archaeology*, Ciliberto, E. and Spoto, G. (eds.) 321-361. New York: John Wiley & Sons.

Bajraszewski, T., Gorczynska, Rouba, B., I., Targowski, P., 'Spectral domain Optical Coherence Tomography as the Profilometric Tool for Examination of the Enviromental Influence on Paintings on Canvas', in *Proceedings of the 6th International Congress on Lasers in the Conservation of Artworks (LACONA VI '05)*, J. Nimmrichter, W. Kautek, and M. Schreiner, Eds., Vienna, Austria, September 2006.

Bayerer, F. 1996, '*Die Untersuchung von Kunstobjekten mit Hilfe der bildgebenden Spektroskopie*', München: Herbert Utz Verlag Wissenschaft.

Berns, R. S., de la Rie, E. R., ,The relative importance of surface roughness and refractive index in the effect of varnishes on the appearance of paintings', *ICOM Committee for Conservation, 13th Triennial Meeting*, Rio de Janeiro, Vol. I, 211-216 (2002).

Birney, D. S., Gonzalez, G., Oesper, D., 2006. *Observational Astronomy*. Cambridge University Press.

Bohren C. F. & Huffman D. R., 2004. *Absorption and scattering of light by small particles*. Wiley-VCH Verlag, Weinheim.

Born, M. & Wolf, E., 1999. *Principles of Optics: Electromagnetic Theory of Propagation, Interference and Diffraction of Light*. 7th ed. Cambridge University Press.

Brezinski, M.E., 2006. *Optical Coherence Tomography: Principles and Applications*. Burlington: Academic Press (Elsevier).

Brill, T. B., 1980. *Light: Its Interaction with Art and Antiquities*. New York: Plenum Press.

Bomford, D., 2002. *Art in the Making: Underdrawings in Renaissance Paintings*. Butler and Tanner.

Carl Zeiss Meditec AG. 2006. Visante™ OCT Anterior Segment Imaging & Biometry. A new perspective in clinical confidence. [online]. Jena: Carl Zeiss Meditec AG. Available at: http://www.meditec.zeiss.com/88256DE3007B916B/0/A188B8428919BC35882571B1005DED22/$file/visanteoct_engl.pdf [accessed 18 May 2008].

de la Rie, E. R., 'The influence of varnish on the appearance of paintings', *Studies in Conservation*, 32, 1-13 (1987).

Delaney, J.K., Metzger, C., Walmsley, E., Fletcher, C., 'Examination of the Visibility of Underdrawing Lines as a Function of Wavelength', *ICOM Committee for Conservation, 10th Triennial Meeting*, Washington, D.C., Vol. I, 15-19 (1993).

Delaney, J. K., Walmsley, E., Berrie, B. H., Fletcher, C. F., 'Multispectral imaging of paintings in the infrared to detect and map blue pigments', Sackler NAS Colloquium – Scientific Examination of Art: Modern Techniques in Conservation and Analysis, 120-136 (2005).

Gargano, M., Ludwig, N., Poldi, G., 'A new methodology for comparing IR reflectographic systems', *Infrared Physics & Technology*, Volume 49, Issue 3, p. 249-253 (2006).

Gora, M., Targowski, P., Rycyk, A., Marczak, J., 'Varnish Ablation Control by Optical Coherence Tomography', *Laser Chemistry*, Article ID 10647 (2006).

Gorczynska, I., Wojtkowski, M., Szkulmowski, M., Bajraszewski, T., Rouba, B., Kowalczyk, A., Targowski, P., 'Varnish Thickness Determination by Spectral Optical Coherence Tomography', in *Proceedings of the 6th International Congress on Lasers in the Conservation of Artworks LACONA VI, Vienna, Austria 2005*, Springer, Berlin, Germany, 2006.

Hecht, E., 2003. *Optics*. 4th ed. Amsterdam: Addison-Wesley Longman.

Huang, D., Swanson, E., Lin, C., Schuman, J., Stinson, W., Chang, W., Hee, M., Flotte, T., Gregory, K., Puliafito, C., and Fujimoto, J., 'Optical Coherence Tomography', Science, Vol. 254, pp. 1178-1181 (1991).

Kubelka, P., Munk, F., 'Ein Beitrag zur Optik der Farbanstriche', *Zeits. f. tech. Phys.* 12, S. 593-601 (1931).

Kubelka, P., 'New Contributions to the Optics of Intensely Light Scattering Materials. Part I', *Journal of the Optical Society of America*, Volume 38, Number 5, 448-454 (1948).

Liang, H., Cid, M., Cucu, R., Dobre, G., Jackson, D., Pannell, C., Pedro, J., Saunders, D., Podoleanu, A., 'Application of OCT to examination of easel paintings', *Second European Workshop on Optical Fibre Sensors*, Proc. SPIE 5502, 378-381 (2004).

Liang, H., Cid, M., Cucu, R., Dobre, G., Podoleanu, A., Pedro, J. and Saunders, D., 'En-face optical coherence tomography – a novel application of non-invasive imaging to art conservation', *Opt. Express* 13, 6133-6144 (2005a).

Liang, H., Cid, M., Cucu, R., Dobre, G., Kudimov, B., Pedro, J., Saunders, D., Cupitt, J., and Podoleanu, A., 'Optical Coherence Tomography: A non-invasive technique applied to conservation of paintings', SPIE, Munich, Germany, 261-269, (2005b).

Liang, H., Peric, B., Spring, M., Saunders, D., Hughes, M., Podoleanu, A., 'Non-invasive imaging of subsurface paint layers with optical coherence tomography', *Conservation*

Science 2007, Milan, *10-11 May 2007*, Joyce Townsend et al., eds. (Archtype publishing, London, 2008), pp. 171-17 (2007a).

Liang, H., Peric, B., Hughes, M., Podoleanu, A., Spring, M., Saunders, D., 'Optical coherence tomography for art conservation and archaeology', *Proc. SPIE*, Vol. 6618, O3A: Optics for Arts, Architecture, and Archaeology, 2007, pp. 661805-1..661805-12 DOI: 10.1117/12.726032 (2007b).

Maruyama, H., Inoue, S., Mitsuyama, T., Ohmi, M., Haruna, M., 'Low-coherence interferometer system for the simultaneous measurement of refractive index and thickness', *Applied Optics*, Vol. 41, No. 7, 1315-1322 (2002).

McNeil, L. E., French, R. H., ‚Light scattering from red pigment particles: Multiple scattering in a strongly absorbing system', *Journal of Applied Physics*, Volume 89, Number 1, 283-293 (2001).

Phenix, A., Sutherland, K., 'The cleaning of paintings: effects of organic solvents on oil paint films', *Reviews in Conservation*, Number 2, 47-60 (2001).

Phillips-Invernizzi, B., Dupont, D., Caze, C., 'Bibliographical review for reflectance of diffusing media', *Opt., Eng.*, 40(6), 1082-1092 (2001).

Saunders, D., Billinge, R., Cupitt, J., Aktinson, N, Liang, H., ‚A New Camera for High-Resolution Infrared Imaging of Works of Art', *Studies in Conservation* 51, 277-290 (2006).

Stifter, D., 'Beyond biomedicine: a review of alternative applications and developments for optical coherence tomography', *Appl. Phys. B*, Vol. 88, p. 337-357(2007).

Sutherland, K., 2001. *Solvent extractable components of oil paint films*. Ph. D., University of Amsterdam.

Szkulmowska, A., Gora, M., Targowska, M., Rouba, B., Stifter, D., Breuer, E., and Targowski, P., 'The application of optical coherence tomography at 1.55 μm to the examination of oil paintings', in *Proceedings of the 6th International Congress on Lasers in the Conservation of Artworks (LACONA VI '05)*, J. Nimmrichter, W. Kautek, and M. Schreiner, Eds., Vienna, Austria, September 2006.

Targowski, P., Rouba, B., Wojtkowski, M., and Kowalczyk, A., 'The application of optical coherence tomography to non-destructive examination of museum objects', *Studies in Conservation* 49, 107-114 (2004).

Targowski, P., Gora, M., Bajraszewski, T., Szkulmowski, M., Rouba, B., Lekawa-Wyslouch, T., Tyminska-Widmer, L., 'Optical Coherence Tomography for Tracking Canvas Deformation', Laser Chem., Article ID 93658, 8 pages (2006a).

Targowski, P., Gora, M., Wojtkowski, M., 'Optical coherence tomography for artwork diagnostics', Laser Chem., Article ID 35373, 11 pages (2006b).

Taylor, D., 'Optical Properties of Pigments in the Near Infra-Red', *The Journal of the Oil and Colour Chemists' Association* 41, No. 10 (1958).

Tearney, G. J., Brezinski, M. E., Southern, J. F., Bouma, B. E., Hee, M. R., Fujimoto, J. G., 'Determination of the refractive index of highly scattering human tissue by optical coherence tomography', *Optics Letters*, 20 (21), 2258-2260 (1995) .

The Burlington Magazine, 'Editorial: The National Gallery Cleaning Controversy', *The Burlington Magazine*, Vol. 104, No. 707, pp. 49-50. (1962).

Tomlins, P. H., Wang, R. K., ,Theory, developments and applications of optical coherence tomography', *Appl. Phys.* 38, 2519-2535 (2005).

Townsend, J. H., 'The Refractive Index of 19th-Century Paint Media: A Preliminary Study', *ICOM Committee for Conservation, 10th Triennial Meeting*, Washington, D.C., Vol. II, 586-592 (1993).

van Asperen de Boer, J. R. J., 'Infrared Reflectograms of Panel Paintings', *Studies in Conservation*, Vol. 11, No. 1., 45-46 (1966).

van Asperen de Boer, J. R. J., 'Infrared Reflectography: a Method for the Examination of
Paintings', *Applied Optics* 7, 1711-1714 (1968).

van Asperen de Boer, J. R. J., 'Reflectography of paintings using an infra-red vidicon television system', *Studies in Conservation* 14, 96-118 (1969).

Walmsley, E., Metzgerm, C., Delaney, J. K., Fletcher, C., 'Improved visualization of underdrawings with solid-state detectors operating in the infrared', *Studies in Conservation* 39, 217-231 (1993).

Wang, H. W., Izatt, J. A., and Kulkarni, M. D., 2002. *Handbook of Optical Coherence Tomography*, ed. B. E. Bouma, and G. J. Tearney (New York: Dekker), chapter 10, pp. 275-298.

Wang, X., Zhang, C., Zhang, L., Xue, L., Tian, J., 'Simultaneous refractive index and thickness measurements of bio tissue by optical coherence tomography', Journal of Biomedical Optics, Vol. 7, No. 4, 628-632 (2002).

Westphal, V., Rollins, A. M., Radhakrishnan, S., Izatt, J. A., 'Correction of geometric and refractive image distortion in optical coherence tomography applying Fermat's principle', *Opt. Express* Vol. 10, No. 9, 397-404 (2002).

White, R., Roy, A., 'GC-MS and SEM studies on the effects of solvent cleaning on old master paintings from the National Gallery, London', *Studies in Conservation* 43, 159–176 (1998).

Yang, M.-L., Lu, C.-W., HSU, I.-J., Yang, C. C., ,The use of optical coherence tomography for monitoring the subsurface morphologies of archaic jades', *Archaeometry* 46, 171-182 (2004).

Appendix

A Reflectance Graphs

a. Blue Pigments in Egg Tempera and Linseed Oil

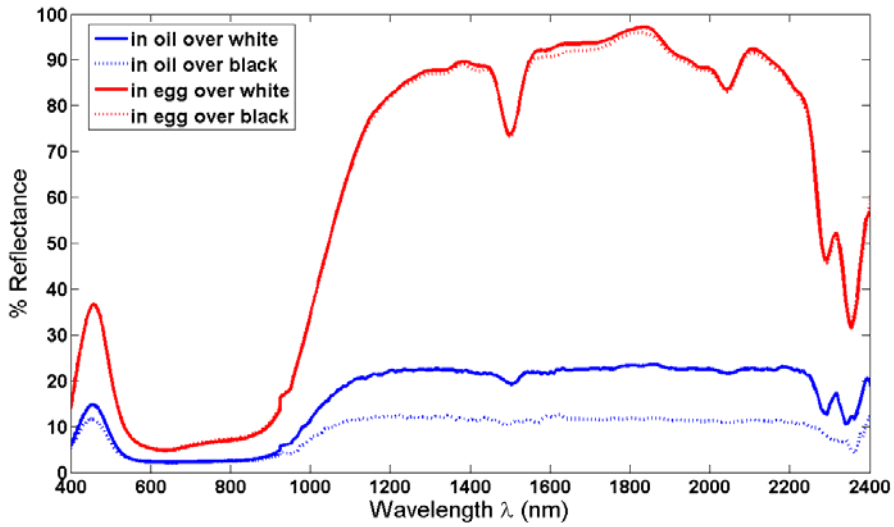

Figure a.1: Spectral reflectance of azurite (grade 1) in egg tempera and linseed oil.

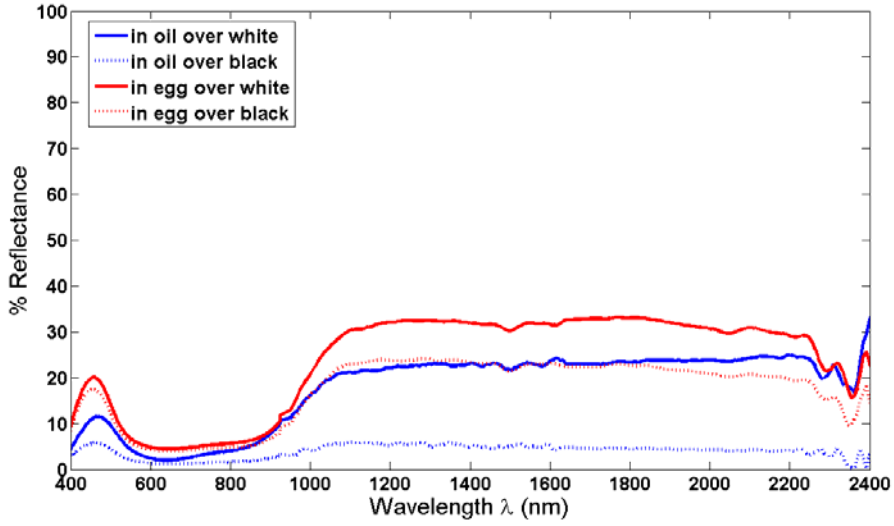

Figure a.2: Spectral reflectance of azurite (MP) in egg tempera and linseed oil.

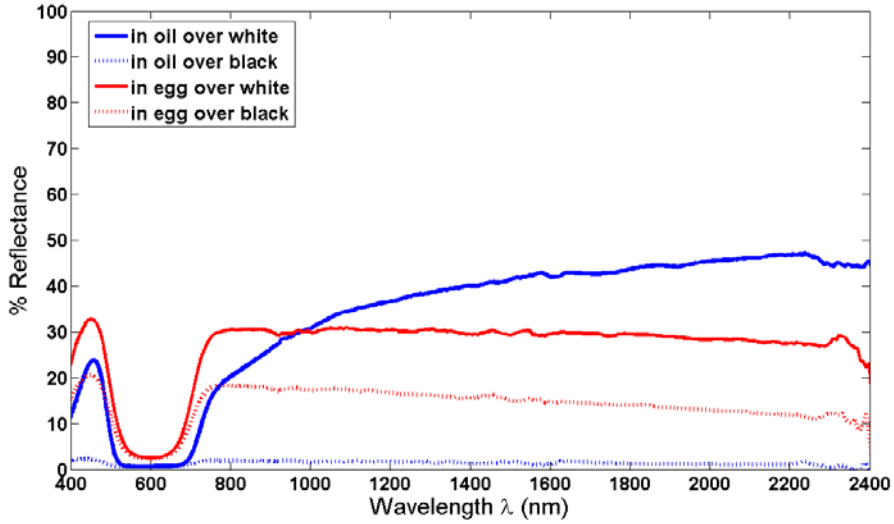

Figure a.3: Spectral reflectance of artificial ultramarine dark in egg tempera and linseed oil.

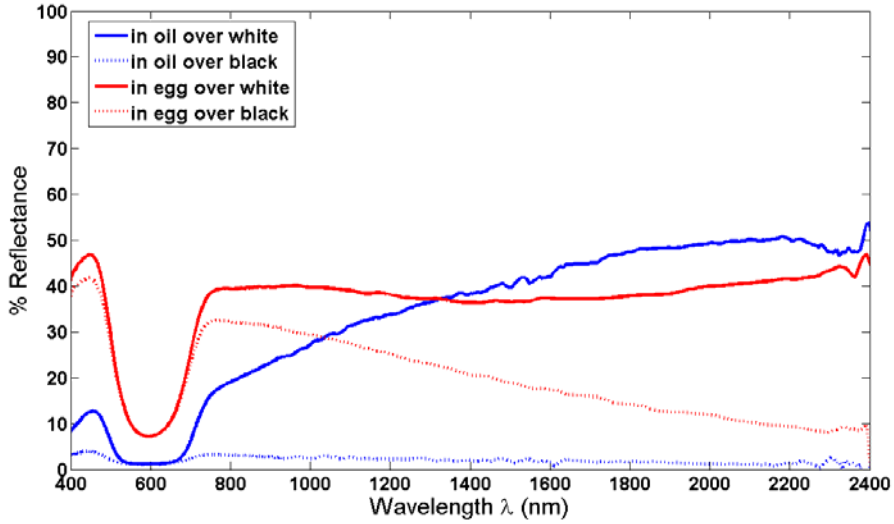

Figure a.4: Spectral reflectance of artificial ultramarine light in egg tempera and linseed oil.

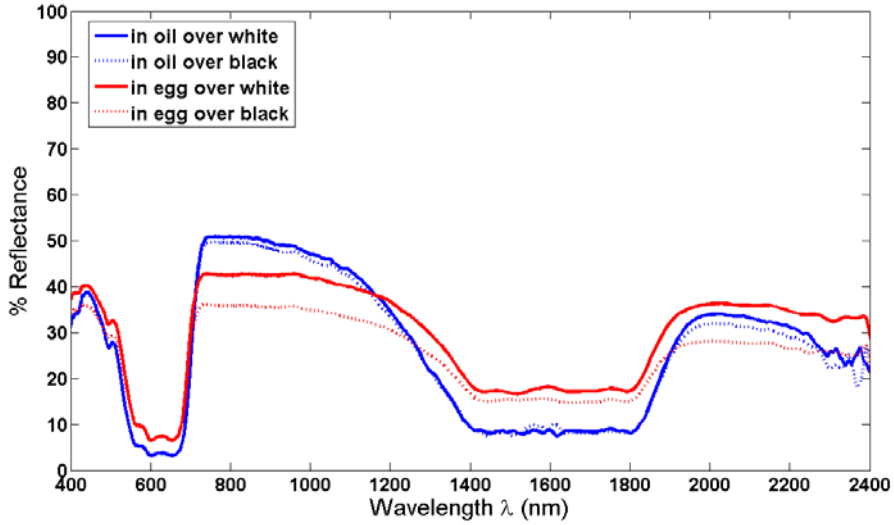

Figure a.5: Spectral reflectance of cerulean blue in egg tempera and linseed oil.

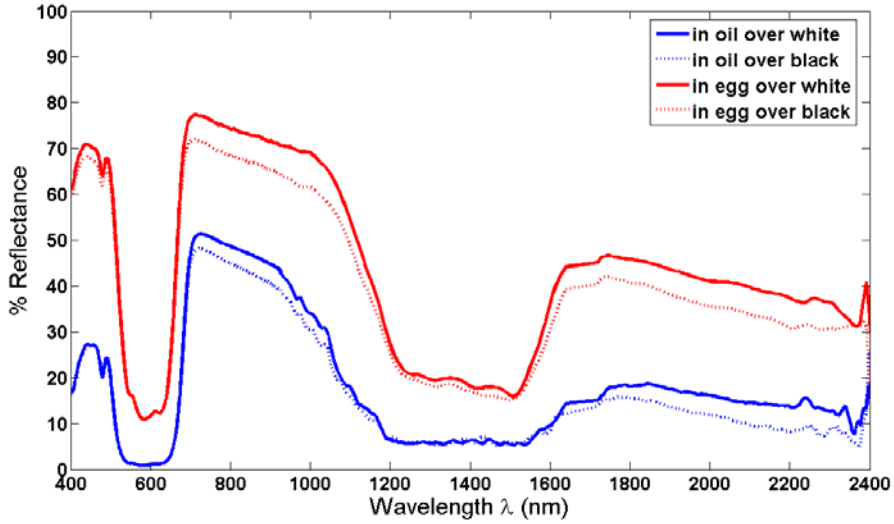

Figure a.6: Spectral reflectance of cobalt blue in egg tempera and linseed oil.

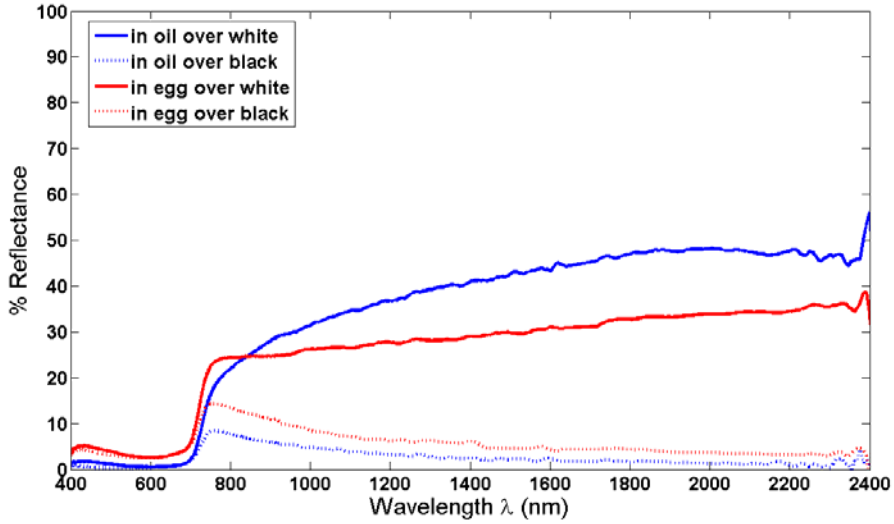

Figure a.7: Spectral reflectance of indigo in egg tempera and linseed oil.

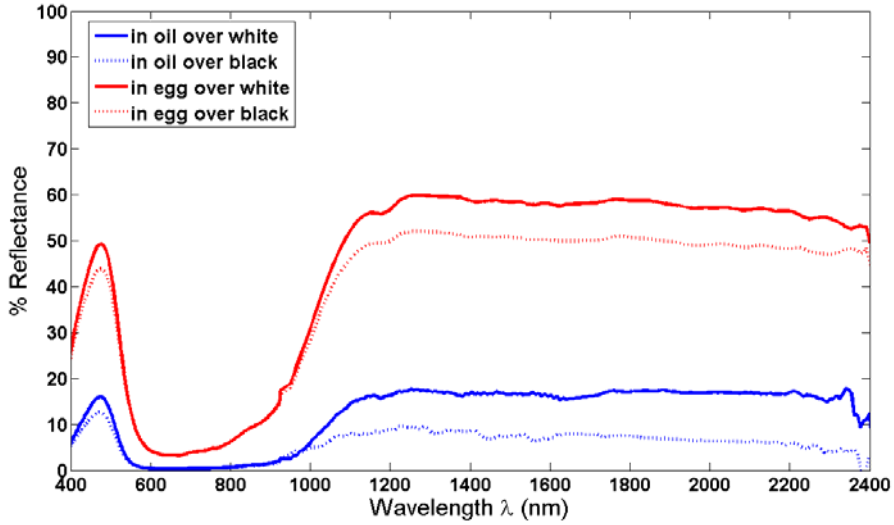

Figure a.8: Spectral reflectance of manganese blue in egg tempera and linseed oil.

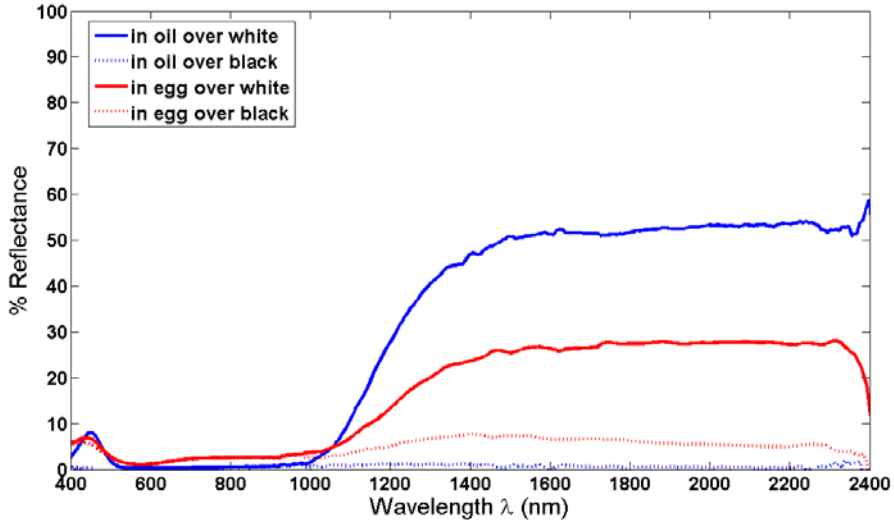

Figure a.9: Spectral reflectance of Prussian blue in egg tempera and linseed oil.

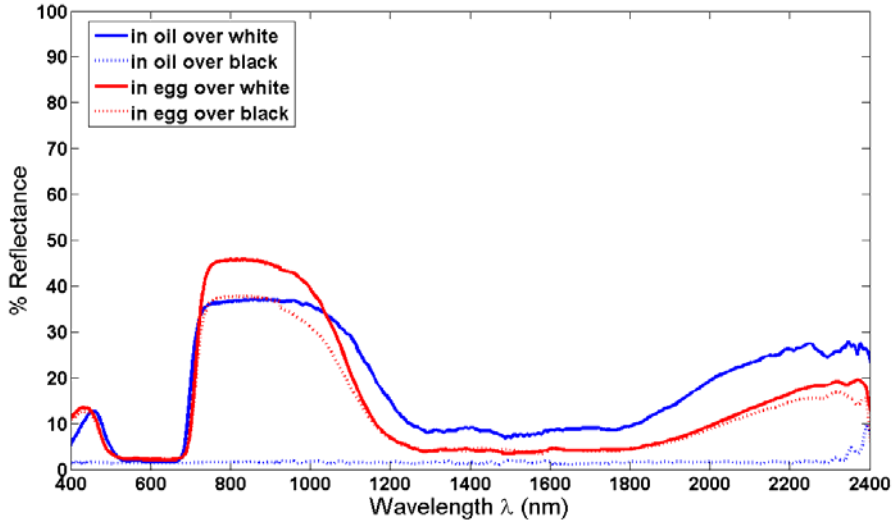

Figure a.10: Spectral reflectance of smalt in egg tempera and linseed oil.

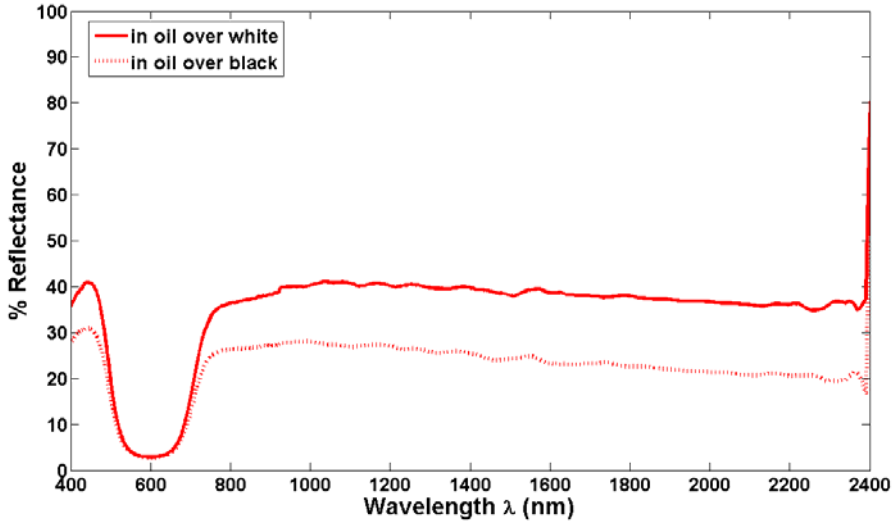

Figure a.11: Spectral reflectance of lapis lazuli deep in egg tempera.

b. Green Pigments in Egg Tempera and Linseed Oil

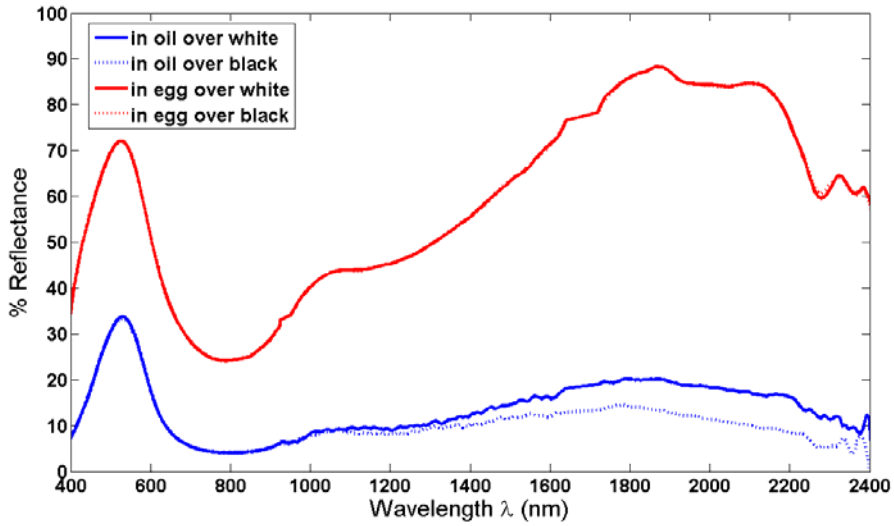

Figure b.1: Spectral reflectance of artificial malachite in egg tempera and linseed oil.

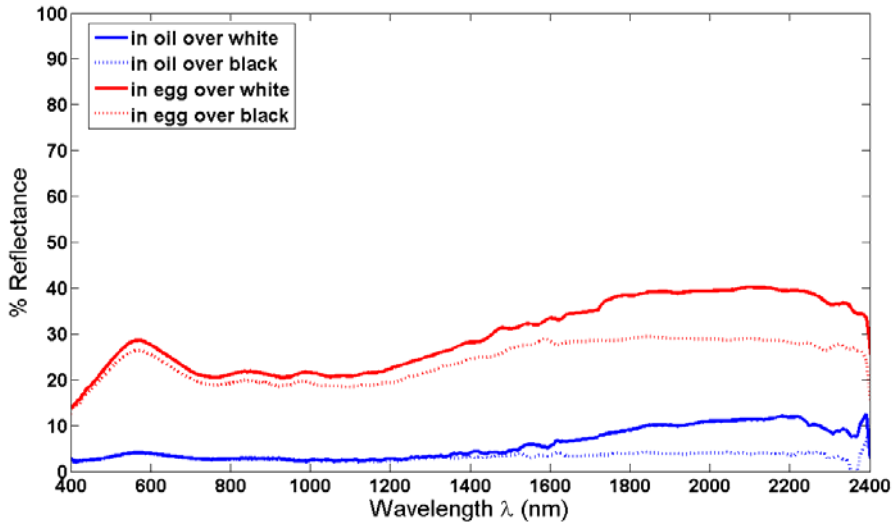

Figure b.2: Spectral reflectance of Bavarian green earth in egg tempera and linseed oil.

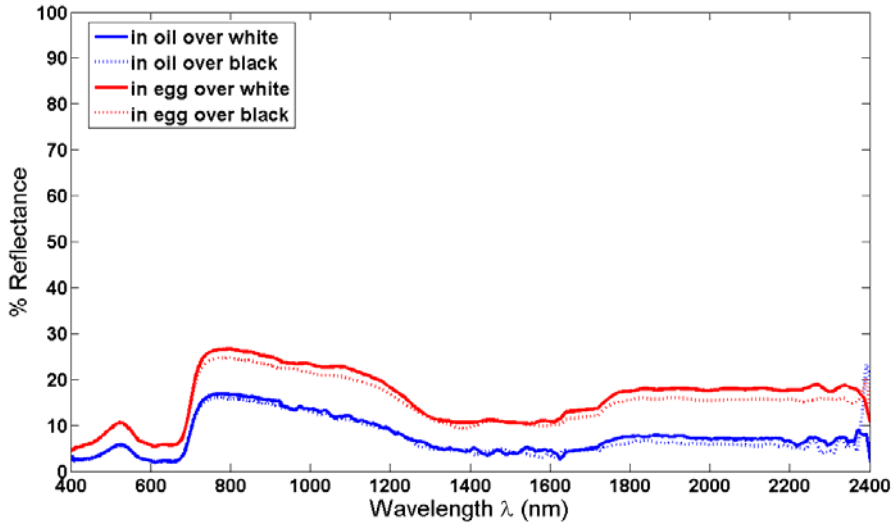

Figure b.3: Spectral reflectance of cobalt bottle green in egg tempera and linseed oil.

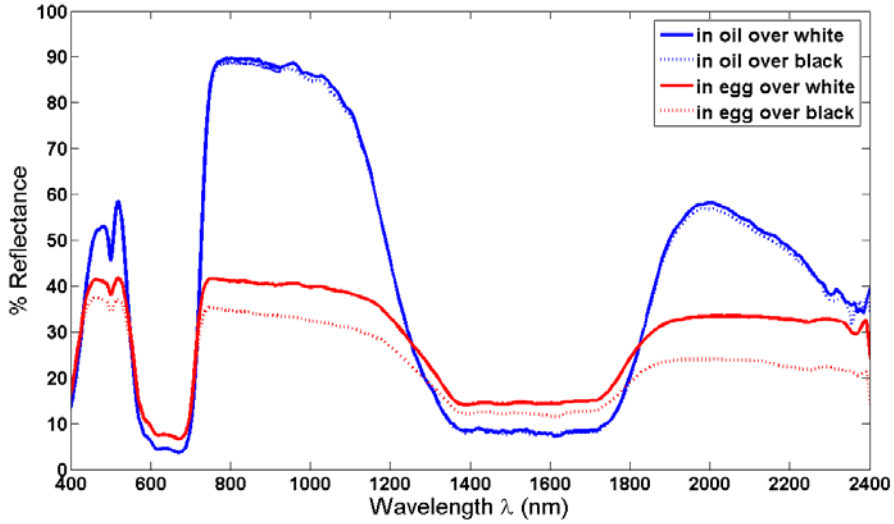

Figure b.4: Spectral reflectance of cobalt turquoise in egg tempera and linseed oil.

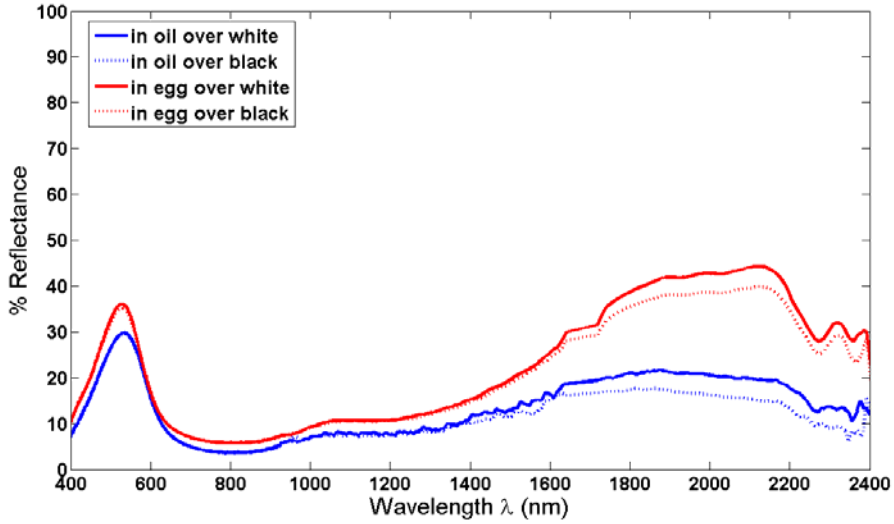

Figure b.5: Spectral reflectance of natural malachite (grade 1) in egg tempera and linseed oil.

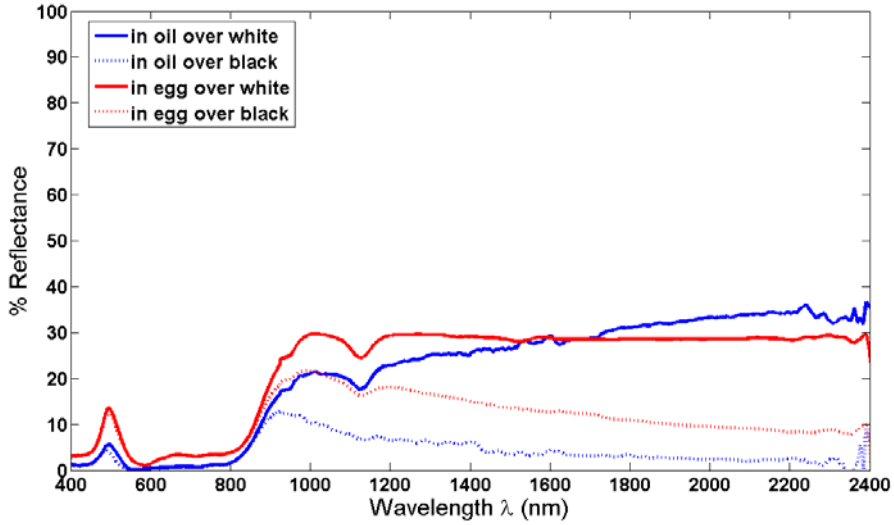

Figure b.6: Spectral reflectance of phthalo green in egg tempera and linseed oil.

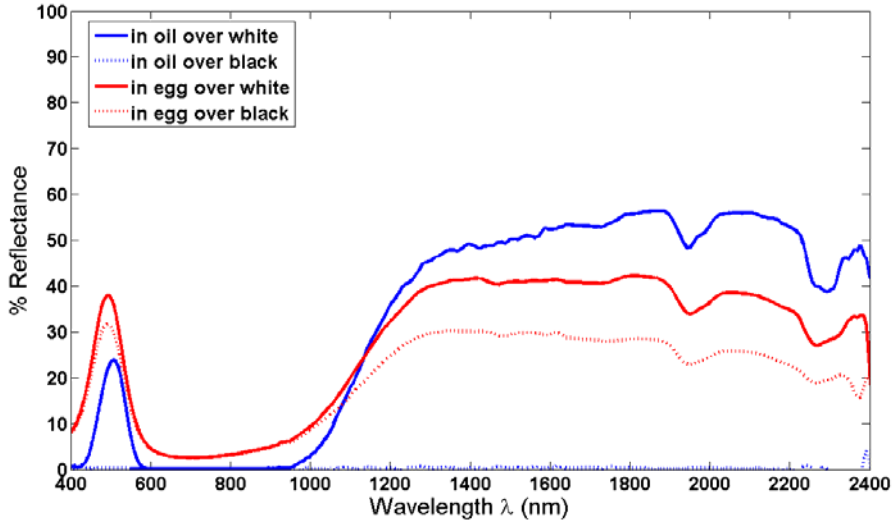

Figure b.7: Spectral reflectance of verdigris in egg tempera and linseed oil.

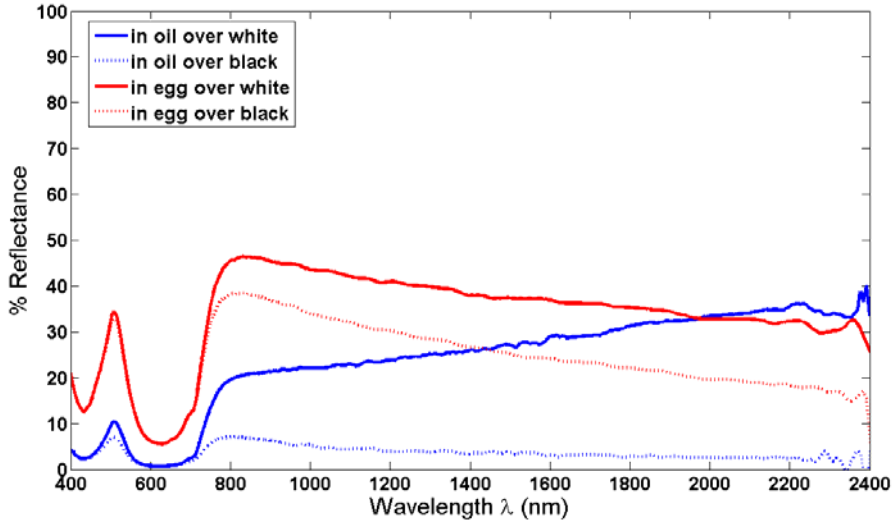

Figure b.8: Spectral reflectance of viridian green in egg tempera and linseed oil.

c. Red Pigments in Egg Tempera and Linseed Oil

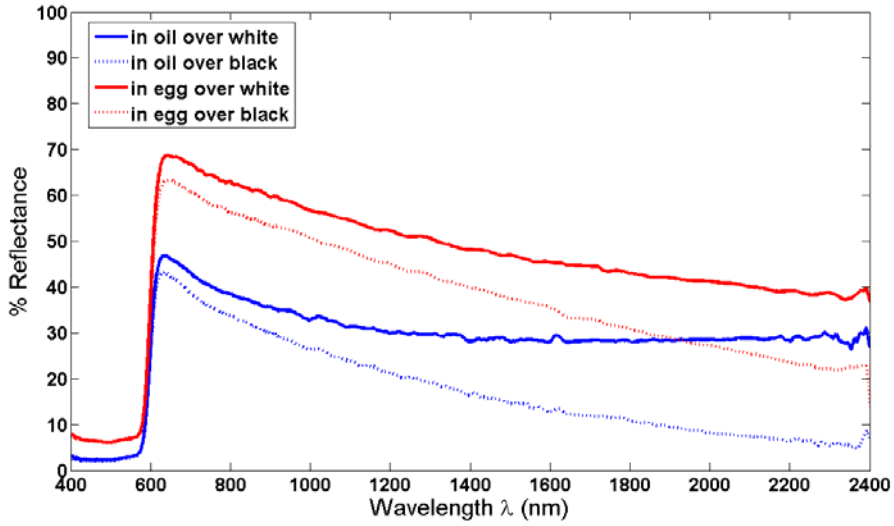

Figure c.1: Spectral reflectance of cadmium red in egg tempera and linseed oil.

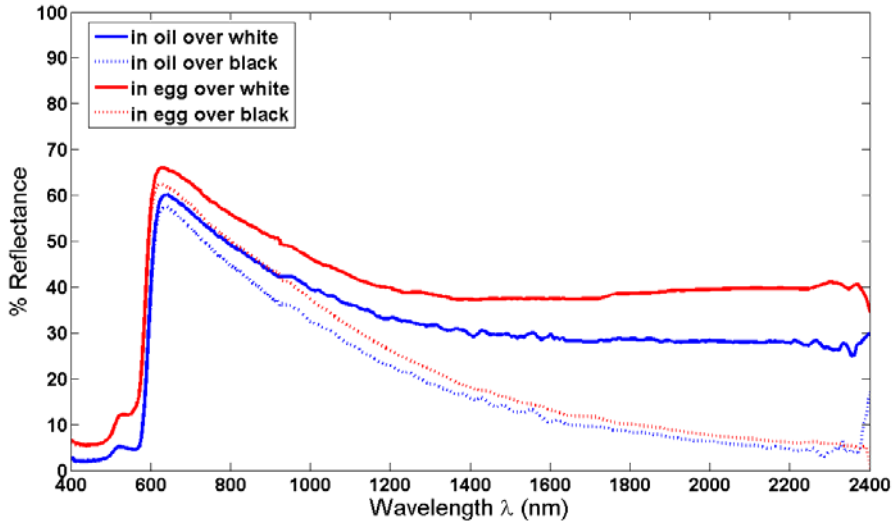

Figure c.2: Spectral reflectance of chrome red in egg tempera and linseed oil.

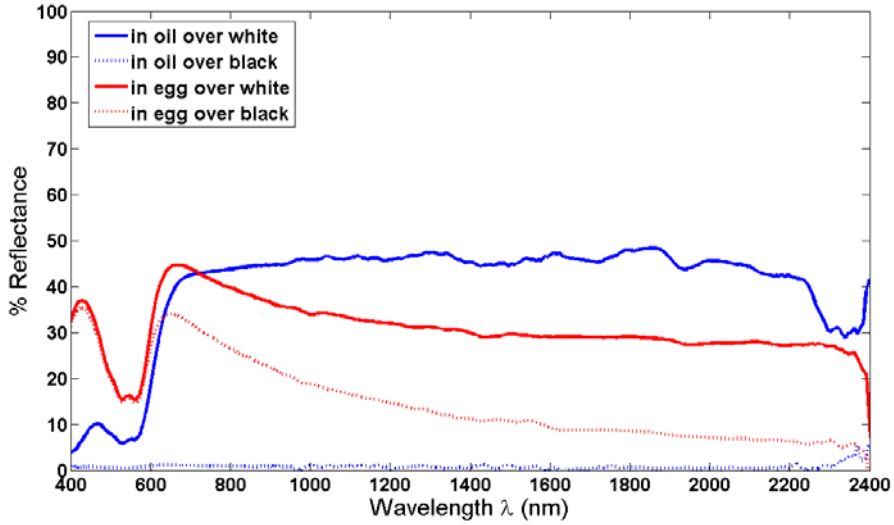

Figure c.3: Spectral reflectance of cochineal lake in egg tempera and linseed oil.

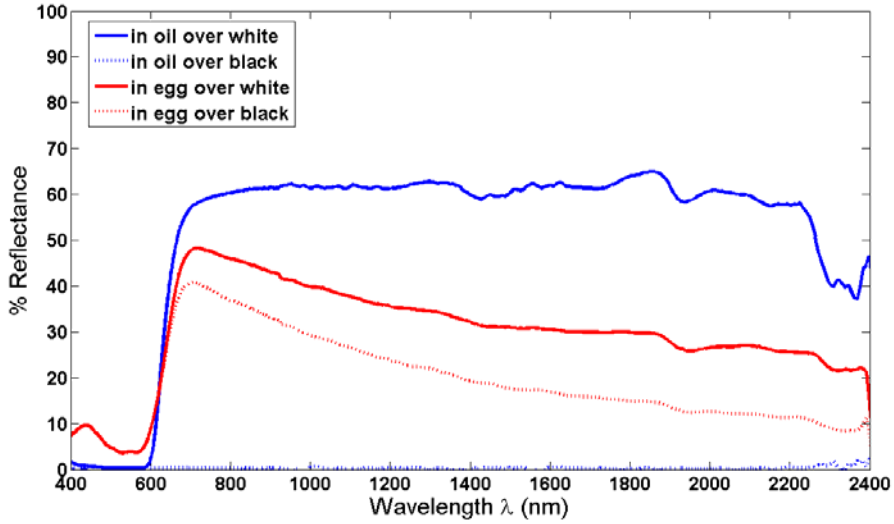

Figure c.4: Spectral reflectance of lac lake in egg tempera and linseed oil.

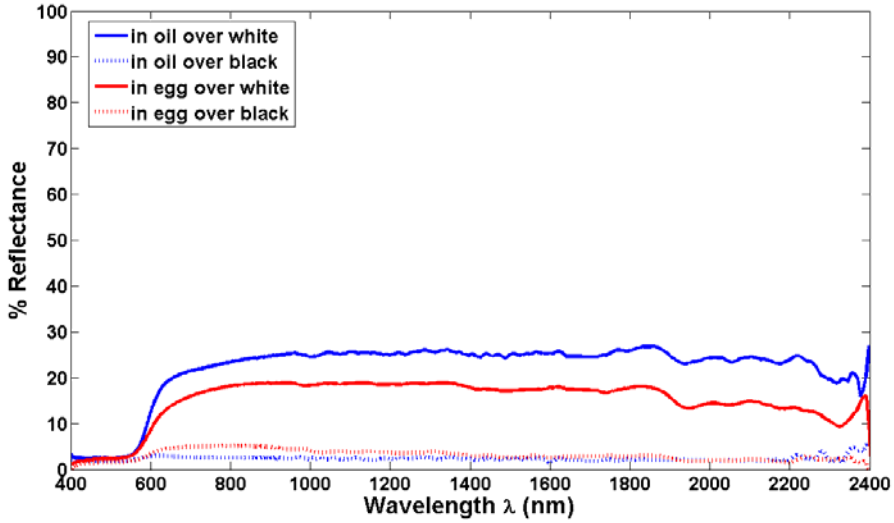

Figure c.5: Spectral reflectance of madder lake (from dyed wool) in egg tempera and linseed oil.

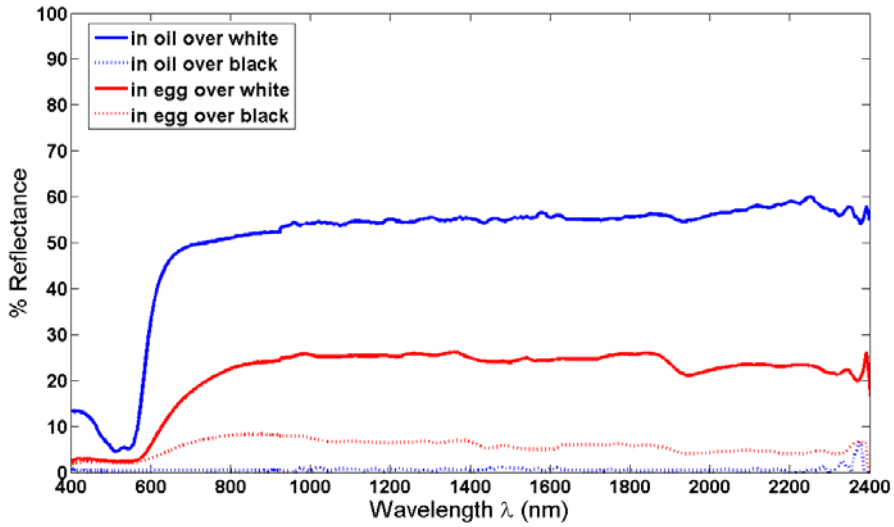

Figure c.6: Spectral reflectance of madder lake (MODHT) in egg tempera and linseed oil.

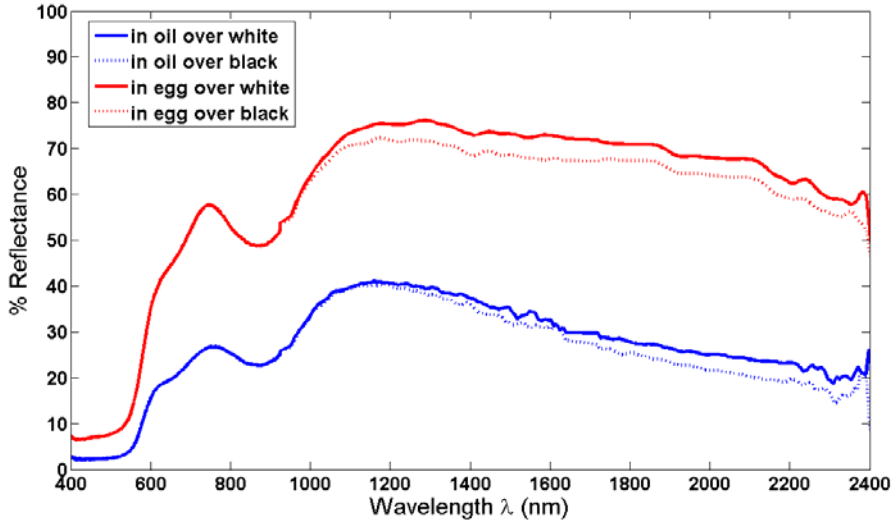

Figure c.7: Spectral reflectance of natural red earth in egg tempera and linseed oil.

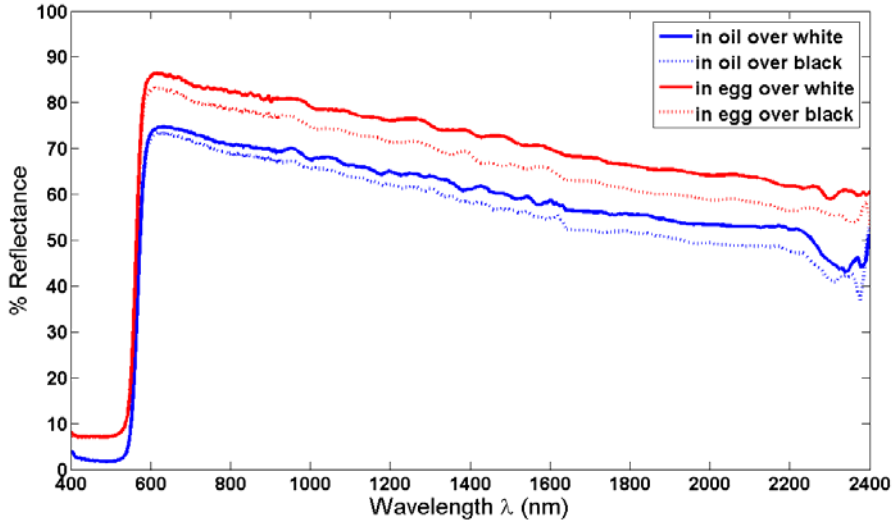

Figure c.8: Spectral reflectance of red lead in egg tempera and linseed oil.

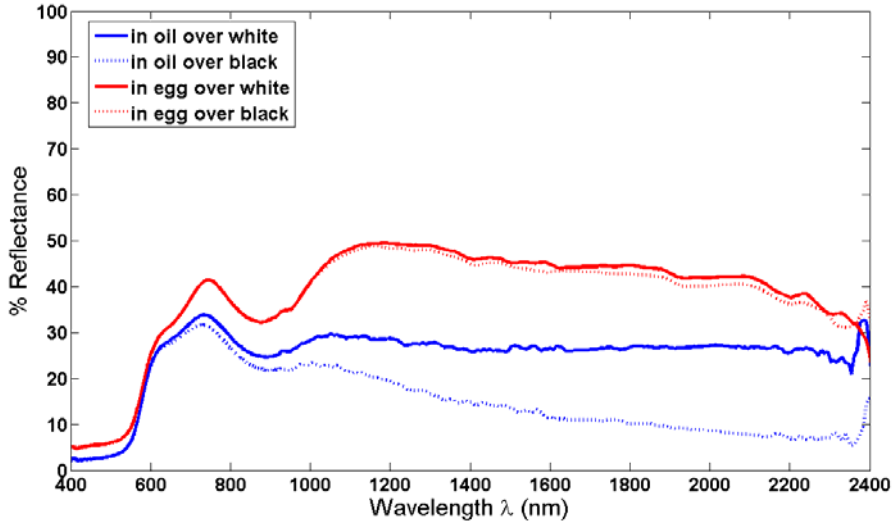

Figure c.9: Spectral reflectance of red ochre in egg tempera and linseed oil.

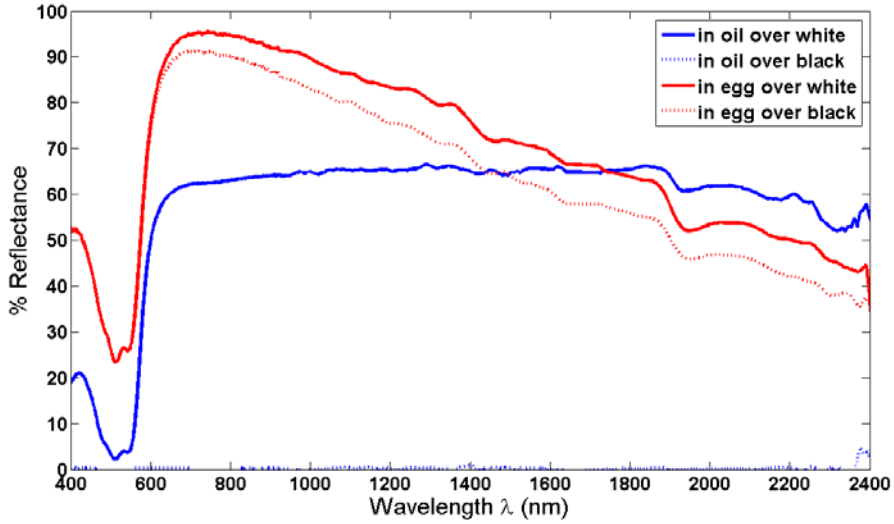

Figure c.10: Spectral reflectance of rose madder in egg tempera and linseed oil.

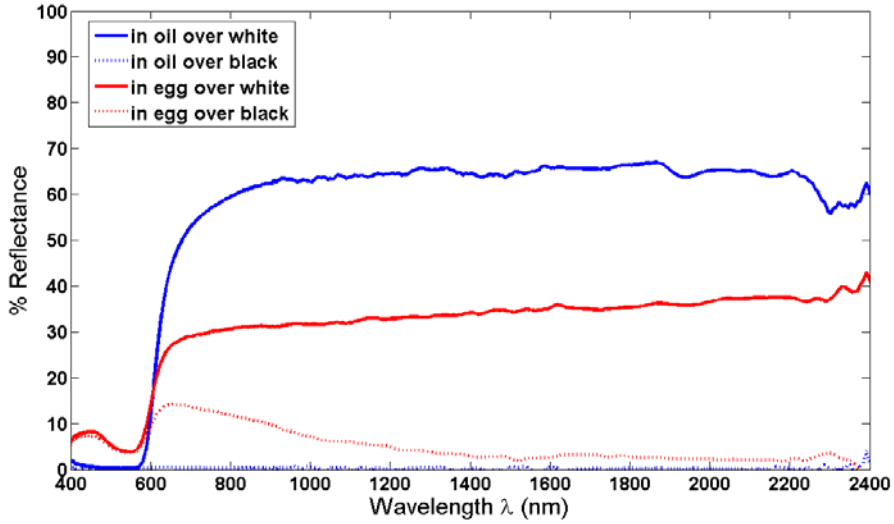

Figure c.11: Spectral reflectance of sappanwood lake in egg tempera and linseed oil.

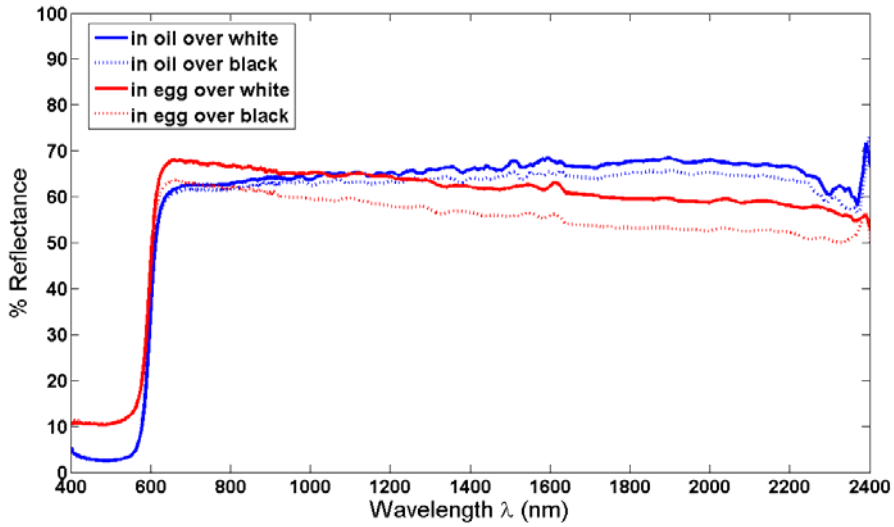

Figure c.12: Spectral reflectance of vermillion (grade 3) in egg tempera and linseed oil.

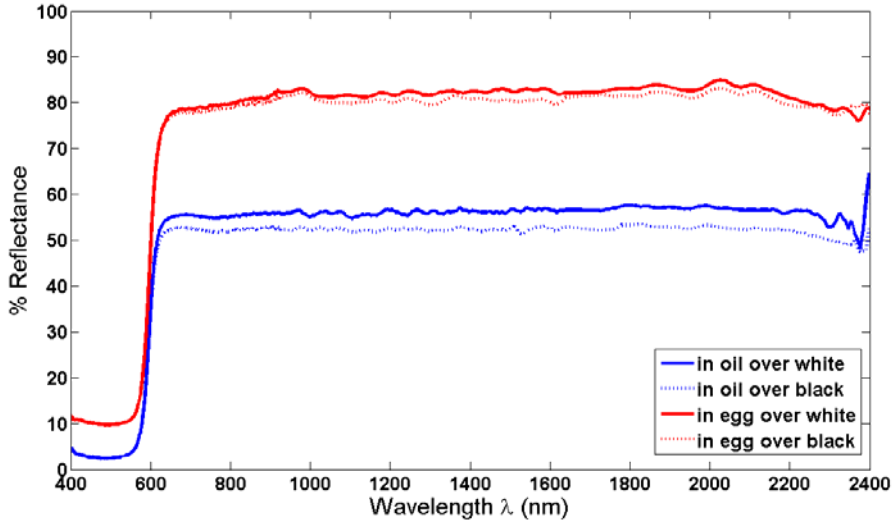

Figure c.13: Spectral reflectance of vermillion light in egg tempera and linseed oil.

d. Yellow Pigments in Egg Tempera and Linseed Oil

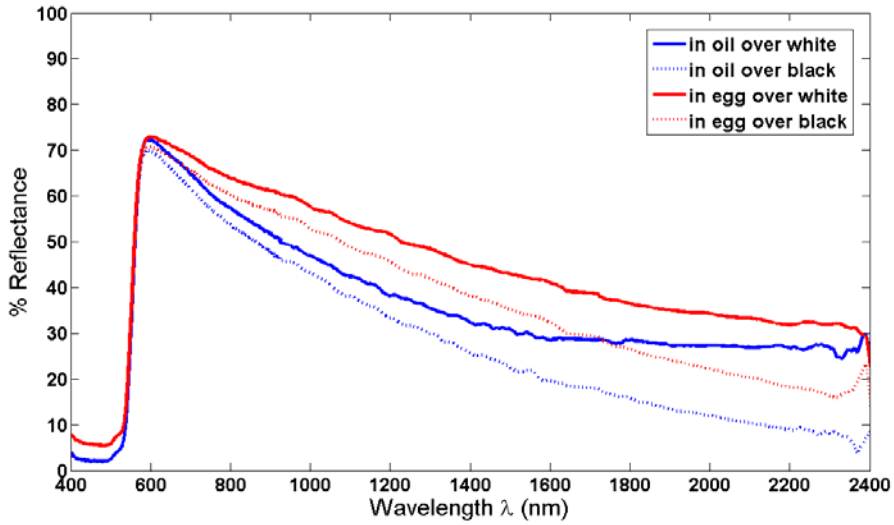

Figure d.1: Spectral reflectance of cadmium yellow deep in egg tempera and linseed oil.

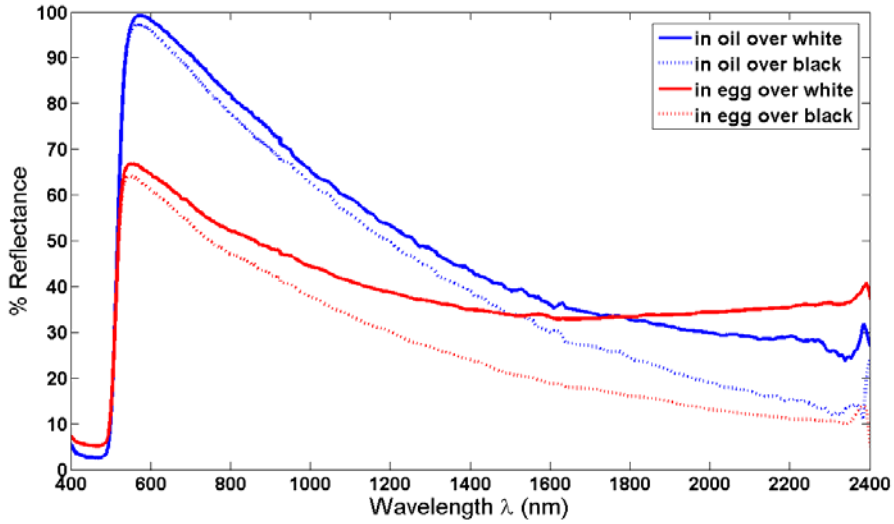

Figure d.2: Spectral reflectance of cadmium yellow light in egg tempera and linseed oil.

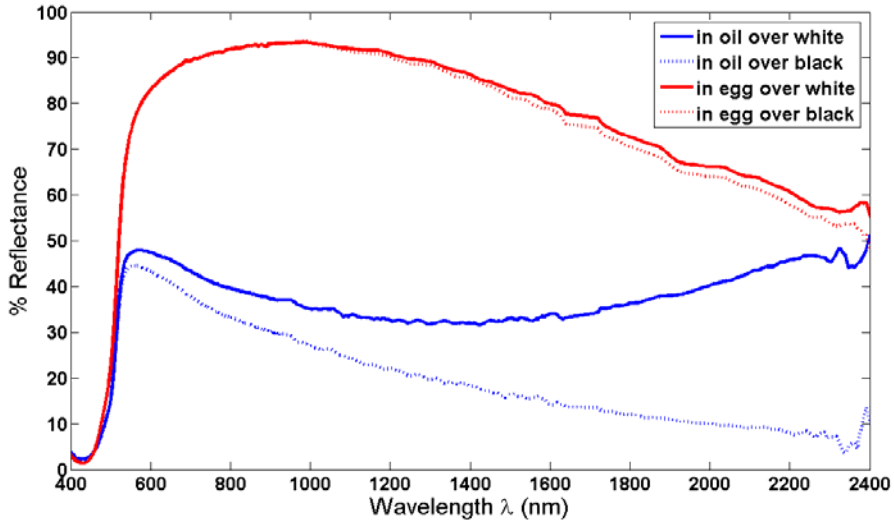

Figure d.3: Spectral reflectance of chrome yellow medium in egg tempera and linseed oil.

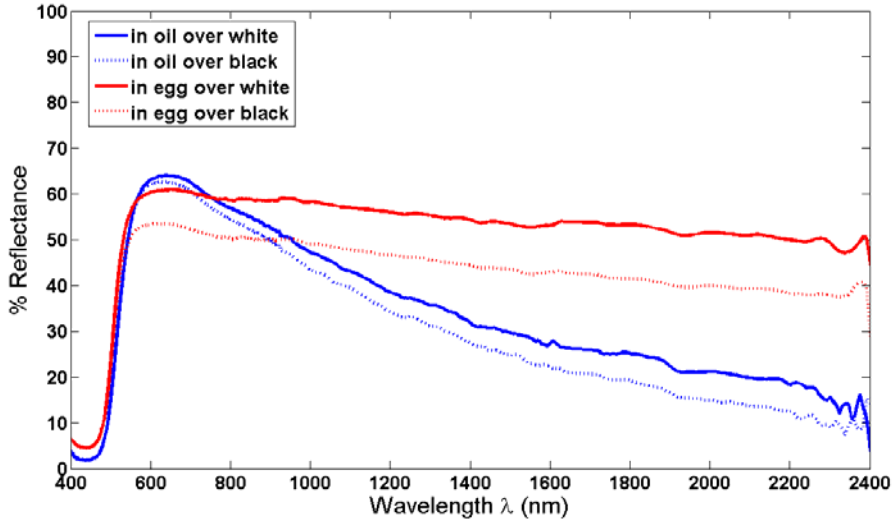

Figure d.4: Spectral reflectance of cobalt yellow (Aureolin) in egg tempera and linseed oil.

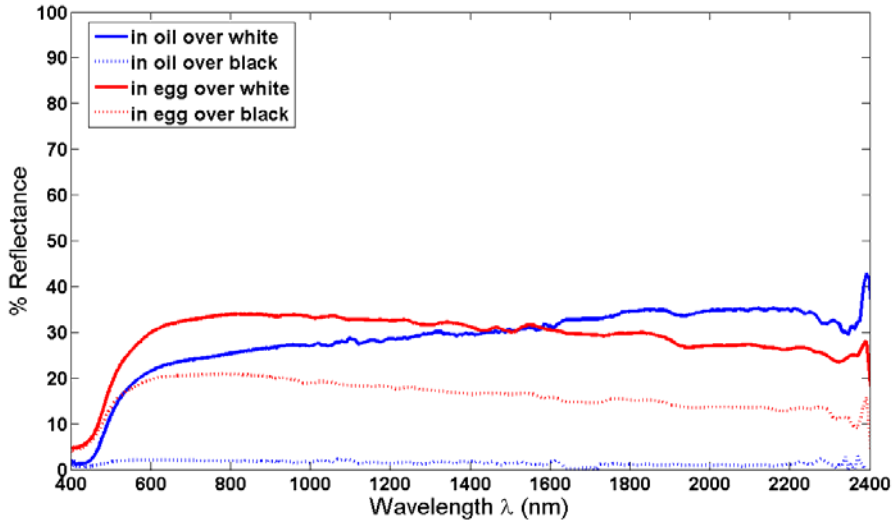

Figure d.5: Spectral reflectance of Dyer's broom lake in egg tempera and linseed oil.

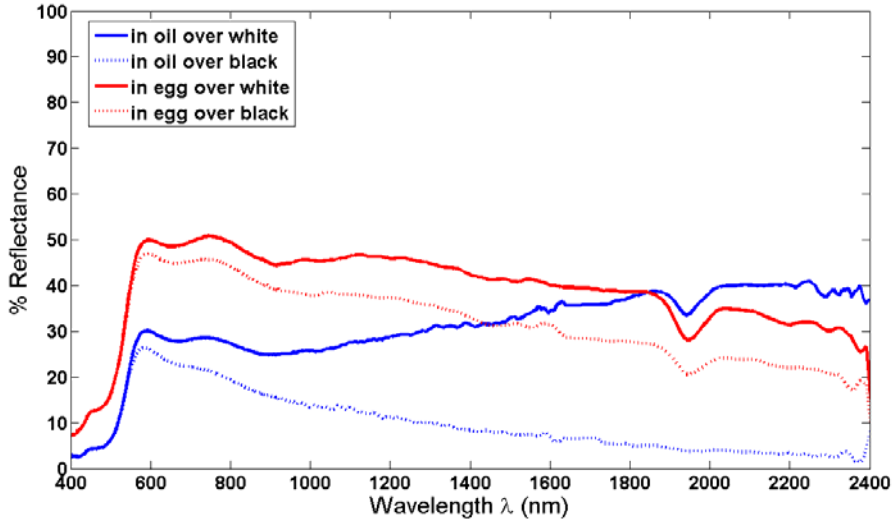

Figure d.6: Spectral reflectance of Italian golden ochre in egg tempera and linseed oil.

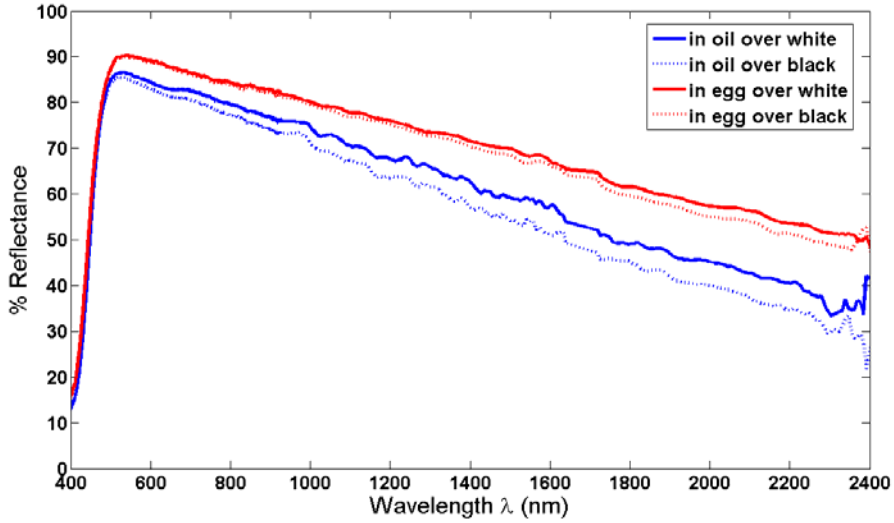

Figure d.7: Spectral reflectance of lead tin yellow in egg tempera and linseed oil.

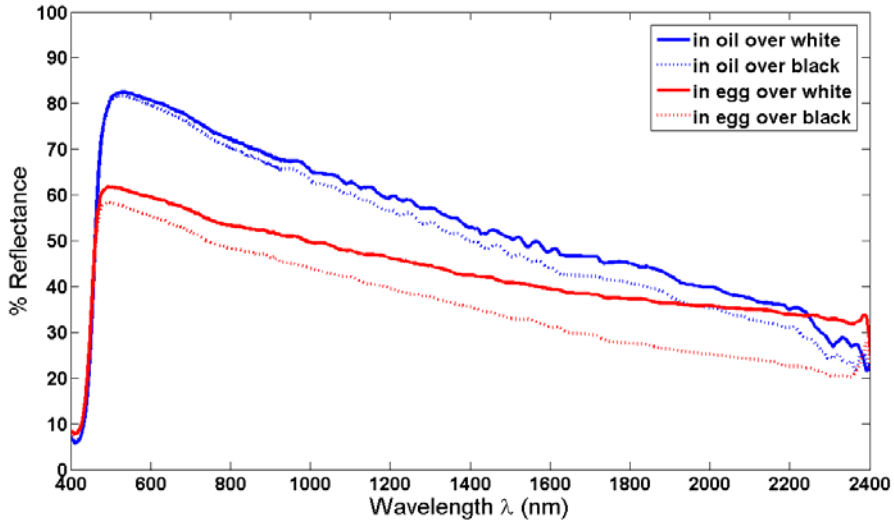

Figure d.8: Spectral reflectance of lemon yellow in egg tempera and linseed oil.

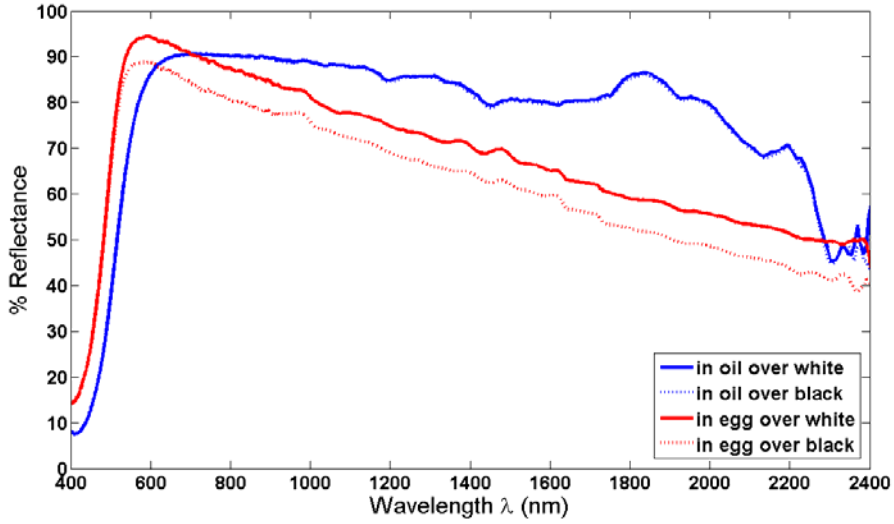

Figure d.9: Spectral reflectance of naples yellow light in egg tempera and linseed oil.

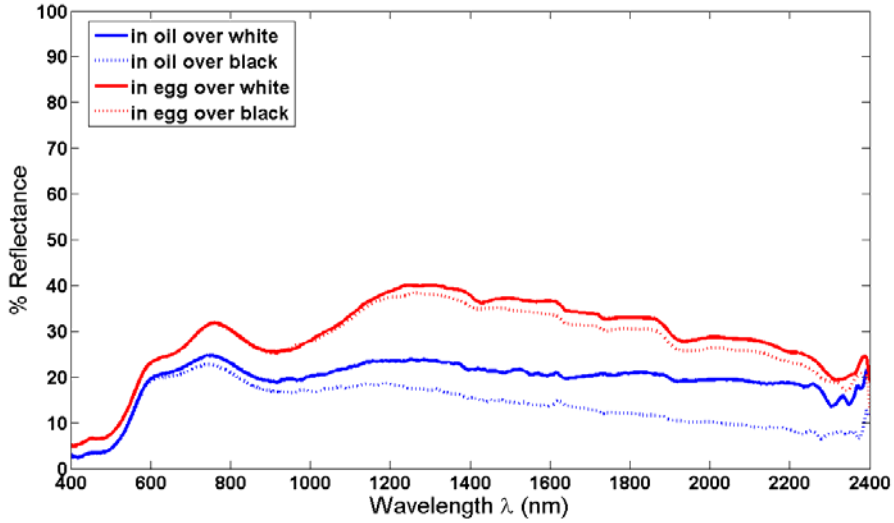

Figure d.10: Spectral reflectance of natural Italian tierra di Sienna in egg tempera and linseed oil.

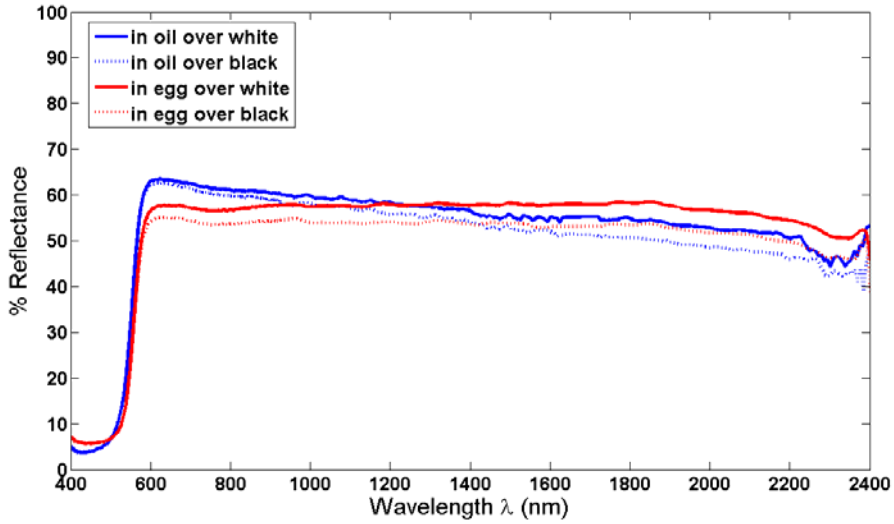

Figure d.11: Spectral reflectance of orpiment (grade 3) in egg tempera and linseed oil.

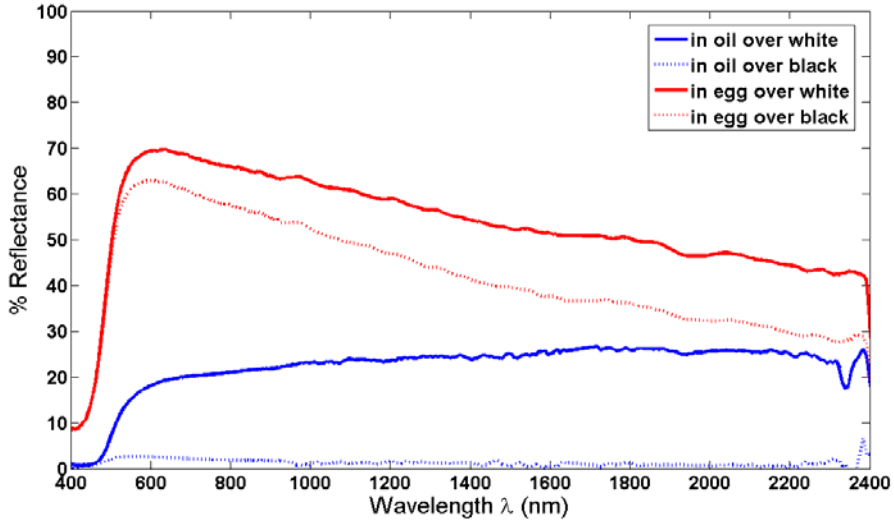

Figure d.12: Spectral reflectance of weld lake in egg tempera and linseed oil.

e. Purple Pigments in Egg Tempera and Linseed Oil

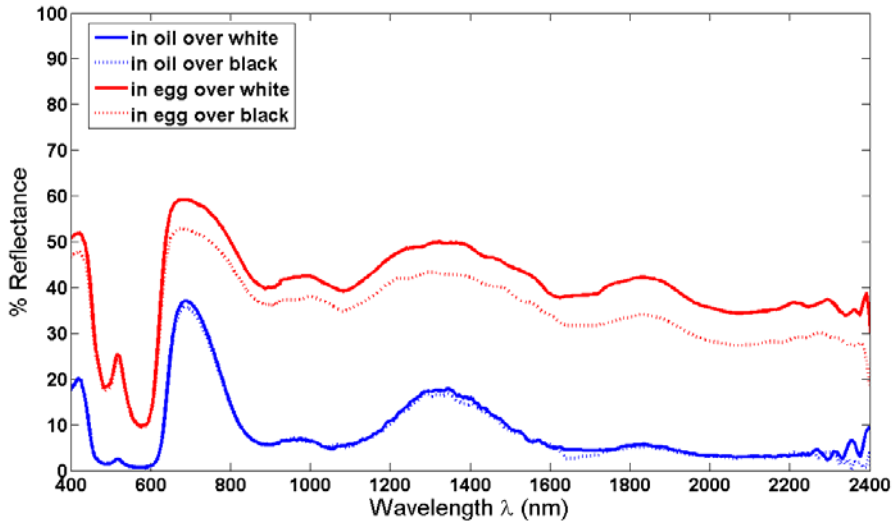

Figure e.1: Spectral reflectance of cobalt violet dark in egg tempera and linseed oil.

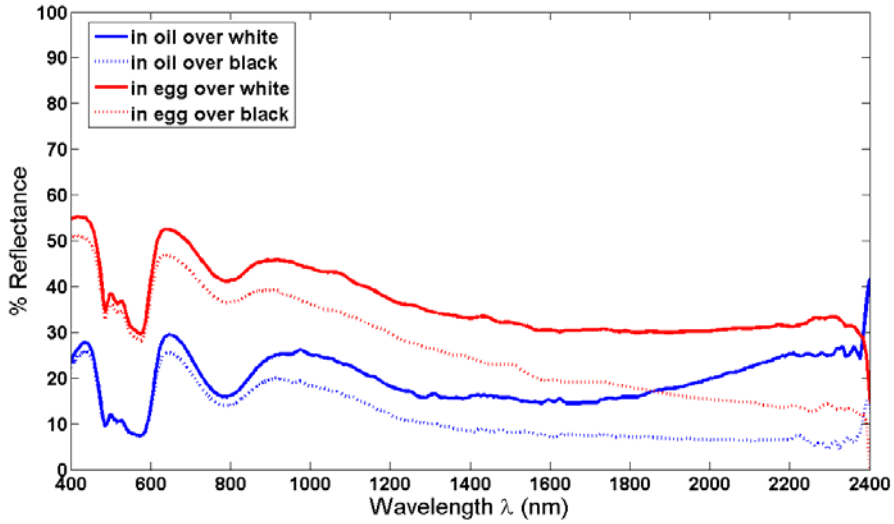

Figure e.2: Spectral reflectance of cobalt violet light in egg tempera and linseed oil.

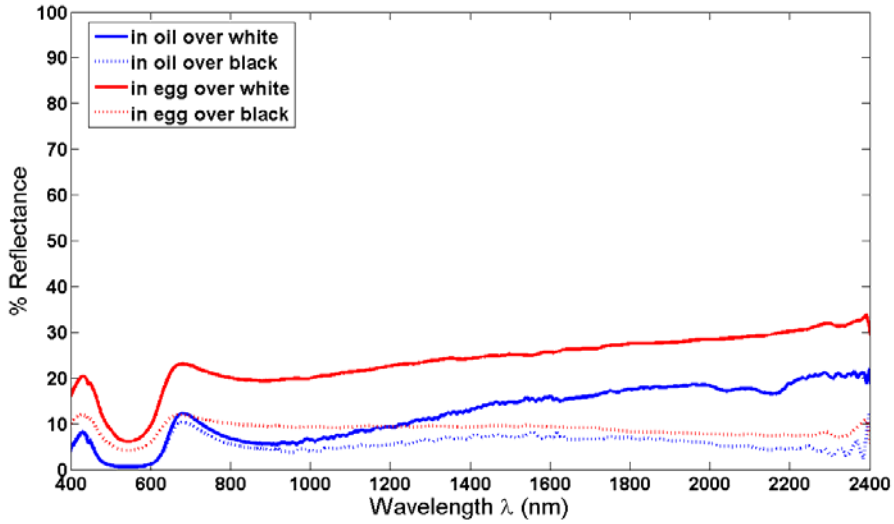

Figure e.3: Spectral reflectance of manganese violet in egg tempera and linseed oil.

f. White and Black Pigments in Egg Tempera and Linseed Oil

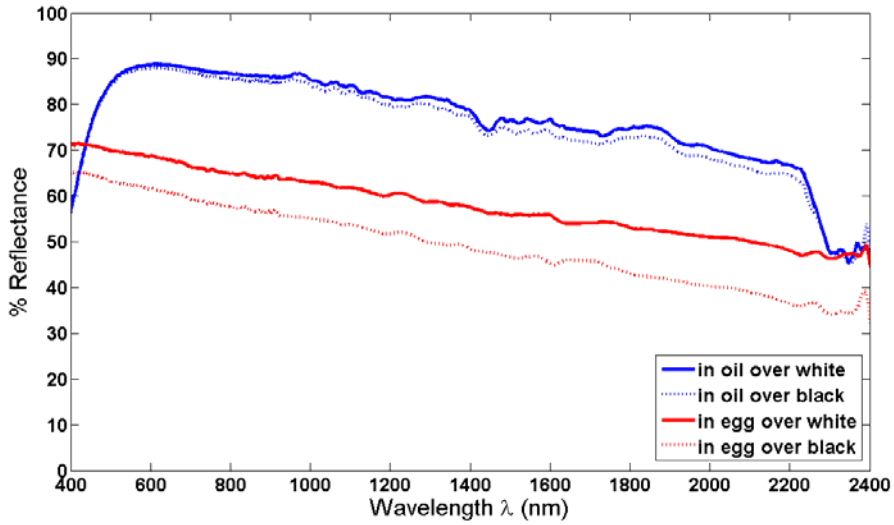

Figure f.1: Spectral reflectance of lead white in egg tempera and linseed oil.

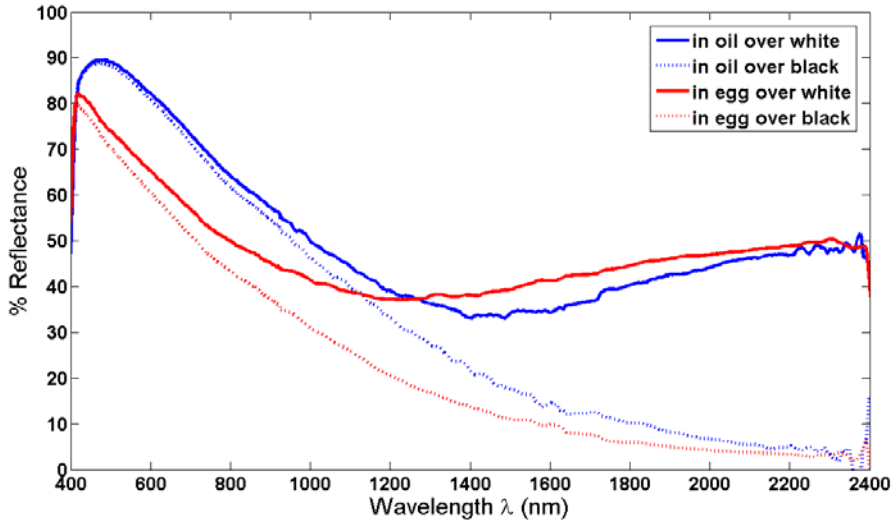

Figure f.2: Spectral reflectance of titanium white in egg tempera and linseed oil.

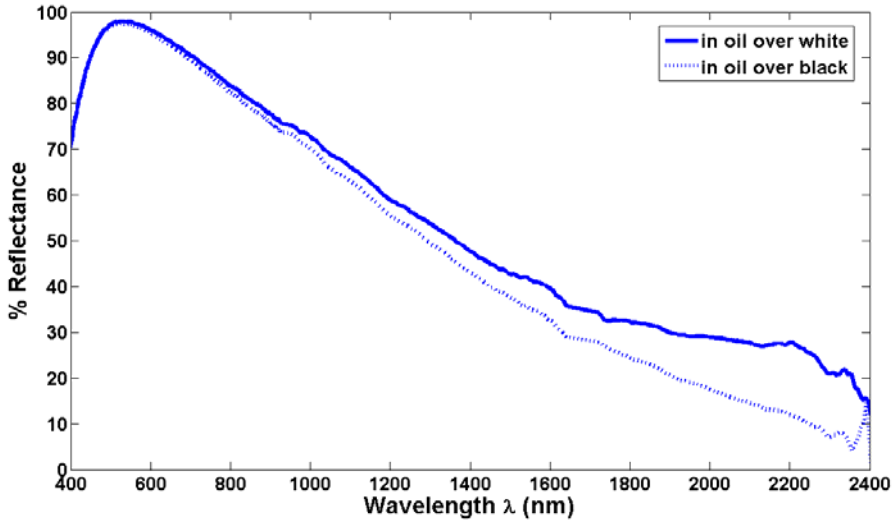

Figure f.3: Spectral reflectance of zinc white in linseed oil.

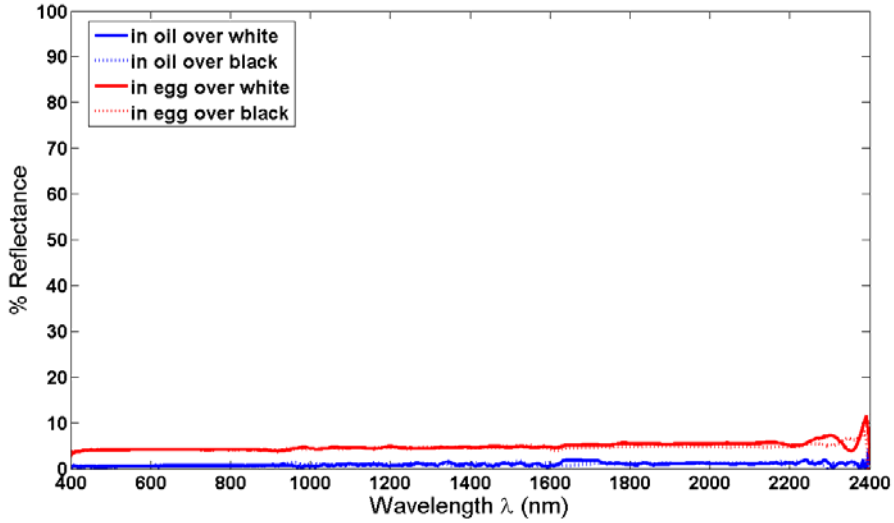

Figure f.4: Spectral reflectance of bone black in egg tempera and linseed oil.

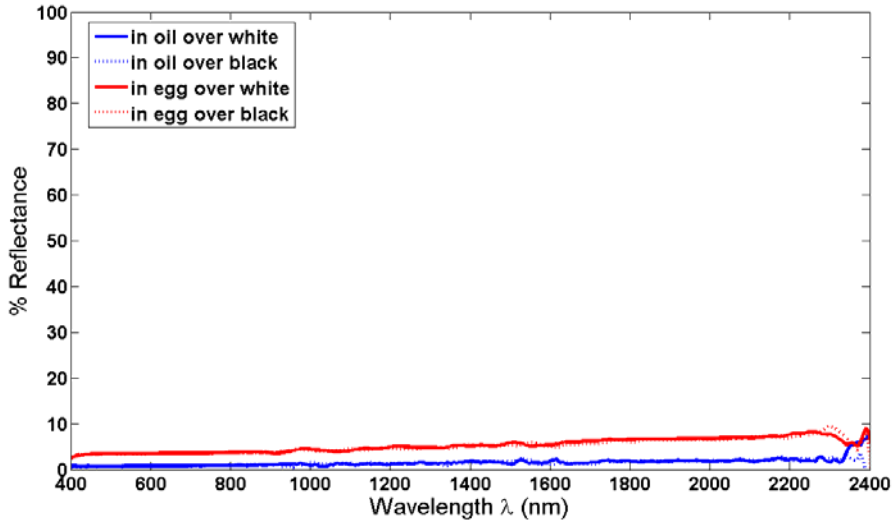

Figure f.5: Spectral reflectance of charcoal in egg tempera and linseed oil.

B List of Publications

Papers

H. Liang, B. Peric, M. Spring, D. Saunders, M. Hughes, A. Podoleanu, 'Non-invasive imaging of subsurface paint layers with optical coherence tomography', *Conservation Science 2007*, Milan, *10-11 May 2007*, Joyce Townsend et al., eds. (Archtype publishing, London, 2008), pp. 171-17 (refereed conference proceeding)

H. Liang, B. Peric, M. Hughes, A. Podoleanu, M. Spring, D. Saunders, 'Optical coherence tomography for art conservation and archaeology', *Proc. SPIE*, Vol. 6618, O3A: Optics for Arts, Architecture, and Archaeology, 2007, pp. 661805-1..661805-12 DOI: 10.1117/12.726032

H. Liang, K. Keita, T. Vajzovic, B. Peric, 'Pigment Identification with Optical Coherence Tomography and Multispectral Imaging', OSAV'08, The 2nd International Topical Meeting on Optical Sensing and Artificial Vision, Saint Petersburg, 2008, in press

M. Spring, H. Liang, B. Peric, D. Saunders, A. Podoleanu, 'Optical Coherence tomography - a tool for high resolution non-invasive 3D-imaging of the subsurface structure of paintings', in *International Council of Museums (ICOM) Committee for Conservation 15th Triennial Conference, Preprints Vol. II, New Delhi, 22-26 September 2008*, (Allied Publishers, New Delhi, 2008), pp. 916-923 (refereed conference proceeding)

H. Liang, B. Peric, M. Hughes, A. Podoleanu, M. Spring, S. Roehrs, 'Optical Coherence Tomography in Archaeological and Conservation Science - A new emerging field', 1st Canterbury workshop on Optical Coherence Tomography & Adaptive Optics, Canterbury, September 2008, in press

Poster

B. Peric, S. Martin-Simpson, M. Spring, H. Liang, 'Spectral Transparency of Historic Artists' Pigments', in *Conservation Science 2007*, *Milan, 10-11 May 2007,* Joyce Townsend et al., eds. (Archtype Publishing, London, 2008), pp. 185-186)

To appear in Conservation Science 2007, Milan

Non-invasive imaging of subsurface paint layers with optical coherence tomography

Haida Liang[*a], Borislava Peric [a], Marika Spring [b], David Saunders[c], Michael Hughes [d], Adrian Podoleanu[d]

[a]School of Science and Technology, Nottingham Trent University, Nottingham NG11 8NS, UK

[b]Scientific Department, The National Gallery, London WC2N 5DN, UK

[c]Department of Conservation, Documentation and Science, The British Museum, London WC1B 3DG, UK

[d]School of Physical Sciences, University of Kent, Canterbury, CT2 7NR, UK

ABSTRACT

Optical Coherence Tomography (OCT) systems are fast scanning infrared Michelson interferometers designed for the non-invasive examination of the interiors of the eye and subsurface structures of biological tissues. OCT has recently been applied to the non-invasive examinations of the stratigraphy of paintings and museum artefacts. So far this is the only technique capable of imaging non-invasively the subsurface structure of paintings and painted objects. Unlike the traditional method of paint cross-section examination where sampling is required, the non-invasive and non-contact nature of the technique enables the examination of the paint cross-section anywhere on a painting as there is no long an issue with conservation ethics regarding the taking of samples from historical artefacts. A range of applications of the technique including the imaging of stratigraphy of paintings and painted artefacts, the imaging of underdrawings to the analysis of the optical properties of paint and varnish layers are presented. Future developments in the context of a Leverhulme Trust funded project on the application of OCT to art conservation are discussed.

Keywords: optical coherence tomography, Michelson interferometer, art conservation, paint, varnish, infrared imaging, infrared reflectography, 3D imaging, refractive index, confocal microscopy

1. INTRODUCTION

Conservation ethics place an increasing emphasis on non-destructive and non-invasive methods of analysis and preventive conservation. In the case of paintings, conservation ethics limits sampling to regions of damage and edges of paintings which can be unrepresentative of the painting as a whole. In general, non-invasive techniques not only reduce the need to take samples from artefacts, but also enable examinations on any area of an object hence providing a global and representative view.

Technology is often the driving force for the direction a discipline takes. For example, in the 1930s non-invasive optical methods were routine in the scientific examination of works of art and microchemical analysis was a new emerging method viewed as giving limited information but was useful in providing supplementary information to those routine imaging techniques (Getten 1933). Nowadays, as a consequence of technological developments since the 1930s, microchemical analysis is considered routine and the new emerging non-invasive optical methods are considered desirable but ineffective at examining the interior beneath the surface. However, this perception may change with new developments in imaging technology. It is particularly beneficial to borrow imaging technologies in other disciplines such as biomedical imaging where there is a similar need for non-invasive methods, and astronomy or remote sensing where there is no alternative to remote, therefore non-invasive, methods.

[*]haida.liang@ntu.ac.uk; phone 44 115 848 3448; fax 44 115 848 6636;

Most non-invasive techniques currently used for point (i.e. non-imaging) analysis of painting materials can only examine surface layers (eg Fiber-optic FTIR, micro Raman), or analyse all the paint layers together (eg XRF), so that it is not possible to obtain the information on stratigraphy and the composition of the separate layers that can be achieved through analysis of cross sections of paint samples. Current routine non-invasive imaging methods of examination of paintings include X-radiography, infrared reflectography, macrophotography, UV-fluorescence and raking light imaging. The last three methods give information mostly on the conditions of the surface of a painting. X-radiography is routinely employed to examine the structure of the support of a painting, as well as details of areas painted with pigments containing heavy elements. Infrared reflectography is one of the most useful techniques for studying the underdrawings beneath the painted layers, which would be otherwise invisible to the eye. Both X-radiography and infrared reflectography reduce the 3D information of a painting into 2D, thus losing the detailed depth resolved information on the subsurface stratigraphy. In this paper, we present the applications of a new emerging non-invasive imaging technology to the examination of subsurface structures of paintings and potentially other artefacts.

Ever since the invention of the Michelson interferometer for the detection of ether in 1881, it has been used in a wide range of applications from spectroscopy to metrology and from Astronomy, Chemistry to Biomedical research. In the early 1990s, Optical Coherence Tomography (OCT) - a fast, high resolution, 3-D scanning technique based on the Michelson interferometer, was first developed for *in vivo* scanning of the eye and other biological tissues (Huang et al. 1991). Since the pioneering work by our group and others, OCT has been applied to art conservation to produce cross-sectional images of paintings and archaeological objects non-invasively (Liang et al. 2004, Targowski et al. 2004, Yang et al. 2004, Liang et al. 2005a). OCT typically operates in the near infrared and probes the subsurface structure of an object by measuring the back-scattering light at each depth position. Since OCT is based on the Michelson interferometer, interference between the light reflected back from the reference mirror and the light back-scattered from the object occur when the optical path length between the two are within the coherence length. The depth resolution given by half the coherence length is decoupled from the transverse X-Y resolution given by the numerical aperture of the objective. To achieve high depth resolution, short coherence length or wide-band sources are required, since the coherence length is given by

$$l_c = \frac{2\ln 2}{\pi}\frac{\lambda_0^2}{\Delta\lambda}$$

where λ_0, $\Delta\lambda$ are the central wavelength and bandwidth of the light source. This is in contrast to a confocal microscope where both the depth resolution and the transverse resolution are given by the numerical aperture of the objective. Hence, for the same depth resolution, OCT can operate at a greater working distance than confocal microscopes. This may be one reason why confocal microscopy has not been used directly on paintings because of the close working distances required (a few millimetres) rendering the technique potentially hazardous. In addition, OCT compared to confocal microscopy is able to probe up to three times the penetration depth in scattering media, since it takes advantage of the coherence properties of light and registers only coherent signals (Izatt et al. 1994). Since OCTs are designed for *in vivo* examinations of a highly sensitive organ – the eye, it has the added advantage of a comfortably remote working distance of typically ~1-2 cm.

Currently, there are two main types of OCT – Time-Domain OCT (TD-OCT) and Fourier-Domain OCT (FD-OCT). Wide-band sources such as superluminescent diode (SLD), Kerr lens mode-locked laser and supercontinuum sources have been used to achieve high depth resolution. Sub-micron resolutions are achievable using specialized ultra-wide band sources (Drexler 2004). However, these novel broad band sources are currently very expensive. Figure 1 shows the schematic diagrams of the two types of OCT. A recent review of OCT is given by Tomlins et al. (2005). TD-OCT scans the depth of an object through moving the position of the reference mirror. In contrast, the reference mirror position is fixed in a FD-OCT and a spectrometer is used to record the interference spectrum and later Fourier transformed back to obtain the depth resolved structure of the object. Within TD-OCT technology, the most common type collects a series of 2-D cross-section images which are then stacked to obtain a 3-D image. An alternative to this kind of conventional TD-OCT is the *en-face* TD-OCT (Podoleanu et al. 1996, 2000) which takes images in planes parallel to the painting surface one after another in depth which is particularly convenient for the examination of paintings. The *en-face* scans provide an instant comparison to the familiar sight of a painting. Features seen with the naked eye could easily be compared with features hidden below the surface.

In biomedical applications, the speed of acquisition is crucial for *in vivo* examination of biological tissues. However, in the case of examination of paintings, speed is of less importance except for the examination of temporal effects such as tracking the deformation of canvas and laser cleaning (Targowski et al. 2006a; Gora et al. 2006). Currently, FD-OCT is the most promising in biomedical applications, as it is faster at achieving the same sensitivity, however, FD-OCT has a number of drawbacks compared to TD-OCT (for a detailed discussion see Leitgeb et al. 2003). For paintings, the main drawback of the FD-OCT is ghost images associated with highly reflective surfaces such as a freshly varnished painting or gilded areas. In addition, for wavelength longer than 1μm, FD-OCTs are significantly more expensive than TD-OCTs. Paint is in general more transparent to near infrared light at longer wavelength than 1μm which makes longer wavelength OCTs more desirable for the examination of paintings (see Peric et al. this volume).

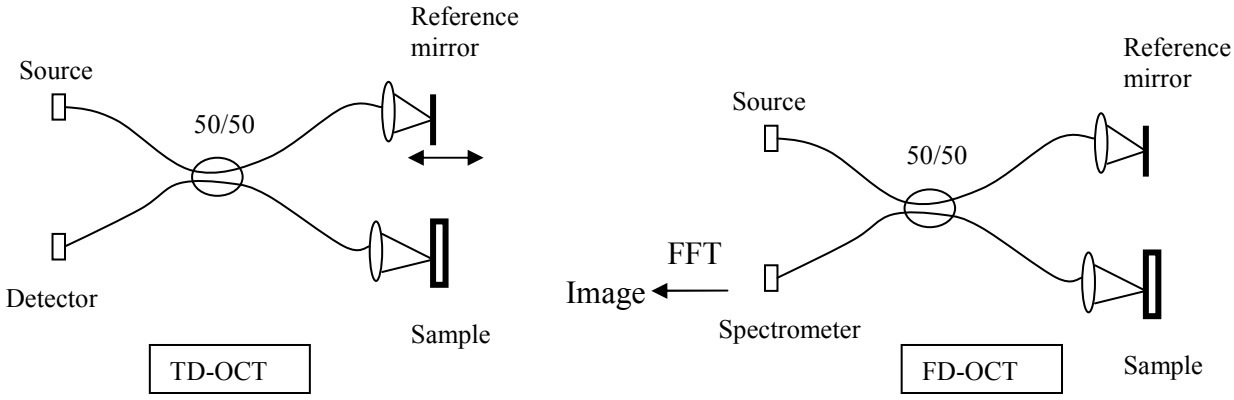

Fig. 1 Schematic diagram of fibre based OCT systems. The back-scattered light from the sample is combined with back-reflected light from the mirror and the interference signal is detected either directly (TD-OCT) or through a spectrometer (FD-OCT). Left: TD-OCT where the depth information is probed by scanning the reference mirror; Right: FD-OCT where the reference mirror position is fixed and the detector is replaced with a spectrometer and the depth resolved structure is recovered through a fast Fourier transform.

2. APPLICATION TO TECHNICAL EXAMINATION OF PAINTING

In this paper, we will concentrate on the application of OCT to the examination of paintings. The OCT systems used in this paper range from *en-face* TD-OCT to FD-OCT with wavelengths of 930nm, 1300nm and depth resolutions of 6 μm and 20 μm. Table 1 gives the specifications of the two OCT systems. The systems should not be considered as typical of their types. They were used simply because we had access to these systems. The typical speed of acquisition of a cross-section image is between 2-10 frames/second. System 1 is a commercial system from Thorlabs and system 2 is a prototype laboratory system (Liang et al. 2005a).

Table 1 Specifications of the OCT systems used in this paper

OCT system	Type	wavelength (nm)	depth resolution (μm)	transverse resolution (μm)
1	FD-OCT	930	6	9
2	*En face* TD-OCT	1300	20	25

2.1 Non-invasive, non-contact imaging of paint cross-sections

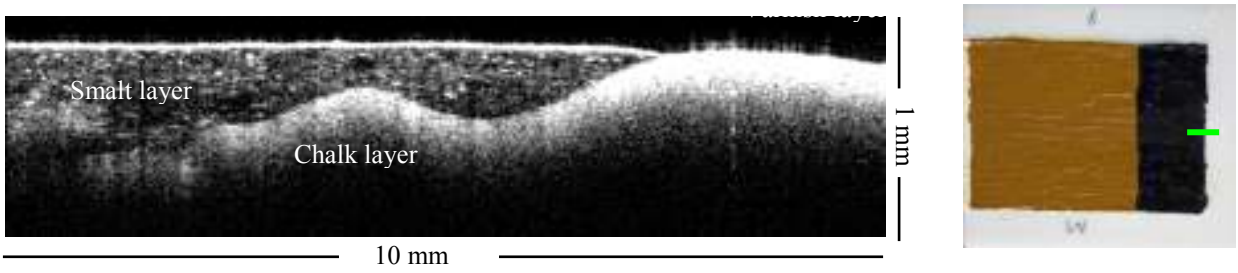

Fig. 2 Left: An OCT cross-section image of a painted panel of smalt in linseed oil over a chalk layer; Right: the test panel and the position of where the scan was taken.

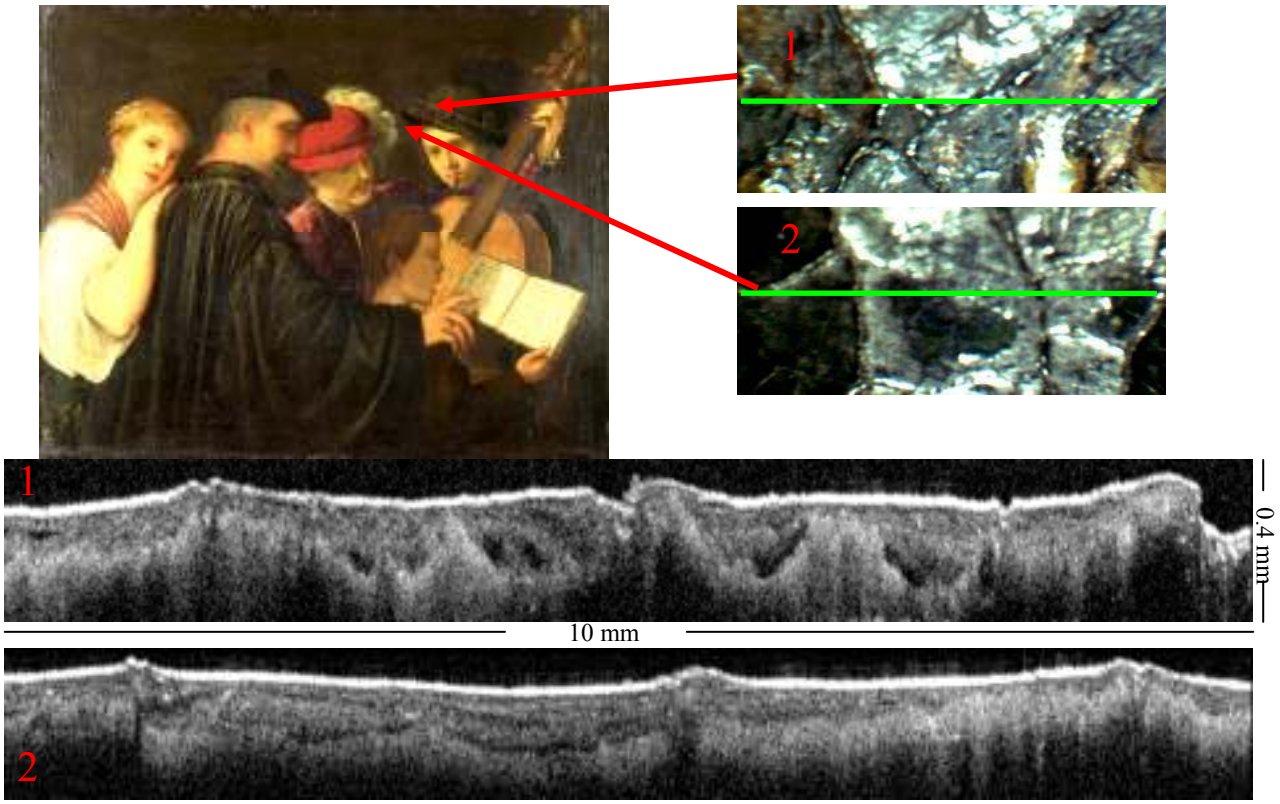

Fig. 3 Top Left: *A Concert* (1600-50), after Titian (National Gallery No. 3); Top Right: details of two regions on the painting examined by OCT system 1; Bottom: OCT cross-section images of the two regions at positions marked by the green line segment.

A test panel was prepared with a traditional ground layer of chalk mixed with rabbit skin glue, on top of which a layer of smalt in linseed oil was painted. An image of a cross-section taken with OCT system 1 is given in Fig. 2, where the bright dots are the smalt particles. The uneven chalk layer under the smalt layer can also be seen. OCT registers the back-scattered light from the sample. The greater the back-scattering, the brighter the image is, hence we can conclude

that the chalk layer is much more scattering than the smalt layer. Back-scattering is greatest at sharp boundaries in refractive indices. The bright edge at the top of the smalt layer is due to the strong reflection at the boundary between air and the smalt layer. Similarly, the smalt particles are seen as bright spots as a result of the scattering due to the difference in refractive index between the pigment particles and the oil medium.

Figure 3 shows an example of OCT images of paint stratigraphy on a 17th C painting from the National Gallery. Multiple paint layers can be seen, and the cross section images show the marked cupping of the paint surface particularly well. Further investigations are needed to fully interpret the layer structures. This example demonstrates the usefulness of combining non-invasive OCT imaging of subsurface structure with the examination of sample cross-sections, where microscope examinations of sample cross-sections can aid the interpretation of OCT images and OCT images in turn can show how similar or different the layer structures are between regions on a painting.

2.2 Imaging of underdrawings

Figure 4 shows that the dynamic range and resolution of the OCT images of underdrawings surpass any conventional infrared images. The separate droplets of the bone black drawings are clearly discernable in the OCT images. The high dynamic range is because interferometers register only coherent signals; hence only back-scattered light with a path length that matches (within the coherence length) the reference path length is registered. Stray light is automatically filtered out. For the imaging of underdrawings, it is most convenient to use an *en-face* scanning OCT where underdrawings can be seen as the 3-D scan is progressing. For other types of OCT, it is necessary to wait until a full 3-D scan has finished before *en-face* slices can be displayed. Figure 4(e) shows that the increased resolution of OCT system 1 compared with OCT system 2 (Fig. 4(d)), gives added information on the way the underdrawings are drawn making it possible to deduce that not only the type of underdrawing (liquid) but also the direction in which it is drawn.

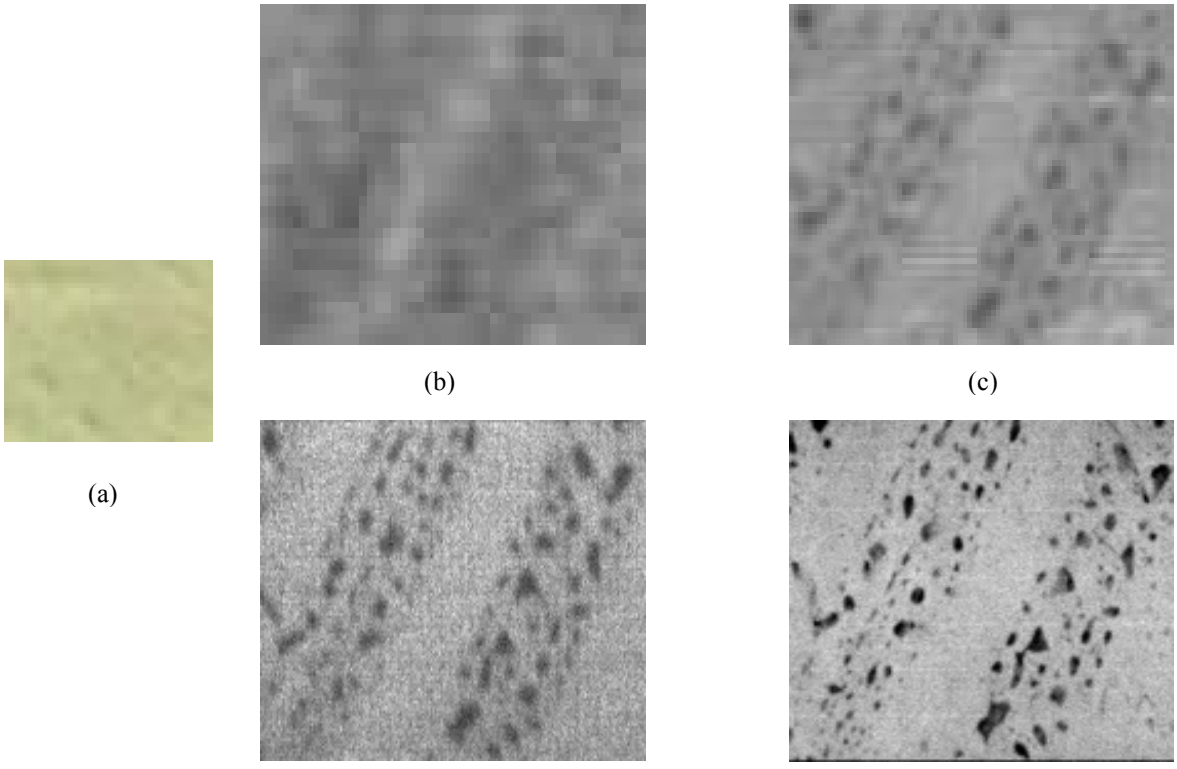

Fig. 4 a) Colour images of a painted patch over underdrawings: it has two layers of lead-tin-yellow paint over underdrawings drawn with a quill pen using an ink of bone black in gum; b) the corresponding near infrared Vidicon images; c) the corresponding near

infrared images taken with a InGaAs camera; d) the corresponding 1300nm OCT image (system 2) of the average of layers containing underdrawings; e) the corresponding 930nm OCT image (system 1).

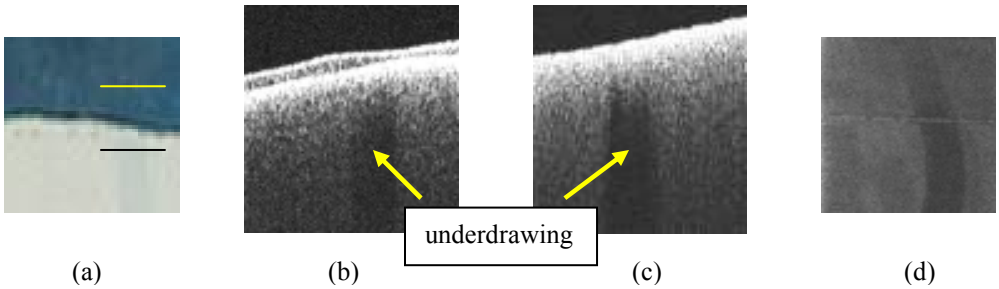

Fig. 5 a) Colour image of a painted panel: the lower part is painted with an imprimatura on top of the underdrawing which is painted on a preparatory ground layer, the upper half has an additional paint layer above the imprimatura; b) cross-section images collected with OCT system 2 of a scan in the top half of the image (line segment marked in yellow) showing the dark shadow of the underdrawing below two layers of paint; c) OCT cross-section image of a scan in the lower half of the image (line segment marked in black) showing the dark shadow of the underdrawing below one layer of paint; d) *en-face* OCT image (system 2) of the underdrawing.

Figure 5 shows that unlike conventional infrared images such as infrared reflectography, OCT images can show the exact depth location of an underdrawing, e.g. whether the underdrawing was drawn above or below an imprimatura. The underdrawing absorbs the incident light hence casting a shadow in the layers below.

An example of imaging underdrawings in a 16th C painting is shown in Figure 6. In this painting, the underdrawing beneath drapery painted with red lake was easily visible to the naked eye. An area where the underdrawing lines could be seen was imaged with the aim of determining whether the underdrawing line was visible in the OCT cross section image. The layers of red lake paint and varnish are clearly discernable. The dark lines/shadows lower down in the cross section correspond to the underdrawing lines which seems to be directly below the red lake layer and above another layer which could be either the chalk ground or a priming layer.

2.3 Monitoring cleaning process

OCT cross-section images are particularly effective at showing translucent layers, including multiple varnish layers, and so can be used to monitor varnish removal. Given the fast acquisition speed, OCT can potentially be used for dynamic monitoring of the cleaning process. Figure 7 shows an example where part of an old degraded yellow varnish has been removed. The painting has an interesting layer structure where paint has been applied over a gold layer. The OCT image shows the varnish, paint and gold layers. On the extreme left is the area where the bare gold layer is exposed, in the middle is the blue paint layer (probably ultramarine) over gold and on the right is the area where there is still the old varnish on top of the paint layer. Effects of multiple scattering in the paint layer give the impression of a thick layer below the gold layer. If the paint layer is strongly scattering, light can bounce off a few times within the paint layer before being collected by the OCT. A photon collected by the OCT that was scattered more than once would have a longer path length than if it was scattered once. Since OCT registers optical depth rather than physical depth, these multiply scattered photons would appear to the OCT as coming from a deeper layer. This is why some of the multiply scattered light from the blue paint layer above the gold layer appears to be coming from below the gold layer. This highlights the importance of combining knowledge about the instrument and the painting in interpreting the images (which is what microscopists had to learn in the past to interpret cross-section images). Similarly, caution has to be employed in interpreting cross-section images in biomedical applications. However, paintings are perhaps more varied than the human eye or skin.

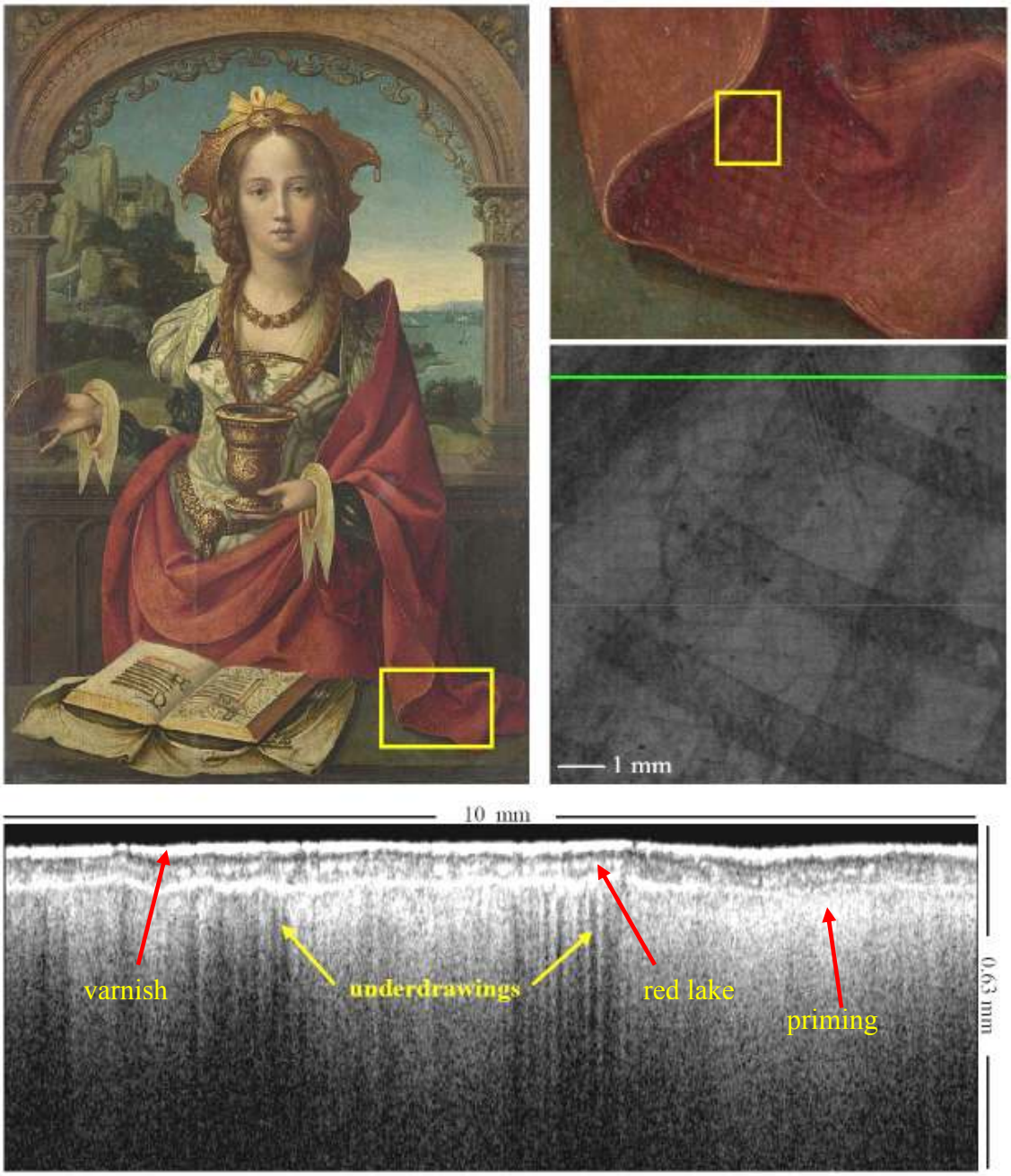

Fig. 6 Top: A region on the red drapery in the painting *The Magdalen* by an anonymous Netherlandish artist (National Gallery No. 719); Right middle: OCT (system 1) *en-face* image at the depth of the underdrawing corresponding to the region marked by a yellow box in the top right image; Bottom: OCT (system 1) cross-section image of the region marked by a green line segment on the *en-face* underdrawing image.

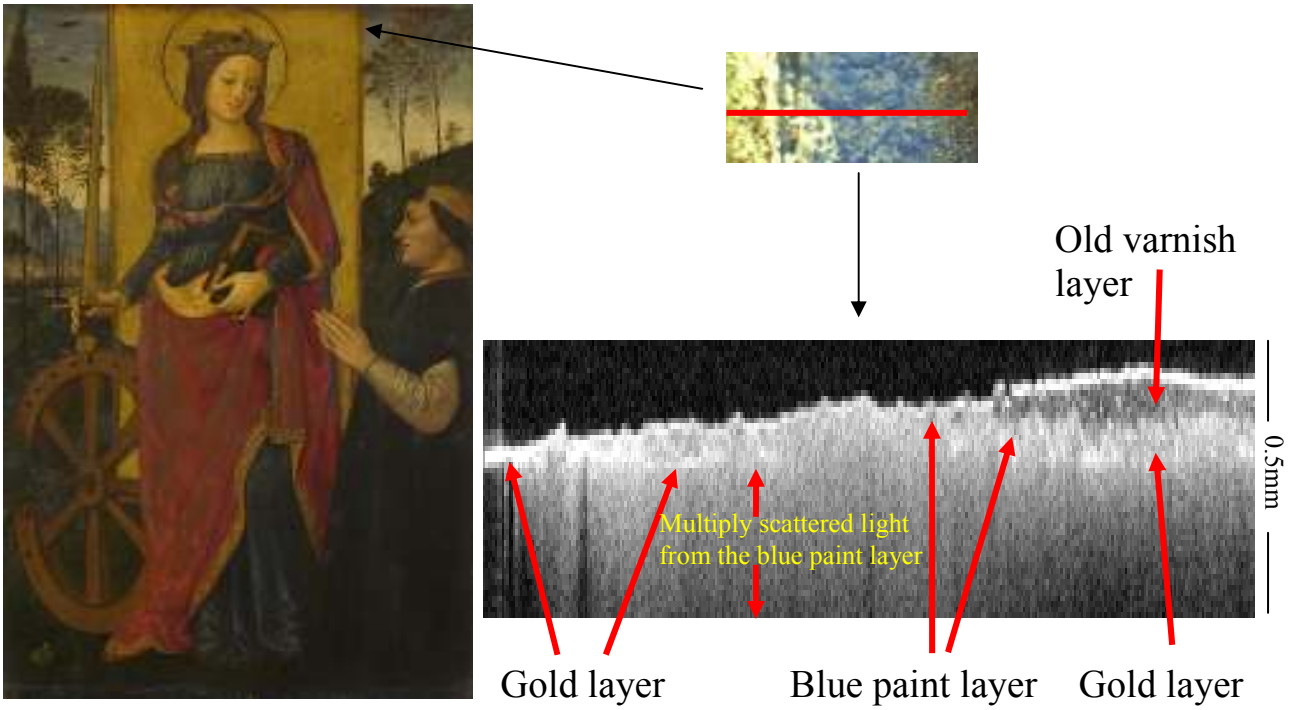

Fig. 7 Left: *Saint Catherine of Alexandria with a Donor* (1480-1500) by Pintoricchio (National Gallery No. 693); Top right: a detail from the painting where the right hand side is covered with an old yellowed varnish; the old varnish has been cleaned off on the left. Bottom right: an OCT (system 1) image of a scan through the centre of the area showing the old varnish region on the right and the cleaned area on the left.

2.4 Measurement of optical properties of paint and varnish layers

The visual qualities of a painting are determined by optical parameters such as refractive index, thickness, absorption and scattering coefficients, and surface roughness of the varnish and paint layers. Measurement of these parameters can be useful for conservation treatment and in studies of deterioration processes. OCT makes it possible to study ageing processes using naturally aged 'real' paintings as a statistical sample, rather than relying on artificially aged samples. The OCT images at 930nm in Fig. 8 show a clear difference in scattering properties of an old degraded varnish compared to a relatively new varnish. The chemical changes occurred in an old varnish makes it change colour and become less homogeneous giving it a hazy and yellowed appearance. This can be seen in the OCT image as increased scattering in the old varnish layer.

The traditional method of measuring refractive index (RI) of paint and varnish layers of a painting requires taking tiny samples and observing under a microscope the changes in their transparency when immersed in a series of liquids with calibrated RI (Townsend 1993). When the RI of the sample matches that of the liquid, the sample 'disappears'. We have demonstrated that OCT is capable of measuring RI non-invasively for varnish layers (Liang et al. 2005b). In Fig. 8(b), the top of the paint layer below the varnish layer appears to be lower than the top of the paint layer next to it where the varnish had fallen off. This is because OCT measures the optical depth rather than physical depth, as varnish has a higher refractive index than air. The ratio between the optical thickness of the varnish (l_1) compared to its physical thickness (l_0) gives the refractive index of the varnish. The non-invasive measurements of RI of paint layers will be reported in a forth-coming publication.

Another application of OCT is in the dynamic monitoring of the drying and wetting processes of varnish layers. Preliminary studies (Liang et al. 2005b) on the monitoring of the drying processes of different varnishes confirmed that the varnish surface generally follows the roughness of the substrate as it dries and the degree of roughness depends on

the type of varnish as suggested by Berns and de la Rie (2003). Further work on the topic using OCT has also been reported in Targowski et al. (2006b).

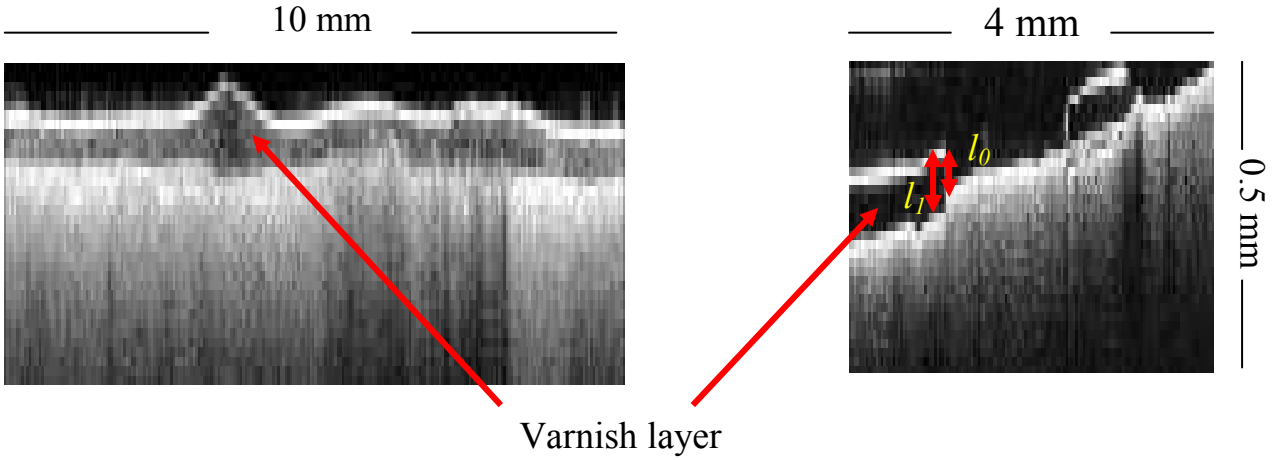

Fig. 8 Left: an OCT (system 1) image of an old degraded varnish (>120 years old) from the painting in Fig. 7; Right: a relatively new varnish (<50 years old).

3. CONCLUSIONS & FUTURE DEVELOPEMENTS

Optical Coherence Tomography, a low coherence 3-D scanning Michelson's interferometer, shows the potential to be a powerful non-invasive technique for probing into the depth of paintings, providing 3-D infrared image cubes that can show not only the structure of the paint and varnish layers, reveal the underdrawings and their depth positions, but also provide some quantitative measurements of the optical properties of varnish and paint layers.

We have a started a three year Leverhulme Trust funded project on OCT for art conservation, where we aim to achieve the following objectives:

- To find the best method of obtaining quantitative measurements of optical parameters, such as refractive index, thickness, absorption and scattering coefficients, of the paint and varnish layers using OCT;
- To conduct a study of how the paint and varnish material of historic paintings or painted objects age in terms of their optical properties;
- To use OCT to assist practical conservation, address various issues in conservation and art historical studies;
- To find the optimum wavelength bands in the visible to near infrared spectrum (400-2500 nm) for a dedicated OCT system for the conservation of painted objects (this has been found to be around 2.2µm, see Peric et al. this volume);
- To add extra wavelength channels to an existing OCT system to explore the potentials of spectral measurements for the identification of different materials in the paint layers;
- To specify a design for an ideal OCT system tailored for museum use.

ACKNOWLEDGEMENT

We are grateful to the Leverhulme Trust for funding the project. We would like to thank colleagues at the National Gallery and the British Museum for providing samples, studio space and for useful discussion.

REFERENCES

Berns, R. S., and de la Rie, E. R., 2003. 'Exploring the optical properties of picture varnishes using imaging techniques', Studies in Conservation, 48(2), 73-83.

Drexler, W., 2004. 'Ultrahigh-resolution optical coherence tomography', Journal of Biomedical Optics, 9, 47.

Getten, R., 1933. 'An equipment for the microchemical examination of pictures and other works of art', Technical Studies in the Field of the Fine Arts, 2, 185.

Gora, M., Targowski, P., Rycyk, A., Marczak, J., 2006, 'Varnish ablation control by optical coherence tomography', Laser Chemsitry 2006: Article ID 10647

Huang, D., Swanson, E. A., Lin, C. P., Schuman, J. S., Stinson, W. G., Chang, W., Hee, M. R., Flotte, T., Gregory, K., C. Puliafito, C. A., Fujimoto, J. G., 1991. 'Optical coherence tomography', Science, 254, 1178.

Izatt, J.A., Hee, M.R., Owen, G.M., Swanson, E.A., Fujimoto, J.G., 1994. 'Optical Coherence Microscopy in scattering media ', Optics Letter, 19, 590.

Leitgeb, R., Hitzenberger, C. K., Fercher, A. F., 2003, 'Performance of Fourier domain vs. time domain optical coherence tomography', Optics Express, Vol. 11, 889-894.

Liang, H., M. Gomez Cid, R. Cucu, G. Dobre, D. Jackson, C. Pannell, J. Pedro, D. Saunders, A. Podoleanu, 2004. 'Application of OCT to examination of easel paintings', Second European Workshop on Optical Fibre Sensors, Proc. SPIE, 5502, 378.

Liang, H., Cid, M.G., Cucu R.G., Dobre, G.M., Podoleanu, A.Gh., Pedro, J., Saunders, D., 2005a. `En-face Optical Coherence Tomography – a novel application of non-invasive imaging to art conservation', Optics Express, Vol. 13, 6133-6144. http://www.opticsexpress.org/abstract.cfm?id=85276

Liang, H., Cid, M.G., Cucu R.G., Dobre, G.M., Kudimov, B., Pedro, J., Saunders, D., Cupitt, J., Podoleanu, A.Gh., 2005b. `Optical Coherence Tomography – a non-invasive technique applied to conservation of paintings', Proceedings of SPIE, Vol. 5857, Optical Methods for Arts and Archaeology, Munich.

Peric, B., Martin-Simpson, S., Spring, M., Liang, H., 2007. 'Spectral transparency of historic artists' pigments', this volume.

Podoleanu, A. Gh., Rogers, J. A., Jackson, D. A., and Dunne, S., 2000. 'Three dimensional OCT images from retina and skin', Optics Express, 7(9), 292. http://www.opticsexpress.org/framestocv7n9.htm

Podoleanu, A. Gh., Dobre, G. M., Webb, D. J., Jackson, D. A., 1996 'Coherence imaging by use of a Newton rings sampling function', Optics Letters, 21(21), 1789.

Targowski, P., Rouba, B., Wojtkowski, M., Kowalczyk, A., 2004. 'The application of optical coherence tomography to non-destructive examination of museum objects", Studies in Conservation, 49(2), 107.

Targowski, P., Gora, M., Bajraszewski, T. et al., 2006a, 'Optical Coherence Tomography for Tracking Canvas Deformation', Laser Chemistry 2006: Article ID 93658

Targowski, P., Gora, M. and Wojtkowski, M., 2006b, 'Optical Coherence Tomography for Artwork Diagnostics', Laser Chemistry 2006: Article ID 35373

Tomlins, P. H., Wang, R. K., 2005, 'Theory, developments and applications of optical coherence tomography', J. Phys. D: Appl. Phys., 38, 2519-2535.

Townsend, J. H., 1993. 'The Refractive Index of 19th-Century Paint Media: A Preliminary Study', ICOM Committee for Conservation, Working Group 16, Vol. II, 586.

Yang, M.-L., Lu, C.-W., Hsu, I.-J., Yang, C.-C., 2004. 'The use of optical coherence tomography for monitoring the subsurface morphologies of archaic jades', Archaeometry, 46(2), 171.

Optical Coherence Tomography for Art Conservation & Archaeology

Haida Liang[*a], Borislava Peric [a], Michael Hughes [b], Adrian Podoleanu[b], Marika Spring [c], David Saunders[d]
[a]School of Science and Technology, Nottingham Trent University, Nottingham NG11 8NS, UK
[b]School of Physical Sciences, University of Kent, Canterbury, CT2 7NR, UK
[c]Scientific Department, The National Gallery, London WC2N 5DN, UK
[d]Department of Conservation, Documentation and Science, The British Museum, London WC1B 3DG, UK

ABSTRACT

Optical coherence tomography (OCT) is a fast scanning Michelson interferometer originally designed for in vivo imaging of the eye. In 2004, our group along with two other groups first reported the application of OCT to art conservation and archaeology. Since that time we have been conducting a project to investigate systematically the potential of OCT as a new tool for non-invasive examinations of a wide range of museum objects and to design an OCT optimised for *in situ* use in museums. Here we present the latest results from this ongoing project, which include the determination of the optimum spectral windows for OCT imaging of paintings and painted objects executed using traditional techniques, and non-invasive imaging of the subsurface stratigraphy of painted layers at multiple wavelengths. OCT imaging in assisting spectral pigment identification and in measuring refractive indices of paint will also be presented to illustrate the potential of the technique.

Keywords: optical coherence tomography, low coherence interferometry, art conservation, paint, pigment, varnish, infrared imaging, infrared reflectography, 3D imaging, refractive index

1. INTRODUCTION

Optical coherence tomography (OCT) is a non-invasive and non-contact 3D imaging technique based on the Michelson interferometer using a broadband source with fast 2D or 3D scanning. It was first developed in the early 1990s for the *in vivo* imaging of the eye and skin tissue in the near infrared spectral range[1]. There are two ways of probing into the depth of the sample: physically moving the reference mirror on a translation stage or fixing the reference mirror but measure the fringes in the spectral domain using a spectrometer and Fourier transform it into the spatial domain. The first type is called a time domain OCT (TD-OCT) and the second type is called a Fourier domain OCT (FD-OCT)[2]. A standard TD-OCT collects a series of closely-spaced parallel scans in a plane perpendicular to the surface of the object to give a series of cross section images that can be combined to form a 3D tomogram, and an *en face* image at a given depth can only be obtained after manipulation of the images with software and not while collecting the scans. An alternative type of TD-OCT collects a series of *en face* 2D images parallel to the surface of the object at gradually increasing depths, which again are combined to form a 3D image[3]. The depth resolution of an OCT at a given wavelength is given by the spectral bandwidth of the illuminating source. In an OCT, the depth (axial) resolution is decoupled from the transverse (*en face)* resolution making it possible to achieve high depth resolution at a comfortable distance from the object being examined.

In 2004, the application of optical coherence tomography (OCT) to the examination of paintings, porcelain and ancient jade was first reported[4,5,6]. Since then most of the efforts have been concentrated on new applications of OCT to the examination of paintings[7,8,9]. Apart from the non-invasive examination of the stratigraphy of paint and varnish layers, OCT has also been shown to be the most sensitive technique for revealing preparatory sketches or underdrawings beneath paint layers[7] owing to its high dynamic range and depth selection capabilities. The high speed of acquisition of OCT has proven to be useful in monitoring the laser cleaning of varnish[10]. OCT has also been shown to have the

[*]haida.liang@ntu.ac.uk; phone 44 115 848 3448; fax 44 115 848 6636;

O3A: Optics for Arts, Architecture, and Archaeology
edited by Costas Fotakis, Luca Pezzati, Renzo Salimbeni
Proc. of SPIE Vol. 6618, 661805, (2007) · 0277-786X/07/$18 · doi: 10.1117/12.726032

potential for monitoring the wetting and drying process of varnish and paint[8], the deformation of canvas as the result of environmental changes such as humidity[11] and the solvent cleaning of varnish on paintings[12]. It has also been shown that it is possible to obtain non-invasive measurements of refractive indices of varnish layers using OCT[8].

Given the initial success, we have started a systematic study to investigate the potential of OCT as a non-invasive technique for a variety of applications to a wide range of museum objects. In this paper, we report some of the new results from this ongoing project. In Section 2, we present results of a trial run of applying a portable FD-OCT on old master paintings from the National Gallery and fragments of non-accessioned objects from the British Museum in a conservation studio of the National Gallery in London. Section 3 is separated into two parts where the first part gives the results of a systematic study of the spectral transparency of historic artists' paint in the visible and near infrared and the second part discusses non-invasive refractive index measurements of some of these paints using OCT. A discussion of the design specifications of an OCT optimized for *in situ* use in a museum is given in Section 4. In Section 5, we present a dual wavelength OCT and some preliminary results on test samples and finally in Section 6 we present the potential for pigment identification with OCT and reflectance spectroscopy.

2. EXAMPLES OF OCT IMAGING OF MUSEUM OBJECTS

At the last Munich conference on optics for art two years ago, we reported our work on OCT applications on paintings based mainly on samples and test paintings. Here we present a trial run using a FD-OCT for *in situ* examination of old master paintings in a conservation studio of the National Gallery. The FD-OCT operates at 930 nm with an axial resolution of 6 μm, transverse resolution of 9 μm and a maximum depth range of 1.6 mm. A number of paintings from the National Gallery and a few fragments of different objects from the British Museum were examined. Here we present example scans of a painting and a fragment of degraded glass to illustrate the different problems encountered in scanning a highly scattering material (e.g. a painting) and a transparent material such as glass.

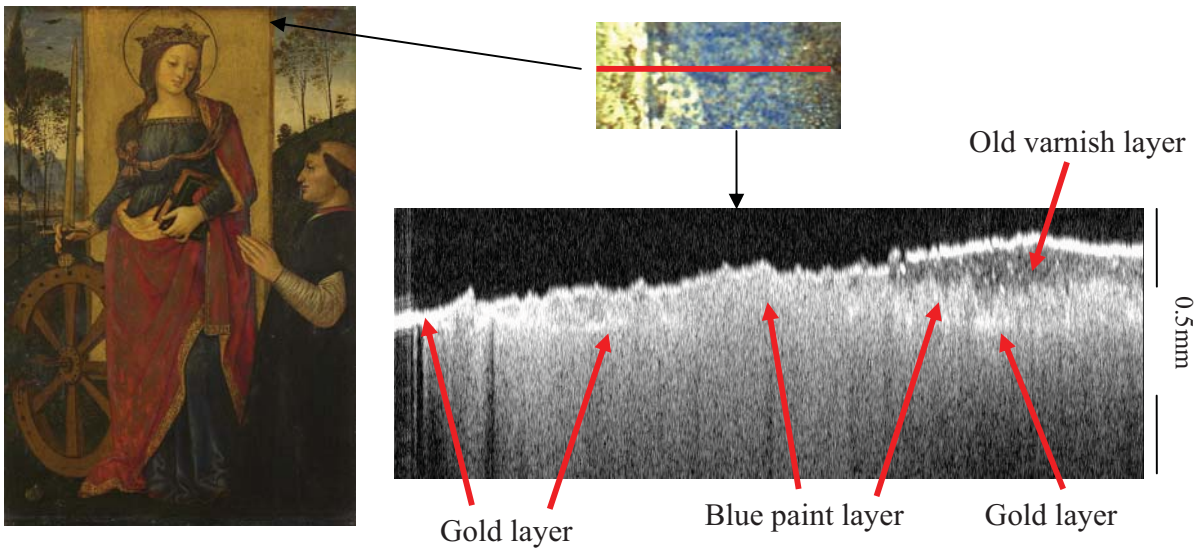

Fig. 1. Left: *Saint Catherine of Alexandria with a Donor* (1480-1500) by Pintoricchio (National Gallery No. 693); Top right: a detail from the painting where the right hand side is covered with an old yellowed varnish; the old varnish has been cleaned off on the left; the OCT scan direction is marked in red. Bottom right: a 930nm OCT image of a scan through the centre of the area showing the old varnish region on the right and the cleaned area on the left.

Figure 1 shows an example where part of an old degraded yellow varnish has been removed. The painting has an interesting layer structure where paint has been applied over a gold layer. The OCT image shows the varnish, paint and

gold layers. On the extreme left is the area where the bare gold layer is exposed, in the middle is the blue paint layer (probably ultramarine) over gold and on the right is the area where there is still the old varnish on top of the paint layer. Effects of multiple scattering in the paint layer give the impression of a thick layer below the gold layer. Multiply scattered light has a longer optical path length than singly scattered light from the same depth. Some of the multiply scattered light from the blue paint layer above the gold layer appears to be coming from below the gold layer where the light had only been scattered back once. An example of this effect is shown clearly in Fig. 3 where a layer of madder lake pigment in egg tempera is painted on top of a glass microscope slide. In Fig. 3, both the air/paint and the paint/glass boundaries are clearly discernable, but the image also shows back-scattered light that appears to be from below the paint/glass boundary indicating multiple scattering in the paint layer. This highlights the importance of combining knowledge about the instrument and the painting in interpreting the images. Similarly, caution had to be employed in interpreting cross-section images for biomedical applications. However, paintings are perhaps more varied than the human eye or skin and as the project progresses one of the important outcomes will be the development of experience in interpretation of OCT images from paintings, and a knowledge of which of the various types of stratigraphy or materials encountered in painting are most likely to be successfully imaged by OCT.

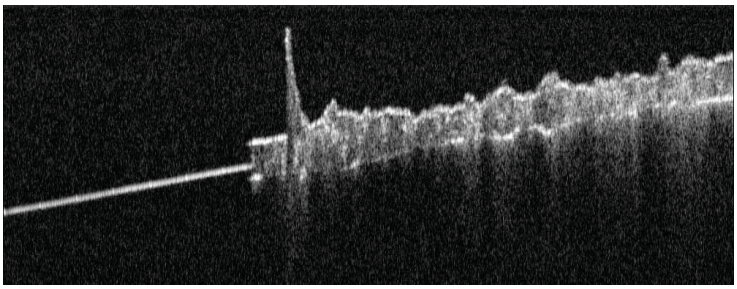

Fig. 3. A 930nm OCT cross section image of madder lake in egg tempera painted on top of a glass microscope slide showing clear evidence for multiple scattering.

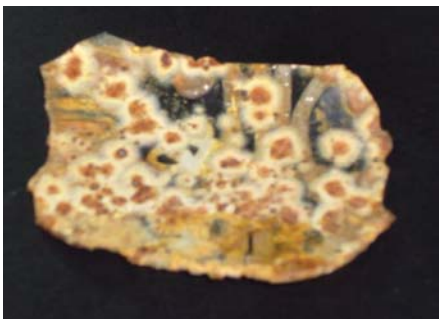

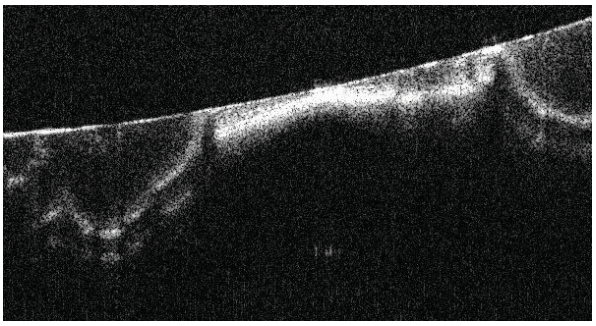

Fig. 4. Left: a piece of 17th Century Antwerp facon de Venise glass showing typical deterioration patterns. Right: an OCT cross-section scan through some of the areas of corrosion.

In contrast, Fig. 4 shows an OCT scan of a highly transparent material, a piece of corroded 17th Century Antwerp facon de Venise glass, a non-accessioned object from the British Museum. The OCT image shows the corrosion spots in cross section where there seem to be multiple corrosion fronts. Note that the glass has a greater optical thickness than the depth range of the OCT, which is why the bottom surface of the glass is not seen in the cross section. One of the limitations of FD-OCT is the short depth range (limited by the number of pixels of spectrometer detector and the depth of focus of the objective lens)[13] which is usually not a problem for highly scattering material where the scattering limits the penetration depth, but is clearly not adequate for highly transparent material. In the case of the FD-OCT used for this application, the depth range was 1.6 mm which means it can only image glass up to a maximum thickness of ~1 mm.

3. OCT & OPTICAL PROPERTIES OF PAINT MATERIAL

3.1 Spectral Transparency of Traditional Paint

Since the invention of infrared reflectography for the imaging of underdrawings, there have been studies conducted to directly or indirectly determine the optimum spectral window for infrared imaging[14,15,16]. However, there has not been a comprehensive survey of the transparency of historic artist pigments over the full near infrared (NIR) range. A set of paint-outs consisting of a wide variety of ~50 historic artists' pigments in both egg tempera and linseed oil has been prepared. The pigments were chosen to be representative of those found on paintings and the compositions of the pigments were verified with EDX, FTIR and XRD measurements. The samples were prepared with known pigment volume concentration and thickness. A list of the pigments is given in Table 1. In order to measure the transparency of the paint layers, one set of paint-outs was prepared over thin glass microscope slides.

Table 1 Pigment List

Hue	Pigment	Supplier	Hue	Pigment	Supplier
red	Natural red ochre (French)	Kremer Pigmente	green	Natural malachite	Kremer Pigmente
	Cadmium red	L.Cornelissen and Son		Artificial malachite	Kremer Pigmente
	Vermilion	The Pigment Factory Bejing		Viridian green	L.Cornelissen and Son
	Vermilion light	Kremer Pigmente		Cobalt turquoise (Rimmans green)	L.Cornelissen and Son
	Sappanwood lake	prepared by National Gallery		Cobalt bottle green	Kremer Pigmente
	Lac lake	prepared by National Gallery		Verdigris	Kremer Pigmente
	Red lead	Kremer Pigmente		Bavarian green earth	Kremer Pigmente
	Chrome red	Kremer Pigmente		Phthalo green (Monastral)	L.Cornelissen and Son
	Cochineal lake	prepared by National Gallery	blue	Smalt	L.Cornelissen and Son
	Madder lake (from dyed wool)	prepared by National Gallery		Azurite MP	Kremer Pigmente
	Madder lake (from ground madder root)	prepared by National Gallery		Azurite	The Pigment Factory Bejing
	Rose madder (genuine)	L.Cornelissen and Son		Prussian blue (Milori)	Kremer Pigmente
	Natural iron oxide red	Kremer Pigmente		Cerulean blue	Kremer Pigmente
yellow	Lemon yellow (barium chromate)	L.Cornelissen and Son		Manganese blue	Kremer Pigmente
	Naples yellow light	Kremer Pigmente		Cobalt blue medium	Kremer Pigmente
	Lead tin yellow (type I)	Kremer Pigmente		Artificial ultramarine blue light	Kremer Pigmente
	Orpiment	The Pigment Factory Bejing		Artificial ultramarine blue dark	Kremer Pigmente
	Aureolin (cobalt yellow)	L.Cornelissen and Son		Indigo	Kremer Pigmente
	Cadmium yellow deep	L.Cornelissen and Son	purple	Manganese violet	Kremer Pigmente
	Chrome yellow medium	Kremer Pigmente		Cobalt violet dark	Kremer Pigmente
	Cadmium yellow light	L.Cornelissen and Son		Cobalt violet light	Kremer Pigmente
	Dyer's Broom lake	prepared by National Gallery	white	Titanium white	L.Cornelissen and Son
	Italian golden ochre	Kremer Pigmente		Lead white	Kremer Pigmente
	Weld lake	prepared by National Gallery	black	Bone black	Kremer Pigmente
	Natural Italian terra di siena (raw)	Kremer Pigmente		Charcoal (made from beech)	Kremer Pigmente

The transparency of a paint layer depends on both the scattering and absorption properties, since light is both scattered and absorbed when it travels through the layer. For a strongly scattering paint layer (painted on glass), we expect to find the backscattered light and hence the reflectance to be high and independent of whether the sample was placed on a white or black background. A highly absorbing paint layer would have low reflectance on a white or black background. In contrast, a highly transparent layer will have high reflectance when it is placed on a white background but low reflectance when placed over a black background. For paint layers, the depth penetration of an OCT is limited by multiple scattering rather than absorption since OCT is more sensitive to scattering than absorption.

An Ocean Optics HR2000 fibre optic spectrometer (200-1100nm), a Polychromix DTS 1700 (900-1700nm) and DTS 2500 (1700-2500nm) fibre optic spectrometer were used to measure the spectra between 400 nm and 2500 nm. The spectral resolutions of the three spectrometers are 0.9 nm, 12 nm and 22 nm. By comparing the spectral reflectance over white and over black, we find that almost without exception all paint samples have highest transparency (or least extinction) at 2.2-2.3 μm. There are six pigments that have slightly higher (but comparable) transparency in other regions of the spectra. This is best illustrated by defining a transparency factor (η) as

$$\eta(\lambda) = \frac{S_W(\lambda) - S_B(\lambda)}{S_W(\lambda)} \qquad (1)$$

where S_W is the spectral reflectance of the paint measured over a standard white background and S_B is the spectral reflectance of the paint when it is placed far away from any reflecting background (this is equivalent to placing it over a non-reflecting black background). Figure 5 shows median transparency of the sample of pigments painted in oil and in egg tempera as a function of wavelength, which illustrates the general increase in transparency into the infrared and that the maximum transparency is at 2.2-2.3 μm. Figure 6 shows how the spectral transparency determined from the

reflectance measurements over white and black background of two paint samples corresponds to their OCT cross section images. The reflectance spectra show that verdigris in linseed oil is highly absorbent at 930 nm but transparent at 1310 nm which is confirmed by the OCT images at these two wavelengths. Similarly, the reflectance spectra show that cobalt blue in linseed oil is transparent at 930 nm but highly absorbent at 1310nm which is what we see in the OCT images.

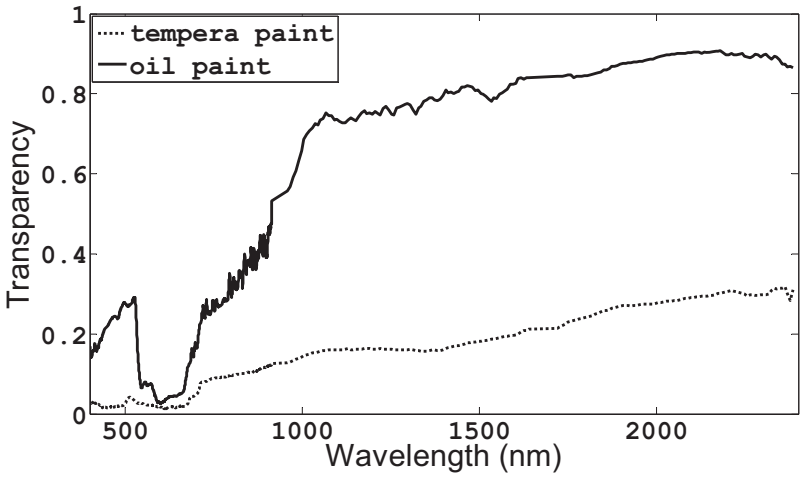

Fig. 5. Transparency (η) as defined in Eq. (1) is plotted as a function of wavelength after taking the median transparency of the sample of pigments painted in oil and in egg tempera.

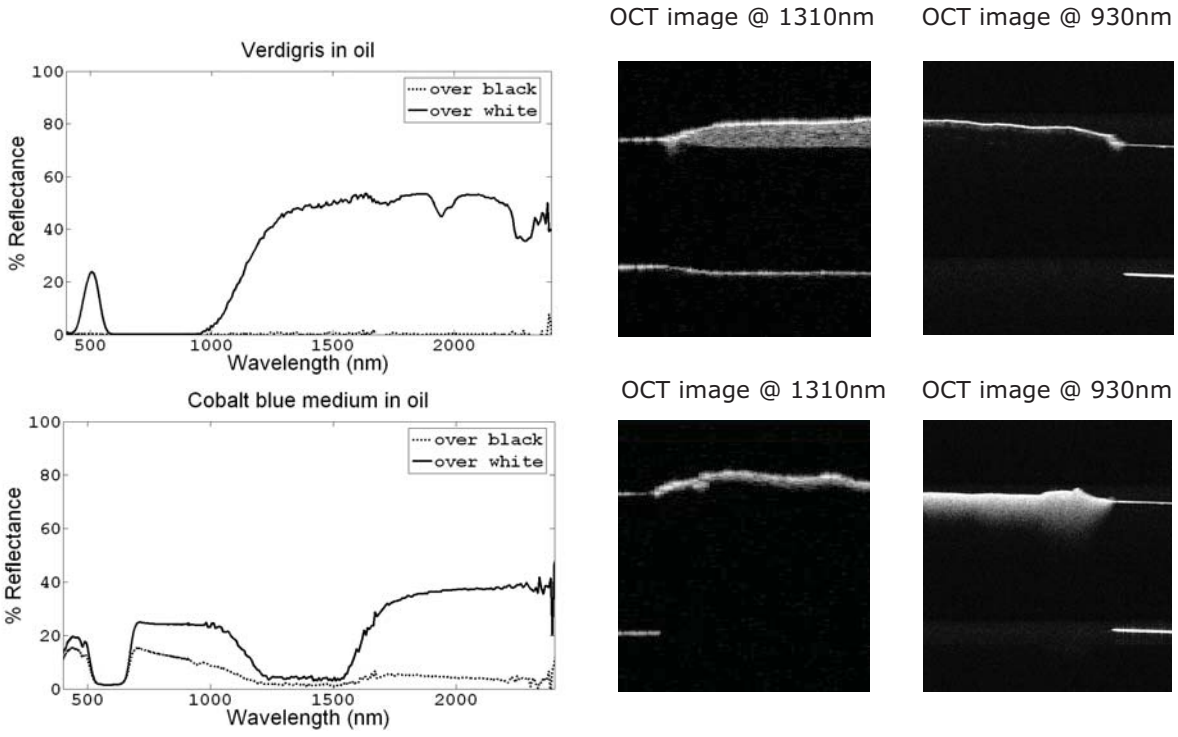

Fig. 6. Spectral reflectance and OCT images at 930 nm and 1300 nm of verdigris and cobalt blue medium in linseed oil. The OCT image of verdigris at 1300 nm is transparent and at 930 nm it is highly absorbent consistent with the spectral reflectance data. Similarly the OCT image of cobalt blue medium is more absorbent at 1300 nm.

3.2 OCT Measurements of Refractive Indices of Traditional Artists' Paint

Knowledge of the refractive index of paint layers is useful in converting optical thickness to real physical thickness. Refractive indices of the paint samples on glass microscope slides can be measured directly with an OCT. Figure 7 shows one way of measuring the refractive index, where the group refractive index can be measured from the ratio between the optical thickness and the physical thickness of the paint layer as $n = \frac{t_o}{t_r}$. The measurement is repeated at various points on the paint sample to obtain the mean refractive index and uncertainty. The accuracy of the measurement is limited by the thickness of the paint layer and the depth resolution of the OCT. Another source of error is the overestimation of the optical thickness because of multiple scattering. In order to check if the paint layer is multiply scattering, a second method shown in Fig. 8 measures the optical thickness of the paint layer by subtracting the optical thickness of the glass from the optical thickness of paint and glass and the refractive index is given by $n = \frac{t_w - t_g}{t_r}$. This second method gives a more accurate measure of the refractive index because it avoids measuring the weak paint/glass interface and measures the well defined air/glass and glass/air interfaces. Similarly, the measurements are repeated at various points on the paint sample to increase accuracy of the measurement. Unfortunately, the second method can not be used with the 930nm FD-OCT because of the limited depth range of the FD-OCT.

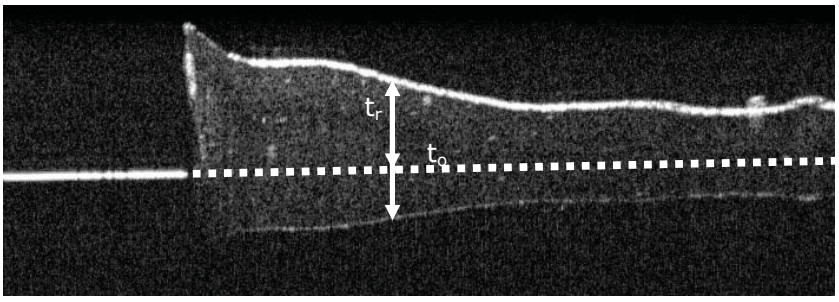

Fig. 7. Refractive index measurement of Rose Madder in linseed oil using a 930 nm FD-OCT (method 1).

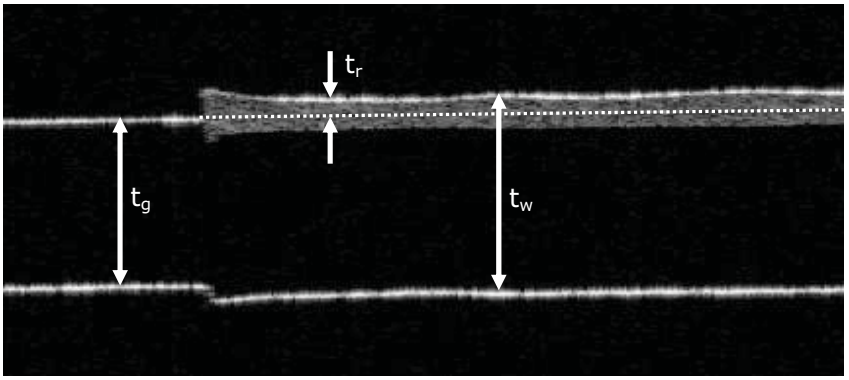

Fig. 8. Refractive index measurement of Rose Madder in linseed oil using a 1310 nm TD-OCT (method 2).

We present the results of refractive index measurements of two paint samples, cochineal lake in linseed oil and rose madder in linseed oil, both were painted at a wet thickness of ~200 μm. The measurements were taken with the 930nm FD-OCT (depth resolution 6 μm) and a 1310nm TD-OCT (depth resolution 18 μm). For cochineal, the results are

$n = 1.55 \pm 0.02$ at 930nm, $n = 1.45 \pm 0.12$ at 1310nm using the first method and $n = 1.53 \pm 0.07$ at 1310nm using the second method. Similarly for rose madder, $n = 1.59 \pm 0.09$ at 930nm, $n = 1.59 \pm 0.08$ at 1310nm using the first method and $n = 1.61 \pm 0.07$ at 1310nm using the second method. The uncertainties quoted are one standard deviation. Both paints are in the single scattering regime.

4. OCT FOR ART CONSERVATION AND ARCHAEOLOGY

What kind of OCT is best suited to museum applications? In biomedical applications, the demand is for fast OCTs for *in vivo* imaging which means there is a trade-off between imaging speed and integration time. Current OCTs are mostly designed for biomedical applications where sensitivity is sacrificed for speed[13]. In the case of museum objects, apart from applications such as laser cleaning (Targowski this volume), speed is not crucial as the objects are stationary. We need to re-consider the traditional trade-off in OCT design. In the shot noise limited regime (which is the case for current OCTs), increase of integration time improves the S/N. It is worth considering either increasing the integration time for OCT acquisition or averaging multiple frames.

Current wisdom considers FD-OCT the future for OCT design because of the higher sensitivity and speed of acquisition. However, for stationary art objects in a studio, speed is no longer a fundamental advantage and FD-OCT has a number of drawbacks compared with TD-OCT. In a FD-OCT, the depth range is limited by the spectral resolution of the spectrometer and the depth of field of the objective lens in the case of high resolution imaging. There is a trade off between the transverse resolution and the depth of field. For example, a transverse resolution of 1 μm corresponds to a depth of field of less than 10 μm in the near infrared. In the case of TD-OCT, especially *en-face* OCTs it is possible to overcome the limitation in depth of field by incorporating dynamic focusing mechanism. Another issue is that FD-OCTs are more prone to ghost images, especially when imaging highly reflective surfaces such as freshly varnished paintings. In addition, FD-OCT operating beyond the CCD sensitivity range, i.e. $\lambda > 1$ μm are much more expensive because it needs either an infrared array detector for the spectrometer or a relatively expensive source such as a swept source OCT[17].

While museum objects do not move, their environment may not be stationary. In our recent trial run of using a FD-OCT to examine old master paintings in a conservation studio in the National Gallery, we found that vibrations from air conditioning plant as well as soprano voices are noticeable from the OCT scans. Figure 7 (Left) shows the image acquired at the National Gallery of a single cross-section scan consisting of 1000 individual depth scans. The acquisition frequency of the single depth scans is 5 kHz which means one cross-section scan is acquired at 5 frames per second. Figure 7 (Right) shows the average of 11 successive frames which is clearly blurred. Closer examination showed that the frequency of the vibration is less than ~1 kHz (c.f. frequency of human voice is between ~80Hz and ~3 kHz) with a peak-to-peak amplitude of ~20 μm. For comparison, Fig. 8 shows images acquired by the same OCT in the NTU Imaging Laboratory; the left image is a single cross-section frame and the right image is the average of 11 successive frames which shows no visible blurring. This result shows that vibration effect needs to be taken into account when deciding on the length of the integration time. In situations where vibration can not be avoided, it would be best to average a series of frames of shorter integration time (after some image processing to align the individual frames).

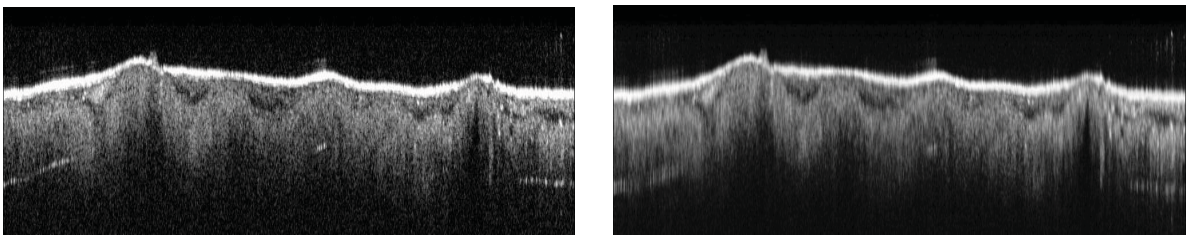

Fig. 7. OCT cross-section images of an area on a large canvas painting in a conservation studio in the National Gallery. Left: one frame Right: average of 11 frames

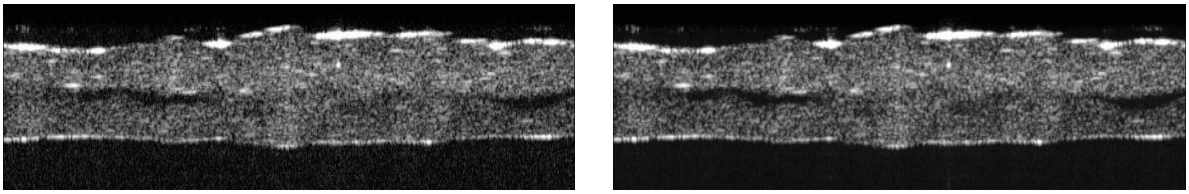

Fig. 8. OCT cross-section images of a paint sample (cochineal lake in linseed oil) on a glass substrate in the NTU Imaging Lab. Left: one frame Right: average of 11 frames

Comparison between images of paint sample cross-section viewed under a microscope and non-invasive subsurface stratigraphy of paintings viewed through an OCT, shows that the limiting factors in information content of an OCT image are the high scattering properties of some of the paint, the relatively low resolution of an average OCT and the lack of colour information. While an average OCT, using an inexpensive SLD source, can give depth resolutions of ~10 μm in free space, OCTs using expensive novel broad-band light sources such as Kerr lens mode locked Ti:sapphire laser and photonic crystal fibre based non-linear light sources have been demonstrated to provide ~1μm depth resolution[18]. With such high resolution, it would be possible to resolve many of the pigment particles, making the information on paint structure in the OCT images closer to that from conventional cross sections of paint samples examined with a microscope.

A three-colour wide-field OCT using colour LEDs was recently reported to give colour subsurface images of bees, leaves and apples[19]. Given the high scattering properties of paint in the visible, such a three-colour OCT would have very limited depth penetration in paint. As paint material is more transparent in the near infrared than the visible, a three infrared channel OCT providing false colour cross-section images would be more useful.

While it has been established for a long time that paint material is more transparent in the near infrared than in the visible, it was not clear in which spectral window paint materials are most transparent. The systematic study of the spectral transparency in the visible and the near infrared (400nm – 2400nm) of paint made of historic artists' pigments and media described in Section 3.1 showed that the best wavelength for transparency to be ~2.2 μm. An OCT at ~2.2 μm would be able to probe deeper into traditional paint material than the ones currently available.

5. A DUAL WAVELENGTH OCT

A dual wavelength *en-face* TD-OCT was constructed to test the idea of using multiple wavelength OCT to probe the subsurface structure of paint layers and identify the material. An *en-face* OCT takes images in planes parallel to the painting surface one after another at increasing depth[3] which is particularly convenient for the examination of paintings[7]. The OCT is fitted with two SLD sources at 670 nm and 1300 nm. The setup shown in Fig. 9 enables the acquisition of cross-sectional or *en-face* scans at both 670 nm and 1300 nm simultaneously. The configuration is comprised of two essentially complete OCT systems, whose object arms are superimposed immediately after decoupling from the fibre and prior to scanning by the galvo mirrors. This is achieved using a dichroic beamsplitter, a cold mirror selected with a transition wavelength of 1 μm. After reflection from the object, the same beamsplitter is used to direct the two wavelengths back into their respective fibre sub-systems. The two systems are further linked by the use of a single translation stage to provide scanning in both reference arms, ensuring that the two channels are synchronised in depth. By placing a mirror in the object arm, the reference optical path for both wavelengths are aligned to within the axial resolution of the system, and hence images obtained for the two channels represent a single spatial region. The axial resolutions are ~20 μm in both wavelengths. The transverse resolutions are 10 μm and 20 μm at 670 nm and 1300 nm respectively.

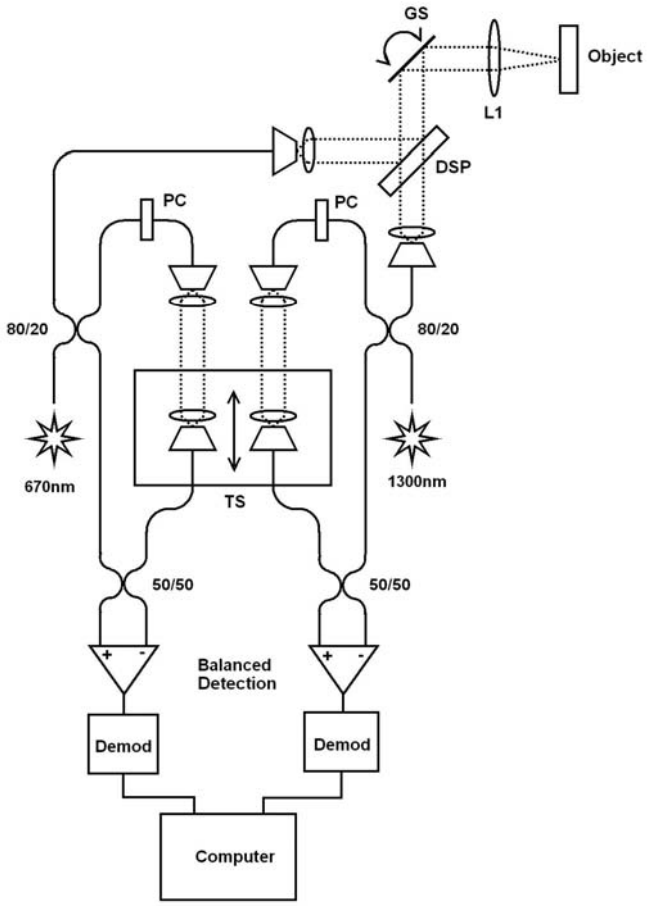

DSP: Dichromatic Beam Splitter
TS: Translation Stage
GS: Galvo Scanners
PC: Polaristaion Controller
Demod: Demodulation Electronics
L1: Object Lens, achromatic doublet

Fig. 9. The dual wavelength optical coherence tomography system architecture

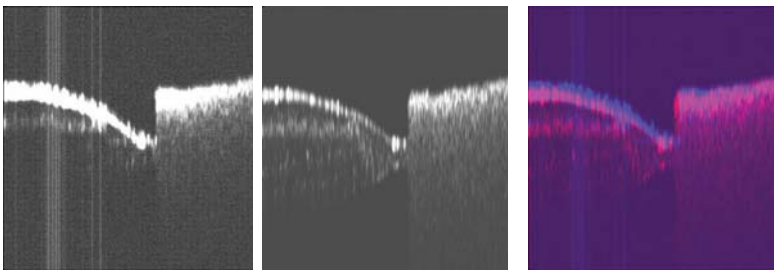

(a) (b) (c)

Fig. 10. Dual wavelength cross section scan of a test sample of Malachite in egg tempera painted over a piece of microscope glass and a piece of white paper as a reference sample. (a) A 670nm scan of the test sample (on the left) showing a couple of top layers and a piece of white paper on the right; (b) simultaneous 1300nm scan of the test sample and white paper showing 5 layers of the paint; (c) an overlay of the two images where the 670nm image is in blue and the 1300nm is in red.

A test sample of malachite in egg tempera (a medium-rich mixture) that was painted in five layers was imaged with the dual wavelength OCT. Figure 10a,b show the simultaneous cross section images at the two wavelengths of the same position on the sample. The 1300 nm image shows all five layers, but the 670 nm image shows only the top three layers. The relative intensity of the two images were adjusted such that the white paper used as a reference would give roughly equal backscattered light in the upper portion of the paper where scattering is seen at both wavelengths. The two images are superimposed in Fig. 10c showing the potential for a multiple wavelength OCT scan providing structure as well as "colour" information.

6. PIGMENT IDENTIFICATION WITH SPECTRAL REFLECTANCE AND OCT DATA

An alternative method of obtaining both structure and spectral/colour information non-invasively is to combine the structural information from an OCT image with the spectral reflectance measurements (another non-invasive method). Pigment identification using reflectance spectroscopy is both an established technique and one that has not been successful enough to have been met with much enthusiasm in the field of art conservation. The problems are twofold. Firstly, the focus has mainly been on identifying the reflectance spectra of pigments in the visible wavelength region. As such, unique identification of a spectrum to a particular pigment is often difficult as the spectra of pigments of similar hues can look alike. Secondly, it has been difficult to identify mixtures of chromatic pigments with confidence from reflectance spectra alone, especially when it is restricted to the visible spectral range. By extending the wavelength range into the near infrared, additional spectral features that are unique to each pigment are often revealed, allowing more conclusive identification. However, non-invasive spectral pigment identification is still a rather challenging task when it comes to mixtures of pigments. OCT provides additional structural information when the paint layers are translucent and even when they are not, it gives information on the scattering and absorption properties of the material. Similarly, even though for most OCTs, it is currently not possible to resolve the individual pigment particles for most pigments, bulk optical properties of the material can still be extracted. Figure 11 shows an example of OCT images being used to distinguish between a paint of pure smalt in egg tempera and one where it is mixed with a white pigment. The addition of a white pigment does not change the spectral features of a paint mixture significantly as shown in Fig. 11. However, the OCT data shows significant difference between the pure smalt paint and the paint mixed with lead white.

With current technology, it appears that the combination of high resolution spectral data combined with OCT data offers a promising new direction for non-invasive pigment identification. While it does not provide as much of the structural information as is given by a conventional microscope image of a cross section of a sample, it offers more spectral information as well as the additional data on absorption and scattering properties.

7. CONCLUSIONS

OCT is the first non-invasive imaging technique to date that allows direct *in situ* imaging of subsurface structure of works of art. However, research and experience is still needed to interpret OCT images before it can be usefully applied for routine examination. While varnish layers are transparent in the near infrared, many of the paint layers are highly scattering limiting the penetration depth. We have conducted a systematic study of the spectral transparency of historic artitsts' paint and identified the spectral region best suited to OCT imaging of paint layers. In the visible and near infrared (400-2400 nm), paint material is most transparent at ~2.2 μm. In designing OCTs specific for museum use, we need to re-consider the traditional OCT design criteria meant for in vivo biomedical applications. Museum objects are stationary and hence speed is less important than sensitivity.

Since the initial success of applying OCT to works of art, we are now conducting a systematic study on how to exploit it further in obtaining quantitative information such as measuring the optical properties and assisting non-invasive pigment identification.

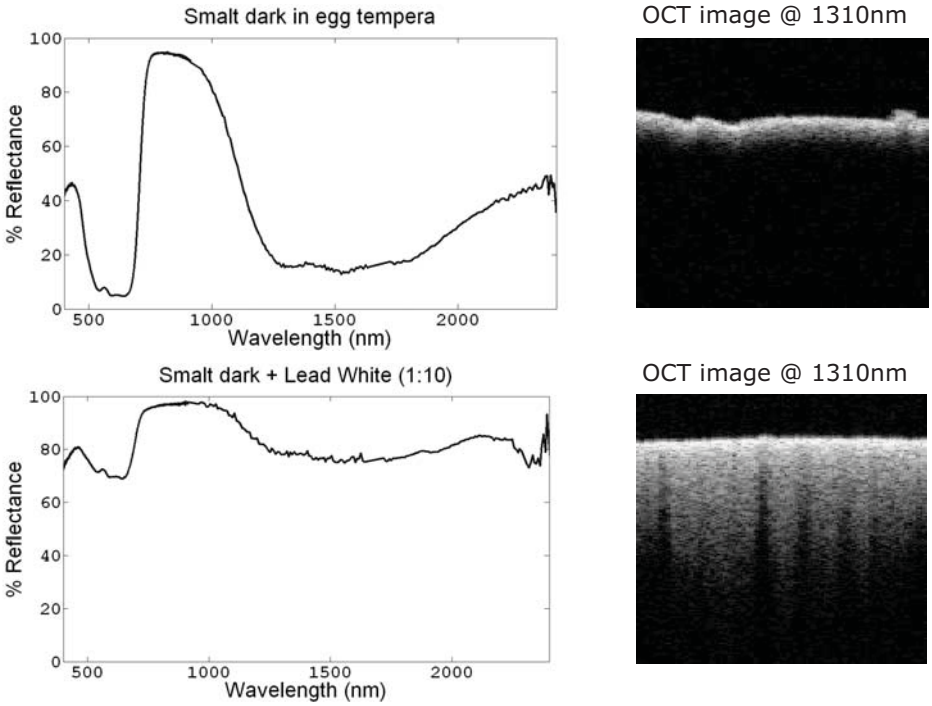

Fig. 11. Top Left: spectral reflectance of pure smalt in egg tempera; Top Right: OCT cross section image at 1300 nm of the same sample showing low scattering and high absorption. Bottom Left: spectral reflectance of smalt in egg tempera mixed with lead white; Bottom right: OCT cross section image at 1300 nm of the same sample showing strong scattering because of the presence of lead white;

ACKNOWLEDGEMENT

This project is funded by the Leverhulme Trust. We would like to thank colleagues at the National Gallery and the British Museum for providing samples, studio space and for useful discussion. We would also like to acknowledge Sophie Martin-Simpson for preparing the historic artists' paint samples.

REFERENCES

1 D. Huang, E. A. Swanson, C. P. Lin, J. S. Schuman, W. G. Stinson, W. Chang, M. R. Hee, T. Flotte, K. Gregory, C. A. Puliafito, J. G. Fujimoto, "Optical coherence tomography", Science, 254, 1178, 1991.

2 A. F. Fercher, C. K. Hitzenberger, G. Kamp, S. Y. El-Zaiat, "Measurement of intraocular distances by backscattering spectral interferometry", Opt. Commun. 117, 43, 1995.

3 A. Gh. Podoleanu, J. A. Rogers, D. A. Jackson and S. Dunne, "Three dimensional OCT images from retina and skin", Optics Express, 7(9), 292, 2000.

4 H. Liang, M. Gomez Cid, R. Cucu, G. Dobre, D. Jackson, C. Pannell, J. Pedro, D. Saunders, A. Podoleanu, "Application of OCT to examination of easel paintings", Second European Workshop on Optical Fibre Sensors, Proc. SPIE, 5502, 378, 2004.

5 P. Targowski, B. Rouba, M. Wojtkowski, and A. Kowalczyk, "The application of optical coherence tomography to non-destructive examination of museum objects", Studies in Conservation, 49(2), 107, 2004.

6 M.-L. Yang, C.-W. Lu, I.-J. Hsu, C. C. Yang, "The use of optical coherence tomography for monitoring the subsurface morphologies of archaic jades", Archaeometry, 46(2), 171, 2004.

7 H. Liang, M. G. Cid, R. G. Cucu, G. M. Dobre, A. Gh. Podoleanu, J. Pedro, D. Saunders, "En-face Optical Coherence Tomography – a novel application of non-invasive imaging to art conservation", Opt. Express, 13, 6133, 2005a. http://www.opticsexpress.org/abstract.cfm?id=85276.
8 H. Liang, M. G. Cid, R. G. Cucu, G. M. Dobre, B. Kudimov, J. Pedro, D. Saunders, J. Cupitt, A. Gh. Podoleanu, "Optical Coherence Tomography – a non-invasive technique applied to conservation of paintings", Proceedings of SPIE, 5857, Optical Methods for Arts and Archaeology, Munich, 2005b
9 P. Targowski, G. Michalina, M. Wojtkowski, "Optical coherence tomography for artwork diagnostics", Laser Chemistry, Article ID 35373, 2006
10 M. Gora, P. Targowski, A. Rycyk, J. Marczak, "Varnish abalation control by optical coherence tomography", Laser Chemistry, Article ID 10647, 2006
11 P. Targowski, M. Gora, T. Bajraszewski et al., "Optical coherence tomography for tracking canvas deformation", Laser Chemistry, Article ID 93658, 2006
12 H. Liang, B. Peric, M. Spring, D. Saunders, M. Hughes, A. Gh. Podoleanu, "Non-invasive imaging of subsurface paint layers with optical coherence tomography", Conservation Science 2007, Milan.
13 P. H. Tomlins and R. K. Wang, "Theory, developments and applications of optical coherence tomography", J. Phys. D: Appl. Phys., 38, 2519, 2005.
14 J. R. J., van Asperen de Boer, "Reflectography of paintings using an infra-red vidicon television system", Studies in Conservation, 14, 96, 1969
15 J. Delaney, C. Metzger, E. Walmsley, C. Fletcher, "Examination of the Visibility of Underdrawing Lines as a Function of Wavelength", in *ICOM Committee for Conservation, 10th Triennial Meeting*, Washington DC, 15–19, 1993
16 M. Gargano, N. Ludwig, G. Poldi, "A new methodology for comparing IR reflectographic systems", Infrared Physics & Technology, 49, 249, 2007.
17 R. Huber, M. Wojtkowski, K. Taira, J. G. Fujimoto, "Amplified, frequency swept lasers for frequency domain reflectometry and OCT imaging: design and scaling principles", Opt. Express, 13, 3513, 2005
18 A. Unterhuber, B. Povazay, K. Bizheva et al., "Advances in broad bandwidth light sources for ultrahigh resolution optical coherence tomography", Phys. Med. Biol., 49, 1235, 2004
19 L. Yu and M. K. Kim, "Full color three-dimensional microscopy by wide-field optical coherence tomography", Opt. Express, 12, 6632, 2004.

Pigment identification with optical coherence tomography and multispectral imaging

H. Liang, K. Keita, B. Peric, T. Vajzovic

Nottingham Trent University, School of Science & Technology
Clifton Lane, Nottingham NG11 8NS, UK
E-mail: haida.liang@ntu.ac.uk

ABSTRACT

We describe a new method for non-invasive pigment identification by combining the spectral reflectance in the visible spectrum with near infrared OCT cross-section images of the subsurface layer structure.

Keywords: optical coherence tomography, multispectral imaging, spectral imaging, pigment identification, scattering coefficient

1. INTRODUCTION

Routine identification of pigments on a painting or painted object is carried out in museums by taking a tiny sample to examine under a microscope. To identify pigments in various layers, the sample is prepared and polished to examine the cross-section. An experienced microscopist can visually identify the pigments according to their colour and shape. The disadvantage of the method is that it is invasive and conservation ethics restricts sampling to regions of damage or edges of the art work, hence it is difficult to obtain a global view of the material composition of the whole piece.

It has long been recognised that spectral reflectance can be used as a signature of a pigment to offer non-invasive identification of pigments. For the last 10 years, multispectral imaging which offers an efficient measurement of spectral reflectance over a large area has been used for spectral pigment identification[1,2]. However, this non-invasive technique has not been met with enthusiasm in the conservation community partly because the identification of mixtures of pigments is unreliable and it cannot identify a pigment if it has deteriorated. The difference between spectral pigment identification and the examination of a sample under a microscope is that the latter offers not only colour but shape information whereas spectral pigment identification gives spectral (hence colour) information but without any shape information on the pigment particles.

Recently, another non-invasive imaging technique, optical coherence tomography (OCT), has been successfully applied to the imaging of subsurface paint layers[3-9]. It has been shown that in certain cases where the paint is transparent and if the pigment particles are of a few microns in size, it is possible to see the individual particles[5,9]. Even when it is not possible to see the individual particles, the scattering properties of the paint will contribute additional information to the identification of the material. Since paint is more transparent in the near infrared and most efficient OCT sources are in the near infrared, it is preferable to use an infrared OCT rather than an OCT that operates in the visible range. Unlike cross-sections of paint samples viewed under a microscope, OCT cross-section images do not have colour information. However, a combination of OCT images of paint cross-section and multispectral imaging of

the same area can yield structural and spectral (hence colour) information non-invasively. In addition, even when the pigment particles can not be resolved by the OCT, the scattering and absorption properties can be still be measured from the OCT cross-section images. This additional information can also assist spectral pigment identification.

We will show in this paper to what extent the combination of OCT imaging with multispectral imaging can be used to identify pigments. We will use the novel portable multispectral camera, PRISMS[10] (Portable Remote Imaging System for Multispectral Scanning) for spectral pigment identification.

2. SPECTRAL PIGMENT IDENTIFICATION

A paint consists of pigments in a binding medium. A given type of pigment can be painted out in different binding medium, concentration, particle size, thickness and roughness. In order to identify a pigment through the spectral reflectance of its paint, it is important to distinguish the spectral features of the pigment from variations due to the above factors. In the following section, we examine the effects on the spectral reflectance as a result of each of these variations.

Figures 1 to 5 show that none of the above variations change the key spectral features significantly, i.e. the position of the peaks associated with a pigment type. Incomplete hiding of paint layer does not change the spectral reflectance significantly. Positions of the peaks can shift by ~20nm with concentration, particle size and binding media. Binding medium gives the greatest variation in spectra changing the relative height between peaks, but the basic characteristics of the spectra are still preserved. Finally, the application of paint by hand gives similar spectral reflectance when painted by the same person in the same manner. This shows that the key spectral features in a reflectance spectrum is mostly determined by the pigments in the paint, at least for the spectral range 400-1000nm. For this reason, the identification of pigments in single pigment paint mixtures in paintings has been successful as long as there is no deterioration[1,2,13].

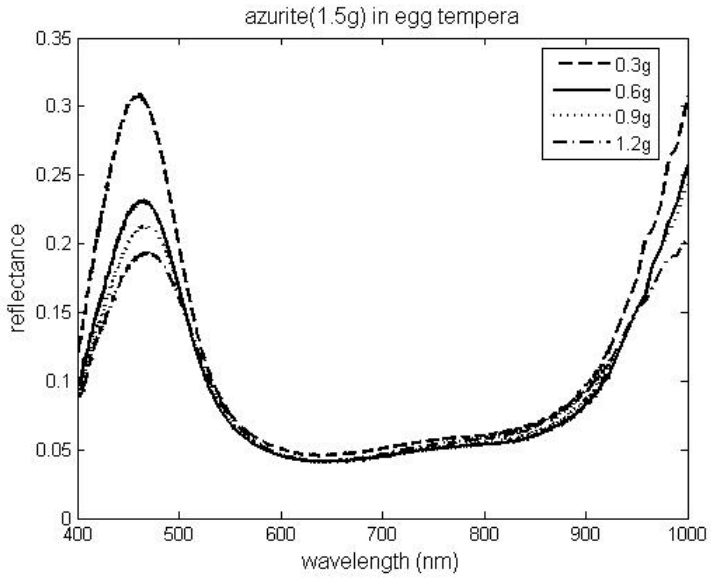

Figure 1. Spectral reflectance of paint consisting of various concentrations of azurite pigments in an egg tempera binding medium. The legends indicate the amount of egg tempera added to 1.5g of azurite.

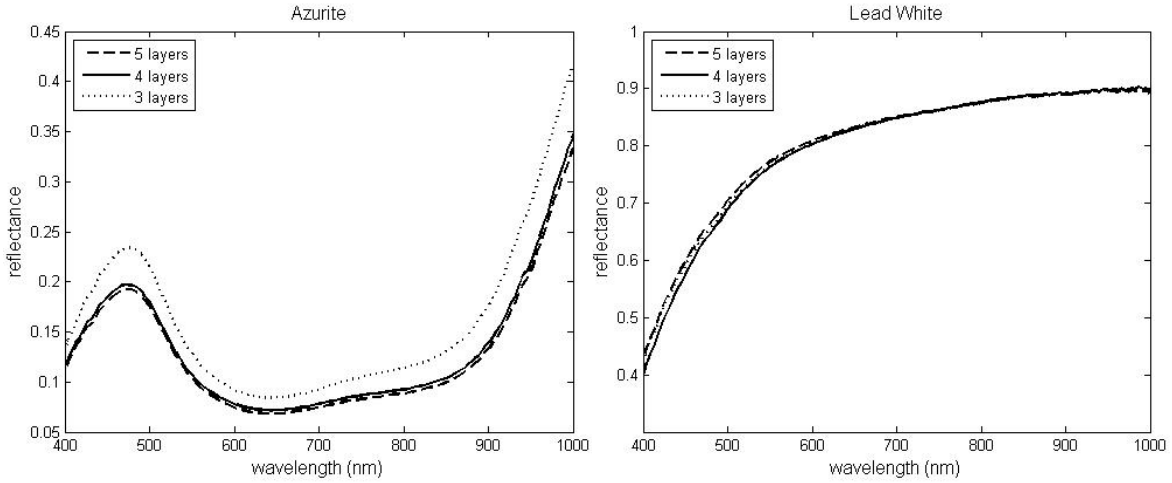

(a) (b)

Figure 2. Effect of thickness of paint on the spectral reflectance of a) azurite in egg tempera and b) lead white in egg tempera (the higher the number of layers the thicker the final paint layer).

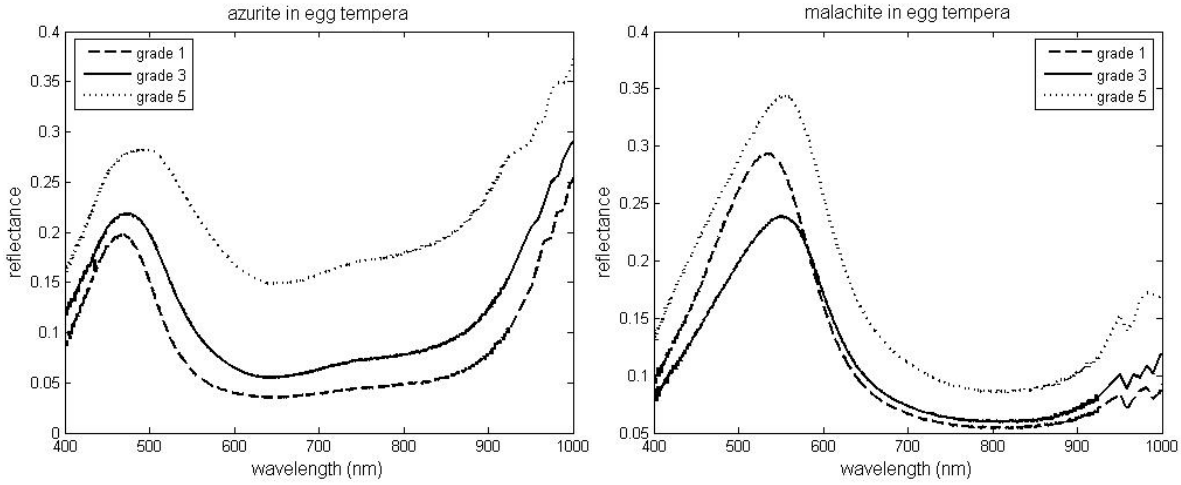

(a) (b)

Figure 3. Effect of particle size on the spectral reflectance of paint: a) azurite in egg tempera and b) malachite in egg tempera with 3 different particle sizes. Particle size decreases with increasing grade.

For pigment identification involving paint mixtures, Kubelka-Munk (KM) theory[11] provides a convenient way of modelling the expected reflectance from a paint layer consisting a mixture of pigments[13]. The KM theory is a simple approximation to the full radiative transfer model, where the diffuse reflectance (R) of the layer without interfaces is related to the effective absorption (K) and scattering coefficients (S) through

$$R = \frac{1 - R_g[a - b\coth(bSh)]}{a + b\coth(bSh) - R_g},$$

where $a = \frac{K+S}{S}$, $b = \sqrt{a^2 - 1}$, h is the layer thickness and R_g is the reflectance of the substrate. KM theory assumes diffuse illumination and collection, however, in practice measurements are often made with collimated normal illumination. Saunderson's correction[12] is normally applied to correct for the reflection at the air/paint and paint/air interfaces. If it is possible to measure the reflectance of the same paint layer over a black and white substrate,

then K/S can be deduced. For a paint layer with infinite optical thickness, the diffuse reflectance is directly related to *K/S*.

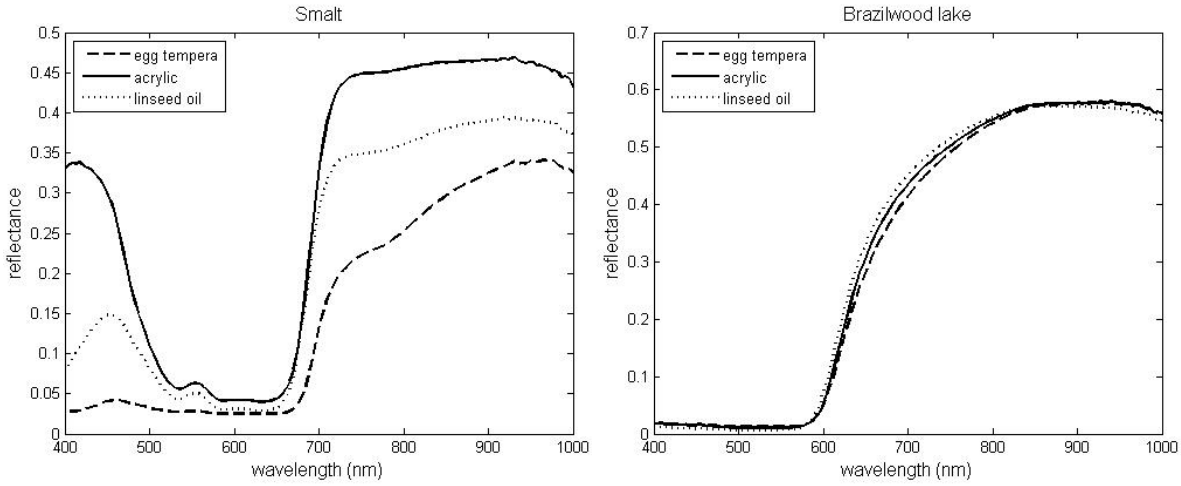

(a) (b)

Figure 4. Effect of binding media on the spectral reflectance of paint: a) smalt pigment and b) Brazil wood lake pigment in an egg tempera, linseed oil and acrylic binding medium.

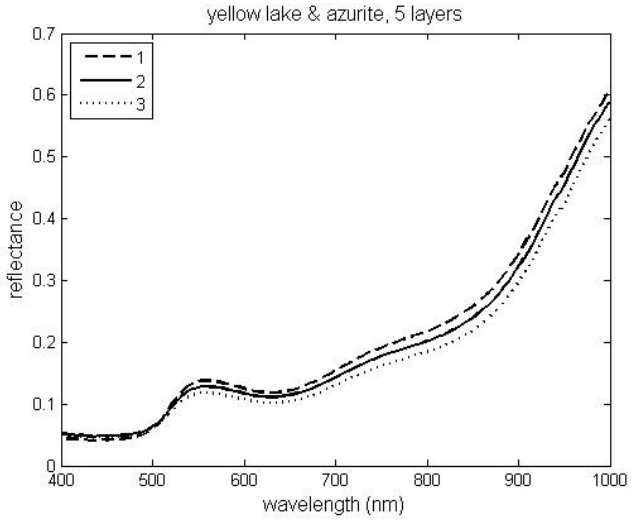

Figure 5. Spectral reflectance of 3 paint patches of Buckthorn lake mixed with azurite in egg tempera painted on 3 separate occasions by the same person. Each paint patch was painted in 5 layers.

If a mixture of different paint components can be modelled as a linear combination of *K/S*, then we can predict the reflectance of the paint mixture. In this case, log(*K/S*) versus wavelength curves shift by a constant for different concentrations which means that the shape of log(K/S) is concentration invariant. To verify how well KM theory can predict the spectral shape of paint mixtures, a set of single pigment paints and their mixtures were painted out and measured with an Ocean Optics fibre optic spectrometer (HR2000) with normal illumination and 45^{o} collection. The measured single pigment spectral reflectances were used to predict the spectra of the mixtures using KM theory. Since our aim here is to identify the pigments in a mixture, the concentrations of the single pigments were set as free parameters to find the best fit of the predicted spectrum to the actual measured spectrum of the mixture. Figure 6 shows a couple of examples of two pigment mixtures where the KM theory with the appropriate concentrations of each pigment is able to give a spectrum very similar to the actual measured spectrum of the mixture. It is found that in general the method works well except when highly

absorbing blue pigments like Prussian blue and indigo are involved. However, by increasing the relative strength of scattering to absorption by adding lead white to the highly absorbing pigment and treating the white added mixture as one component, the method works again. Based on the above study, an algorithm is devised to automatically identify pigments by fitting different combinations to the unknown spectrum. The best fit for each combination is then cross-correlated with the unknown spectrum. The best identification is the one with the highest normalised cross-correlation coefficient at zero offset. An extra 20 nm range around zero offset should be allowed to account for the slight shift in peaks due to different binding medium, concentration and particle size. When the algorithm was applied to 7 two pigment paint mixtures, at least one of the two pigments was identified correctly in each case and in two cases both pigments were identified correctly.

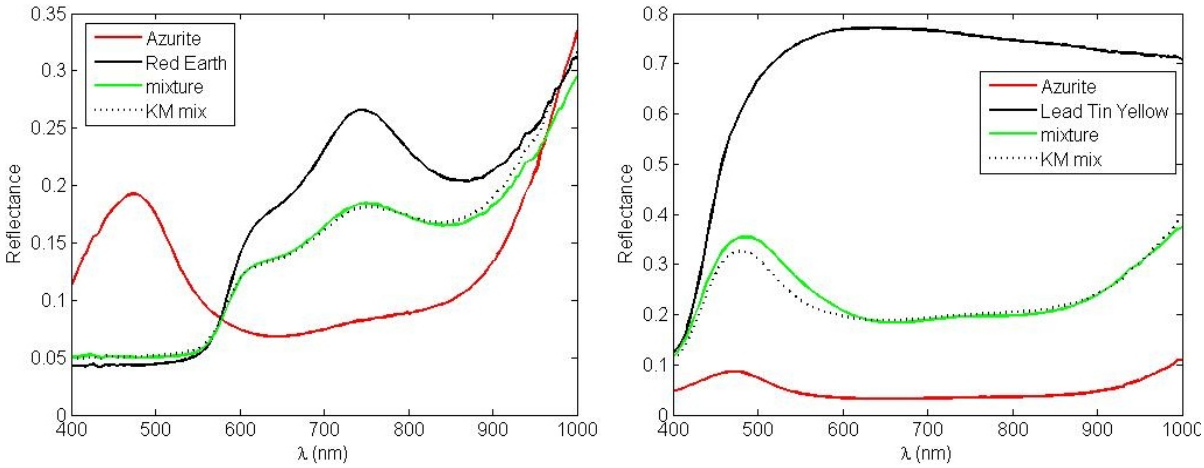

(a) (b)

Figure 6. Kubelka-Munk theory predicting mixture of pigments. The dotted curve gives the predicted spectrum and the green curve give the measured spectrum of the actual mix. a) Measured reflectance of azurite (red), red earth (solid black) and a mixture of the two (green) in egg tempera compared with the predicted spectrum (dotted black) b) measured reflectance of azurite (red), lead tin yellow (solid black) and a mixture of the two (green) compared with the predicted spectrum (dotted black).

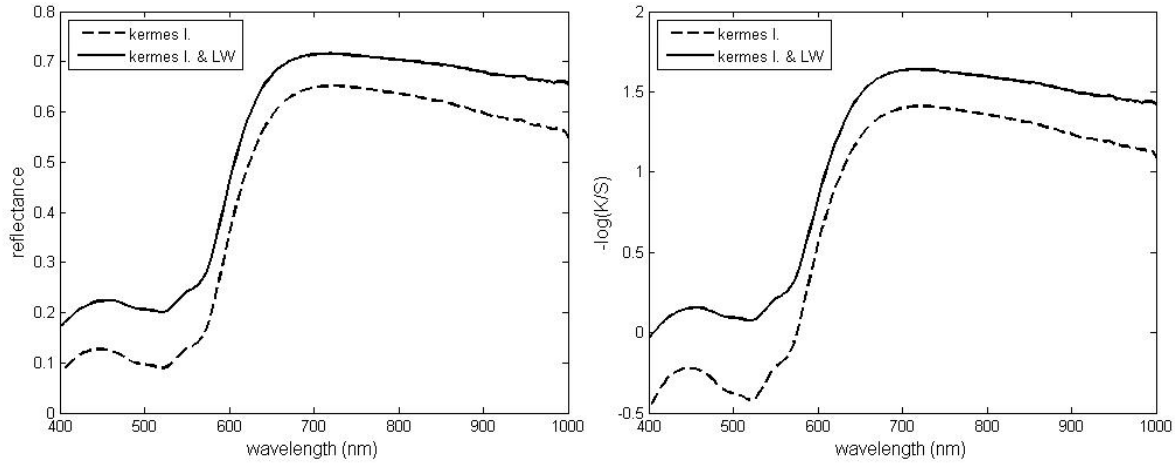

(a) (b)

Figure 7. a) measured reflectance of kermes lake pigment in linseed oil (dashed) and kermes lake mixed with lead white in linseed oil (solid) b) same as a) but plotted in terms of -log(K/S).

The reason for the incorrect identification is that two different pigment combinations can sometimes give spectra with similar shape. A simple example is given in Figure 7 where the spectral shape of kermes lake painted over a white substrate and kermes lake mixed with lead

white are similar. However, we know that the scattering properties of the two are very different. If we have a paint layer painted over a transparent material such as glass, then it is possible to measure *K* and *S* using KM theory by measuring the reflectance over a white and a black background. However, this is not possible on a painting as the substrate is typically opaque. The following section shows a method of measuring the scattering properties non-invasively on a painting.

3. COMBINED OCT AND MUTISPECTRAL IMAGING FOR PIGMENT IDENTIFICATION

A Fourier domain OCT (Thorlabs SROCT) at 930nm was used for the non-invasive imaging of paint layers. It has a 9μm transverse resolution and a 6μm depth resolution (in air). Figure 8 shows the cross-section images obtained with the OCT of a highly absorbing pigment (charcoal), a weakly scattering and absorbing pigment (sappon wood lake), a medium scattering and absorbing pigment (artificial ultramarine dark) and a highly scattering pigment (Ti white). OCT readily shows the scattering and absorption properties of paint layers. Figure 9 shows that while kermes lake and kermes lake mixed with lead white have similar shape in spectral reflectance, their scattering properties are very different as shown in their OCT images.

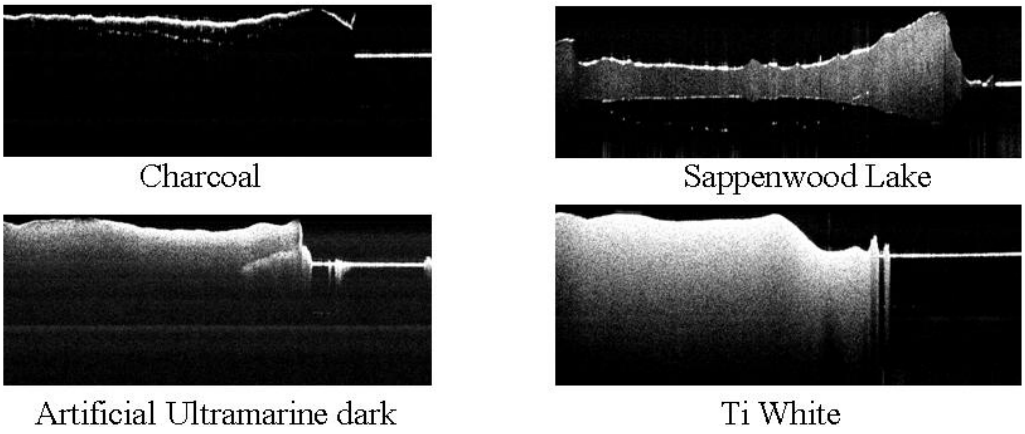

Figure 8. OCT cross-section images of various pigments (in a linseed oil binding medium) painted on glass microscope slides.

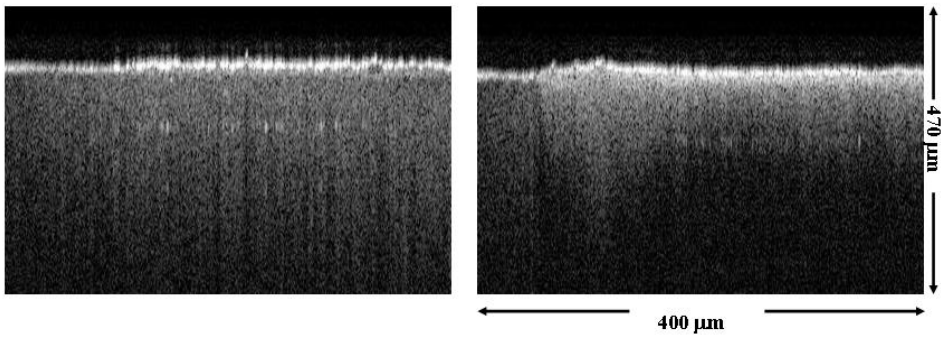

Figure 9. OCT cross-section images of a) Kermes lake in linseed oil (~8 μm thick layer); b) lake with lead white in linseed oil (~12 μm thick layer) painted on a white Teflon board (short section on the left of the images are regions of bare Teflon). The faint dotted lines in the middle of the images are ghost images.

PRISMS[6] (Portable Remote Imaging System for Multispectral Scanning) was originally designed for in situ remote high resolution multispectral imaging of wall paintings from the

ground level. It consists of a filter system operating between 400nm and 880nm (9 filters evenly spaced between 400 and 800nm with 40nm bandwidth and one filter at 880nm with 70nm bandwidth) and a CCD camera mounted on a small telescope. Since this is a multispectral camera designed in our lab and readily available, we used it in combination with the Thorlabs OCT at 930nm to image an easel painting to demonstrate the advantages of combining OCT with multispectral imaging for pigment identification. PRISMS was place 6m from the painting giving an image resolution of ~45μm per pixel on the painting. The OCT probe was placed 1cm from the painting surface on a motorised X-Y-Z micrometer stage to scan a 1cm by 2.5cm area. The individual cross-section images are stacked together and resliced in the plane parallel to the paint surface to give an en face image. Figure 10 shows a direct comparison of the multispectral image at 880nm and the OCT image at 930nm of a painting. The OCT with 5 times better resolution shows more clearly the brush strokes.

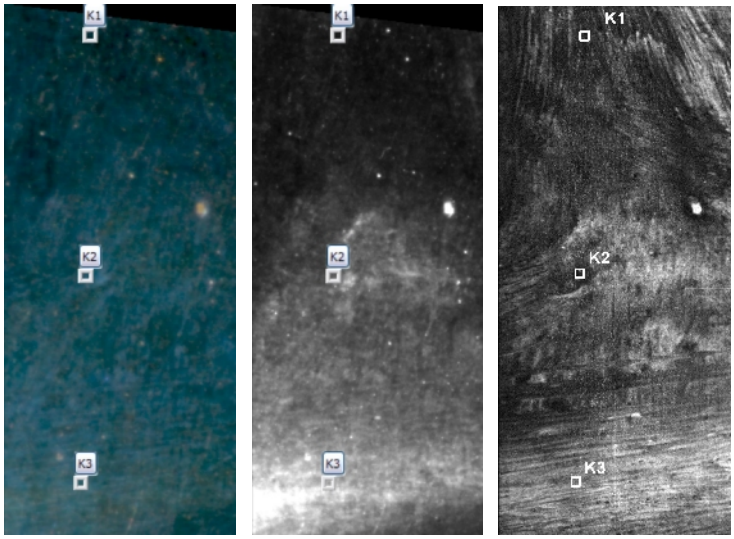

(a) (b) (c)

Figure 10. Multispectral image and *en-face* OCT image of the virgin's blue cloak in *Virgin and Child with an Angel* by an imitator of Francia (National gallery NG 3927). a) colour image deduced from the multispectral image cube assuming D65 illumination and 1931 2^{o} standard observer; b) 880nm image from PRISMS; c) *en face* OCT image at 930nm. The images are 1cm by 2.5cm.

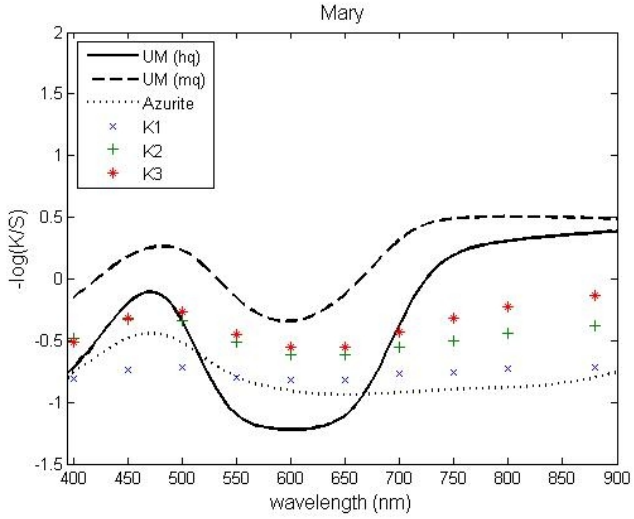

Figure 11. Spectral reflectance converted to –log(*K/S*) measured with PRISMS at positions marked in Fig. 10 compared with spectral reflectance of ultramarine and azurite from a reference library.

Figure 11 shows the spectra corresponding to 3 different locations indicated in Fig.10 obtained from a multispectral image cube captured by PRISMS along with spectral reflectance of known pigments in linseed oil. While the spectra do not agree with either azurite or ultramarine, they seem to have spectral features more in common with ultramarine. OCT images at the same locations show that the shadow areas to be more absorbing than pure ultramarine and the high light area to be more scattering than pure ultramarine (see Fig. 12). It is likely that the shadow areas are painted with ultramarine mixed with a highly absorbing black pigment and the highlight to be ultramarine mixed with a highly scattering white pigment. Figure 13 shows the spectrum in the shadow area K1 agrees better with ultramarine mixed with charcoal than pure ultramarine or azurite mixed with charcoal. The spectra of ultramarine and azurite mixed with charcoal were calculated from KM theory. Similarly, the spectrum at K3 agrees better with ultramarine mixed with white than azurite mixed with white. Microscopic images of sample cross-sections from a similar area on the painting showed that there are black and white pigments mixed with ultramarine (Helen Howard private communication).

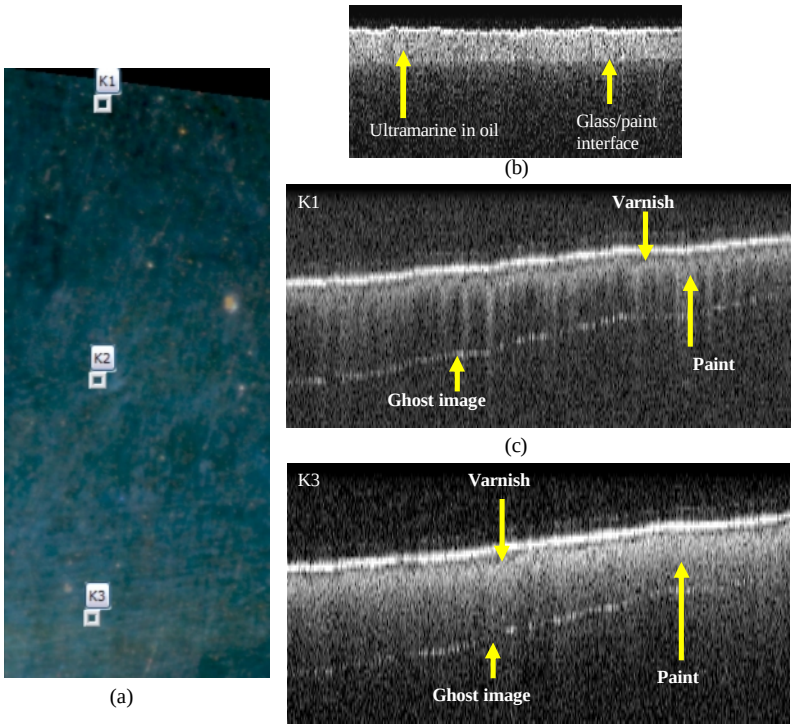

(a) (b) (c) (d)

Figure 12. OCT cross-section image of the virgin's blue cloak in *Virgin and Child with an Angel* by an imitator of Francesco Francia (National gallery NG 3927). a) colour image of the blue area; b) an ultramarine in linseed oil paint layer over a glass microscope slide; c) an OCT cross-section image at K1 in the horizontal direction (1cm across and 600 μm in depth); d) same as c) but at K3.

4. CONCLUSIONS & FUTURE WORK

OCT combined with multispectral imaging gives both structural and spectral information for the paint layers. OCT assisted spectral pigment identification provides stronger constraints than spectral identification alone as it provides scattering and absorption information. Future development will involve quantitative measurements of effective scattering and absorption coefficients using OCT and multispectral imaging.

We would like to thank Marika Spring and Helen Howard from the National Gallery for providing information on the painting and sample analysis.

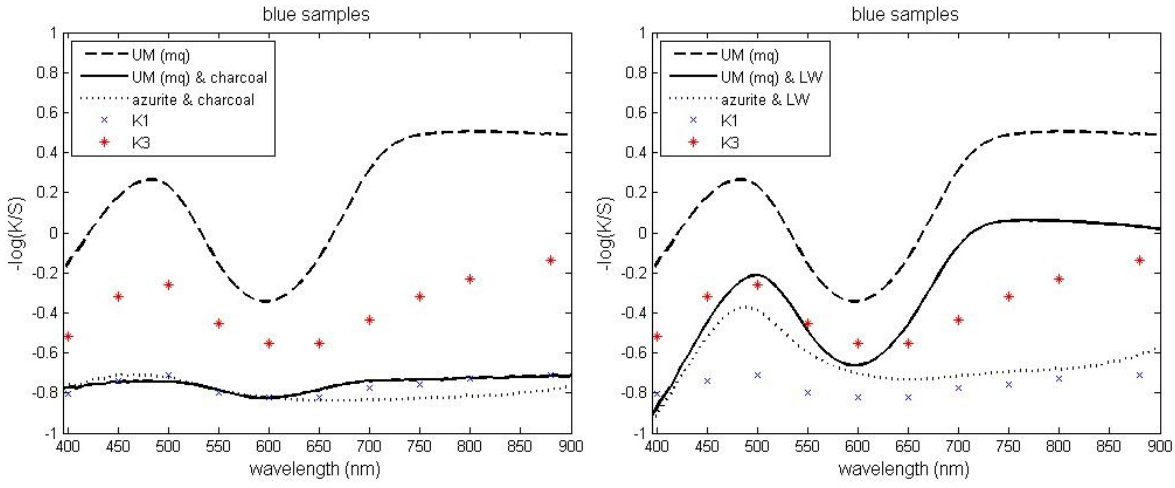

(a) (b)

Figure 13. Spectra of ultramarine, azurite mixed with a) charcoal and b) lead white compared with the measured spectra on the painting in the highlight area K3 and the shadow area K1. Note that the spectra for ultramarine mixed with lead white and azurite mixed with lead white was the best fit to the spectra at K3 using KM theory by setting the relative concentration as free parameters.. The same applies to the mixture with charcoal.

REFERENCES

1. S. Baronti, A., Casini, F., Lotti, S., Porcinai, 'Multispectral imaging system for the mapping of pigments in works of art by use of principal-component analysis', *Applied Optics*, vol. 37, pp.1299 (1998).
2. H. Liang, D. Saunders, J. Cupitt, 'A new multispectral imaging system for examining paintings', *Journal of Imaging Science & Technology*, vol. 49, pp.551 (2005a).
3. P.Targowski, B.,Rouba, M.,Wojtkowski, A.,Kowalczyk, 'The application of optical coherence tomography to non-destructive examination of museum objects', *Studies in Conservation*, vol. 49, pp.107 (2004).
4. H. Liang, M., Gomez Cid, R., Cucu, G., Dobre, D., Jackson, C., Pannell, J., Pedro, D., Saunders, A., Podoleanu, 'Application of OCT to examination of easel paintings', *Second European Workshop on Optical Fibre Sensors, Proc. SPIE*, vol. 5502, pp. 378 (2004).
5. H. Liang, M., Gomz Cid, R., Cucu, G., Dobre, A., Podoleanu, J., Pedro, D., Saunders, 'En-face Optical Coherence Tomography – a novel application of non-invasive imaging to art conservation', *Optics Express*, vol. 13, pp.6133-6144 (2005b) http://www.opticsexpress.org/abstract.cfm?id=85276
6. T. Arecchi, M. Bellini, C. Corsi, R. Fontana, M. Materazzi, L. Pezzati, and A. Tortora, "A new tool for painting diagnostics: Optical coherence tomography", *Opt. Spectrosc.*, vol. 101, pp. 23-26 (2006).
7. P. Targowski, G. Michalina, M. Wojtkowski, 'Optical coherence tomography for artwork diagnostics', *Laser Chemistry*, Article ID 35373 (2006).
8. H. Liang, B. Peric, M. Hughes, A. Podoleanu, M. Spring, and D. Saunders, "Optical coherence tomography for art conservation and archaeology", *Proc.SPIE*, vol. 6618, 661805 (2007).
9. G. Latour, J. Moreau, M. Elias, and J.-M. Frigerio, "Optical Coherence Tomography: non-destructive imaging and spectral information of pigments", *Proc. SPIE*, vol. 6618, 661806-9 (2007).

10. H. Liang, K. Keita, T., Vajzovic, 'PRISMS: A portable multispectral imaging system for remote in situ examination of wall paintings', in O3A: Optics for Arts, Architecture, and Archaeology, *Proc. SPIE*, vol. 6618, 661815 (2007).
11. P. Kubelka, "New contributions to the optics of intensely light scattering materials. Part I", *J. Opt. Soc. Am.*, vol. 38, pp.448-457 (1948).
12. J. L. Saunderson, *J. Opt. Soc. Am.*, vol. 32, pp.727-736 (1942).
13. R. Berns, J. Kreuger, M. Swicklik, 'Multiple pigment selection for inpainting using visible reflectance spectrophotometry', *Studies in Conservation*, vol. 47, pp. 46 (2002).

Optical coherence tomography – a tool for high resolution non-invasive 3D-imaging of the subsurface structure of paintings

Marika Spring*
National Gallery
Trafalgar Square
London WC2N 5DN
United Kingdom
E-mail: marika.spring@ng-london.org.uk

Haida Liang and Borislava Peric
Nottingham Trent University
Clifton Lane
Nottingham NG11 8NS
United Kingdom
E-mail: haida.liang@ntu.ac.uk; boco.peric@ntu.ac.uk
Website: http://www.ntu.ac.uk/research/school_research/bns/staff/55616gp.html

David Saunders
The British Museum
Great Russell Street
London WC1B 3DG
United Kingdom
E-mail: dsaunders@thebritishmuseum.ac.uk

Adrian Podoleanu
School of Physical Sciences
University of Kent
Canterbury CT2 7NH
United Kingdom
E-mail: A.G.H.Podoleanu@kent.ac.uk

*Author for correspondence

Keywords

optical coherence tomography, painting, imaging, cross-section, non-destructive, underdrawing, overpainting

Abstract

Optical Coherence Tomography (OCT) is an imaging technique originally developed for high-resolution 3D imaging of the human eye. In 2004, Targowski et al. and Liang et al. first reported its application to paintings, demonstrating that it was possible to produce cross-section images non-invasively with this technique. In 2005 Liang et al. explored further applications such as imaging of underdrawing at a resolution and contrast greater than that achievable with infrared reflectography. Since then the authors have been conducting a project to investigate systematically the potential of OCT as a new tool in the non-invasive examination of paintings and to design an OCT optimised for use in museums. This paper discusses recent developments in this work and presents examples of the use of OCT on paintings undergoing conservation treatment in the National Gallery, London.

Résumé

La Tomographie à Cohérence Optique (OCT) est une technique d'imagerie mise au point à l'origine pour une imagerie 3D à haute résolution de l'oeil humain. En 2004, Targowski et al. et Liang et al. ont été les premiers à faire part de son application sur les peintures, en démontrant que cette technique permettait de produire des images en coupe transversale, de manière non invasive. En 2005, Liang et al. ont exploré d'autres applications telles que l'imagerie des dessins sous-jacents à une résolution et un contraste plus élevés que ceux obtenus par la réflectographie infrarouge. Depuis, les auteurs ont mené un projet pour étudier systématiquement le potentiel de l'OCT comme nouvel outil pour un examen non invasif des peintures, et pour créer un OCT optimisé pour une utilisation dans les musées. L'article discute des récents développements de ces travaux et présente des exemples d'utilisation de l'OCT sur les peintures en cours de traitements conservatoires dans la Galerie Nationale de Londres.

Synopsis

La tomografía de coherencia óptica (TCO) es una técnica de imagen desarrollada originalmente para obtener imágenes tridimensionales de alta resolución del ojo humano. En 2004,

Introduction

Optical Coherence Tomography (OCT) is an imaging technique originally developed for high-resolution 3D imaging of the human eye (Huang et al. 1991). Targowski et al. (2004) and Liang et al. (2004) first reported its application to paintings, demonstrating that it could produce cross-section images non-invasively. An increasing emphasis is placed on non-destructive methods in the field of cultural heritage science, but those currently routinely used cannot provide the information on stratigraphy and composition of the separate layers that can be achieved through analysis of cross-sections of paint samples. The ability to obtain the same information non-invasively would reduce the need to take samples, and also enable examination of any area of an object, providing a more representative view than a single cross-section. OCT allows 3D imaging, so that as well as cross-sections perpendicular to the paint surface, an *en-face* image from a plane parallel to the surface at a given depth can be extracted. Liang et al. (2005a) demonstrated that *en-face* OCT could be used to image underdrawing at a resolution and contrast greater than that achievable with current infrared reflectography equipment. An advantage over infrared reflectography and X-radiography is that it is

Targowski et al. y Liang et al. presentaron por primera vez su aplicación en las pinturas, demostrando que con esta técnica era posible producir imágenes de secciones transversales de una forma no invasiva. En 2005, Liang et al. investigaron otras aplicaciones, como la obtención de imágenes de una sinopia a una resolución y contraste mayores que los alcanzados con la reflectografía infrarroja. Desde entonces, los autores han estado llevando a cabo un proyecto para investigar sistemáticamente el potencial de la TCO como nueva herramienta en el análisis no invasivo de pinturas y para diseñar una TCO optimizada que pueda usarse en los museos. Este artículo presenta los avances recientes de este trabajo y ejemplos sobre el uso de la TCO en pinturas que están siendo restauradas en la Galería Nacional de Londres.

possible to image only the plane of interest, so that the paint lying on top and the priming layer below does not contribute to, or interfere with, the image.

An overview of OCT and the examination of works of art can be found in Targowski et al. (2006a). It has been used for dynamic monitoring of the drying of different varnishes and examination of differences in topography once dry (Liang et al. 2005b, Targowski et al. 2006a), as well as measurement of refractive indices of varnish and paint samples (Liang et al. 2005b, 2007a, 2007b). On paintings with several different varnish layers the high sensitivity of OCT enables the interfaces between them to be seen (Liang et al. 2005a). Gora et al. (2006) used a Fourier-domain OCT for monitoring laser ablation of varnish and Targowski et al. (2006b) showed it can be used for tracking canvas deformation caused by humidity changes.

This paper will discuss recent developments in a project investigating the potential of OCT for the non-invasive examination of paintings, to design an OCT optimised for use in museums. As part of this project, a commercial OCT instrument was used to examine a range of paintings in the National Gallery, London. As well as identifying possible practical applications that could be useful to conservators, this survey aimed to give a sense of the type of painting and circumstances under which OCT would be an appropriate imaging method. It will also inform the design of an OCT tailored to the study of paintings, indicating what depth range, sensitivity and resolution would be desirable. Some of the results that have been obtained so far will be presented here.

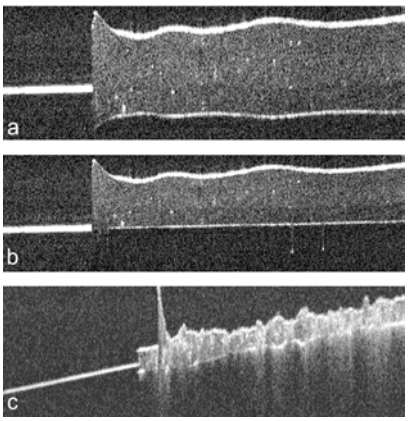

Figure 1. OCT cross-section images of paint on glass microscope slides: a) a transparent paint of rose madder in linseed oil; b) same as (a) but corrected for optical depth to show the true sample thickness; c) madder lake in egg tempera showing evidence for multiple scattering

Principles of OCT

Optical Coherence Tomography (OCT) is a fast, high-resolution 3D scanning Michelson interferometer. A near infrared source of very low power but high spatial concentration (small spot size) is generally used for illumination of both the reference mirror and the object. Interference fringes occur when the optical path of the backscattered light from within the object matches, within the coherence length, the optical path from the reference mirror, thus enabling depth determination. The depth resolution is therefore given by the coherence length, which depends on the bandwidth of the light source. The intensity at a point in the image corresponds to the strength of the backscattered light from the corresponding point inside the object (Figure 1). Mapping produces either cross-section images or *en-face* images at various depths; a series of these can be combined to give 3D information. The transverse resolution is determined by the numerical aperture of the objective lens. The depth range depends on both the type of OCT and the scattering properties of the material. It is particularly suited to the examination of translucent layers such as varnishes and glazes, although it has been shown that under certain circumstances it is capable of imaging the layer structure as far as the preparation layer.

Typical OCT speed of acquisition is at least a few frames per second. Most OCTs use superluminescent diodes (SLD), which can achieve a depth resolution of around 10 μm, although a depth resolution of the order of 1 μm has been achieved with expensive laser sources (Drexler 2004). Recently, preliminary results were shown from an inexpensive way of achieving 1 μm depth resolution (at the expense of sensitivity or speed) through a full field OCT using a tungsten halogen source (Gurov et al. 2007, Latour et al. 2007).

In this paper, an adapted commercial instrument operating at a wavelength of 930 nm, an axial resolution of 6 μm, transverse resolution of 9 μm and depth range of 1.6 mm, capable of automatically scanning a 15 × 15 cm area, was used to examine paintings in the National Gallery. The instrument is small and portable, operating at a safe distance of around 1 cm from the paint surface.

A guide to interpreting OCT images

Although the OCT cross-section images appear deceptively similar to real cross-sections, there are crucial differences and it is important to combine

knowledge about the instrument with an understanding of the behaviour of different types of paint when interpreting them.

Figure 1a shows an OCT cross-section image of a transparent paint, rose madder in linseed oil, on a glass microscope slide. On the left of the image where there is no paint, a bright straight line is seen at the interface between air and glass, since the glass surface is highly reflective; on the right the bright curved line shows the interface between air and paint and the pigment particles are seen as bright spots inside the paint because of the increased scattering at the pigment/medium interface; the fainter curved line at the bottom is the interface between the paint and the glass. OCT measures the optical depth rather than the physical depth; the ratio between these gives the refractive index of the paint. This explains why the interface between the paint and the glass in Figure 1a is not flat nor at the same level as the air/glass interface. Figure 1b shows the cross-section image after correction for optical depth.

Multiply-scattered light has a greater optical path length than singly-scattered light from the same depth. An example of this effect is shown in Figure 1c where madder lake in egg tempera is painted on a glass microscope slide. The air/paint and the paint/glass boundaries are clear, but the image also shows back-scattered light that appears to be from below the paint/glass boundary, indicating multiple scattering in the paint layer. The bright signal from below the paint/glass interface is clearly an artefact, but it also gives useful information about the optical properties of the paint. It indicates that madder lake in egg tempera scatters light more strongly than madder lake in linseed oil.

OCT is particularly suited to the imaging of underdrawings, since it can produce an image at the depth at which the underdrawing is located. In addition OCT offers greater resolution and dynamic range than any direct imaging method. Figure 2 shows that the *en-face* OCT image of underdrawing on a test panel is far superior than even the images from the state-of-art infrared camera SIRIS using InGaAs technology (Saunders et al. 2006). The liquid droplets of the ink and the direction in which it is drawn can be seen in the OCT image.

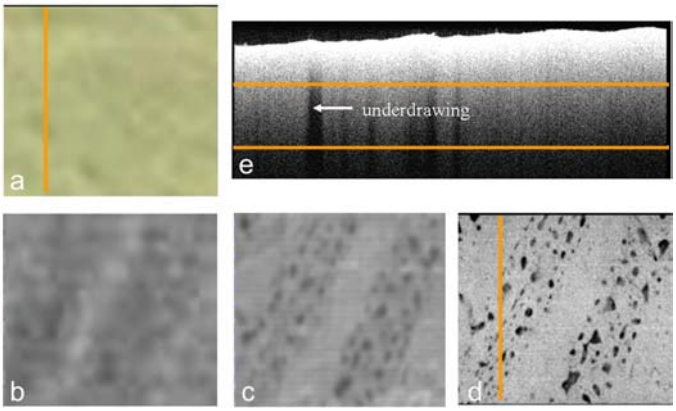

Figure 2. Near infrared images of a painted patch of two layers of lead-tin yellow over underdrawing of bone black in gum executed with a quill pen: a) colour image; b) Near infrared Vidicon image; c) Near infrared image from SIRIS, an InGaAs camera; d) 1300 nm OCT image, averaging the en-face *images between the horizontal lines in (e), where the underdrawing information is located; e) OCT cross-section image of a scan marked with a line in images (a) and (d)*

OCT imaging of paintings in the National Gallery, London

One of the paintings examined using OCT imaging was *A Distant View of Dordrecht, with a Milkmaid and Four Cows, and Other Figures*, by Aelbert Cuyp, dating from around 1650, which was undergoing conservation treatment. The old mastic resin varnish had yellowed considerably. There were also patches of a discontinuous brownish layer in some areas, as well as old brown

discoloured retouchings. Samples were taken to investigate the composition and layer structure in these areas, as the status of the brownish layers was not immediately clear. Examination by OCT imaging at the same time gave the opportunity to consider how it could contribute to the technical examination being carried out in support of treatment, and the real cross-sections could be used to verify the interpretation of layer structure seen in the 'virtual' OCT cross-section images.

26 areas of the painting were examined using OCT. In each case a series of cross-section images were collected from an area 10 mm wide at intervals of 19 μm, scanning a length varying between 3 and 10 mm. The equipment is capable of scanning an area of 15 × 15 cm, but at the time was not yet automated to allow images to be acquired effectively from such a large area. The cross-section images were processed to produce a 3D cube, allowing *en-face* images at different depths parallel to the paint surface to be extracted. A corresponding series of video images was also collected at each point.

When the uppermost varnish had been removed there was still a patchy staining visible in some areas of the sky, particularly in the troughs of the brushstrokes. It was not clear whether this was the remains of an older surface coating or whether it was caused by an uneven change in the paint. A real cross-section showed a thin surface layer, fluorescent under ultraviolet light, measuring only around 5 microns in the area sampled. Figure 3a shows an image of the area of the sky examined with OCT. Figure 3b is made by averaging a series of *en-face* OCT images from below the surface, and shows the cracks clearly, locating the exact area imaged, as well as each individual cross-section image. In the OCT cross section (Figure 3c) there is a layer which appears dark at the surface of a highly scattering layer (which appears light), the lead-white-containing sky paint. The layer which is dark in the OCT cross-section is thicker in the hollows of the brushstrokes and in the centre of the image it can be seen to run over a crack in the paint and to continue across the top of the raised paint either side of the crack. The 295 closely-spaced OCT cross-section images that were collected give a better indication of the variation in thickness and distribution across the surface than can be gained from the real paint cross-section.

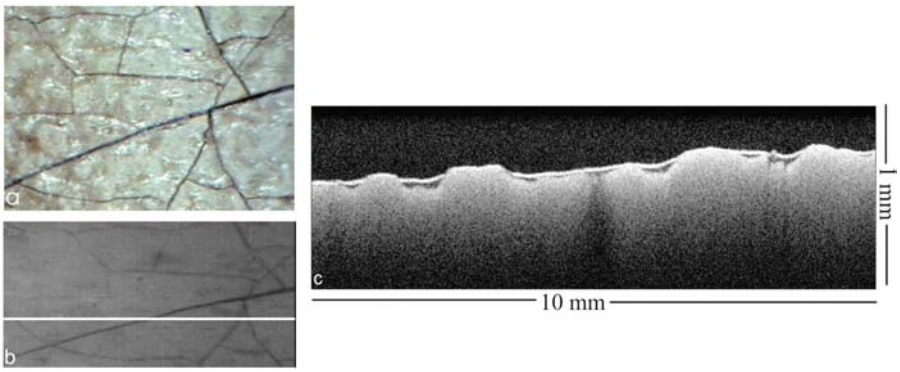

Figure 3. Aelbert Cuyp, A Distant View of Dordrecht, with a Milkmaid and Four Cows, and Other Figures: *a) Image of the area of the sky examined by OCT; b)* En-face *OCT image; c) OCT cross-section. The line in (b) indicates its location*

Figure 4a shows an area in the foreground of the painting where a patchy brown translucent surface layer is present. It is particularly visible in this area because it lies over yellow-green paint. This area was examined by OCT and a sample was also taken (Figures 4d and e). The real cross-section shows that the paint consists mainly of yellow lake (with a calcium carbonate substrate) mixed with a small amount of lead white (basic lead carbonate), Kassel earth and vivianite (hydrated iron phosphate). The strong fluorescence in ultraviolet light of the brown surface layer suggests that it is the remains of an old varnish; this was confirmed by Gas-Chromatography – Mass-Spectrometry.[1]

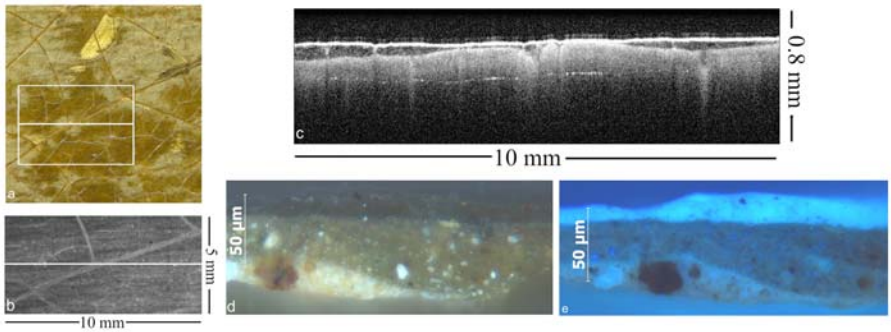

Figure 4. a) Detail of the lower right foreground of the painting by Cuyp showing the patchy brown layer on the surface. Photo © The National Gallery, London; b) en-face *OCT image of the area marked by a box in image (a); c) OCT cross-section through the line marked in (a) and (b); d) Cross-section from an area of the foreground where there is a translucent brown layer on the surface: normal light; e) Cross-section in (d) in ultraviolet light*

The results of OCT examination of a similar area are shown in Figure 4. Below the bright white line in the OCT cross-section, caused by the first surface reflection at the air/paint interface, is a layer which appears dark, corresponding to the brown translucent residual varnish seen in the real cross-section. The OCT cross-section shows that it varies in thickness between 15 and 75 µm in the area of the painting examined, consistent with the thickness of 20 µm measured from the real cross-section. The dark layer corresponding to the old varnish can be seen to run over a crack in the paint layer at the right and in the middle of the OCT cross-section, further evidence that it is not an original layer. A patch in the middle of the detail of the surface (Figure 4a) appears much greener, and the residual brown varnish can be seen to be much thinner in the middle of the OCT cross-section image.

The OCT images of the edge of a branch at the left of the painting illustrate that the original brown translucent paint appears different from the brown translucent surface accretions, and can therefore be distinguished from it (Figure 5). In the *en-face* image, the brown branch can be seen as a darker patch, because of its stronger absorbance at 930 nm than the surrounding paint. This is also why, in the cross-section image, the paint of the branch (at the left) appears darker than the paint at the right (below the scattering that occurs at the surface of the layer). A brown patch which appears to run over the cracks is visible towards the bottom right of the visible image (Figure 5a). A second OCT cross-section (Figure 5d) from near the bottom of the area scanned confirms that this is a later surface accretion, as a dark layer can be seen at the right of the image running over a crack in the layer below. The *en-face* image is from a plane below the accretion; the crack is visible

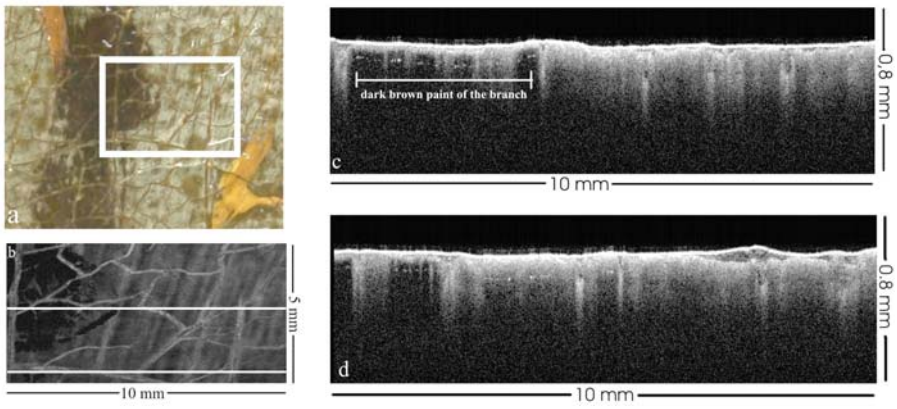

Figure 5. a) Detail of a branch at the left of the painting. Photo © The National Gallery, London; b) en-face *OCT image of the area in the box in image: a); c) OCT cross-section through the line in the centre of image (b); d) OCT cross-section through the line near the bottom of image b)*

confirming observations from other images, but it also demonstrates that the accretion is covering paint rather than a loss.

In another area of the foreground there were remnants of overpaint from previous restoration campaigns. A sample (Figures 6a and b) was taken from the edge of a crack and at the left of the cross-section multiple varnish and overpaint layers can be seen where they remain in the crack. Under ultraviolet light these are almost all fluorescent, but some contain pigment and are probably overpaint with a resinous binding medium, while one layer is more fluorescent, does not contain any particles, and is probably varnish. In the OCT cross-section from a similar area a comparable series of layers can be seen on top of the highly scattering paint, at the left of the image (Figure 6c), including a darker, less scattering layer which could be varnish and which appears cupped.

Figure 6. a) Cross-section from the foreground of the painting by Cuyp, with a crack at the left in which there are several varnish and overpaint layers, normal light; b) Cross-section in ultraviolet light; c) OCT cross-section of a similar area with multiple varnish and overpaint layers visible on the paint surface at the left of the image

The OCT images from an area just above a branch running diagonally across the painting at the left included an area of paint loss covered with varnish and overpaint (Figure 7). At the left of the OCT cross-section image this can be seen as a hollow filled with overpaint, which also extends across the rest of the cross-section. The *en-face* image, taken from below the surface, clearly shows the area of loss at the left (which is hidden by overpaint in the normal light image). The X-radiograph of this painting confirmed that there was a small loss in this area, but it is dominated by the thick lead-white-containing priming layer, and in general it is difficult to see the upper paint layers, losses in them and overpaint. This illustrates the advantage of OCT in a case such as this where an *en-face* OCT image can be extracted from a certain depth range, so that the priming layer is not included in the image.

The ability to produce *en-face* images which do not include the paint is one of the reasons why underdrawing can be imaged so effectively using this technique, as demonstrated with the test panel described above. The SIRIS digital infrared camera had shown that *The Virgin and Child with an Angel*, ascribed to Francesco Francia (NG 3927), has detailed underdrawing which includes pouncing as well as lines which appear to have been drawn with a

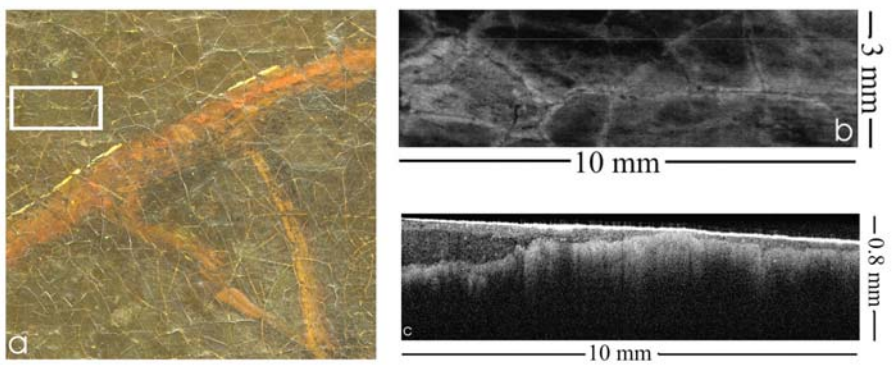

Figure 7. a) Detail of a branch in the left foreground of the painting by Cuyp. Photo © The National Gallery, London; b) en-face *OCT image showing a loss in the paint at the left; c) OCT cross-section from the line marked on image (b), showing the loss filled with what appears to be overpaint at the left*

dry medium. The high resolution and dynamic range of the OCT image of the angel's eye is immediately evident when compared with that from the SIRIS camera (Figure 8). This is particularly useful when considering the nature of the medium used for the drawing, as it is often the quality of the lines that gives this information.

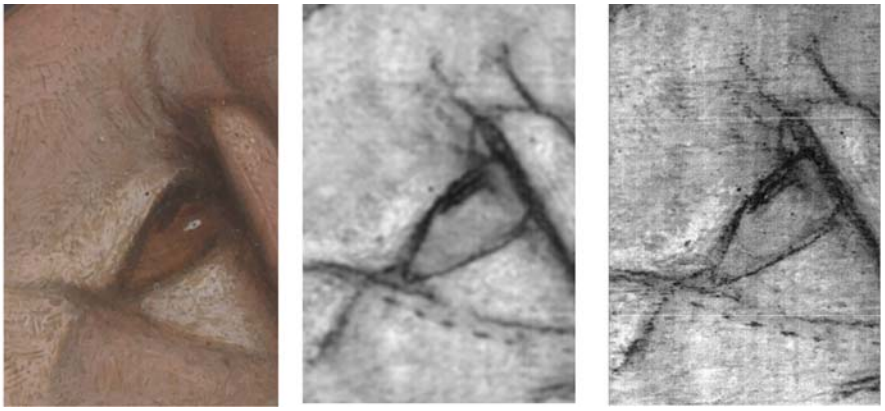

Figure 8. a) Francesco Francia, The Virgin and Child with an Angel *(NG 3927), detail of the angel's eye. Photo © The National Gallery, London; b) Infrared image of the same region using the SIRIS camera; c)* En-face *OCT image at 930 nm; the size of the area on the painting is 10 by 15 mm*

Conclusion

OCT imaging shows great promise for the examination of paintings, and could be a useful tool for answering questions that arise during conservation treatment. Particularly valuable is its ability to reveal the layer structure of a painting, including both paint and varnish, in a non-invasive manner. This allows many more areas of the painting to be examined than would be possible by conventional sampling methods, but it is likely to be most effective when used in combination with the information gained from sampling to provide a more representative view. Acquisition of 3D information broadens even further the range of possible applications, making it a technique that could extend and complement the imaging techniques currently available.

The examinations carried out with a commercial OCT system presented here demonstrated its potential and will contribute towards the design of an OCT system specifically suited to the examination of paintings. It may be possible to obtain layer structure to a greater depth and higher resolution by varying the parameters of the instrument such as wavelength and bandwidth of the light source. A systematic study of the transparency of pigments as a function of wavelength has been conducted for around 50 historic pigments in linseed oil and egg tempera, and the best spectral window for OCT was found to be ~2.2 μm (Peric et al. 2007, Liang et al. 2007b). Multi-wavelength OCT, which could provide spectral information on the paint layers, is also being explored (Liang et al. 2007b), as well as measurement of optical parameters such as refractive index and scattering properties by OCT, which have the potential to provide information on the composition of the layers.

Acknowledgements

We are grateful to David Peggie and Rachel Morrison (Scientific Department, National Gallery, London) for the analysis reported in note 1, and to Rachel Billinge (Conservation Department, National Gallery, London) for the infrared reflectogram in Figure 8b.

Note

1 GC-MS analysis detected heat-bodied linseed oil, as well as degraded pine and oxidised triterpenoid resin components consistent with a degraded oil-resin varnish. The fatty acid methyl ester ratios were: P/S = 1.5; A/P = 2.5; Sub: Az = 1:2.3. Significant quantities of 7-oxodehydroabetic acid methyl ester and 7-oxo, 15–OH–dehydroabetic acid methyl ester were detected. Several oxidised components of the dammarenone type were also seen, suggesting the presence of an aged triterpenoid resin, possibly dammar.

References

Drexler, W. 2004. Ultrahigh-resolution optical coherence tomography. *Journal of Biomedical Optics*, 9, 47–74.

Gora, M, Targowski, P, Rycyk, A and Marczak, J. 2006. Varnish ablation control by optical coherence tomography. *Laser Chemistry* 2006: Article ID 10647.

Huang, D, Swanson, E A, Lin, C P, Schuman, J S, Stinson, W G, Chang, W, Hee, M R, Flotte, T, Gregory, K C, Puliafito, C A and Fujimoto, J G. 1991. Optical coherence tomography. *Science*, 254, 1178–1181.

Gurov, I, Karpets, A, Margariants, N and Vorobeva, E. 2007. Full-field high-speed optical coherence tomography system for evaluating multilayer and random tissues. *O3A: Optics for Arts, Architecture, and Archaeology, Proceedings of SPIE*, 6618, 661807.

Latour, G, Moreau, J, Elias, M and Frigerio, J. 2007. Optical coherence tomography: non-destructive imaging and spectral information of pigments. *O3A: Optics for Arts, Architecture, and Archaeology, Proceedings of SPIE*, 6618, 661806.

Liang, H, Gomez Cid, M, Cucu, R, Dobre, G, Jackson, D, Pannell, C, Pedro, J, Saunders, D and Podoleanu, A. 2004. Application of OCT to examination of easel paintings. *Second European Workshop on Optical Fibre Sensors, Proceedings of SPIE*, 5502, 378–381.

Liang, H, Cid, M G, Cucu, R G, Dobre, G M, Podoleanu, A Gh, Pedro, J and Saunders, D. 2005a. *En-face* Optical Coherence Tomography – a novel application of non-invasive imaging to art conservation. *Optics Express*, 13, 6133–6144. http://www.opticsexpress.org/abstract.cfm?id=85276.

Liang, H, Cid, M G, Cucu, R G, Dobre, G M, Kudimov, B, Pedro, J, Saunders, D, Cupitt, J and Podoleanu, A Gh. 2005b. Optical Coherence Tomography – a non-invasive technique applied to conservation of paintings. *Optical Methods for Arts and Archaeology, Munich., Proceedings of SPIE, 5857, 58570W.*

Liang, H, Peric, B, Spring, M, Saunders, D, Hughes, M and Podoleanu, A. 2007a. Non-invasive imaging of subsurface paint layers with optical coherence tomography. *Conservation Science 2007*, Milan, in press.

Liang, H, Peric, B, Hughes, M, Podoleanu, A, Spring, M and Saunders, D. 2007b. Optical coherence tomography for art conservation and archaeology. *O3A: Optics for Arts, Architecture, and Archaeology, Proceedings of SPIE*, 6618, 661805.

Peric, B, Martin-Simpson, S, Spring, M and Liang, H. 2007. Spectral transparency of historic artists' pigments. *Conservation Science 2007*, Milan, in press.

Saunders, D, Billinge, R, Cupitt, J, Atkinson, N and Liang, H. 2006. A new camera for high-resolution infrared imaging of works of art. *Studies in Conservation*, 51, 277–290.

Targowski, P, Rouba, B, Wojtkowski, M and Kowalczyk, A. 2004. The application of optical coherence tomography to non-destructive examination of museum objects. *Studies in Conservation*, 49, 107–114.

Targowski, P, Gora, M and Wojtkowski, M. 2006a. Optical Coherence Tomography for Artwork Diagnostics. *Laser Chemistry* 2006: Article ID 35373.

Targowski, P, Gora, M and Bajraszewski, T. et al. 2006b. Optical Coherence Tomography for Tracking Canvas Deformation. *Laser Chemistry* 2006: Article ID 93658.

Invited Paper

Optical Coherence Tomography in Archaeological and Conservation Science – A new emerging field

Haida Liang[*a], Borislava Peric [a], Michael Hughes [b], Adrian Podoleanu[b], Marika Spring [c], Stefan Roehrs[d]
[a]School of Science and Technology, Nottingham Trent University, Nottingham NG11 8NS, UK;
[b]School of Physical Sciences, University of Kent, Canterbury, CT2 7NR, UK;
[c]Scientific Department, The National Gallery, London WC2N 5DN, UK
[d]Department of Conservation and Scientific Research, The British Museum, London WC1B 3DG, UK

ABSTRACT

There has been a long tradition of applying biomedical imaging techniques to the examination of historical artefacts, owing to similar demands for non-invasive methods in both fields. Optical Coherence Tomography (OCT) is no exception. We review the achievements on OCT applications to art conservation and archaeology since the publication of the first papers in 2004. Historical artefacts include a much broader range of materials than biological tissues, hence presenting a greater and somewhat different challenge to the field of OCT. New results will be presented to illustrate the various applications of OCT including both qualitative and quantitative analysis.

Keywords: optical coherence tomography, low coherence interferometry, infrared imaging, 3D imaging, refractive index, scattering, absorption, art conservation, archaeology

1. INTRODUCTION

There has been a long tradition of applying biomedical imaging techniques to the examination of historical artefacts owing to similar demands for non-invasive methods in both fields. For example, the introduction of X-ray imaging to the examination of paintings started soon after the invention of X-rays and its application to medicine [1]. It is then not surprising that OCT has recently been applied to paintings and other cultural artefacts. In 2004, OCT was first applied to the examination of jade [2], ceramics [3] and paintings [3,4]. Direct comparisons between OCT cross-section images and real cross-sections of paint samples showed the extent OCT cross-section imaging is able to reflect the real paint layers [6,7]. Apart from the non-invasive examination of the stratigraphy of paint and varnish layers, OCT has also been shown to be the most sensitive technique for revealing preparatory sketches or underdrawings beneath paint layers owing to its high dynamic range and depth selection capabilities [5,12]. It was shown that the high sensitivity of OCT enables the interface between different varnish layers on a painting to be seen [5]. OCT has been used for dynamic monitoring of the wetting and drying of different varnish, the examination of the difference between the roughness of the dried surface for the different types of varnish [8,15] and the monitoring of the aging and solvent cleaning of varnish [9]. Measurements of refractive indices of varnish and paint samples using OCT were given in [8,9]. To exploit the fast imaging capability of Fourier-domain OCT, it has been demonstrated that a fast imaging OCT is capable of monitoring real time laser ablation of varnish layers [10] and real time tracking of canvas deformation due to environmental changes such as humidity [11]. OCT imaging of gold punch marks on paintings to identify the tools used has been demonstrated in [12]. OCT has found application in the examination of ancient glass [9,14], parchment [13] and faience [15].

In this paper, we review the different OCT applications in archaeological and conservation science. The example images shown in the paper are obtained with a Thorlabs SROCT. The SROCT is a portable Fourier-domain OCT operating at a wavelength of 930nm with an axial resolution of ~6μm, transverse resolution of ~9μm and depth range of 1.6mm. We

[*]haida.liang@ntu.ac.uk; phone 44 115 848 8056; fax 44 115 848 6636;
http://www.ntu.ac.uk/research/school_research/sat/staff/55616gp.html

1st Canterbury Workshop on Optical Coherence Tomography and Adaptive Optics
edited by Adrian Podoleanu, Proc. of SPIE Vol. 7139, 713915 · © 2008 SPIE
CCC code: 0277-786X/08/$18 · doi: 10.1117/12.819499

have adapted the instrument for in situ examination of paintings by mounting the light weight probe on a computer controlled XYZ micrometer stage which makes it capable of scanning an area as large as 15cm x 15cm. The instrument is small and portable, operating at a safe distance of around 1cm from the paint surface. The experience gained in using the instrument has helped inform the design of an *en face* time domain OCT for in situ application in museums which complements the capabilities of the SROCT. Section 2 is devoted to a review of OCT imaging of paintings including new results; Section 3 shows new results on OCT imaging of various other historical artefacts from the British Museum collection; Section 4 discusses the specific requirements in the specification of an OCT in the applications to paintings and other historical artefacts.

2. OCT IMAGING OF PAINTINGS

Western European paintings were usually painted on either panel or canvas which were normally prepared with a ground layer (e.g. chalk in animal skin glue). Depending on the style and the historical period, preparatory sketches were sometimes made before paint layers were applied. To enhance the appearance of the painting and for protection, a varnish layer would then be applied once the paint was dry. Paint consists of pigments mixed in a binding medium which in most cases are either egg tempera or oil. Most types of paint are highly scattering compared to the average biological tissue. In most paint layers, multiple scattering dominates.

2.1 Non-invasive examination of varnish and paint layers

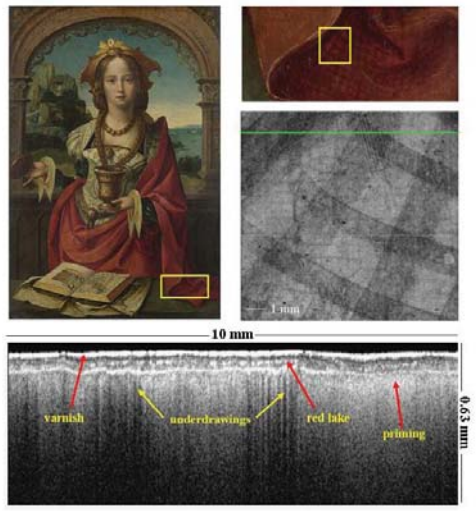

Fig. 1. OCT used to examine the layer structure of varnish and paint, revealing underdrawings of a painting. Top right: A region on the red drapery in the painting *The Magdalen* by an anonymous Netherlandish artist (National Gallery No. 719); Right middle: OCT *en-face* image at the depth of the underdrawing corresponding to the region marked by a yellow box in the top right image; Bottom: OCT cross-section image of the region marked by a green line segment on the *en-face* underdrawing image.

Figure 1 shows an OCT cross-section image of a painting where a varnish layer, a transparent red lake paint layer and a more opaque (highly scattering) paint layer can be seen [16]. Vertical dark bands in the cross-section image correspond to the underdrawings which have a high absorption coefficient at 930nm. The lower half of the cross-section image is dominated by multiply scattered light with scattering centres located in the upper half of the image. This is the result of OCT registering only the optical path length rather than the true physical depth. OCT has been used to detect areas of paint loss hidden beneath the overpaint showing not only the damaged area but also the location of the loss [17]. These areas of loss are not detected in X-ray images.

2.2 Underdrawing

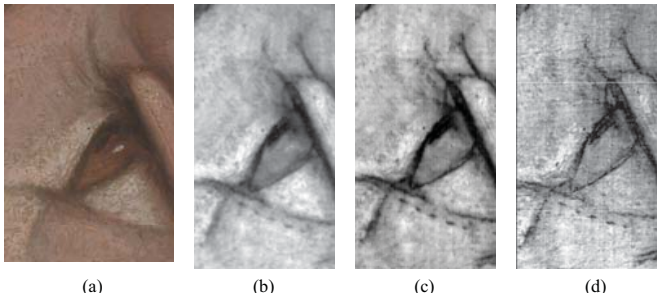

Fig. 2. a) colour image b) 880nm CCD image c) 900-1700nm NIR InGaAS image d) 930nm OCT image (median of 40 en face images) of the eye of the angel in a 15th C painting attributed to Francesco Francia (National Gallery collection NG3937)

As shown in Fig. 1, OCT can be used to image the underdrawing of a painting through scanning a region and taking *en face* slices. The best images are obtained through taking the median of a series of *en face* images at various depths [5,8,9,12]. Figure 2 gives a comparison of near infrared images of part of a painting using a CCD camera through a bandpass filter at 880nm, a state of the art InGaAs digital infrared camera sensitive to 900-1700nm and a 930nm OCT image (a median image of a series of 40 *en face* slices in depth). The OCT image gives the highest resolution and dynamic range showing that the underdrawing was drawn with a solid substance. In addition, OCT imaging of underdrawing has the advantage of depth selection, i.e. it can locate the depth position of the underdrawings and median/average only those layers that contain the underdrawing information. Taking the median has the advantage of eliminating the ghost image in any Fourier domain OCT. Speckle noise is also greatly reduced through taking the median or averaging a series of images at different depth. Figure 1 shows that as a result of multiple scattering in the lower paint layers, the shadows of the underdrawing extend far beyond the actual depth location of the underdrawing or the surrounding paint layer. The *en face* slices below the location of the underdrawing can have higher contrast than at the position of the underdrawing because of the multiply scattered light from the paint layer above the underdrawing. Large area scans of 10cm x 10cm have been achieved through mosaicing of adjacent *en face* images.

2.3 Monitoring the cleaning of varnish

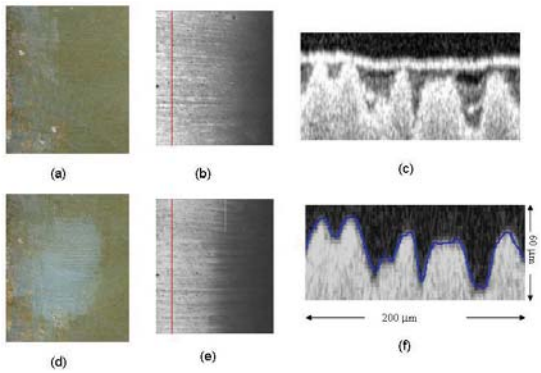

Fig. 3. OCT monitoring of solvent cleaning of varnish: a) part of a painting before cleaning; b) en face OCT image slice at the paint surface below the varnish; c) OCT cross-section image at the position marked in red on the image in b); d) same as a) but after cleaning with industrial methylated spirit/white spirit; e) same as b) but after cleaning; f) same as c) but after cleaning, the blue curve is the paint surface before cleaning obtained from c).

Varnishes have long been applied to traditional Western European paintings for both protective and aesthetic purposes. However, varnishes (especially natural varnishes) degrade over time and become yellow and hazy. It is a routine practice for conservators to remove old varnish and replace it with a coat of new varnish using a solvent that dissolves the old varnish but not the paint. It has not been possible in the past to directly prove that the paint surface is not damaged by the cleaning process. OCT has the potential to directly investigate this as shown in Fig. 3. Figure 3c shows the three varnish

layers and the paint layer before cleaning. The surface profile of the paint layer before cleaning is obtained after correcting for the optical path length through the varnish above the paint. This paint surface is plotted in blue over the cross-section image at the same position after cleaning. In this case, the difference between the paint surface before and after cleaning is within the measurement error margin.

OCT was first applied to the in situ monitoring of laser cleaning of test paintings by Gora et al. [10]. The full advantage of the fast imaging capability of a Fourier domain OCT was demonstrated in the monitoring of laser cleaning which requires a quick response.

2.4 Monitoring canvas deformation and vibration

Canvas deformation as a result of changes in environment such as humidity was first demonstrated using a Fourier domain OCT by Targowski et al. [11]. It was demonstrated that OCT was able to continuously monitor the deformation of the canvas in 3D similar to electronic speckle pattern interferometry. Vibration of canvas paintings as a result of air current from air conditioning ducts and human voice was measured by the Thorlabs SROCT in a conservation studio [9]. In the worst case a peak to peak vibration of ~20μm was found.

2.5 Measurement of optical properties of paint

Refractive indices of varnish and paint samples have been measured using OCT [8, 9] by either directly measuring the physical thickness and the corresponding optical thickness or using the focus tracking method which has the advantage that it can be used *in situ*. However, the measurement errors for both methods are large (accuracy of 0.01 to 0.09) because of the rather thin layers (tens of microns) and the opacity in the case of paint samples. The methods are limited to transparent layers and can not be applied to paint sample that are highly scattering.

The scattering and absorption coefficients of paint samples can be measured from OCT depth scans and calibrated with the coefficients measured from the Kubelka-Munk theory [22]. Details of this work will be presented in a forth coming publication.

OCT measurements of the scattering and absorption properties can also assist the spectral identification of pigments by providing additional constraints [23].

3. OCT IMAGING OF OTHER MUSEUM OBJECTS

3.1 Glass

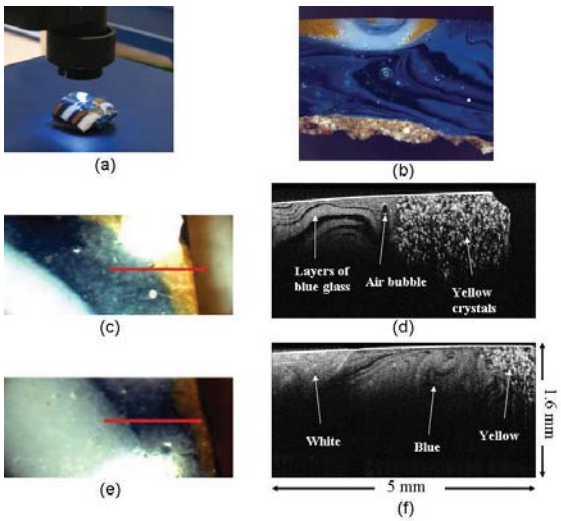

Fig. 4 Egyptian core formed glass from the British Museum (~1500 BC) a) OCT probe scanning the glass fragment; b) microscope image of the cross-section of the glass fragment; d) OCT B-scan image of the region marked by the red line segment in c); f) OCT B-scan image of the region marked by the red line segment in e).

OCT has been applied to the subsurface examination of the deterioration of glass [9] and the examination of the internal structure of stained glass [14]. Figure 4 shows the OCT B-scan image of a fragment of Egyptian glass from the British

Museum compared with a conventional microscope image of the cross-section in a similar region. The blue, yellowish and white areas have different optical properties and structure. The scattering particles are much smaller in the blue and white regions than those in the brown regions. Flow lines and air bubbles are seen in the blue glass. The opacifier crystals in the brown area are well resolved in the OCT image. Opacifiers are normally added to make the glass less transparent and more scattering, typically calcium antimonate crystals are found in white opaque glass and lead antimonate crystals are found in yellow opaque glass [18]. The OCT cross-section image shows that the white layers and the brown layers were applied after the blue layer and that the downward turning of the flow line near the boundaries between the white and blue regions is likely to be the result of the white glass being applied. The ancient manufacturing process of such glass is still a topic for debate. It is thought that the glass was either trailed onto the core by rotating it or the core was dipped into molten glass. The white and yellow decorations were probably added later to the still soft blue glass. A 3D OCT scan gives a 1cm x 1cm x 1.6mm volume cube that shows that the blue glass consists of different curved layers with very different scattering properties throughout the imaged volume. The best way to test the two hypotheses is to use OCT to image glass samples made by the different proposed methods.

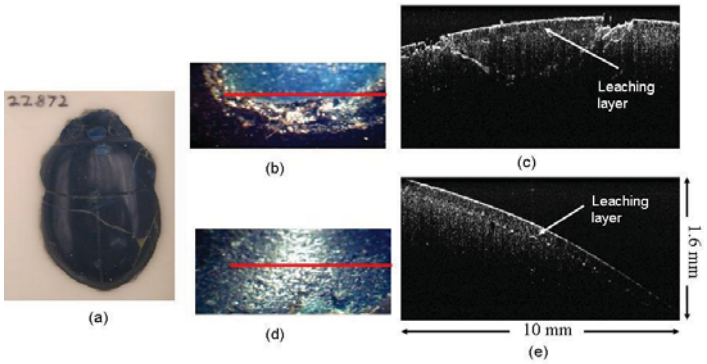

Fig. 5 An Egyptian glass scarab from the British Musuem (a) showing effect of corrosion in OCT images c) & d)

Figure 5 shows how OCT can be used to detect glass corrosion non-invasively. The Egyptian scarab has an unstable glass composition which leads to corrosion. Fragments have already fallen off and had to be repaired. The OCT image in Fig. 5c shows how well the glued-in piece fits in the body of the scarab. Figure 5c and 5e show that both the glued-in piece and the original show a leaching layer that extends ~170 micron in optical thickness below the surface (or ~110 microns assuming a refractive index of 1.5). The layer has presumably lost its sodium ions and the corrosion starts. OCT can potentially give early warning to glass corrosion.

3.2 Jade

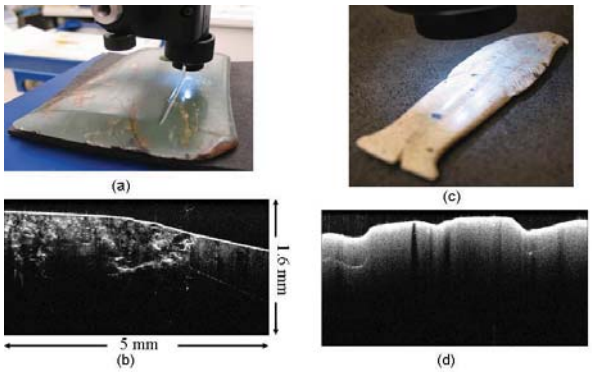

Fig. 6. a) A Nephrite Jade blade from the British Museum (Neolithic); b) OCT B-scan showing the crystal structure; c) A weathered jade fish from the British Museum; d) B-scan showing strong scattering.

Figure 6 shows that jade is translucent at 930nm and OCT can image the mineral structure of jade, however, weathered jade is highly scattering with much lower penetration depth at 930nm. OCT imaging can potentially help to identify the type of jade through their mineral structure. Yang et al. (2004) studied the weathering patterns on jade using OCT in an attempt to distinguish natural weathering from artificial weathering. Figure 6d shows some strongly absorbing particles (dark particles seen in Fig. 6c) embedded in the surrounding highly scattering material.

3.3 Ceramics

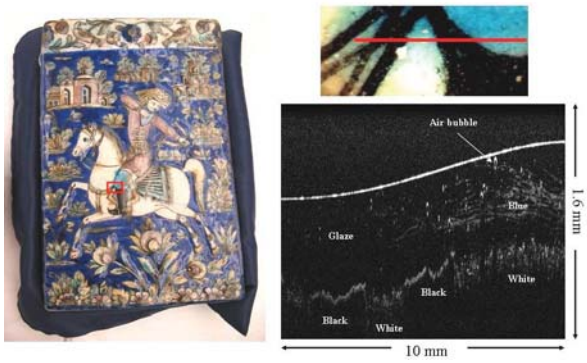

Fig. 7. A 19th century Persian under glaze painted ceramic tile from the British Museum collection.

Micro-XRF (X-ray fluorescence) is used to study the elemental composition of the glaze of the ceramic tile in Fig.7, however, it is difficult without measurements of the thickness of the glaze to know whether the X-rays detected were due to the glaze or the paint layer further down. The OCT image in Fig. 7 shows that the glaze layer is ~800 μm in optical thickness which translates to a physical thickness of 400 to 570μm for a refractive index in the range of 1.4 to 2.0 (range of refractive indices found for glass). Theoretical values of the information depth for XRF measurements in an alkaline glass were estimated for a signal fraction of 95% for various X-ray energy levels. The energy levels for Ca-K alpha line, the Fe-K alpha line and Pb-L alpha line are 3.7 keV, 6.4 keV, and 10.5 keV respectively and X-rays at these energy levels can penetrate a depth of about ~20 μm, ~60 μm and ~200 μm respectively [19]. Therefore, the quantification of these main components of the glaze seems to be possible as long as elements with higher energy X-rays are only present as traces. However, the OCT image also shows that most of the blue pigments have dissolved into the glaze, hence XRF measurements of the glaze in this blue area would be contaminated by the blue pigment.

3.4 Painted enamel

Painted enamels are made from layers of glass. As in the case of the ceramic tile, XRF is commonly used to identify the material non-invasively. However, an independent method of imaging the layer structure and thickness is needed to associate the elements detected with the correct layer. The OCT images in Fig. 8 show the various layers of glass the enamel is made from. The blue, green and brown layers are transparent, but the white layer is highly scattering and the dark drawings are highly absorbing. In many cases, the layers are transparent enough for the copper plate to be seen in the OCT images. Air bubbles seem to concentrate toward the top surface. The total optical thickness of the enamel layer is ~800 μm.

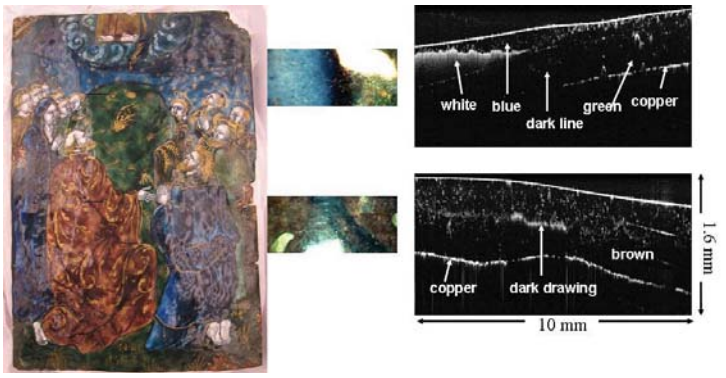

Fig. 8. Painted enamel from the British Museum collection.

4. REQUIREMENTS FOR OCT IN MUSEUM APPLICATIONS

While speed is the focus for OCT development in the biomedical field for in vivo imaging, in the field of archaeology and art conservation speed is less of an issue as the objects are stationary. The only applications that require high speed are laser cleaning, tracking of canvas deformation and vibration monitoring. Large area scans can also benefit from higher speed of acquisition even though high speed is not essential for image quality. Most applications in this field do not require high speed. The trade-off between speed and signal to noise ratio is different here. Increase of integration time does not improve the S/N of strong OCT signals as these are speckle noise limited. However, for weak signals significant improvements can be made by increasing the integration time. Figure 8 shows the improvement in signal to noise ratio for weak signals in a depth scan through a Ti white paint sample using the 930nm Fourier domain OCT.

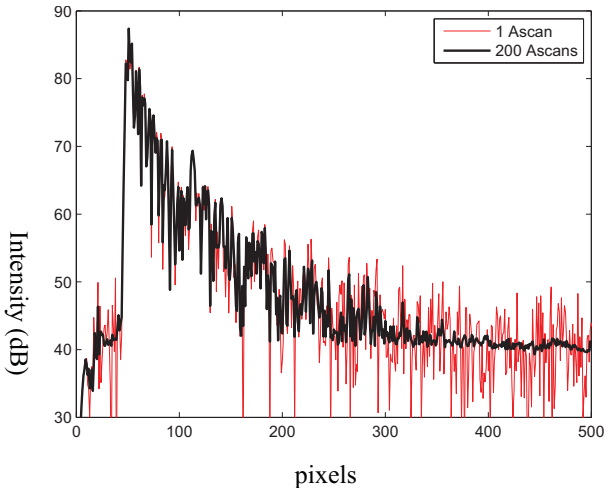

Fig. 9. A depth scan (A-scan) through a Ti white oil paint sample showing the improved signal to noise ratio for an average of 200 A-scans (black) compared with one A-scan (red).

Fourier domain OCT has the advantage of high speed capturing however it has limited depth range which makes imaging of relatively transparent and thick objects difficult. For the Thorlabs SROCT the depth range is 1.6 mm, the relative distance from zero path length gives a 10 dB drop in signal over 0.9mm and the relative distance from the focus position gives another 20dB drop in signal over 0.9mm.

We have designed and built a portable time-domain system for use *in situ* at the British Museum and National Gallery. The system is illuminated by an 850 nm centred broadband source (super-luminescent diode) with a FWHM of 50 nm, yielding an axial resolution of approximately 6.7 microns (theoretical) and 8 microns (observed). Depth scanning (scanning of the reference arm) is achieved using mirrors mounted on a translation stage, while lateral scanning is by a

pair of galvo-mirrors (x and y). For en-face (transversal) imaging, modulation of the carrier wave is provided by the x (fast) scanner, no additional phase modulator is required [20]. The system employs balanced detection to reduce excess photon noise [21] and a log scaling of the demodulated signal prior to digitisation in order to preserve dynamic range. The system is enclosed and designed to be easily transportable to imaging sites.

Although the time-domain modality A-scan rate is slower than for Fourier domain OCT, this system has the advantage than it can generate en-face slices at 1Hz. This finds significant utility in the alignment phase of imaging, since the investigator is presented with a live image which is oriented in the same way as for conventional microscopy (or indeed naked eye viewing), permitting a more intuitive interpretation of structure. The advantage is strongest when investigating features which lie in a plane orthogonal to the optical axis (such as underdrawings) and which may be more difficult to identify in B-scans.

Time-domain OCT also offers the opportunity to acquire single shot images of thick, transparent objects, subject to the limitations of the confocal window (or depth of focus) - the 4 cm focal length lens normally used provides a (theoretical) depth of focus of 5 cm in air, for a lateral resolution of 15 microns. This range could, in principle, be extended using dynamic focus, although this has not been implemented at the current time.

5. CONCLUSIONS

OCT has great potential to become a routine non-invasive tool in museums for the examination of subsurface structure of painting and other museum objects. As OCT imaging is non-invasive, this means cross-section imaging is possible anywhere on a painting or an intact object where there are no other methods of obtaining the depth information. OCT can go beyond qualitative imaging toward quantitative measurements of optical properties for monitoring the ageing of material and assist material identification.

We would like to thank Kafing Keita of Nottingham Trent University for providing Figure 8, Rachel Billinge of the National Gallery for providing Figure 2c, Margaret Sax and Caroline Cartwright of the British Museum for helpful discussion and David Saunders for support and encouragement.

REFERENCES

[1] J. Padfield, D. Saunders, J. Cupitt, R. Atkinson, “Improvements in the acquisition and processing of X-ray images of paintings,” The National Gallery Technical Bulletin 23, 62-75 (2002).

[2] M.-L. Yang, C.-W. Lu, I.-J. Hsu, C. C. Yang, “The use of optical coherence tomography for monitoring the subsurface morphologies of archaic jades”, Archaeometry, 46(2), 171-182 (2004).

[3] P. Targowski, B. Rouba, M. Wojtkowski, and A. Kowalczyk, “The application of optical coherence tomography to non-destructive examination of museum objects”, Studies in Conservation, 49(2), 107-114 (2004).

[4] H. Liang, M. Gomez Cid, R. Cucu, G. Dobre, D. Jackson, C. Pannell, J. Pedro, D. Saunders, A. Podoleanu, “Application of OCT to examination of easel paintings”, Second European Workshop on Optical Fibre Sensors, Proc. SPIE, 5502, 378-381, (2004).

[5] H. Liang, M. G. Cid, R. G. Cucu, G. M. Dobre, A. Gh. Podoleanu, J. Pedro, D. Saunders, “En-face Optical Coherence Tomography – a novel application of non-invasive imaging to art conservation”, Opt. Express, 13, 6133-6144, (2005). http://www.opticsexpress.org/abstract.cfm?id=85276.

[6] T. Arecchi, M. Bellini, C. Corsi, R. Fontana, M. Materazzi, L. Pezzati, and A. Tortora, "Optical coherence tomography for painting diagnostics", Proc.SPIE 5857, 278-282 (2005).

[7] A. Szkulmowska, M. Góra, M. Targowska, B. Rouba, D. Stifter, E. Breuer, and P. Targowski, "The Applicability of Optical Coherence Tomography at 1.55 um to the Examination of Oil Paintings", in Lasers in the Conservation of Artworks, LACONA VI Proceedings, Vienna, Austria, Sept. 21 - 25, 2005, J. Nimmrichter, W. Kautek, and M. Schreiner, eds. (Springer Verlag, Berlin-Heidelberg-New York, 2007), pp. 487-492

[8] H. Liang, M. G. Cid, R. G. Cucu, G. M. Dobre, B. Kudimov, J. Pedro, D. Saunders, J. Cupitt, A. Gh. Podoleanu, “Optical Coherence Tomography – a non-invasive technique applied to conservation of paintings”, Proceedings of SPIE, 5857, 261-269 (2005).

[9] H. Liang, B. Peric, M. Hughes, A. Podoleanu, M. Spring, and D. Saunders, “Optical coherence tomography for art conservation and archaeology”, Proc. SPIE 6618, 661805 (2007)
[10] M. Góra, P. Targowski, A. Rycyk, J. Marczak “Varnish ablation control by Optical Coherence Tomography”, Laser Chemistry, Article ID 10647, (2006)
[11] P. Targowski, M. Gora, T. Bajraszewski et al., “Optical coherence tomography for tracking canvas deformation”, Laser Chemistry, Article ID 93658, 2006
[12] D. C. Adler, J. Stenger, I. Gorczynska, H. Lie, T. Hensick, R. Spronk, S. Wolohojian, N. Khandekar, J. Y. Jiang, and S. Barry, "Comparison of three-dimensional optical coherence tomography and high resolution photography for art conservation studies", Opt. Express, 15, 15972-15986 (2007).
[13] M. Góra, M. Pircher, E. Götzinger, T. Bajraszewski, M. Strlic, J. Kolar, Ch.K. Hitzenberger, P. Targowski “Optical Coherence Tomography for Examination of Parchment Degradation”, Laser Chemistry, Article ID 68679, (2006)
[14] P. Targowski, B. Rouba, M. Góra, L. Tymińska-Widmer, J. Marczak, and A. Kowalczyk, “Optical Coherence Tomography in Art Diagnostics and Restoration” Applied Physics A, 92, 1-9 (2008).
[15] P. Targowski, M. Góra, M. Wojtkowski, “Optical Coherence Tomography for Artwork Diagnostics” , Laser Chemistry, Article ID 35373, (2006) http://www.hindawi.com/GetArticle.aspx?doi=10.1155/2006/35373
[16] H. Liang, B. Peric, M. Spring, D. Saunders, M. Hughes, A. Podoleanu, “A non-invasive imaging of subsurface paint layers with optical coherence tomography”, Conservation Science 2007, 171-176, Archtype publishing.
[17] M. Spring, H. Liang, B. Peric, D. Saunders, A. Podoleanu, “Optical Coherence Tomography – a tool for high resolution non-invasive 3D-imaging of the subsurface structure of paintings”, Proceeding of ICOM-CC Triennial Conference, 2008, Delhi, Vol. II, 916-923
[18] P. T. Nicholson and J. Anderson, in ‘Ancient Egyptian Materials and Technology’, P.T. Nicholson & I. Shaw eds. Cambridge University Press (2000)
[19] Mantler, M., Beckhoff, B. *private communication*
[20] Podoleanu, A. Gh., Dobre, G.M., Jackson, D.A., “En-face Coherence Imaging Using Galvanometer Scanner Modulation,” Opt. Letters 23, 147-149 (1998).
[21] Podoleanu, A. Gh., “Unbalanced versus balanced operation in an optical coherence tomography system,” Applied Optics 39(1), 173-182 (2000).
[22] P. Kubelka, “New contributions to the optics of intensely light scattering materials. Part I”, J. Opt. Soc. Am. 38, 448-457 (1948).
[23] H. Liang, K. Keita, B. Peric, T. Vajzovic, “Pigment identification with optical coherence tomography and multispectral imaging’’, The 2nd international topical meeting on optical sensing and artificial vision (OSAV08), May 2008, St Petersburg, in print.

Spectral transparency of historic artists' pigments

Borislava Peric[a], Sophie Martin-Simpson[a], Marika Spring[b], Haida Liang[a*]
[a]School of Biomedical and Natural Sciences, Nottingham Trent University, Clifton Lane, Nottingham NG11 8NS, UK
[b]Scientific Department, The National Gallery, London WC2N 5DN, UK

ABSTRACT

The VIS-NIR (400 nm – 2500 nm) reflectance spectra of a wide variety (~50) of historic artists' pigments have been measured with the aim to produce a reference set of spectra that will be made widely available for use by the conservation community. The spectra will provide the basis for infonation to further understand the optical properties of pigments as well as a reference library for spectral pigment identification. Analysis of the reflectance spectra provides a recommendation for the best spectral windows with which to use OCT and IRR to most successfully image subsurface structure of paintings and their underdrawings.

1. INTRODUCTION

Since the invention of IRR for the imaging of underdrawings, there have been studies conducted to directly or indirectly determine the optimum spectral window for IRR (van Asperen de Boer 1969, Delaney et al. 1993, Delaney et al. 2005). However, there has not been a comprehensive survey of the transparency of historic artist pigments over the full near infrared (NIR) range. The recent developments of another non-invasive imaging technique, OCT which enables non-contact imaging of the stratigraphy of paint layers, have prompted a renewed interest in studying the transparency of pigments in the NIR range (e.g. Liang et al. 2004, 2005, Targowski et al. 2004, Szkulmowska et al. 2006).

2. THE SAMPLE

A set of paint-outs consisting of a wide variety of ~50 historic artist's pigments in both egg tempera and linseed oil has been prepared. The pigments were chosen to be representative of what is found on paintings and the compositions of the pigments were verified with EDX, FTIR and XRD measurements. The samples were prepared with known pigment volume concentration and thickness. A list of the pigments is given in Table 1. In order to measure the transparency of the paint layers, one set of paint-outs was prepared over thin glass microscope slides.

Fig. 1 Pigment samples

Hue	Pigment	Supplier
red	Natural red ochre (French)	Kremer Pigmente
	Cadmium red	L.Cornelissen and Son
	Vermilion	The Pigment Factory Bejing
	Vermilion light	Kremer Pigmente
	Sapperwood lake	prepared by National Gallery
	Lac lake	prepared by National Gallery
	Red lead	Kremer Pigmente
	Chrome red	Kremer Pigmente
	Cochineal lake	prepared by National Gallery
	Madder lake (from dyed wool)	prepared by National Gallery
	Madder lake (from ground madder root)	prepared by National Gallery
	Rose madder (genuine)	L.Cornelissen and Son
	Natural iron oxide red	Kremer Pigmente
yellow	Lemon yellow (barium chromate)	L.Cornelissen and Son
	Naples yellow light	Kremer Pigmente
	Lead tin yellow (type I)	Kremer Pigmente
	Orpiment	The Pigment Factory Bejing
	Aureolin (cobalt yellow)	L.Cornelissen and Son
	Cadmium yellow deep	L.Cornelissen and Son
	Chrome yellow medium	Kremer Pigmente
	Cadmium yellow light	L.Cornelissen and Son
	Dyer's Broom lake	prepared by National Gallery
	Italian golden ochre	Kremer Pigmente
	Weld lake	prepared by National Gallery
	Natural Italian terra di siena (raw)	Kremer Pigmente
green	Natural malachite	Kremer Pigmente
	Artificial malachite	Kremer Pigmente
	Viridian green	L.Cornelissen and Son
	Cobalt turquoise (Rimmans green)	L.Cornelissen and Son
	Cobalt bottle green	Kremer Pigmente
	Verdigris	Kremer Pigmente
	Bavarian green earth	Kremer Pigmente
	Prthalo green (Monastral)	L.Cornelissen and Son
blue	Smalt	L.Cornelissen and Son
	Azurite MP	Kremer Pigmente
	Azurite	The Pigment Factory Bejing
	Prussian blue (Milori)	Kremer Pigmente
	Cerulean blue	Kremer Pigmente
	Manganese blue	Kremer Pigmente
	Cobalt blue medium	Kremer Pigmente
	Artificial ultramarine blue light	Kremer Pigmente
	Artificial ultramarine blue dark	Kremer Pigmente
	Indigo	Kremer Pigmente
purple	Manganese violet	Kremer Pigmente
	Cobalt violet dark	Kremer Pigmente
	Cobalt violet light	Kremer Pigmente
white	Titanium white	L.Cornelissen and Son
	Lead white	Kremer Pigmente
black	Bone black	Kremer Pigmente
	Charcoal (made from beech)	Kremer Pigmente

Table 1 Pigment list

3. SPECTRAL MEASUREMENTS

In order to determine the best spectral windows for NIR imaging, either to reveal underdrawings in the case of IRR or to penetrate deeper into the paint layers in the case of non-contact cross-section imaging using OCT, we need to measure the relative spectral transparency of the paint samples.

The transparency of a paint layer depends on both the scattering and absorption properties, since light is both scattered and absorbed when it travels through the layer. For paint layers, the depth range of an OCT is limited by multiple scattering rather than absorption since OCT has high sensitivity and dynamic range. For a strongly scattering paint layer (painted on glass), we expect to find the backscattered light hence reflectance to be high and independent of whether the sample was placed on a white or black background. A highly absorbing paint layer would have low reflectance on a white or black background. In contrast, a highly transparent layer will have high reflectance when it is placed on a white background but low reflectance when placed over a black background.

3.1 Experimental setup

An Ocean Optics HR2000 fibre optic spectrometer (200-1100nm), a Polychromix DTS 1700 (900-1700nm) and DTS 2500 (1700-2500nm) fibre optic spectrometer were used to measure the spectra between 400 nm and 2500 nm. The spectral resolutions of the three spectrometers are 0.9 nm, 12 nm and 22 nm.

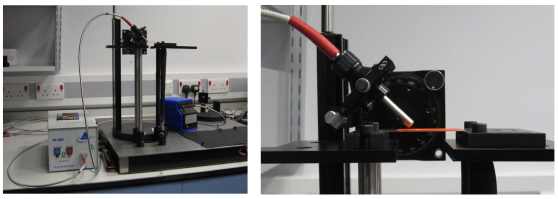

Fig. 2 Experimental setup for reflectance measurements: the sample is placed on a stage 30cm from the optical table (covered in black) such that no light will be reflected back from the background into the fibre.

3.2 Spectral reflectance data

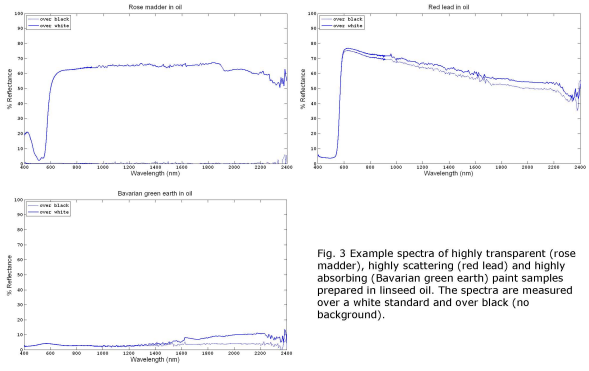

Fig. 3 Example spectra of highly transparent (rose madder), highly scattering (red lead) and highly absorbing (Bavarian green earth) paint samples prepared in linseed oil. The spectra are measured over a white standard and over black (no background).

* haida.liang@ntu.ac.uk

3.3 Spectral transparency

By comparing the spectral reflectance over white and over black, we find that almost without exception all paint samples have best transparency (or least extinction) at ~2.2μm. There are 6 pigments that have slightly better (but comparable) transparency in other regions of the spectra.

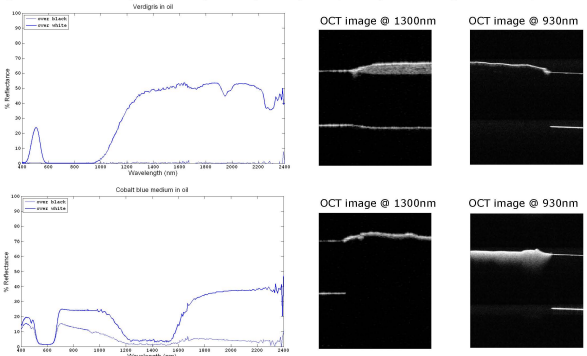

Fig. 4 Spectral reflectance and OCT images at 930 nm and 1300 nm of Verdigris and Cobalt blue medium in linseed oil. The OCT image of Verdigris at 1300 nm is transparent and at 930 nm it is highly absorbent consistent with the spectral reflectance data. Similarly the OCT image of Cobalt blue medium is more absorbent at 1300 nm.

3.4 Effects of binding media

The binding medium changes the transparency of a paint significantly as can be seen in Fig. 5 where the paints in egg tempera are significantly less transparent compared to oil. This is partly due to the difference in refractive indices of egg tempera (n=1.346) and linseed oil (n=1.478). As pigments tend to have larger refractive indices than either medium, we expect higher reflection at the pigment to medium interface when the difference in refractive indices is greater. In addition, egg tempera is less homogeneous compared with linseed oil and hence more scattering.

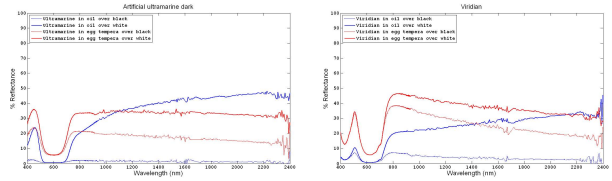

Fig. 5 Spectral reflectance of artificial ultramarine dark and Viridian, both in egg tempera and linseed oil, over a white standard and over no background (black).

3.4 Effects of concentration

As expected for both examples in Fig. 6, the paint with lower pigment to medium concentration is more transparent.

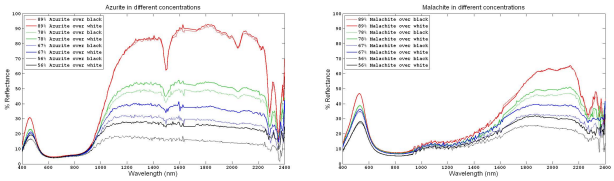

Fig. 6 Azurite and Malachite in different mass concentrations.

3.5 Effects of particle size

The two examples in Fig.7 show that the smaller the particle size, the more scattering and less transparent the paint is.

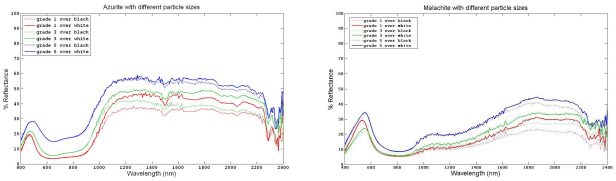

Fig. 7 Effect of particle size for Azurite (in egg tempera) and Malachite (in egg tempera). The particle size is described as grade 1, 3 and 5 (grade 1 is the largest particle size and grade 5 is the smallest).

4. CONCLUSIONS

We have identified the best spectral band for OCT and IRR imaging of paintings to be ~2.2 μm over the 400-2400 nm range. The general trend is that the pigments in linseed oil or egg tempera are more transparent with increasing wavelength over the VIS-NIR spectral range.

This comprehensive survey of VIS-NIR reflectance spectra also provides a reference library for the identification of historic artists' pigments. By extending the wavelength range into the NIR, additional spectral features that are unique to each pigment are revealed, allowing more conclusive identification (e.g. Bacci 2000, Bayerer 1996). The positions of the peaks in the spectra are found to shift as either the concentration or the particle size changes, which needs to be considered when identifying pigments based on their spectra. The successes and limitations of non-invasive identification of pigments on actual paintings using this VIS-NIR reference spectral library along with newly developed algorithms for spectral identification will be reported in a future publication.

REFERENCES

van Asperen de Boer, J. R. J. 1969. 'Reflectography of paintings using an infra-red vidicon television system', Studies in Conservation, 14, 96-118
Bacci, M., 2000, 'UV-VIS-NIR, FT-IR, and FORS spectroscopies'. In *Modern Analytical Methods in Art and Archaeology*, Ciliberto, E. and Spoto, G. (eds.) 321-361. New York: John Wiley & Sons.
Bayerer, F. 1996, 'Die Untersuchung von Kunstobjekten mit Hilfe der bildgebenden Spektroskopie', München: Herbert Utz Verlag Wissenschaft
Delaney, J., Metzger, C.,Walmsley, E., Fletcher, C. 1993. 'Examination of the Visibility of Underdrawing Lines as a Function of Wavelength', in *ICOM Committee for Conservation. 10th Triennia Meeting*, Washington DC, 15–19
Delaney, J. K., Walmsley, E., Berrie, B. H., Fletcher, C. F. 2005. 'Multispectral imaging of paintings in the infrared to detect and map blue pigments', Sackler NAS Colloquium – Scientific Examination of Art: Modern Techniques in Conservation and Analysis, 120-139
Liang, H., Gomez Cid, M., Cucu, R., Dobre, G., Jackson, D., Pannell, C., Pedro, J., Saunders, D., Podoleanu, A., 2004. 'Application of OCT to examination of easel paintings', Second European Workshop on Optical Fibre Sensors, Proc. SPIE 5502, 378-381
Liang, H., Gomez Cid, M., Cucu, R., Dobre, G., Podoleanu, A., Pedro, J., Saunders, D., 2005. 'En-face optical coherence tomography, a novel application of non-invasive imaging to art conservation,' Optics Express, 13 (16), 6136.
Szkulmowska, A., Gora, M., Targowska, M. et al., 2006, 'The application of optical coherence tomography at 1.55mm to the examination of oil paintings', Paper presented at the 6th International Congress on Lasers in the Conservation of Artworks, Vienna, September 2006.
P. Targowski, B. Rouba, M. Wojtkowski, and A. Kowalczyk, 2004. 'The application of optical coherence tomography to non-destructive examination of museum objects', Studies in Conservation 49, 107-114.